plants

MDPI

Article

Anti-Inflammatory Effect of Liverwort (*Marchantia polymorpha* L.) and Racomitrium Moss (*Racomitrium canescens* (Hedw.) Brid.) Growing in Korea

So-Yeon Kim [1], Minji Hong [1], Tae-Hee Kim [1,2], Ki Yeon Lee [1,2], Se Jin Park [1], Sun Hee Hong [3], Kandhasamy Sowndhararajan [4,*] and Songmun Kim [1,*]

1 School of Natural Resource and Environmental Science, Kangwon National University, Chuncheon 24341, Korea; ykims95@kangwon.ac.kr (S.-Y.K.); alswl0356@kangwon.ac.kr (M.H.); hanmi230@naver.com (T.-H.K.); lky6520@korea.kr (K.Y.L.); sejinpark@kangwon.ac.kr (S.J.P.)
2 Agriproduct Processing Experiment Station, Gangwon-do Agriculture Research and Experiment Services, Chuncheon 24203, Korea
3 Department of Plant Life and Environmental Science, Hankyong National University, Ansung 17579, Korea; shhong@hknu.ac.kr
4 Department of Botany, Kongunadu Arts and Science College, Coimbatore 641029, India
* Correspondence: sowndhar1982@gmail.com (K.S.); perfume@kangwon.ac.kr (S.K.); Tel.: +91-422-2642095 (K.S.); +82-33-250-6447 (S.K.)

Abstract: Bryophytes contain a variety of bioactive metabolites, but studies about the anti-inflammatory effect of bryophytes are meager. Therefore, the present study aimed to compare the anti-inflammatory effect of methanol extract of *Marchantia polymorpha* L. (liverwort) and *Racomitrium canescens* (Racomitrium moss) in lipopolysaccharide (LPS)-induced HaCaT cells. To evaluate the anti-inflammatory effect of liverwort and Racomitrium moss, the levels of nitric oxide (NO) production and the mRNA expression of inducible nitric oxide synthase (iNOS), cyclooxygenase-2 (COX-2) and tumor necrosis factor-α (TNF-α), and interleukin (IL)-6 and IL-1β in LPS-induced HaCaT cells were measured. The methanol extract of liverwort and Racomitrium moss significantly decreased LPS-induced NO production in HaCaT cells. When compared with Racomitrium moss extract, pre-treatment with methanol extract of liverwort markedly inhibited the expression of iNOS, COX-2, IL-6, and IL-1β at the concentration of 100 μg/mL with the exception of TNF-α. Further, liverwort extract markedly attenuated the production of TNF-α, IL-6, and IL-1β in the culture medium. In addition, ethyl acetate and butanol fractions obtained from the methanol extract of liverwort showed remarkable inhibitory activity against the production of NO in LPS-stimulated HaCaT cells. The LC-MS data revealed the presence of bisbibenzyl types of bioactive components in the methanol extract of liverwort. These data demonstrate that liverwort extract exhibits effective inhibitory activity against the production of inflammatory mediators in LPS-induced HaCaT cells and may be useful for the treatment of inflammation-mediated diseases.

Keywords: liverwort; *Marchantia polymorpha*; *Racomitrium canescens*; anti-inflammatory; nitric oxide; HaCaT cell

check for updates

Citation: Kim, S.-Y.; Hong, M.; Kim, T.-H.; Lee, K.Y.; Park, S.J.; Hong, S.H.; Sowndhararajan, K.; Kim, S. Anti-Inflammatory Effect of Liverwort (*Marchantia polymorpha* L.) and Racomitrium Moss (*Racomitrium canescens* (Hedw.) Brid.) Growing in Korea. *Plants* **2021**, *10*, 2075. https://doi.org/10.3390/plants10102075

Academic Editor: Mariangela Marrelli

Received: 25 August 2021
Accepted: 28 September 2021
Published: 30 September 2021

Publisher's Note: MDPI stays neutral with regard to jurisdictional claims in published maps and institutional affiliations.

Copyright: © 2021 by the authors. Licensee MDPI, Basel, Switzerland. This article is an open access article distributed under the terms and conditions of the Creative Commons Attribution (CC BY) license (https://creativecommons.org/licenses/by/4.0/).

1. Introduction

The human epidermis, mainly comprised of keratinocytes (about 95%), is a principal portion of the skin's immune system. Keratinocytes provide the first line of defense against various external harmful agents, such as microorganisms and toxic chemicals [1,2]. In the inflamed skin, keratinocytes play an important role in the structural integrity of skin and the inflammatory responses by producing various pro-inflammatory cytokines such as interleukin-6 (IL-6), IL-1β, tumor necrosis factor-α (TNF-α), inducible nitric oxide synthase (iNOS) derived nitric oxide (NO), and cyclooxygenase-2 (COX-2) prostaglandins [3]. Cytokines are the most important contributors in the regulation of the immune system.

Although cytokines and other mediators contribute to normal homeostatic mechanisms in the skin, overproduction of pro-inflammatory mediators may lead to various inflammatory diseases [4]. Hence, the suppression of pro-inflammatory mediators may play a key role in the treatment of inflammation-mediated skin diseases.

Many synthetic drugs have shown an appreciable anti-inflammatory effect but they have certain side effects, including gastric bleeding and ulceration [5]. Therefore, there is a growing trend to develop safer natural products for the treatment of inflammation-mediated diseases. Lipopolysaccharides (LPS), the major component of the Gram-negative bacterial cell wall, are one of the most powerful stimulators of the production of pro-inflammatory cytokines [6]. The HaCaT cell line is routinely employed to confirm the effects of drugs on epidermal inflammation. Hence, the inhibition of pro-inflammatory mediator's production in LPS-stimulated HaCaT cells is a potential way to screen the anti-inflammatory effect of extracts/compounds.

In the plant kingdom, bryophytes are the second most diverse group of terrestrial plants after angiosperms with about 25,000 species found throughout the world. Bryophytes are classified into mosses, liverworts, and hornworts [7]. They contain a variety of biologically active components such as fatty acids, terpenoids, flavonoids, and polyphenols [7–9]. In traditional systems of medicine, bryophyte plants have been used to cure various ailments in India, China, and North America, including burns, external wounds, snake bites, pulmonary tuberculosis, cardiovascular diseases, bone fractures, hepatic disorders, and skin diseases [10].

Mosses are the largest group of bryophytes, playing a significant role in the ecosystem of terrestrial biodiversity. Traditionally, mosses have been used to treat wounds, burns, and other diseases. In these, the genus *Racomitrium* (Grimmiaceae) is an important component of various terrestrial ecosystems [11]. *Racomitrium canescens* (Hedw.) Brid. (Racomitrium moss) is widely distributed from the northern temperate to arctic zones (Figure 1). However, only a few studies have been conducted on this genus, especially from a taxonomic point of view [11]. Liverworts are the second important group of bryophytes, containing about 6000 species, and are considered to be the oldest aquatic-terrestrial plants [12,13]. Liverworts mainly contain volatile components (terpenoids) in addition to a wide variety of other bioactive components. In particular, some terpenoid compounds such as the pinguisane group of sesquiterpenoids and the sacculatane group of diterpenoids are not identified in other plant species [14]. *Marchantia* is one of the important genera in the family of Marchantiaceae. The common liverwort *Marchantia polymorpha* L. (liverwort) is mainly found in temperate regions (Figure 1) [15]. This plant has been traditionally used to treat boils, fractures, poisonous snakebites, abscesses, wounds, and hepatic disorders. Liverwort has also been used as a diuretic agent in European countries [10,16,17]. The extracts and compounds isolated from liverwort exhibited various biological activities such as antimicrobial [17,18], antioxidant [19], anti-inflammatory [20] activities, and cytotoxic potential against cancer cell lines [21]. However, there has been no study in relation to the anti-inflammatory potential of liverwort and Racomitrium moss in LPS-induced HaCaT cells.

Based on the highly acclaimed properties of liverwort and Racomitrium moss, we investigated the anti-inflammatory effects of methanol extract of liverwort and Racomitrium moss by measuring its ability to inhibit NO production and mRNA expression of iNOS, COX-2, TNF-α, IL-6, and IL-1β in LPS-stimulated HaCaT cells.

(**a**) Liverwort

(**b**) Racomitrium moss

Figure 1. Morphology of liverwort and Racomitrium moss.

2. Results and Discussion

2.1. The Effect of Extract on the Viability of HaCaT Cells

Keratinocytes, a major part of epidermal cells, play an important role in the pathogenesis of inflammatory skin lesions by producing pro-inflammatory mediators [22,23]. First, we determined the viability of HaCaT cells in the presence of methanol extracts of liverwort and Racomitrium moss for 24 h to evaluate their possible cytotoxic effect. For this purpose, the HaCaT cells were incubated with different concentrations of methanol extracts of liverwort and Racomitrium moss. After the treatment, the survival of HaCaT cells was not significantly affected by 24 h incubation with up to 100 μg/mL concentration of both the extracts (cell viability > 90%) (Figure 2). Therefore, non-toxic concentrations of liverwort and Racomitrium moss extracts up to 100 μg/mL were used for further experiments.

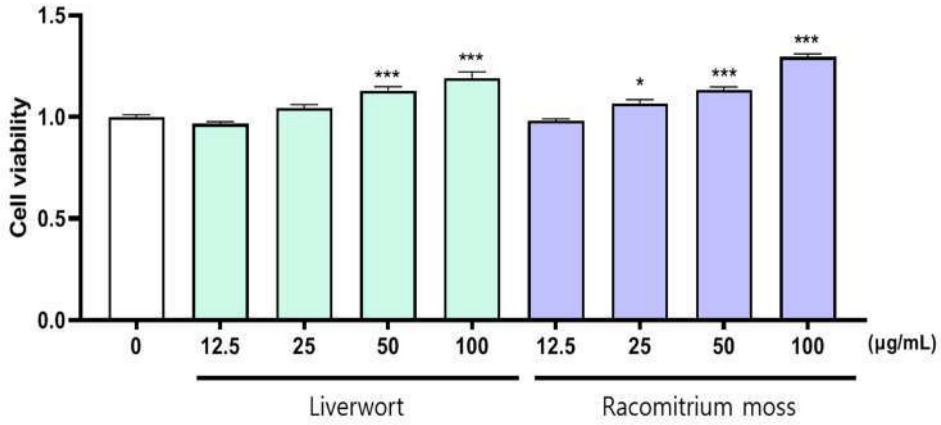

Figure 2. The effect of methanol extract of liverwort and Racomitrium moss on the cell viability of HaCaT cells. Values are mean of three replicate determinations (n = 3) ± standard deviation. * $p < 0.05$, *** $p < 0.001$ vs. 1% MeOH alone.

2.2. Inhibition of Nitric Oxide Production in LPS-Stimulated HaCaT Cells

It is well established that LPS can lead to the release of various pro-inflammatory cytokines, including adhesion molecules such as nitric oxide (NO) [24]. Under normal physiological conditions, NO regulates many biological functions such as host defense, platelet aggregation, vasoregulation, and neurotransmission. However, excessive production of NO and other inflammatory mediators is linked with the development of many diseases [25]. Hence, we determined the inhibitory effect of the methanol extract of liverwort and Racomitrium moss on NO production in LPS-induced HaCaT cells (Figure 3).

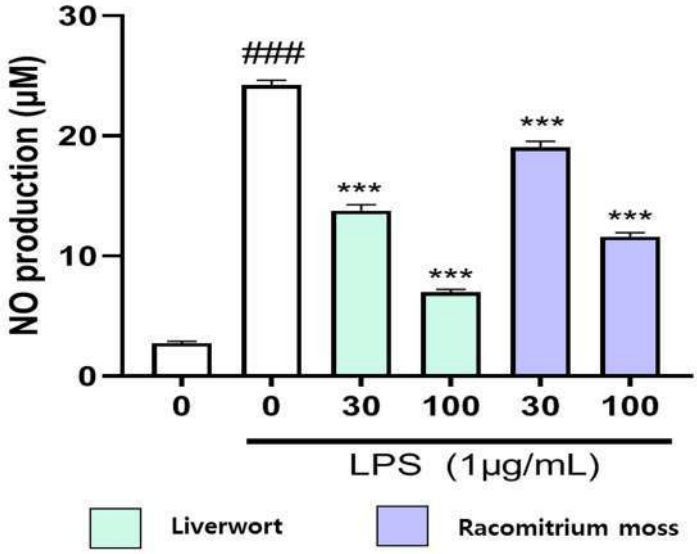

Figure 3. Inhibitory effect of methanol extract of liverwort and Racomitrium moss on NO production by LPS-stimulated HaCaT cells. Values are mean of three replicate determinations (n = 3) ± standard deviation. ### $p < 0.001$ vs. 1% MeOH alone, *** $p < 0.001$ vs. LPS alone.

To accomplish this experiment, HaCaT cells were activated by LPS, and the production of NO was measured as nitrite concentration in the cell culture supernatant. The LPS treatment (1 μg/mL) significantly increased NO production by HaCaT cells by accumulating a higher level of nitrite (24.24 μM). To determine the effect of liverwort and Racomitrium moss extracts on NO production, cells were simultaneously treated with 1 μg/mL LPS and two different concentrations of extracts (30 and 100 μg/mL). When compared to the untreated control, the cells pre-treated with methanol extracts of liverwort and Racomitrium

moss significantly ($p < 0.001$) decreased the production of NO in the medium to 6.99 and 11.61 μM, respectively, at the concentration of 100 μg/mL (Figure 3). The inhibitory effect of liverwort and Racomitrium moss extracts on NO production was not owing to the damage of cells (viability > 90%) as measured in the MTT cell viability assay. There has been no study on the inhibitory effect of moss or liverworts on NO production in HaCaT cells. However, these results were comparable with those previously obtained by other researchers on RAW 264.7 cells. In LPS-induced RAW 264.7 cells, compounds isolated from liverworts such as *Mastigophora diclados* [26], *Porella densifolia* [27], *Lepidozia reptans* [28], and *Jamesoniella autumnalis* [29] showed a potent inhibitory effect on the production of NO.

2.3. The Effect of Extracts on mRNA Expression of iNOS, COX-2, TNF-α, IL-6, and IL-1β

We also analyzed the mRNA expression of iNOS, COX-2, TNF-α, IL-6, and IL-1β in LPS-stimulated HaCaT cells using RT-PCR in order to confirm the inhibitory effects of methanol extracts of liverwort and Racomitrium moss on pro-inflammatory mediators. HaCaT cells were pre-treated with two different concentrations of extracts (30 and 100 μg/mL) to determine the mRNA expression of pro-inflammatory mediators stimulated by LPS. Treatment with LPS alone (1 μg/mL) significantly upregulated the mRNA expression of iNOS, COX-2, TNF-α, IL-6, and IL-1β in HaCaT cells (Figures 4 and 5). On the other hand, pre-treatment with methanol extract of liverwort (at 100 μg/mL) significantly ($p < 0.001$) suppressed the mRNA expression of iNOS, COX-2, IL-6, and IL-1β in LPS-stimulated HaCaT cells when compared to that of Racomitrium moss extract. However, there was no significant downregulation of mRNA expression of TNF-α. Further, Racomitrium moss extract did not show significant downregulation of mRNA expression of COX-2. These data suggest that the methanol extract of liverwort and Racomitrium moss effectively reduced the nitrite accumulation by downregulating the mRNA expression of these pro-inflammatory mediators.

The iNOS and COX-2 and their reaction products are highly connected with inflammatory diseases [30]. Previous studies demonstrated that plant extracts/compounds can selectively suppress the expression of iNOS and COX-2. In addition, a strong correlation between NO production and iNOS expression was observed, as shown by other authors [31,32]. The present study also proved that the methanol extract of liverwort remarkably suppressed the expression of iNOS and COX-2 in LPS-stimulated HaCaT cells. Similarly, dollabellane- and ent-kaurane-type diterpenoids isolated from Chinese liverwort, *Lepidozia reptans*, effectively attenuated the mRNA expression of IL-6, IL-β, IL-α, TNF-α, and COX-2 in LPS-stimulated RAW264.7 cells [28].

In LPS-stimulated cell lines, nuclear factor kappa B (NF-κB) is an important transcription factor in the expression of iNOS and COX-2 genes [33,34]. In LPS-induced human keratinocyte HaCaT cells, He et al. [35] found that feruloylserotonin suppressed the toll-like receptor (TLR4)/NF-κB pathway and promoted the translocation of Nuclear factor-erythroid 2 related factor 2 (Nrf2). The chloroform fraction of *Carpinus tschonoskii* inhibited the protein and mRNA of chemokine in HaCaT cells by downregulating STAT1 in the IFN-γ signaling pathway [36]. Another study indicated that peat moss extracts induced the sequestration of NF-κB in the cytoplasm by inhibiting the degradation of IκBα in the LPS-stimulated RAW 264.7 cells. Further, peat moss extracts suppressed the activation of MAPKs and facilitated the activation of Nrf2, and enhanced heme oxygenase-1 (HO-1) expression [30]. A study indicated that miR-127 is involved in the inhibitory effect of Schisandrin A on LPS-induced inflammation injury in HaCaT cells via inactivating p38MAPK/ ERK and JNK signaling pathways [37]. It can be observed that downregulation of the NF-κB and MAPK pathways play a crucial role in the regulation of pro-inflammatory mediators. The suppression of NO production and the downregulation of mRNA expression of various pro-inflammatory mediators are effective therapeutic approaches to block the potentially harmful production of pro-inflammatory mediators by keratinocytes [38]. Moreover, the results of the present study throw some light on the inhibitory effect of liverworts on the production of pro-inflammatory mediators in HaCaT cells.

2.4. The Effect of Extracts on the Production of TNF-α, IL-16, and IL-1β

As shown in Figure 6, the production of TNF-α (4528 pg/mL), IL-6 (808 pg/mL), and IL-1β (306 pg/mL) were enhanced by the LPS treatment. However, LPS-induced production of TNF-α (1867 pg/mL), IL-6 (29 pg/mL), and IL-1β (40 pg/mL) in HaCaT cells were effectively suppressed upon the treatment of methanol extract of liverwort (at 100 μg/mL) than Racomitrium moss extract. Further, Racomitrium moss extract did not show any significant effect on the production of TNF-α. These data indicated that methanol extracts of liverwort and Racomitrium moss could protect HaCaT cells against LPS-induced cell injury.

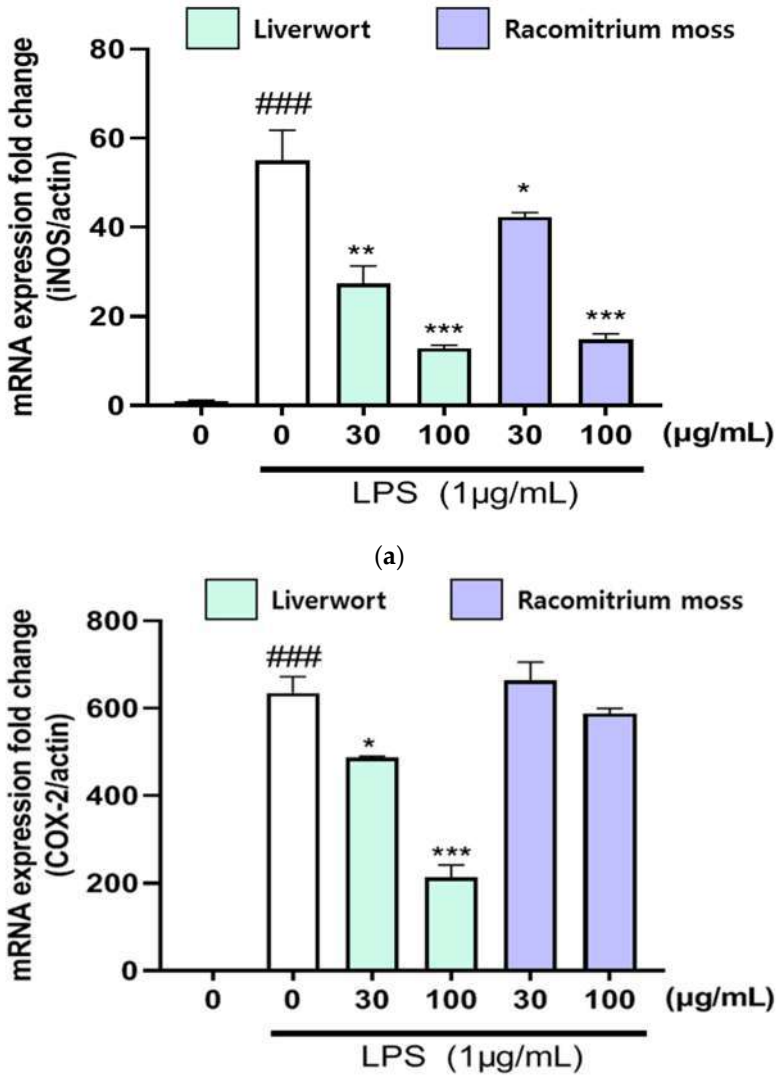

Figure 4. The effect of methanol extract of liverwort and Racomitrium moss on mRNA expressions of iNOS and COX-2 in LPS-stimulated HaCaT cells. (**a**) mRNA expression of iNOS; (**b**) mRNA expression of COX-2. Values are mean of three replicate determinations ($n = 3$) ± standard deviation. ### $p < 0.001$ vs. 1% MeOH alone, * $p < 0.05$, ** $p < 0.01$, *** $p < 0.001$ vs. LPS alone.

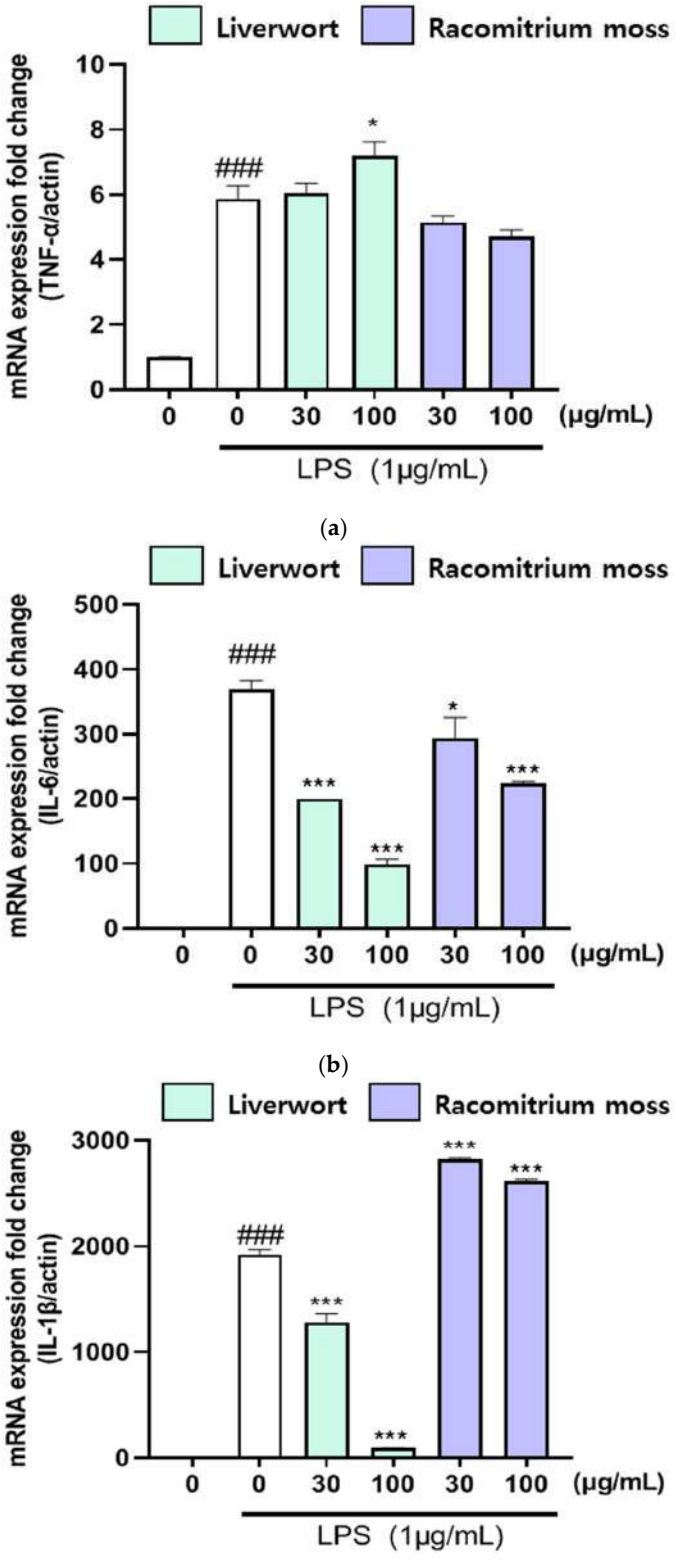

Figure 5. The effect of methanol extract of liverwort and Racomitrium moss on mRNA expressions of TNF-α, IL-6, and IL-1β in LPS-stimulated HaCaT cells. (**a**) mRNA expression of TNF-α; (**b**) mRNA expression of IL-6; (**c**) mRNA expression of IL-1β. Values are mean of three replicate determinations ($n = 3$) ± standard deviation. ### $p < 0.001$ vs. 1% MeOH alone, * $p < 0.05$, *** $p < 0.001$ vs. LPS alone.

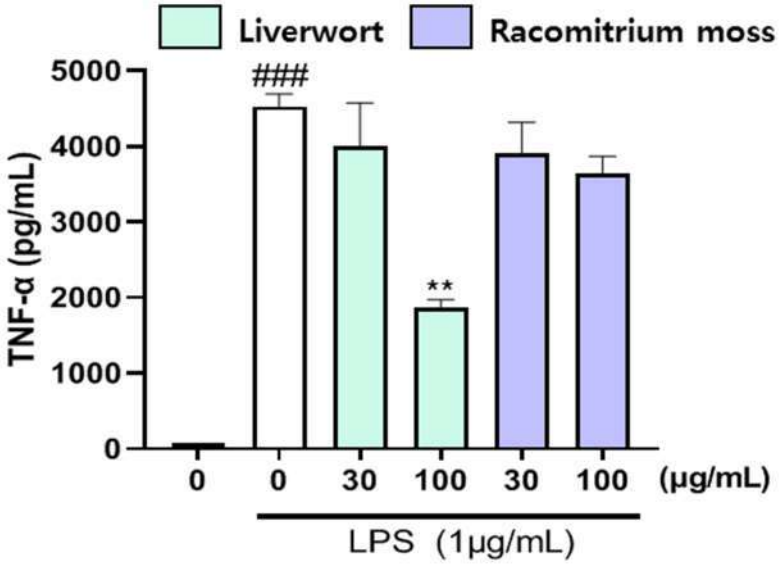

(**a**)

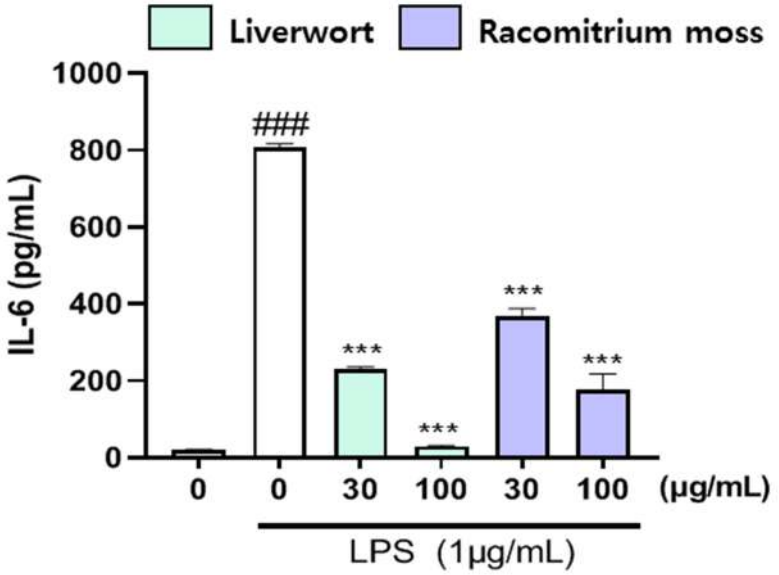

(**b**)

Figure 6. *Cont*.

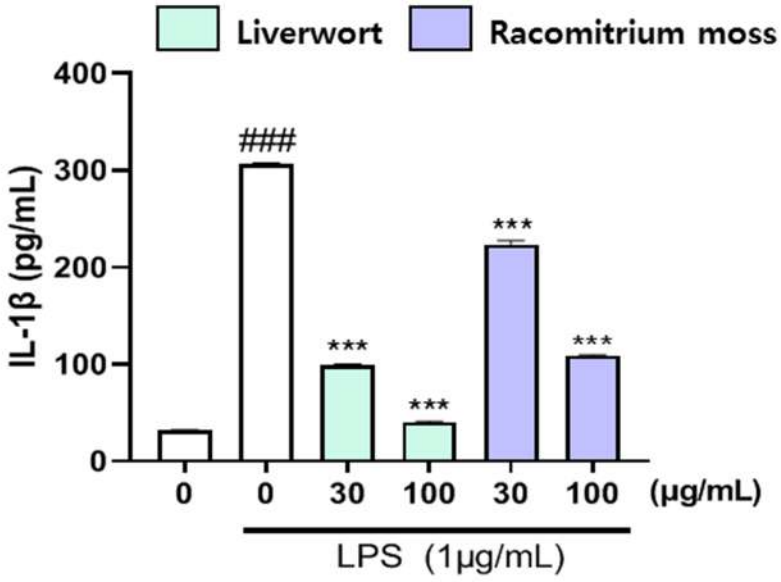

(**c**)

Figure 6. The effect of methanol extract of liverwort and Racomitrium moss on the level of TNF-α, IL-6, and IL-1β in the culture medium of LPS-stimulated HaCaT cells. (**a**) the level of TNF-α; (**b**) the level of IL-6; (**c**) the level of IL-1β. Values are mean of three replicate determinations (n = 3) ± standard deviation. ### $p < 0.001$ vs. 1% MeOH alone, ** $p < 0.01$, *** $p < 0.001$ vs. LPS alone.

2.5. The Effect of Fractions of Liverwort on Nitric Oxide Production

In the cell viability assay, butanol fraction obtained from the methanol extract of liverwort exhibited no cytotoxicity effect against HaCaT cells at 100 μg/mL. Moreover, ethyl acetate fraction showed a low cytotoxic effect at 100 μg/mL. However, hexane, chloroform, and water fractions significantly reduced the cell viability (absorbance < 0.7) at the concentration of 100 μg/mL (Figure 7). Hence, ethyl acetate and butanol fractions were selected for further NO production assay. The cells pretreated with ethyl acetate and butanol fractions significantly ($p < 0.001$) inhibited the production of NO in a concentration-dependent manner by reducing the level of nitrite in the medium (Figure 8). Further studies in connection with the isolation of bioactive components from these fractions are under progress.

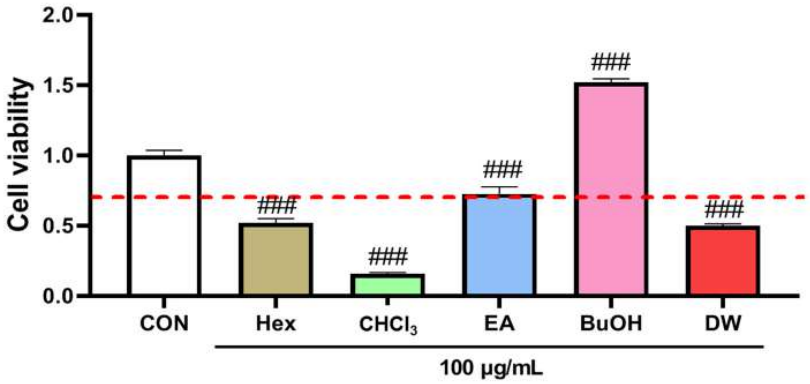

Figure 7. The effect of different fractions (at 100 μg/mL) obtained from methanol extract of liverwort on the cell viability of HaCaT Cells. CON, control; Hex, hexane fraction; $CHCl_3$, chloroform fraction; EA, ethyl acetate fraction; BuOH, butanol fraction; DW, water fraction. Values are mean of three replicate determinations (n = 3) ± standard deviation. ### $p < 0.001$ vs. 1% MeOH alone.

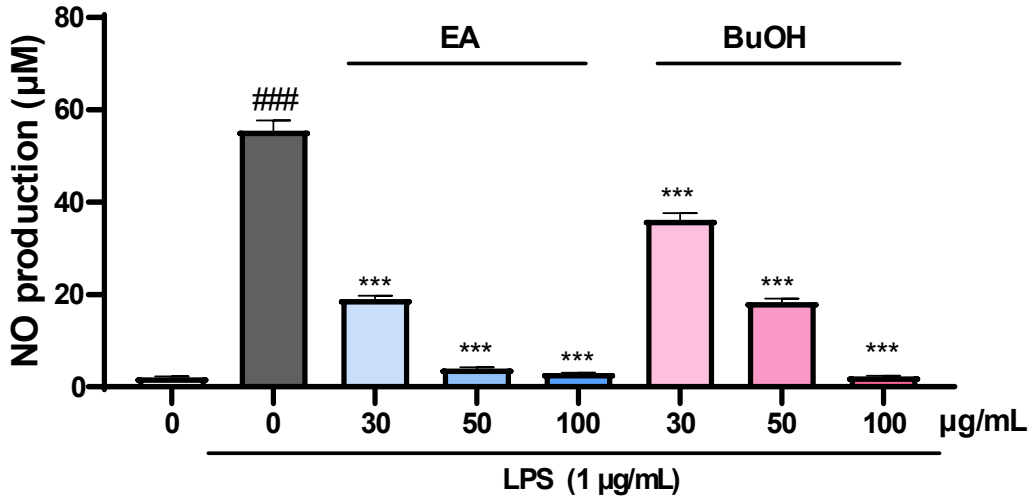

Figure 8. Inhibitory effect of ethyl acetate and butanol fractions of methanol extract of liverwort on NO production by LPS-stimulated HaCaT cells. EA, ethyl acetate fraction; BuOH, butanol fraction; Values are mean of three replicate determinations (n = 3) ± standard deviation. ### $p < 0.001$ vs. 1% MeOH alone, *** $p < 0.001$ vs. LPS alone.

2.6. Liquid Chromatography-Mass Spectrometry (LC-MS) Analysis of Methanol Extracts

It was reported that liverworts are an exceptionally rich source of terpenoids, particularly sesqui- and diterpenoids [39]. Tosun et al. [13] also stated that the sesquiterpene-group components are partially responsible for the anti-inflammatory and antinociceptive properties of different liverworts. However, bryophytes contain a variety of other secondary metabolites with potent biological properties. The methanol extracts of liverwort and Racomitrium moss were subjected to LC-MS analysis (Figures 9 and 10). The molecular mass and fragments of the identified compounds in the methanol extracts of liverwort and Racomitrium moss are presented in Table 1. Eleven components were identified from the methanol extract of liverwort and four components were identified from the methanol extract of Racomitrium moss. In positive mode ionization, the mass data show a similar fragmentation profile with *m/z* at 543, 527, and 381, which is correlated to pinoresinol-di-*O*-*β*-D-glucopyranoside (Figure 11) [40]. Pinoresinol-di-*O*-*β*-D-glucopyranoside exhibited remarkable inhibitory activity against the production of PGE_2 in LPS-induced RAW264.7 cells [41]. In methanol extract of liverwort, peak 9 shows *m/z* at 439, 331, and 226; this compound could be identified as marchantin G [42]. The peak 3 at *m/z* at 423, 411, and 213 and the peak 8 *m/z* at 479, 239, and 211 represent unidentified bisbibenzyls (Figure 11) [43,44]. In addition, peak 2 from Racomitrium moss shows *m/z* at 931, 767, and 753 corresponding to dioscoreside A [45].

The LC-MS data indicated that the methanol extract of liverwort mainly contains the bisbibenzyl group of components. They are aromatic compounds and have one or two diaryl ether or biphenyl bonds mainly found in liverworts, including *Riccardia*, *Marchantia*, *Plagiochila*, etc. [46]. Previously, seven confirmed bisbibenzyls and twelve unconfirmed bisbibenzyl components were detected in the ethanol extract of *M. polymorpha* [44]. Sabovljević et al. [42] studied the comparison of LC-MS analysis of methanol extracts from natural and cultured liverwort. The results indicated the presence of marchantin A in both natural and cultured liverwort. On the other hand, marchantin E, G, and/or C, and dehydromarchantin A were found only in the cultured liverwort. Harinantenaina et al. [46] investigated the inhibitory effect of nineteen bisbibenzyls on NO production in LPS-stimulated RAW 264.7 cells. Among the tested components, marchantin A exhibited strong inhibitory activity against NO production and mRNA expression of iNOS. Previous studies demonstrate that the presence of bisbibenzyl-type components in the methanol extract of liverwort may be responsible for its anti-inflammatory activity.

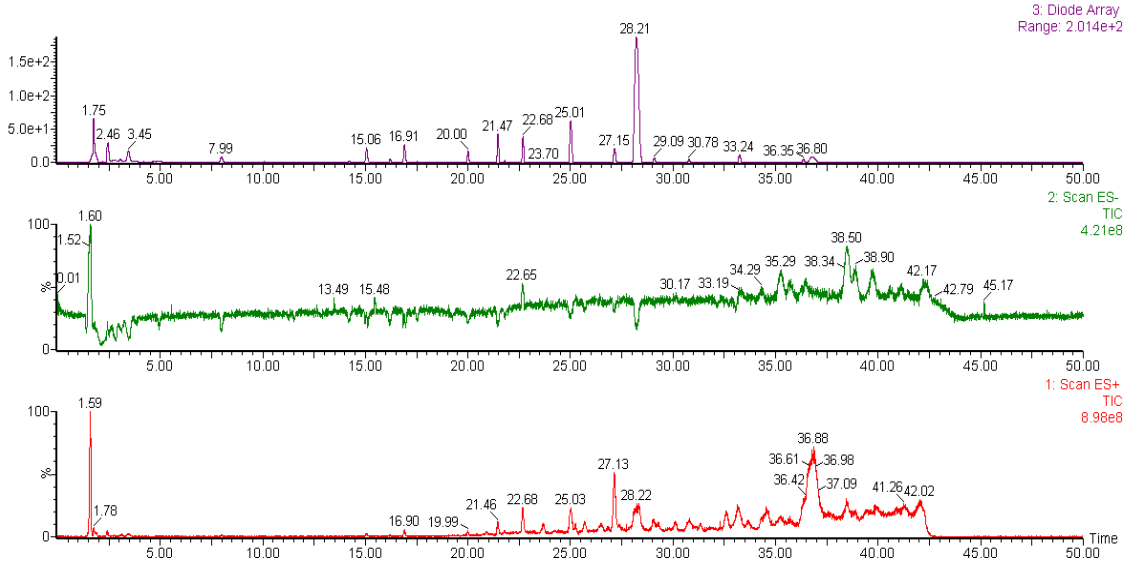

Figure 9. The LC-MS chromatogram of the methanol extract of liverwort.

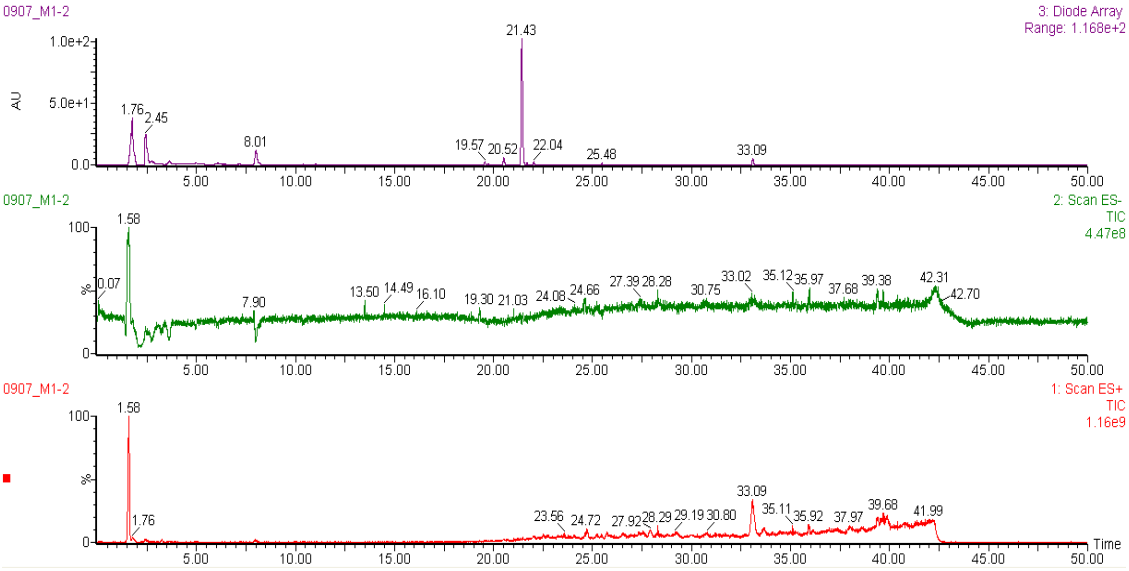

Figure 10. The LC-MS chromatogram of the methanol extract of Racomitrium moss.

Table 1. Identification of chemical constituents from methanol extracts of liverwort and Racomitrium moss by LC-MS.

Peak	Tentative Identification	Retention Time (min)	Molecular Mass (Da)	Fragments (m/z)	References
		Liverwort			
1	Pinoresinol-di-*O*-*β*-D-glucopyranoside	1.59	705	707, 543, 527, 381, 365	[40]
2	Unknown	1.78	517	826, 625, 517, 381, 204	-
3	Unconfirmed bisbibenzyl	15.05	421	463, 423, 411, 309, 213	[43]
4	Unknown	16.90	447	621, 447, 271, 145	-
5	Unknown	19.90	674	970, 806, 772, 674, 597	-
6	Unknown	21.46	565	903, 858, 565, 431, 322,	-
7	Unknown	22.68	658	917, 833, 658, 483, 158	-
8	Unconfirmed bisbibenzyl	25.03	424	479, 452, 417, 239, 142	[44]
9	Marchantin G	27.13	454	493, 439, 331, 313, 226	[42]
10	Unconfirmed bisbibenzyl	28.22	454	463, 458, 333, 224, 197	[44]
11	Unknown	36.88	599	975, 907, 599, 256, 157	-

Table 1. *Cont.*

Peak	Tentative Identification	Retention Time (min)	Molecular Mass (Da)	Fragments (m/z)	References
		Racomitrium moss			
1	Pinoresinol-di-*O*-*β*-D-glucopyranoside	1.58	705	707, 543, 527, 381, 365	[40]
2	Dioscoreside A	7.94	784	931, 793, 767, 753, 268	[45]
3	Unknown	25.75	748	748, 657, 603, 505, 411	-
4	Unknown	33.09	518	518, 497, 263, 215, 205	-

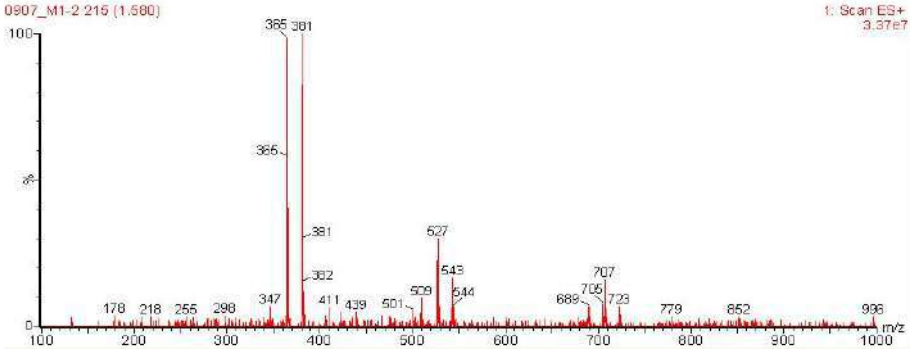

(**a**) Pinoresinol-di-*O*-*β*-D-glucopyranoside

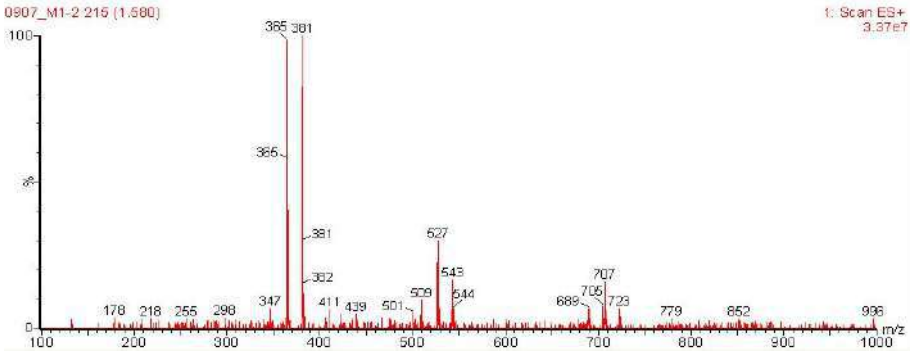

(**b**) Unconfirmed bisbibenzyls

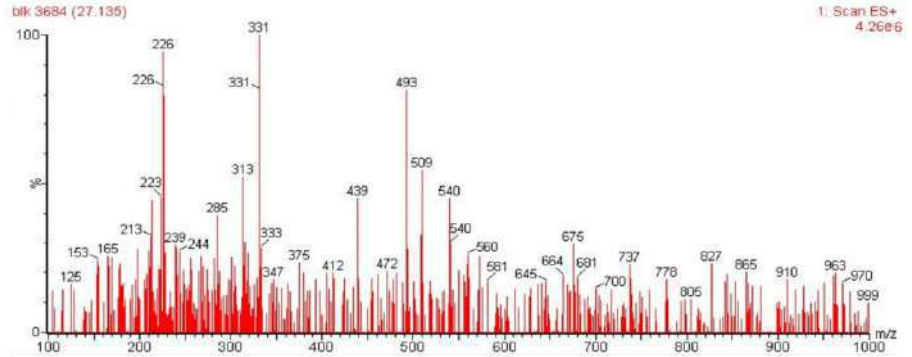

(**c**) Marchantin G

Figure 11. Mass spectra of Pinoresinol-di-*O*-*β*-D-glucopyranoside, unconfirmed bisbibenzyl, and marchantin G from the methanol extract of liverwort.

3. Materials and Methods

3.1. Sample Collection

M. polymorpha and *R. canescens* samples were collected from Songjung-ri, Jinbu-Myeon, Pyeongchang, in Korea during October 2020 (Figure 1). Collected samples were kept in a 4 °C freezer and transported to the laboratory. The soil and plant debris in the samples was removed by washing in running tap water. The samples were authenticated and

deposited in the Herbarium, National Institute of Biological Resources (NIBR), Korea, with voucher numbers NIBRMS 0000107499 and NIBRMS 0000107500, respectively.

3.2. Preparation of Methanol Extract

Plant samples were dried at room temperature, pulverized using a grinder (HANIL HMF-3260S, Hanil Electric Co., Seoul, Korea) up to 0.6 mm. One kilogram of powdered leaves was extracted twice with 4-L of methanol per extraction for 2 days and filtered. The combined filtrates were concentrated using a rotary vacuum evaporator at 40 °C (EYELA NE-1101, Tokyo Rikakikai Co., Ltd., Tokyo, Japan) and the concentrate was dissolved with 50 mL of distilled water. Then the extract was dried using a freeze dryer (FD5505, ILSHIN BIOBASE, Dongduchon, Korea). The obtained extracts of liverwort and Racomitrium moss were dissolved and diluted to 10 mg/mL in methanol as a stock solution.

3.3. Cell Culture

HaCaT cells (human epidermal fibroblast) were provided by the Food Chemistry laboratory at Kangwon National University (Prof. Lee). Cell culture medium was used in Dulbecco's Modified Eagle's Medium (DMEM) with 100 units/milliliter penicillin-streptomycin (P/S) and 10% fetal bovine serum (FBS) [47]. Thereafter, the cells were cultured at 37 °C and 5% CO2, followed by subculture every three days, respectively.

3.4. Cell Viability Analysis

Cell viability was estimated for cytotoxicity of methanol extract of liverwort and Racomitrium moss using the MTT assay. Cultured cells were treated with methanol extract of liverwort and Racomitrium moss at 12.5–100 μg/mL for 24 h. After incubation with MTT solution diluted 10:1 (5 mg/mL in PBS) at 37 °C for 4 h, purple formazan was formed in the cells. The solution in each well was completely removed and then the purple formazan crystals were dissolved in DMSO and isopropyl alcohol at 1:1 (100 μL/well). The optical density was measured at 540 nm using a SpectraMax 190 Microplate Reader (Molecular Devices, San Jose, CA, USA).

3.5. Measurement of Nitric Oxide

HaCaT cells were pre-treated with methanol extract of liverwort and Racomitrium moss at 30 and 100 μg/mL for 1 h, followed by stimulation with LPS (1 μg/mL) for 24 h. Nitrite accumulation in the culture medium as an indicator of NO production was measured using Griess reagent [48]. The culture supernatant (100 μL) was mixed with 100 μL of Griess reagent (equal volumes of 1% (*w*/*v*) sulfanilamide in 0.1% (*w*/*v*) naphthyl ethylenediamine-HCl and 5% (*v*/*v*) phosphoric acid) for 10 min [47]. The optical density was measured at 540 nm using a SpectraMax 190 Microplate Reader (Molecular Devices, San Jose, CA, USA). The amount of nitrite in the medium was determined with reference to a sodium nitrite ($NaNO_2$) standard curve.

3.6. RNA Isolation and Real Time-Polymerase Chain Reaction (RT-PCR)

RT-PCR was used to estimate the mRNA expression of iNOS, COX-2, TNF-α, IL-6, and IL-1β. Total RNA was extracted from HaCaT cells using RNAiso PLUS. Total RNA (1 μg) was used to generate cDNA by reverse transcription using All-in-One First-Strand cDNA Synthesis SuperMix [49]. The synthesized cDNA was used as a template for qRT-PCR using QuantStudio 3 (Applied Biosystems, Foster City, CA, USA) system with FG POWER SYBR Green PCR master mix and gene-specific primers (Table 2) [47]. A dissociation curve analysis of iNOS, COX-2, TNF-α, IL-6, IL-1β, and β-actin showed a single peak. Expression levels of target genes were quantified from duplicate measurements and normalized with the $2^{-\Delta\Delta CT}$ method relative to β-actin.

Table 2. Primer sequences used for quantitative real-time PCR analysis.

Target Gene		Primer Sequence
iNOS	Forward	5′-CATTGATCTCCGTGACAGCC-3′
	Reverse	5′-CATGCTACTGGAGGTGGGTG-3′
COX-2	Forward	5′-GCAGCCATTTCCTTCTCTCC-3′
	Reverse	5′-TGCTGTACAAGCAGTGGCAA-3′
TNF-α	Forward	5′-CTG ATG AGA GGG AGG CCA TT-3′
	Reverse	5′- AGC ACA GAA AGC ATG ATC CG-3′
IL-6	Forward	5′-AAGTGCATCATCGTTGTTCATACA-3′
	Reverse	5′-GAGGATACCACTCCCAACAGACC-3′
IL-1β	Forward	5′-TCGTTGCTTGGTTCTCCTTG-3′
	Reverse	5′-ACCTGCTGGTGTGTGACGTT-3′
β-actin	Forward	5′-TCAGCAATGCCTGGGTACAT-3′
	Reverse	5′-ATCACTATTGGCAACGAGCG-3′

3.7. Enzyme-Linked Immunosorbent Assay (ELISA)

HaCaT cells were pre-treated with methanol extract of liverwort and Racomitrium moss at 30 and 100 μg/mL for 4 h and then treated with LPS (1 μg/mL) for an additional 20 h. The supernatants were collected and analyzed for the levels of TNF-α, IL-6, and IL-1β (Invitrogen, Carlsbad, CA, USA) using ELISA kits according to the manufacturer's protocol.

3.8. Fractionation of Methanol Extract of Liver Wort and Nitric Oxide Measurement

The methanol extract of liverwort was prepared as mentioned in Section 2.2. The crude methanol extract was suspended in deionized water and the aqueous solution was sequentially partitioned with hexane, chloroform ($CHCl_3$), ethyl acetate (EA), butanol (BuOH). The obtained fractions, in addition to the aqueous solution, that remained after the extraction were filtered and concentrated and dried under vacuum. The crude fractions were used for the assessment of cell viability and nitric oxide production assay using HaCaT cells.

3.9. Liquid Chromatography-Mass Spectrometry (LCMS) Analysis of Methanol Extracts

The chemical profile of methanol extracts from liverwort and Racomitrium moss was identified by LC-MS method using the instrument Waters auto-purification system with Waters 3100 single mass system (Waters, USA). The LC system was connected to 3100 single mass (100–1000 m/z) and 2998 Photodiode Array Detector (230–600 nm). Analyte separation was performed on a SunFire C18 (150 mm × 4.6 mm × 5 mm) with a gradient mobile phase consisting of 0.1% trifluoroacetic acid in water (solvent A) and acetonitrile (solvent B). The compositions of mobile phases consisted of the following multistep linear gradient: 0–10 min, 10% B and 90% A; 10–20 min, 20% B and 80% A; 20–30 min, 30% B and 70% A; 30–40 min, 50 % B and 50% A; 40–50 min, 70% B and 30% A. The flow rate was set at 1 mL/min. The sample injection volume was 10 μL. All chromatographic procedures were performed at ambient temperature and the corresponding peaks from the LC-MS analysis of all the samples were identified by comparison with the literature.

3.10. Statistical Analysis

All data analyses were done using GraphPad Prism Version 8.0 (GraphPad, La Jolla, CA, USA). The values expressed were means of three replicate determinations ± SD. All results were analyzed using the Student–Newman–Keuls test for multiple comparisons after analyzed with a one-way analysis of variance (ANOVA). Statistical significance was set at $p < 0.05$.

4. Conclusions

The data of the present study demonstrate that the methanol extract of liverwort effectively inhibited the mRNA expression (except TNF-α) and production of pro-inflammatory mediators in LPS-stimulated HaCaT cells when compared with Racomitrium moss extract. It could be concluded that the methanol extract of liverwort is a potential candidate for the development of an anti-inflammatory drug against inflammation-mediated skin diseases. Further isolation of biologically active metabolites from ethyl acetate and butanol fractions and elucidation of their anti-inflammatory mechanism(s) are required to facilitate the development of therapeutic agents for inflammation-mediated skin diseases.

Author Contributions: Conceptualization, S.K.; methodology, S.J.P., M.H., T.-H.K.; formal analysis, S.-Y.K. and M.H.; investigation, S.-Y.K., T.-H.K. and M.H.; resources, K.Y.L. and S.H.H.; data curation, M.H., S.-Y.K.; writing—original draft preparation, K.S.; writing—review and editing, S.K. and K.S.; supervision, S.K. All authors have read and agreed to the published version of the manuscript.

Funding: This research received no external funding.

Institutional Review Board Statement: Not applicable.

Informed Consent Statement: Not applicable.

Data Availability Statement: The data presented in this study are available within the article.

Acknowledgments: The authors would like to express thanks to Min Ha Kim and Jin Seok Kim at the National Institute of Biological Resources, Korea, for authenticating the bryophyte samples. This work was supported by the Korean Ministry of Environment (Grant no. 2018002270002).

Conflicts of Interest: The authors declare no conflict of interest.

References

1. Kim, H.; Han, T.H.; Lee, S.G. Anti-inflammatory activity of a water extract of *Acorus calamus* L. leaves on keratinocytes HaCaT cells. *J. Ethnopharmacol.* **2009**, *122*, 129–156. [CrossRef] [PubMed]
2. Cho, S.H.; Kim, H.S.; Lee, W.; Han, E.J.; Kim, S.Y.; Fernando, I.P.S.; Ahn, G.; Kim, K.N. Eckol from *Ecklonia cava* ameliorates TNF-α/IFN-γ-induced inflammatory responses via regulating MAPKs and NF-κB signaling pathway in HaCaT cells. *Int. Immunopharmacol.* **2020**, *82*, 106146. [CrossRef] [PubMed]
3. Piktel, E.; Wnorowska, U.; Cieśluk, M.; Deptula, P.; Pogoda, K.; Misztalewska-Turkowicz, I.; Paprocka, P.; Niemirowicz-Laskowska, K.; Wilczewska, A.Z.; Janmey, P.A. Inhibition of inflammatory response in human keratinocytes by magnetic nanoparticles functionalized with PBP10 peptide derived from the PIP2-binding site of human plasma gelsolin. *J. Nanobiotechnol.* **2019**, *17*, 22. [CrossRef] [PubMed]
4. Karin, M.; Lawrence, T.; Nizet, V. Innate immunity gone awry: Linking microbial infections to chronic inflammation and cancer. *Cell* **2006**, *124*, 823–835. [CrossRef]
5. Liang, Q.; Chalamaiah, M.; Liao, W.; Ren, X.; Ma, H.; Wu, J. Zein hydrolysate and its peptides exert anti-inflammatory activity on endothelial cells by preventing TNF-alpha-induced NF-kappa B activation. *J. Funct. Foods* **2020**, *64*, 103598. [CrossRef]
6. Zhao, B.; Li, R.; Yang, F.; Yu, F.; Xu, N.; Zhang, F.; Ge, X.; Du, J. LPS-induced vitamin D receptor decrease in oral Keratinocytes is associated with oral lichen planus. *Sci. Rep.* **2018**, *8*, 763. [CrossRef]
7. Lu, Y.; Eiriksson, F.F.; Thorsteinsdóttir, M.; Simonsen, H.T. Valuable fatty acids in bryophytes—Production, biosynthesis, analysis and applications. *Plants* **2019**, *8*, 524. [CrossRef]
8. Klavina, L.; Springe, G.; Nikolajeva, V.; Martsinkevich, I.; Nakurte, I.; Dzabijeva, D.; Steinberg, I. Chemical composition analysis, antimicrobial activity and cytotoxicity screening of moss extracts (Moss Phytochemistry). *Molecules* **2015**, *20*, 17221–17243. [CrossRef]
9. Tosun, A.; Nagashima, F.; Asakawa, Y. Terpenoid and steroid components of selected liverworts. *Chem. Nat. Compd.* **2015**, *51*, 387–391. [CrossRef]
10. Chandra, S.; Chandra, D.; Barh, A.; Pankaj; Pandey, R.K.; Sharma, I.K. Bryophytes: Hoard of remedies, an ethno-medicinal review. *J. Tradit. Complement. Med.* **2017**, *7*, 94–98. [CrossRef] [PubMed]
11. Stech, M.; Veldman, S.; Larraın, J.; Munoz, J.; Quandt, D.; Hassel, K.; Kruijer, H. Molecular species delimitation in the *Racomitrium canescens* Complex (Grimmiaceae) and implications for DNA barcoding of species complexes in mosses. *PLoS ONE* **2013**, *8*, e53134. [CrossRef]
12. Asakawa, Y.; Ludwiczuk, A. Chemical constituents of bryophytes: Structures and biological activity. *J. Nat. Prod.* **2018**, *81*, 641–660. [CrossRef]

13. Tosun, A.; Küpeli Akkol, E.; Süntar, I.; Özenoğlu Kiremit, H.; Asakawa, Y. Phytochemical investigations and bioactivity evaluation of liverworts as a function of anti-inflammatory and antinociceptive properties in animal models. *Pharm. Biol.* **2013**, *51*, 1008–1013. [CrossRef]
14. Ludwiczuk, A.; Asakawa, Y. Chemotaxonomic value of essential oil components in liverwort species. A review. *Flavour Fragr. J.* **2015**, *30*, 189–196. [CrossRef]
15. Romani, F.; Banić, E.; Florent, S.N.; Kanazawa, T.; Goodger, J.Q.D.; Mentink, R.A.; Dierschke, T.; Zachgo, S.; Ueda, T.; Bowman, J.L. Oil body formation in *Marchantia polymorpha* is controlled by MpC1HDZ and serves as a defense against arthropod herbivores. *Curr. Biol.* **2020**, *30*, 2815–2828. [CrossRef]
16. Asakawa, Y. Biologically active compounds from bryophytes. *Pure Appl. Chem.* **2007**, *79*, 557–580. [CrossRef]
17. Mewari, N.; Kumar, P. Antimicrobial activity of extracts of *Marchantia polymorpha*. *Pharm. Biol.* **2008**, *46*, 819–822. [CrossRef]
18. Guo, X.L.; Leng, P.; Yang, Y.; Yu, L.G.; Lou, H.X. Plagiochin E, a botanic-derived phenolic compound, reverses fungal resistance to fluconazole relating to the efflux pump. *J. Appl. Microbiol.* **2008**, *104*, 831–838. [CrossRef] [PubMed]
19. Gökbulut, A.; Satilmi, B.; Batçioğlu, K.; Çetin, B.; Şarer, E. Antioxidant activity and luteolin content of *Marchantia polymorpha* L. *Turk. J. Biol.* **2012**, *36*, 381–385.
20. Rana, M.; Pant, J.; Jantwal, A.; Rana, A.J.; Upadhyay, J.; Bisht, S.S. In vitro anti-inflammatory and antioxidant activity of ethanolic extract of *Marchantia polymorpha* in Kumaun region. *World J. Pharm. Res.* **2018**, *7*, 864–875.
21. Jensen, J.S.R.E.; Omarsdottir, S.; Thorsteinsdottir, J.B.; Ogmundsdottir, H.M.; Olafsdottir, E.S. Synergistic Cytotoxic Effect of the Micro tubule Inhibitor Marchantin A from *Marchantia polymorpha* and the Aurora Kinase Inhibitor MLN 8237 on Breast Cancer Cells In Vitro. *Planta Med.* **2012**, *78*, 448–454. [CrossRef] [PubMed]
22. Jung, M.R.; Lee, T.H.; Bang, M.H.; Kim, H.; Son, Y.; Chung, D.K.; Kim, J. Suppression of thymus- and activation-regulated chemokine (TARC/CCL17) production by 3-O-β-d-glucopyanosylspinasterol via blocking NF-κB and STAT1 signaling pathways in TNF-α and IFN-γ-induced HaCaT keratinocytes. *Biochem. Biophys. Res. Commun.* **2012**, *427*, 236–241. [CrossRef] [PubMed]
23. Park, J.H.; Kim, M.S.; Jeong, G.S.; Yoon, J. Xanthii fructus extract inhibits TNF-α/ IFN-γ-induced Th2-chemokines production via blockade of NF-κB, STAT1 and p38-MAPK activation in human epidermal keratinocytes. *J. Ethnopharmacol.* **2015**, *171*, 85–93. [CrossRef] [PubMed]
24. Gasparrini, M.; Forbes-Hernandez, T.Y.; Giampieri, F.; Afrin, S.; Mezzetti, B.; Quiles, J.L.; Bompadre, S.; Battino, M. Protective effect of strawberry extract against inflammatory stress induced in human dermal fibroblasts. *Molecules* **2017**, *22*, 164. [CrossRef]
25. Nguyen, P.H.; Zhao, B.T.; Lee, J.H.; Kim, Y.H.; Min, B.S.; Woo, M.H. Isolation of benzoic and cinnamic acid derivatives from the grains of *Sorghum bicolor* and their inhibition of lipopolysaccharide-induced nitric oxide production in RAW 264.7 cells. *Food Chem.* **2015**, *168*, 512–519. [CrossRef]
26. Harinantenaina, L.; Quang, D.N.; Nishizawa, T.; Hashimoto, T.; Kohichi, C.; Soma, G.I.; Asakawa, Y. Bioactive compounds from liverworts: Inhibition of lipopolysaccharide-induced inducible NOS mRNA in RAW 264.7 cells by herbertenoids and cuparenoids. *Phytomedicine* **2007**, *14*, 486–491. [CrossRef]
27. Quang, D.N.; Asakawa, Y. Chemical constituents of the Vietnamese liverwort *Porella densifolia*. *Fitoterapia* **2010**, *81*, 659–661. [CrossRef]
28. Li, S.; Niu, H.; Qiao, Y.; Zhu, R.; Sun, Y.; Ren, Z.; Yuan, H.; Gao, Y.; Li, Y.; Chen, W.; et al. Terpenoids isolated form Chinese liverworts *Lepidozia reptans* and their anti-inflammatory activity. *Bioorg. Med. Chem.* **2018**, *26*, 2392–2400. [CrossRef]
29. Li, Y.; Zhu, R.; Zhang, J.; Wu, X.; Shen, T.; Zhou, J.; Qiao, Y.; Gao, Y.; Lou, H. Clerodane diterpenoids from the Chinese liverwort *Jamesoniella autumnalis* and their anti-inflammatory activity. *Phytochemistry* **2018**, *154*, 85–93. [CrossRef]
30. Choi, W.S.; Jeong, J.W.; Kim, S.O.; Kim, G.Y.; Kim, B.W.; Kim, C.M.; Seo, Y.B.; Kim, W.Y.; Lee, S.Y.; Jo, K.H. Anti-inflammatory potential of peat moss extracts in lipopolysaccharide-stimulated RAW 264.7 macrophages. *Int. J. Mol. Med.* **2014**, *34*, 1101–1109. [CrossRef]
31. Gasparrini, M.; Forbes-Hernandez, T.Y.; Giampieri, F.; Afrin, S.; Alvarez-Suarez, J.M.; Mazzoni, L.; Mezzetti, B.; Quiles, J.L.; Battino, M. Anti-inflammatory effect of strawberry extract against LPS-induced stress in RAW 264.7 macrophages. *Food Chem. Toxicol.* **2017**, *102*, 1–10. [CrossRef]
32. Mo, C.; Wang, L.; Zhang, J.; Numazawa, S.; Tang, H.; Tang, X.; Han, X.; Li, J.; Yang, M.; Wang, Z.; et al. The crosstalk between Nrf2 and AMPK signal pathways is important for the anti-inflammatory effect of berberine in LPS-stimulated macrophages and endotoxin-shocked mice. *Antioxid. Redox Signal.* **2014**, *20*, 574–588. [CrossRef]
33. Kim, D.H.; An, B.J.; Kim, S.G.; Park, T.S.; Park, G.H.; Son, J.H. Anti-inflammatory effect of *Ligularia fischeri*, *Solidago virga-aurea* and *Aruncus dioicus* complex extracts in Raw 264.7 cells. *J. Life Sci.* **2011**, *21*, 678–683. [CrossRef]
34. Liu, Y.W.; Mei, H.C.; Su, Y.W.; Fan, H.T.; Chen, C.C.; Tsai, Y.C. Inhibitory effects of *Pleurotus tuber-regium* mycelia and bioactive constituents on LPS-treated RAW 264.7 cells. *J. Funct. Foods* **2014**, *7*, 662–670. [CrossRef]
35. He, Y.; Kim, B.; Kim, H.E.; Sun, Q.; Shi, S.; Ma, G.; Kim, Y.; Kim, O.; Kim, O. The protective role of feruloylserotonin in LPS-induced HaCaT Cells. *Molecules* **2019**, *24*, 3064. [CrossRef] [PubMed]
36. Kang, G.J.; Kang, N.J.; Han, S.C.; Koo, D.H.; Kang, H.K.; Yoo, B.S.; Yoo, E.S. The chloroform fraction of *Carpinus tschonoskii* leaves inhibits the production of inflammatory mediators in HaCaT keratinocytes and RAW264.7 macrophages. *Toxicol. Res.* **2012**, *28*, 255–262. [CrossRef]
37. Li, S.; Xie, R.; Jiang, C.; Liu, M. Schizandrin A alleviates LPS-Induced injury in human keratinocyte cell HaCaT through a microRNA-127-dependent regulation. *Cell Physiol. Biochem.* **2018**, *49*, 2229–2239. [CrossRef]

38. Sikandan, A.; Shinomiya, T.; Nagahara, Y. Ashwagandha root extract exerts anti-inflammatory effects in HaCaT cells by inhibiting the MAPK/NF-κB pathways and by regulating cytokines. *Int. J. Mol. Med.* **2018**, *42*, 425–434. [CrossRef] [PubMed]
39. Ludwiczuk, A.; Asakawa, Y. Bryophytes as a source of bioactive volatile terpenoids—A review. *Food Chem. Toxicol.* **2019**, *132*, 110649. [CrossRef] [PubMed]
40. Jiao, Q.-S.; Xu, L.-L.; Zhang, J.-Y.; Wang, Z.-J.; Jiang, Y.-Y.; Liu, B. Rapid Characterization and identification of non-diterpenoid constituents in *Tinospora sinensis* by HPLC-LTQ-Orbitrap MS^n. *Molecules* **2018**, *23*, 274. [CrossRef] [PubMed]
41. Qi, Y.; Choi, S.I.; Son, S.R.; Han, H.S.; Ahn, H.S.; Shin, Y.K.; Lee, S.H.; Lee, K.T.; Kwon, H.C.; Jang, D.S. Chemical constituents of the leaves of *Campanula takesimana* (Korean Bellflower) and their inhibitory effects on LPS-induced PGE_2 production. *Plants* **2020**, *9*, 1232. [CrossRef] [PubMed]
42. Sabovljević, M.S.; Vujičić, M.; Wang, X.; Garraffo, H.M.; Bewley, C.A.; Sabovljević, A. Production of the macrocyclic bis-bibenzyls in axenically farmed and wild liverwort *Marchantia polymorpha* L. subsp. ruderalis Bischl. et Boisselier. *Plant Biosyst.* **2017**, *151*, 414–418. [CrossRef]
43. Gao, J.; Li, X.; Lv, B.B.; Sun, B.; Zhu, C.J.; Lou, H.X. LC-DAD/MS/MS detection of macrocyclic bisbibenzyls from the liverwort *Reboulia hemisphaerica* and the cell-based screening of their microtubule inhibitory effects. *Chin. J. Nat. Med.* **2009**, *7*, 123–128. [CrossRef]
44. Xing, J.; Xie, C.; Qu, J.; Guo, H.; Lv, B.; Lou, H. Rapid screening for bisbibenzyls in bryophyte crude extracts using liquid chromatography/tandem mass spectrometry. *Rapid Commun. Mass Spectrom.* **2007**, *21*, 2467–2476. [CrossRef]
45. Li, R.; Zhou, Y.; Wu, Z.; Ding, L. ESI-QqTOF-MS/MS and APCI-IT-MS/MS analysis of steroid saponins from the rhizomes of *Dioscorea panthaica*. *J. Mass Spectrom.* **2006**, *41*, 1–22. [CrossRef]
46. Harinantenaina, L.; Quang, D.N.; Takeshi, N.; Hashimoto, T.; Kohchi, C.; Soma, G.; Asakawa, Y. Bis(bibenzyls) from liverworts inhibit lipopolysaccharide-induced inducible NOS in RAW 264.7 cells: A study of structure-activity relationships and molecular mechanism. *J. Nat. Prod.* **2005**, *68*, 1779–1781. [CrossRef]
47. Yang, Y.I.; Woo, J.H.; Seo, Y.J.; Lee, K.T.; Lim, Y.; Choi, J.H. Protective effect of brown alga Phlorotannins against hyper-inflammatory responses in lipopolysaccharide-induced sepsis models. *J. Agric. Food Chem.* **2016**, *64*, 570–578. [CrossRef]
48. Yang, Y.I.; Shin, H.C.; Kim, S.H.; Park, W.Y.; Lee, K.T.; Choi, J.H. 6,6′-Bieckol, isolated from marine alga *Ecklonia cava*, suppressed LPS-induced nitric oxide and PGE_2 production and inflammatory cytokine expression in macrophages: The inhibition of NF-κB. *Int. Immunopharmacol.* **2012**, *12*, 510–517. [CrossRef] [PubMed]
49. Sapkota, A.; Gair, B.P.; Kang, M.G.; Choi, J.W. S1P2 contributes to microglial activation and M1 polarization following cerebral ischemia through ERK1/2 and JNK. *Sci. Rep.* **2019**, *9*, 12106. [CrossRef] [PubMed]

Hindawi
Evidence-Based Complementary and Alternative Medicine
Volume 2022, Article ID 3781189, 10 pages
https://doi.org/10.1155/2022/3781189

Research Article

Photoprotective Potential, Cytotoxicity, and UPLC-QTOF/MS Analysis on Bioactive Solvent Fractions of *Moringa concanensis* Nimmo Bark

Rameshkumar Santhanam,[1,2] **Thiruventhan Karunakaran**,[3,4] **Kandhasamy Sowndhararajan**,[5] **Muhammad Faiz Zulkifli**,[1] **Mouriya Govindan Kothandaraman**,[1] **Veerasamy Aravindhan**,[5] **and Wan Iryani Wan Ismail**[1,2]

[1]*Faculty of Science and Marine Environment, Universiti Malaysia Terengganu, Kuala Nerus 21030, Terengganu, Malaysia*
[2]*Biological Security and Sustainability Research Group (BIOSES), Faculty of Science and Marine Environment, Universiti Malaysia Terengganu, Kuala Nerus 21030, Terengganu, Malaysia*
[3]*Centre for Drug Research, Universiti Sains Malaysia, Gelugor, Pulau Pinang 11800, Malaysia*
[4]*School of Chemical Sciences, Universiti Sains Malaysia, Gelugor, Pulau Pinang 11800, Malaysia*
[5]*Department of Botany, Kongunadu Arts and Science College (Autonomous), Coimbatore 641029, Tamil Nadu, India*

Correspondence should be addressed to Rameshkumar Santhanam; ramesh@umt.edu.my and Thiruventhan Karunakaran; thiruventhan@usm.my

Received 31 January 2022; Revised 3 April 2022; Accepted 5 April 2022; Published 23 April 2022

Academic Editor: Jelena Zivkovic

Copyright © 2022 Rameshkumar Santhanam et al. This is an open access article distributed under the Creative Commons Attribution License, which permits unrestricted use, distribution, and reproduction in any medium, provided the original work is properly cited.

Moringa concanensis Nimmo (Moringaceae) belongs to the same family of *M. oleifera* (miracle tree) and is a medicinal plant traditionally used by Indians to treat various ailments related to diabetes, tumours, inflammation, and blood pressure. Despite its versatility, the photoprotective properties of the plant remain unclear. This study revealed the UV-protective properties of its methanol bark extract and respective subfractions, chloroform, hexane, and ethyl acetate through total phenolic and flavonoid content (TPC & TFC), antioxidant (DPPH), sun protecting factor (SPF) value, and UV absorption spectra analysis. This study also investigated on the inhibitory effect of the tested samples on collagenases and elastase, which are well-known for their role in the skin. The cytotoxic and H_2O_2 scavenging properties of *M. concanensis* in 3T3-L1 cells were explored. Finally, the phytochemical profiling of the active fraction was conducted through UPLC-QTOF/MS analysis. Among the tested fractions, the chloroform fraction of *M. concanensis* showed the highest TPC (30.92 ± 0.71 mg GAE/DW), TFC (29.05 ± 0.09 mg QE/DW), and antioxidant properties (IC_{50}-6.616 ± 1.90 μgml^{-1}). Additionally, chloroform fraction demonstrated the highest SPF value, 10.46 at 200 μgml^{-1}, compared to the other tested fractions. All the fractions showed a broad absorption spectrum covering both UVA and UVB ranges. The chloroform fraction of *M. concanensis* also showed collagenase (50%) and elastase (IC_{50}-2.95 ± 1.23 μgml^{-1}) inhibition properties similar to the positive control. Cytotoxic results revealed that the chloroform fraction of *M. concanensis* prevented the H_2O_2-induced oxidative damage in 3T3-L1 cells even at lower concentrations (1.56 μgml^{-1}). UPLC-QTOF/MS analysis tentatively identified the presence of bioactive flavonoids and phenolics such as astragalin, quercetin, isoquercetin, and caffeic acid in the active fraction of *M. concanensis* bark. Overall, it is suggested that the chloroform fraction of *M. concanensis* bark has the potency to be used as an active ingredient in sunscreen products.

1. Introduction

In recent times, the intensity of ultraviolet (UV) radiation reaching the earth's surface has increased due to ozone depletion by releasing human-made chemicals into the atmosphere. [1]. Three types of UV (200–400 nm) radiations are available: UVA (320–400 nm), UVB (290–320 nm), and UVC (200–290 nm). UV radiation-stimulated skin damage is highly influenced by its wavelength, intensity, and exposure time [2]. UV radiation directly interacts with the

skin, which leads to the activation of several signaling cascades in the skin layers. Excessive doses of UVA and UVB rays are widely considered the leading causative agent for sunburns, early aging, DNA damage, wrinkle formation, oxidative stress, and skin cancer. [3]. In particular, UVA radiation produces immediate skin pigmentation and skin alterations related to premature aging *via* penetrating the deeper layers of the skin, whereas UVB is responsible for skin damage, including erythema and sunburn, by inducing late pigmentation. UVB is also associated with changes in cellular DNA and can provoke skin cancer [4]. Both rays are capable of promoting lipid peroxidation, which is strongly associated with the generation of reactive oxygen species (ROS) [5]. The excessive production of ROS leads to direct DNA damage; stimulation of proinflammatory cytokines such as IL-1 (interleukin-1), IL-6 (interleukin-6), and TNF-α (tumor necrosis factor); activation of signaling pathways; and the release of matrix metalloproteinases. Overexpression of these biomarkers could damage the matrix proteins such as elastin and collagen, which finally results in phototoxic reactions such as photoallergy, photosensitivity, photoaging, and photocarcinogenesis [6, 7].

Nowadays, sunscreen-based photoprotection is one of the essential strategies utilized to prevent UV-induced damage and other skin-related disorders. Sunscreens can protect the skin from sunburn, sun allergy rash, immune suppression, and other harmful effects induced by UV radiation. These sunscreens are made up of different organic and inorganic filters to protect the skin [3, 4]. Synthetic-based sunscreens are now becoming a serious threat to consumers and a threat to marine lives and the environment. A wide range of novel hypoallergenic cosmetics has been developed using natural products due to the adverse effect of synthetic sunscreen ingredients. Specifically, plant-based products are in high demand due to their myriad benefits such as antioxidant, anti-inflammatory, and immune enhancers [3–9]. Compared to synthetic filters, compounds, fractions, and extracts from plant sources offer a broad range of UV absorption. Several natural products are incorporated into sunscreen products. Previous research reported the usage of numerous traditional plants such as *Moringa. oleifera Lam, Zanthoxylum rhetsa (Roxb.) DC., Parentucellia latifolia Caruel,* and *Nephelium lappaceum L., Camellia sinensis L. Kuntze*, and other plant extracts or fractions that are rich in polyphenols were described to possess appreciable sunscreen properties *via* targeting free radicals, inflammatory pathways (NF-κB, MAPK) and cytokines, and matrix metalloproteinases (MMP1, MMP3, MMP9, etc.) [2, 3, 6, 8, 10, 11]. Though there are studies that revealed the photoprotective potency of some traditional medicinal plants, it remains limited.

Moringa concanensis Nimmo is an important traditional medicinal plant in the family of Moringaceae mainly spotted in the Western Ghats of India and also widely distributed in Asian and Arab countries [12]. This species looks almost similar to the well-known medicinal, nutritional value species *M. oleifera*. However, it has some distinct features such as bipinnate leaves, a strong central trunk with an extremely distinctive layer of very furrowed bark, and the petals and sepals of the flower have green patches at the tip. Moreover, the leaves and flowers of *M. concanensis* are larger compared to *M. oleifera* [13]. In Indian traditional systems of medicine, *M. concanensis* is mainly used to treat fertility problems. The leaves and bark of this species were used to treat skin tumours, tiredness, high blood pressure, jaundice, eye problems, diabetes, and swellings [14] with a wide range of therapeutic properties. Studies revealed that the ethanol extract of *M. concanensis* extract exhibited hyperglycaemic activity and showed protective activity against oxidative tissue damage in the pancreas, liver, and kidney [15]. In this study, the photoprotective properties of various solvent fractions of the *M. concanensis* bark were revealed for the first time using biochemical assays such as total phenolic (TPC) and flavonoid content (TFC), DPPH free radical scavenging activity, SPF value determination, and UVA/UVB absorption spectra analysis. Moreover, the inhibitory effect of the plant extract towards collagenase and elastase was also shown using gelatin digestion and antielastase assay. The cytotoxic and H_2O_2 damage preventive potential of the extracts and fractions were assessed through the cell culture technique using MTT assay. The potential metabolites present in the active fraction responsible for the biological properties of *M. concanensis* bark were identified through UPLC-QTOF/MS analysis.

2. Materials and Methods

2.1. Chemical and Reagents. Solvents such as hexane (CAS No. 110-54-3), chloroform (CAS No. 67-66-3), methanol (CAS No. 67-56-1), and ethyl acetate (CAS No. 141-78-6) used for extraction are of analytical grade obtained from Merck Millipore (Darmstadt, Germany). Collagenase from *Clostridium histolyticum* (CAS No. 9001-12-1), N-succinyl-ala-ala-ala-*p*-nitroanilide (AAAPVN, CAS No. 52299-14-6), 2,2-diphenyl-1-picrylhydrazyl (DPPH, CAS, No. 1898-66-4), gelatin (CAS No. 9000-70-8), porcine elastase (CAS No. 39445-21-1), Coomassie blue R-250 (CAS No. 6104-59-2), ascorbic acid (AA) (CAS No. 50-81-7), epigallocatechin gallate (EGCG, CAS No. 989-51-5), Tris-HCl (CAS No. 1185-53-1), agarose (CAS No. 9012-36-6), acetic acid (CAS No. 64-19-7), dimethyl sulfoxide (DMSO, CAS No. 67-68-5), and 3-(4,5-dimethylthiazol-2-yl)-2,5-diphenyltetrazolium bromide (MTT, CAS No. 57360-69-7) were purchased from Sigma-Aldrich Chemicals (St. Louis, MO, USA). Dulbecco's modified Eagle's medium (DMEM, CAT No. 11-995-073), TrypLE Express (CAT No. 12604–013), fetal bovine serum (FBS, CAT No. 26-140-079), and penicillin/streptomycin (CAT No. 15140–122) were purchased from Gibco (Life Technologies, California, USA).

2.2. Samples Collection and Extraction. The stem bark of *M. concanensis* was collected from Madukkarai, Coimbatore, Tamil Nadu, India. The plant specimen was authenticated, and plant identification certificate was given by Dr. G.V.S. Moorthy, Head of Office, Southern Regional Centre (Letter No. BSI/SRC/5/23/2018/Tech-437), Botanical Survey of India, Coimbatore, Tamil Nadu, India. The Voucher specimen

(BUH-VA-3203/2018) was submitted to the Herbarium of Department of Botany, Bharathiar University, Coimbatore, Tamil Nadu, India. The crude methanolic extract (28 g) from dried and powdered bark (600 g) of *M. concanensis* was obtained using ultrasound-assisted extraction technique according to the literature [6].

2.3. Liquid-Liquid Partitioning. Various solvent fractions of the crude methanol extract of *M. concanensis* were subjected to liquid-liquid partitioning technique using different solvents based on their polarity. Initially, 15 g of the methanol crude extract was mixed with equal volume of hexane and water (1 : 1) and loaded into the separating funnel. After few agitations, the hexane fraction was removed and the chloroform was added to the separating funnel. Then, the same process was repeated with ethyl acetate. Finally using rotavapor, the resultant fractions such as hexane (3.1 g), chloroform (6.2 g), and ethyl acetate (1.8 g) were obtained and dried under vacuum and lyophilized [11].

2.4. Total Phenolic Content. The total phenolic content for all the solvent fractions of *M. concanensis* bark was determined using the Folin–Ciocalteu method [16]. Briefly, 50 μL of the sample (1 mgml^{-1}) in methanol was mixed with 50 μL distilled water, 50 μL of 10% Folin–Ciocalteu's phenol reagent, and 50 μL of 1 M sodium carbonate solution in a 96-well microwell plate and incubated for 60 min at room temperature without exposing it to light. Methanol was used as a blank. The absorbance of the reaction mixture was measured using a microplate reader at 750 nm. The total phenolic content was determined through calibration curve using gallic acid (7.81, 15.62, 31.25, 62.5, 125, 250, and 500 μgmL^{-1}) as standard. Results are expressed as milligram gallic acid equivalents (GAE) per gram of dry plant extract. All tests were done in triplicates.

2.5. Total Flavonoid Content. The total flavonoid content for all the fractions of *M. concanensis bark* was determined using spectrophotometric method [16]. 100 μL of the plant extract (1 mgmL^{-1}) and standard solutions of quercetin (7.81, 15.62, 31.25, 62.5, 125, 250, and 500 μgmL^{-1}) in methanol solution were mixed with 100 μl of 2% $AlCl_3$ solution. Reaction mixtures were incubated for an hour at room temperature. The absorbance was measured using Tecan Infinite F200 Pro plate reader at λmax 415 nm. Total flavonoid contents were expressed as mg quercetin equivalent (QE) per gram of dry plant extract. Experiments were done in triplicates.

2.6. DPPH Scavenging Activity Assay. The crude extract and the fractions of *M. concanensis* bark were tested for their free radical scavenging properties using DPPH free radical scavenging assay [16, 17]. Briefly, 0.12 mM DPPH in methanol was prepared and mixed with various concentrations of test samples at 1 : 1 ratio (100 μL). Ascorbic acid was used as the positive control. Test samples and DPPH solution were incubated at room temperature for 30 min in the dark. After the incubation, the absorbance value of the mixture was recorded on a microwell plate reader at 570 nm. The experiment was done in triplicates. The DPPH radical scavenging activity was calculated using the formula:

$$\text{DPPH radical scavenging activity (\%)} = \frac{\left[\left(\text{Abs}_{\text{control}} - \text{Abs}_{\text{sample}}\right)\right]}{\left[\left(\text{Abs}_{\text{control}}\right)\right]} \times 100, \quad (1)$$

where $\text{Abs}_{\text{control}}$ is the absorbance of DPPH radical-+methanol and $\text{Abs}_{\text{sample}}$ is the absorbance of DPPH radical + samples/positive control.

2.7. SPF Value Determination. The *in vitro* SPF value of the crude extract and solvent fractions of *M. concanensis* were obtained by the method described in the literature [16]. Briefly, the absorbance value of the test sample (200 μgmL^{-1}) was determined on a UV-Visible spectrophotometer at 5 nm intervals within the range of 290–320 nm. The SPF value was then calculated by using the formula:

$$\text{SPF spectrophotometric} = \underset{290}{\overset{320}{\text{CF}}} x \sum \text{EE}(\lambda) x I(\lambda) x \text{Abs}(\lambda), \quad (2)$$

where CF is the correction factor (= 10), EE (λ) is the erythemal effect spectrum, I (λ) is the solar intensity spectrum, Abs (λ) is the absorbance of test sample, where EE (λ) x I(λ) are constants. Methanol was used as a blank, and measurements were made in triplicate.

2.8. UVA/UVB Absorption Spectra. The UV absorption spectrum of the crude extract and solvent fractions of *M. concanensis* (100 μgmL^{-1} in methanol) were measured over a wavelength range of 200–400 nm on a UV-Visible spectrophotometer using a quartz cell (1 cm). The UV absorption spectrum of the samples tested was compared with the positive control, epigallocatechin gallate (EGCG) prepared with the same concentration.

2.9. Gelatin Digestion Assay. The gelatin digestion assay was done according to the method described by Santhanam et al. [6] with slight modifications. Agarose (2%) was prepared in a collagenase buffer (50 mM Tris-HCl, 10 mM $CaCl_2$, 0.15 M NaCl, pH 7.8) and porcine gelatin (0.15%). The mixture was transferred into a petri dish and left at room temperature for 1 h for solidification. Later, the wells were made using a sterile 200 μL microtip. Then, 25 μL of the samples was incubated with 25 μL of bacterial collagenase-1 (0.1 mgmL^{-1}) for 1 h. Finally, the reaction mixture (50 μL) was loaded into the well and further incubated overnight. EGCG was used as a positive control. The next day, the petri dish was visualized by the Coomassie brilliant blue staining method. The degree of gelatin digestion was determined by measuring the area of the light translucent zone formed after destaining over a blue background.

2.10. Antielastase Assay. The antielastase activity of the various solvent fractions of *M. concanensis* was determined according to the methods of Santhanam et al. [6], with minor modifications. The assay was performed in Tris-HCl buffer (0.2 mM, pH 8.0). The stock solution of porcine pancreatic elastase (PE–E.C. 3.4.21.36) was dissolved in sterile water. N-succinyl-ala-ala-ala-p-nitroanilide (AAAPVN) was dissolved in 1 mL Tris-HCl (0.2 mM) buffer (pH 8.0), and the samples were dissolved in buffer. Then, the test samples and elastase were incubated for 15 minutes before adding the substrate to start the reaction. The final reaction mixture contains a buffer, 0.8 mM AAAPVN, 50 μgmL^{-1} PE, and the test samples at various test concentrations in a total volume of 250 μL. EGCG served as the positive control while water served as the negative control. The absorbance value was measured using a Tecan Infinite F200 Pro plate reader (Tecan Group Ltd., Männedorf, Switzerland) at 410 nm.

$$\text{Enzyme inhibition activity (\%)} = \frac{\left[\left(\text{Abs}_{\text{control}} - \text{Abs}_{\text{sample}}\right)\right]}{\left[\text{Abs}_{\text{control}}\right]} \times 100. \quad (3)$$

2.11. Cell Culture. 3T3-L1 cells were maintained in complete Dulbecco's modified Eagle's medium (DMEM) high-glucose media according to the method of Raseetha et al. [18] with slight modification. The media were supplemented with 10% fetal bovine serum (FBS) and 5% of penicillin-streptomycin in a humidified 5% CO_2 incubator at 37°C. Once the cell reaches 70–80% confluence, it was utilized for seeding and treatment.

2.11.1. Cytotoxicity. Cells cytotoxicity was performed using MTT assay based on the method described by Raseetha et al. [18]. The cells were seeded at a density of 1×10^5 cells/well in 96-well plates. Once the cell reaches 80% confluence, the 100 μL of various concentrations of methanol extract and solvent fractions of *M. concanensis* and positive control EGCG were treated in each well. After 24 h, 20 μL of MTT was added to the cells and it was incubated at 37°C for 4 h. The medium was replaced with 100 μL DMSO, and the absorbance for each well was measured at 570 nm on Tecan Infinite F200 Pro plate reader. Cytotoxicity assay was conducted to determine the range of concentrations of the active fraction. Experiments were performed in triplicates.

2.11.2. Protective Effect of Samples against H_2O_2-Induced Oxidative Damage in 3T3-L1 Cells. The protective effect of *M. concanensis* fractions against H_2O_2 was performed according to Chen et al. [19] with slight modification. The 3T3-L1 cells were seeded on 96-well plates at a density of 1×10^5 (in 100 μL medium) per well and incubated at 37°C for 24 h. Once the cell reaches the confluence, the medium was replaced with 100 μl of samples with various concentrations (0–100 μg mL-1) and positive control (ascorbic acid) for 18 h. Then, the cells were treated with H_2O_2 (125 μM) to induce oxidative damage, and the dose concentration was fixed based on the current study. After 6 h, the medium was removed, and the cells were washed thrice with PBS. Next, the MTT solution was added and the cells were further incubated for 4 h. Finally, the formazan crystals were dissolved in DMSO (100 μL per well), and the absorbance value was measured at 540 nm using Tecan Infinite F200 Pro plate reader [20].

2.12. Ultraperformance Liquid Chromatography Quadrupole Time-of-Flight Mass Spectrometry (UPLC-QTOF/MS) Analysis. Phytochemical profiling in chloroform fractions of *M. concanensis* was conducted via ultraperformance liquid chromatography (UPLC-MS) analysis. The analysis was carried out using Waters ACQUITY ultraperformance LC system (Waters, Milford, MA, USA). Chromatographic separation of the respective extract was conducted using a selected column (ACQUITY UPLC HSS T3, 100 mm × 2.1 mm × 1.8 m, Waters, Manchester, UK) maintained at 40°C. The UPLC systems were connected to Vion IMS QTOF detector (Waters, Milford, MA, USA). The mobile phases used in the analysis were 0.1% formic acid (*A*) and acetonitrile (B). The composition of mobile phases was consisted of the following multistep linear gradient: 0 min, 1% B and 99% A; 0.5 min, 1% B and 99% A; 16.00 min, 35% B and 65% A; 18.00 min, 100% B and 0% A; and 20.00 min, 1% B and 99% A, respectively. The injection volume used for the sample was 1 μL while the flow rate was set at 0.6 mL/min. The data were obtained from the UHPLC system coupled with Vion IMS QTOF hybrid mass spectrometer from waters, equipped with a LockSpray ion source. The ion source was operated in negative electrospray ionization (ESI) mode by applying specific conditions such as the capillary voltage at 1.50 kV, reference capillary voltage at 3.00 kV, source temperature at 120°C, desolvation gas temperature at 550°C, desolvation gas flow at 800 L/h, and cone gas flow at 50 L/h, respectively. Nitrogen (>99.5%) was used as desolvation and cone gas. Data were acquired in high-definition MSE (HDMSE) mode ranging between *m/z* 50 and 1500 at 0.1 s/scan. Hence, two independent scans with different collision energies (CE) were alternatively obtained during the run: a low-energy (LE) scan at a fixed CE of 4 eV and a high-energy (HE) scan where the CE was ramped from 10 to 40 eV. Argon (99.999%) was used as collision-induced-dissociation (CID) gas. Data interpretation was carried out using Waters UNIFI Scientific Information System database. Resolved peaks were further identified with the assistance of reported values from previous literature and are shown in Table 1.

2.13. Statistical Analysis. All the data were represented as mean ± SD. Statistical analyses were performed using GraphPad Prism version 5 with one-way ANOVA followed by Dunnett's test. p values < 0.05 were considered to be statistically significant.

3. Results and Discussion

3.1. Total Phenolic and Flavonoid Contents. It is well established that phenolic compounds from various plants are strongly associated with their biological properties.

Table 1: Compounds tentatively identified in the chloroform fraction from the methanol extract of *M. concanensis* bark using UPLC-QTOF/MS analysis.

Peak no.	Tentative identification	Elemental composition	Calculated m/z $[M-H]^-$	Observed m/z $[M-H]^-$	Retention time	References
1	Kaempferol-3-*O*-rutinoside	$C_{27}H_{30}O_{15}$	593.1507	593.1512	6.65	[21]
2	Astragalin	$C_{21}H_{20}O_{11}$	447.0927	447.0937	7.50	[21]
3	Quercetin-3-*O*-glucuronide	$C_{21}H_{18}O_{13}$	477.0670	477.0685	7.83	—
4	Tetra-*O*-galloyl-glucoside	$C_{34}H_{28}O_{22}$	787.0994	787.1005	8.11	—
5	Kaempferol-3-*O*-glucuronosyl methyl ester	$C_{22}H_{20}O_{12}$	475.0876	475.0867	8.61	[21]
6	Isoquercetin	$C_{21}H_{20}O_{12}$	463.0877	463.0884	8.63	[21]
7	Caffeic acid	$C_9H_8O_4$	179.0344	179.0352	9.01	[21]
8	Hydroxy-methoxy-cinnamic acid	$C_{10}H_{10}O_4$	193.0501	193.0511	9.38	—
9	Sinapic acid	$C_{11}H_{12}O_5$	223.0607	223.0613	10.04	—
10	Kaempferol 3-*O*-arabinoside	$C_{20}H_{18}O_{10}$	417.0822	417.0844	10.40	—
11	Secoisolariciresinol	$C_{20}H_{26}O_6$	361.1651	361.1656	10.43	—
12	Kaempferol-3-*O*-rhamnoside	$C_{21}H_{20}O_{10}$	431.0978	431.0995	10.91	[21]
13	Quercetin-3-*O*-glucuronide-methyl-ester	$C_{22}H_{20}O_{13}$	491.0826	491.0842	10.99	—
14	Quercetin	$C_{15}H_{10}O_7$	301.0348	301.0351	11.93	[21]
15	Eugenol	$C_{10}H_{12}O_2$	163.0759	163.0765	12.47	[21]
16	Naringenin	$C_{15}H_{12}O_5$	271.0607	271.0615	13.07	—
17	Trimethoxyflavone	$C_{18}H_{16}O_5$	311.0920	311.0929	13.32	—
18	Demethoxycurcumin	$C_{20}H_{18}O_5$	337.1076	337.1085	15.53	—
19	Sanleng acid	$C_{18}H_{34}O_5$	329.2328	329.2339	15.62	[21]
20	Licoricone	$C_{22}H_{22}O_6$	381.1338	381.1335	15.65	—

Hence, it would be worthwhile to determine the total phenolic and flavonoid contents in the plant extracts [10]. The total phenolic and flavonoid contents of methanol extract and its fractions of *M. concanensis* bark are presented in Table 2. The total phenolic (30.920 ± 0.71 mg GAE/g DW) and flavonoid (29.054 ± 0.09 mg QE/g DW) contents were found to be higher in the chloroform fraction followed by hexane fraction. Phenolic components are regarded as powerful antioxidants and act in redox-sensitive signaling cascades to prevent DNA damage [11].

Data expressed as mean ± SD, $n = 3$. Data with different alphabet superscript letters show significant difference at $p < 0.05$, among different solvents, with multiple comparisons (one-way ANOVA, followed by Dunnett's test).

Table 2: Total phenolic and flavonoid contents of the methanol extract and its fractions from the bark of *M. concanensis*.

Fractions	Total phenolics mg GAE/g DW	Total flavonoids mg QE/g DW
Methanol	9.858 ± 0.036^d	3.655 ± 0.061^d
Hexane	14.306 ± 0.073^b	9.089 ± 0.193^b
Chloroform	30.920 ± 0.717^a	29.054 ± 0.099^a
Ethyl acetate	12.154 ± 0.158^c	4.055 ± 0.056^c

3.2. Antioxidant Activity of *M. concanensis* Bark Fractions

3.2.1. Free Radical Scavenging Assay. The free radical scavenging capacity of the crude methanol extract and other fractions of *M. concanensis* bark were determined using the DPPH assay, and the results are shown in Figure 1. All the samples exhibited varying degrees of concentration-dependent DPPH radical scavenging activity. In that, the chloroform fraction showed the strongest DPPH radical scavenging activity with the IC_{50} value of $6.616 \pm 1.90\ \mu g mL^{-1}$ followed by ethyl acetate fraction ($IC_{50} = 13.4 \pm 2.22\ \mu g mL^{-1}$) which is comparable to the positive control, ascorbic acid (AA). Gori et al. [22] revealed the photoprotective effect of 11 medicinal plants *Atalantia ceylanica (Arn.) Oliv, Argyreia populifolia Choisy*, *Hibiscus furcatus Roxb. ex DC*, *Ipomoea mauritiana Jacq*, *LAsia spinosa (L.) Thw*, *Leucas zeylanica (L.) W.T.Aiton*, *Olax zeylanica Wall., Ophiorrhiza mungos Linn.*, *Plectranthus amboinicus (Lour.)*, and *Mollugo cerviana (L.).Ser.* where the plant that showed high SPF values is closely related to its antioxidant properties. Numerous studies also suggested that the plant fraction which shows high free scavenging properties offers significant protection towards UV-induced damage [16, 22].

3.3. Protective Effect of the *M. concanensis* Fractions against UV

3.3.1. Sunscreen Protection Factor (SPF) Value. SPF value refers to the efficacy of test samples that protects the development of UV radiation-induced erythema [23]. It is a measure of UVB protection offered by sunscreen products. As the value increases, the percentage of UVB protection increases. As shown in Table 3, at the concentration of $200\ \mu g mL^{-1}$, the chloroform fraction of *M. concanensis* bark exhibited the highest SPF value (10.50 ± 0.23 with >87% of UVB protection) compared to the other fractions such as ethyl acetate and hexane. The SPF value of the most active ingredient epigallocatechin gallate (EGCG) from *Camellia sinensis* (Green

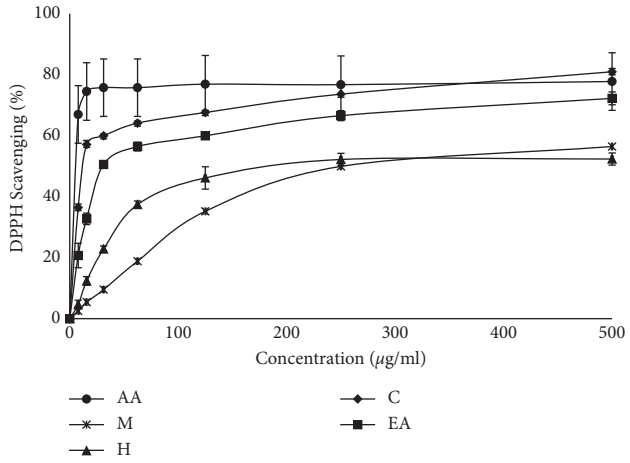

Figure 1: DPPH radical scavenging activity of the methanol extract and its fractions from the bark of *M. concanensis*. AA, ascorbic acid; M, methanol extract; H, hexane extract; C, chloroform extract; EA, ethyl acetate extract. ($n = 3$).

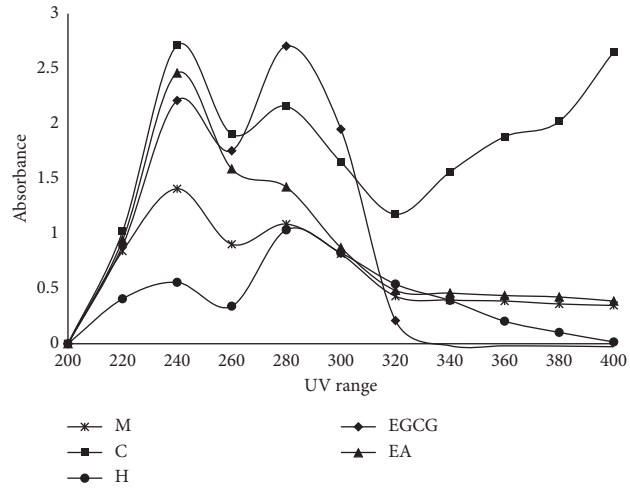

Figure 2: UV absorption spectra of the methanol extract and its fractions from the bark of *M. concanensis*. M, methanol extract; C, chloroform extract; H, hexane extract; EGCG, epigallocatechin gallate; EA, ethyl acetate extract ($n = 3$).

Table 3: The sun protection factor (SPF) value and UVB protection effect of the methanol extract and its fractions from the bark of *M. concanensis*.

Samples (200 μgml^{-1})	SPF value	UVB protection (%)
Methanol	$4.37 \pm 0.17^{***}$	>75
Hexane	$5.49 \pm 0.01^{***}$	>75
Chloroform	10.50 ± 0.23^{ns}	>87
Ethyl acetate	$5.18 \pm 0.01^{***}$	>75
Epigallocatechin gallate	10.34 ± 0.21	>87

Data are expressed as mean ± SD, $n = 3$. Data represent a significant difference at (***) p value < 0.05, among different solvent fractions compared with the positive control (EGCG), using one-way ANOVA, followed by Dunnett's test.

Tea) is 10.34 ± 0.21, which is almost like the SPF value of the chloroform fraction of *M. concanensis* bark. The literature revealed that the seed oil from *M. concanensis* could be a good candidate for sunscreen formulation [24]. The bark extract of medicinal plants such as *Curatella americana* L and *Amburana cearensis (Allemao) A.C. Sm.* showed SPF values 14.74 and 12.21 at 0.2 mgmL^{-1} which is suggested to be the promising source of future skin care products [25]. Similarly, the bark extract of *M. concanensis* could also be utilized as one of the encouraging ingredients in natural product sunscreen formulation.

3.3.2. UV Absorption Spectra. UV absorption spectra of various solvent fractions of *M. concanensis* and the positive control EGCG are shown in Figure 2. The results showed that all the fractions of *M. concanensis* have a wide range of UV absorption; however, among the other fractions, the chloroform fraction of *M. concanensis* showed a broad spectrum of UV absorption which covers UVA (320–400 nm), UVB (280–320 nm), and also UVC (200–280 nm). The positive control EGCG showed the absorption under the UVB range only. Similar patterns of results were observed in the active fraction of *Zanthoxylum rhetsa* (*Roxb.*) *DC.* bark extract which is suggested to be utilized in broad-spectrum sunscreen formulations [6]. Compared to the active fraction of *Z. rhetsa*, the UV absorption spectra of *M. concanensis bark* are high. At present, several studies and regulatory bodies recommend using broad-spectrum natural sunscreen to prevent the damages such as wrinkling and sunburns induced by both UVA and UVB, respectively [26]. The results revealed that the chloroform fraction of *M. concanensis* bark could be an optional ingredient to be used in a natural broad-spectrum sunscreen formulation.

3.4. Gelatin Digestion Assay. Collagenases are one of the important matrix metalloproteinases responsible for the breakdown of collagen present in the skin layers. Studies revealed that continuous exposure of UV radiation could increase the level of collagenases that might damage the matrix proteins and cause wrinkle formation as well as lead to premature aging [27]. The collagenase inhibitory activity of extract and various solvent fractions of *M. concanensis* are presented in Table 4. Compared to the extract and other fractions, the chloroform fraction showed appreciable collagenase inhibitory activity of 50% at the concentration of 200 μgmL^{-1} which is comparable to that of EGCG. However, the hexane and ethyl acetate fractions exhibited a weaker collagenase inhibition activity. Studies revealed that various parts of medicinal plants such as leaves extracts (methanol) of *Aegle marmelos* (*L.*) *Correa, Acalypha indica Linn, Calotropis gigantea* (*L.*) *W.T. Aiton, Nerium oleander* L., and *Nyctanthes arbor-tristis Linn* and a rhizome extract of *Acorus calamus. Linn* at the concentration of 1 mgmL^{-1} showed 50% collagenase inhibitory activity [28], whereas the ethyl acetate fraction of the bark extract of *Z. rhetsa* showed 50% collagenase inhibition at the concentration of 500 μgmL^{-1} [6].

3.5. Antielastase. Elastase is a serine protease, responsible for the breakdown of elastin, an important protein responsible for skin elasticity [29]. The inhibitory activity of

Table 4: Gelatin digestion activity of the methanol extract and its fractions from the bark of *M. concanensis*.

Samples ($200\,\mu gmL^{-1}$)	Zone inhibition (mm)	Enzyme inhibition (%)
Control	20 ± 0.81	0
EGCG	$10 \pm 0.47^{***}$	50
Chloroform	$10 \pm 1.24^{***}$	50
Hexane	$16 \pm 0.47^{***}$	20
Ethyl acetate	$16 \pm 0.47^{***}$	20
Methanol	18 ± 0.81	10

Data are expressed as mean ± SD, $n = 3$. Data represent significant differences at (***) p value < 0.05, among different solvent fractions compared with negative control (water), using one-way ANOVA, followed by Dunnett's test.

methanol extract and its fractions of *M. concanensis* on elastase enzyme were examined. Figure 3 and Table 5 show the effect of methanol extract and its fractions of *M. concanensis* bark against elastase enzyme activity. Among different fractions tested, the chloroform fraction exhibited remarkable elastase inhibition activity with the IC_{50} value of $2.957 \pm 1.23\,\mu gmL^{-1}$ than the standard EGCG (IC_{50}-$39.32 \pm 1.41\,\mu gmL^{-1}$). These findings demonstrated that chloroform fraction of *M. concanensis* may have antiaging potentials by inhibiting elastase enzyme production and delaying the degradation of elastin fibers. Researchers suggested that the plant fraction that is rich in phenolics and flavonoids is reported to possess significant antielastase activity. The ethyl acetate fraction of *Garcinia daedalanthera Pierre.* stem bark extract possesses $43.96 \pm 12.53\%$ elastase inhibitory effect at the concentration of 100 ppm [30]. In this study, the chloroform fraction of *M. concanensis* bark exhibited >50% of elastase inhibitory effect at the concentration of $31.25\,\mu gmL^{-1}$.

3.6. Cytotoxicity of *M. concanensis* Fractions in Cell Culture (3T3-L1 Cell Lines)

3.6.1. MTT Assay. Cytotoxic effect of various solvent fractions of *M. concanensis* was tested in 3T3-L1 cells with a wide range of concentration (0–$500\,\mu gmL^{-1}$). Results revealed that all the fractions of *M. concanensis* bark except the chloroform fraction were nontoxic to the cells up to $250\,\mu gmL^{-1}$. However, the chloroform fraction of *M. cocanensis* was toxic to the cells at the concentration >$25\,\mu gmL^{-1}$, where it showed the strongest cytotoxic activity against 3T3-L1 cells by reducing the cell viability to 16.5% at the concentration of $62.5\,\mu gmL^{-1}$, Figure 4. This is the first study to reveal the cytotoxic effect of various solvent fractions of *M. concanensis* bark against the preadipocyte cells. Previously, the ethanol extract of the leaves of *M. concanensis* was also reported to be nontoxic to 3T3-L1 adipocytes up to $100\,\mu gmL^{-1}$ until 24 h of treatment [15]. Balamurugan et al. [31] tested the crude ethanol extract of *M. concanensis* leaves and bark against HepG2 cell lines and revealed that both parts of *M. concanensis* strongly inhibit the growth of cancerous cells in a dose-dependent manner. In another study, the methanolic root bark extract of *M. concanensis* was found to be toxic against HepG2 cells,

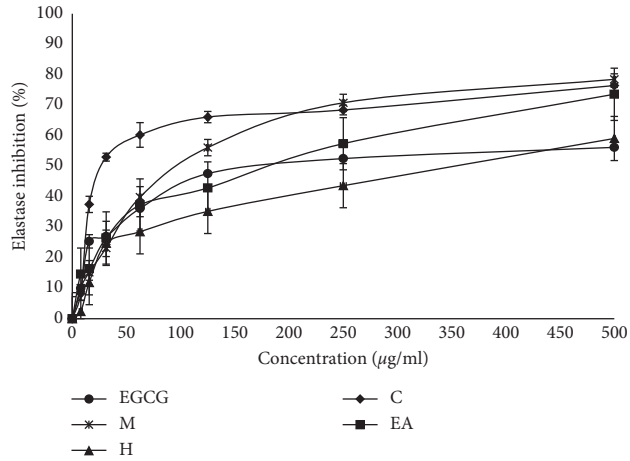

Figure 3: Antielastase activity of the methanol extract and its fractions from the bark of *M. concanensis*. Data are expressed as mean ± SD, $n = 3$.

Table 5: IC_{50} values of elastase inhibition activity of the methanol extract and its fractions from the bark of *M. concanensis*.

Samples	IC_{50} (μgmL^{-1})
EGCG	39.32 ± 1.41
Methanol	$88.53 \pm 1.95^{**}$
Hexane	$78.11 \pm 1.72^{*}$
Chloroform	$2.957 \pm 1.23^{**}$
Ethyl acetate	$176.7 \pm 2.20^{***}$

Data expressed as mean ± SD, $n = 3$. Data represent significant differences at p value < 0.05, among different solvent fractions compared with the positive control (EGCG), using one-way ANOVA, followed by Dunnett's test.

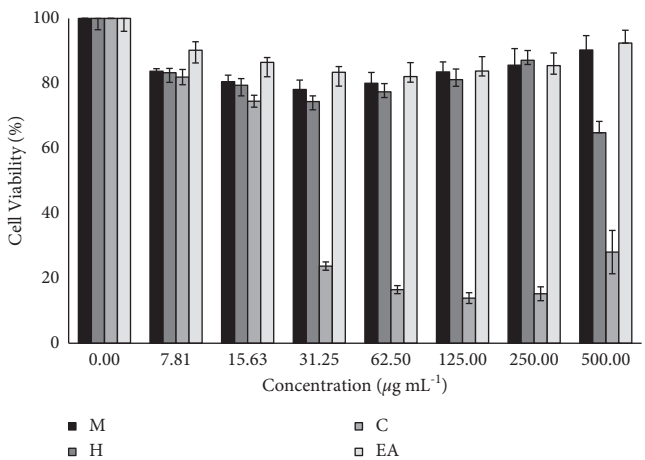

Figure 4: Cytotoxic effect of the methanol extract and various solvent fractions of *M. concanensis* bark treated with 3T3 mouse fibroblasts for 24 h data expressed as mean ± SD, $n = 3$.

whereas it does not induce toxic effect against A549 and HT-29 cell line which demonstrates its selective cytotoxicity [21]. In this study, the crude methanol extract of *M. concanensis* bark does not induce any toxicity against 3T3-L1 cells up to $500\,\mu gmL^{-1}$. Since the other solvent fractions of *M. concanensis* bark have toxic effect >$250\,\mu gmL^{-1}$ and the chloroform fraction has toxic effect >$25\,\mu gmL^{-1}$, on an average, we reduced

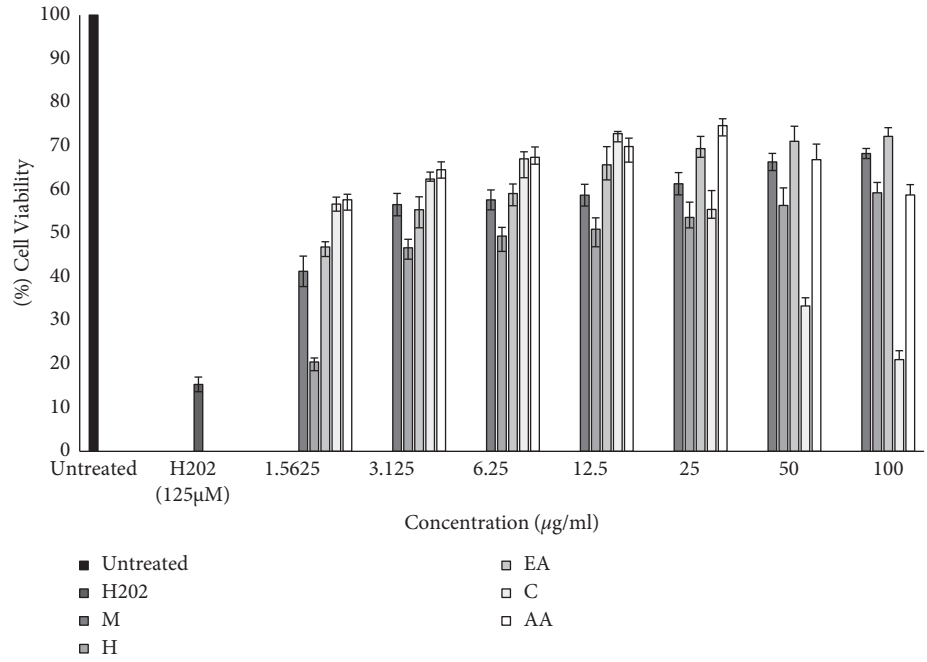

Figure 5: Protective effect of various solvent fractions of *M. concanensis* bark against H_2O_2-induced oxidative damage in 3T3-L1 cells treated for 24 h. Data are expressed as mean ± SD, $n = 3$. Data represent significant difference at p value < 0.05, among different solvent fractions of *M. concanensis* bark (various concentrations) compared with the H_2O_2 (125 μM), using one-way ANOVA, followed by Dunnett's test.

the concentration range of all the extracts/fractions to 0–100 μgmL^{-1} for further assay.

3.6.2. H_2O_2-Induced Damage. The protective effect of various solvent fractions of *M. concanensis* bark against H_2O_2-induced oxidative damage in 3T3-L1 was determined and shown in Figure 5. From the results, it has been clear that the H_2O_2 (125 μM) reduced the viability of cells to 15.35% after 6 h of treatment, whereas the cells pretreated with various solvent fractions of *M. concanensis* bark prevented the cells from oxidative damage. However, the level of protection by each fraction varies and it depends on the concentration and constituents present in each sample. The chloroform fraction of *M. concanensis* bark offers significant protection against H_2O_2-induced damage even at low concentration, where the viability of cells treated with 1.56 μgmL^{-1} protects 56% of cells which was comparable to that of positive control, AA (cell viability—57%). As the concentration increases, up to 12.5 μgmL^{-1}, the chloroform fraction prevented the cells up to 72% where AA prevented up to 69%. However, at the concentration of 25 μgmL^{-1} and above, the viability of cells treated with chloroform fraction got drastically reduced. This might be due to the overdose of chemical constituents present in it. Similar patterns of results were obtained in the cytotoxicity assay, and at low concentration (<15 μgmL^{-1}), the chloroform fraction was nontoxic to 3T3-L1 cells. As the concentration increases, the chloroform fraction is toxic. As reported, the extracts and fractions of various parts of *M. concanensis* are cytotoxic to different cancer cell lines like HepG2 [31, 32], and the chloroform fraction of *M. concanensis* bark could offer a significant cytotoxic effect in other cancerous cell lines. Further research is needed to evaluate the selective cytotoxic effect of chloroform fraction of *M. concanensis* bark.

From this study, it has been evident that compared to other fractions, the chloroform fraction of *M. concanensis* bark has a high sunscreen protection factor value, broad-spectrum UV absorption, appreciable DPPH scavenging, anticollagenase, antielastase, high phenolic, and high flavonoid content. Additionally, it also prevents the H_2O_2-induced oxidative damage in 3T3-L1 cells which was comparable to that of positive control, AA.

3.7. UPLC-QTOF/MS Analysis. From this study, it has been identified that the chloroform fraction is the bioactive fraction of *M. concanensis* bark. UPLC-QTOF/MS analysis was found to be a convenient method to determine the presence of possible phytoconstituents in the studied fraction through the exact mass detection. Polyphenolic compounds such as phenolic acids and flavonoids are naturally abundant and commonly found in the genus *Moringa*. Bioactive flavonols such as quercetin, hyperoside, astragalin, isoquercetin, kaempferol-3-*O*-rutinoside, and rutin were reported previously in this genus especially in the species, *Moringa oleifera* [20]. In this study, 20 different phytoconstituents were identified in the chloroform fraction obtained from the methanol extract of *M. concanensis* bark using UPLC-QTOF/MS analysis, Table 1. The result indicated that the chloroform fraction contains a complex mixture of bioactive tentative annotated phenolics such as kaempferol-3-*O*-rutinoside, astragalin, quercetin-3-*O*-glucuronide, kaempferol 3-*O*-glucuronopyranosyl methyl ester, isoquercetin, kaempferol-

3-*O*-arabinoside, kaempferol-3-*O*-rhamnoside, quercetin-3-*O*-glucuronide-methyl ester, eugenol, quercetin, and caffeic acid. The assignations were carried out on a prediction basis and detailed phytochemistry studies required to be carried out on this species for the affirmation of the presence of the predicted metabolites in the studied fraction/extract in the future. This comprehensive phytochemical profiling analysis has revealed the structural diversity of phenolics and their similar structural patterns as well as the biological potency of the studied fractions.

Moreover, the findings are in agreement with the results obtained from the total phenolic and total flavonoids evaluation conducted on the respective fractions. The existence of flavonoids, especially flavonols, could possibly be the main contributors to photoprotective properties especially in collagenase and elastase inhibitory activities through a synergistic effect [33]. Furthermore, the presence of carbonyl and hydroxyl moieties in the main scaffold of the flavonols might be played the role in giving the inhibitory effects which allow them to bind to metalloenzymes like collagenase and elastase that could alter or inhibit metabolic pathways [34]. However, further studies are required in relation to the detailed identification and isolation of bioactive metabolites from the bark of *M. concanensis* as well as molecular mechanisms of their photoprotective potentials.

4. Conclusion

In summary, the result obtained from the phytochemical analysis showed that chloroform fractions of *M. concanensis* have the highest DPPH, TPC, and TFC values. The photoprotective study also demonstrated a high SPF value for chloroform fractions and gave the same UVB protection as its positive control, EGCG. Besides that, the chloroform fractions have a much broader spectrum of UV absorption that covers both UVA and UVB when compared to others. The inhibitory effect of *M. concanensis* chloroform fractions towards elastase and collagenase proved that the plant extract has potential biological properties that can reduce the breakdown of collagen and elastin within the skin. *In vitro* study showed that some of the fractions possessed low cytotoxicity towards the 3T3-L1 cell line even at higher concentrations (methanol, hexane, and ethyl acetate). However, chloroform fractions obtained from the plant extract exhibit high cytotoxic activity even at lower concentrations (ranging from 31.25 to 500 μgmL^{-1}). All the fractions displayed protective effect against H_2O_2-induced oxidative damage in 3T3-L1 cells, with methanol, hexane, and ethyl acetate having a higher cell viability percentage even at higher concentrations (50 and 100 μgmL^{-1}). Various metabolites especially bioactive flavonols that were tentatively identified using UPLC-QTOF/MS analysis might be the source for the high photoprotective activity. Based on these results, *M. concanensis* has the potential to be a new applicant as an active component in pharmaceutical and cosmetics formulation. However, detailed preclinical research is needed to demonstrate the individual or synergistic effect of the bioactive components involved in the photoprotective mechanism of *M. concanensis*.

Data Availability

Data used to support the findings of this study are obtained from the corresponding author.

Conflicts of Interest

The authors declare that there are no conflicts of interest.

Authors' Contributions

R.S., K.S., and T.K. conceptualized the study; R.S. was responsible for methodology; W.I.W.I., R.S., and T.K. validated the data; M.F.Z., R.S., and T.K. performed formal analysis and investigation; A.V. was responsible for resources; R.S., M.F.Z., and G.K.M. performed experiments; R.S., K.S., T.K., M.F.Z., and V.S. prepared the original draft and reviewed and edited the manuscript; R.S. and W.I.W.I. supervised the study and were responsible for funding acquisition; all authors have read and agreed to the published version of the manuscript.

Acknowledgments

The authors would like to thank Universiti Malaysia Terengganu and Universiti Sains Malaysia for the facilities provided. This research was funded by Universiti Malaysia Terengganu, Malaysia, under the Talent and Publication Enhancement Research Grant (TAPE-RG) scheme. Vote Number: 55256.

References

[1] A. Verma, H. N. Kushwaha, A. K. Srivastava et al., "Piperine attenuates UV-R induced cell damage in human keratinocytes via NF-kB, Bax/Bcl-2 pathway: an application for photoprotection," *Journal of Photochemistry and Photobiology B: Biology*, vol. 172, pp. 139–148, 2017.

[2] Y.-S. Wang, S.-S. Zhou, C.-Y. Shen, and J.-G. Jiang, "Isolation and identification of four antioxidants from *Rhodiola crenulata* and evaluation of their UV photoprotection capacity in vitro," *Journal of Functional Foods*, vol. 66, Article ID 103825, 2020.

[3] M. Radice, S. Manfredini, P. Ziosi et al., "Herbal extracts, lichens and biomolecules as natural photo-protection alternatives to synthetic UV filters. A systematic review," *Fitoterapia*, vol. 114, pp. 144–162, 2016.

[4] G. Schneider, F. L. Figueroa, J. Vega et al., "Photoprotection properties of marine photosynthetic organisms grown in high ultraviolet exposure areas: cosmeceutical applications," *Algal Research*, vol. 49, Article ID 101956, 2020.

[5] H. Sies, "Nutritional protection against skin damage from sunlight," *Oncology Research Featuring Preclinical and Clinical Cancer Therapeutics*, vol. 15, pp. 462-463, 2006.

[6] R. K. Santhanam, S. Fakurazi, S. Ahmad et al., "Inhibition of UVB-induced pro-inflammatory cytokines and MMP expression by *Zanthoxylum rhetsa* bark extract and its active constituent hesperidin," *Phytotherapy Research*, vol. 32, no. 8, pp. 1608–1616, 2018.

[7] A. Kammeyer and R. M. Luiten, "Oxidation events and skin aging," *Ageing Research Reviews*, vol. 21, pp. 16–29, 2015.

[8] M. D. Mota, A. N. da Boa Morte, L. C. R. C. e. Silva, and F. A. Chinalia, "Sunscreen protection factor enhancement through supplementation with Rambutan (*Nephelium lappaceum* L) ethanolic extract," *Journal of Photochemistry and Photobiology B: Biology*, vol. 205, Article ID 111837, 2020.

[9] N. Saewan and A. Jimtaisong, "Natural products as photoprotection," *Journal of Cosmetic Dermatology*, vol. 14, no. 1, pp. 47–63, 2015.

[10] D. Lin, M. Xiao, J. Zhao et al., "An overview of plant phenolic compounds and their importance in human nutrition and management of type 2 diabetes," *Molecules*, vol. 21, no. 10, Article ID 1374, 2016.

[11] Y. C. Boo, "Can plant phenolic compounds protect the skin from airborne particulate matter?" *Antioxidants*, vol. 8, no. 9, p. 379, 2019.

[12] V. Ravichandran, G. Arunachalam, N. Subramanian, and B. Suresh, "Pharmacognostical and phytochemical investigations of *Moringa concanensis* (Moringaceae) an ethnomedicine of Nilgiris," *Journal of Pharmacognosy and Phytotherapy*, vol. 1, pp. 76–81, 2009.

[13] M. Manzoor, F. Anwar, T. Iqbal, and M. I. Bhanger, "Physicochemical characterization of *Moringa concanensis* seeds and seed oil," *Journal of the American Oil Chemists' Society*, vol. 84, no. 5, pp. 413–419, 2007.

[14] S. Anbazhakan, R. Dhandapani, P. Anandhakumar, and S. Balu, "Traditional medicinal knowledge on *Moringa concanensis* Nimmo of perambalur district, tamilnadu," *Ancient Science of Life*, vol. 26, pp. 42–45, 2007.

[15] B. B. Balakrishnan, K. Krishnasamy, and K. C. Choi, "*Moringa concanensis* Nimmo ameliorates hyperglycemia in 3T3-L1 adipocytes by upregulating PPAR-gamma, C/EBP alpha via Akt signaling pathway and STZ- induced diabetic rats," *Biomedicine & Pharmacotherapy*, vol. 103, pp. 719–728, 2018.

[16] R. Santhanam, S. Ahmad, F. Abas, I. S. Ismail, Y. Rukayadi, and K. Shaari, "Photoprotective properties of *Zanthoxylum rhetsa*: an in vitro analysis," *Journal of Chemical and Pharmaceutical Research*, vol. 5, pp. 1512–1520, 2013.

[17] C. Wang, X. Gao, R. K. Santhanam et al., "Effects of polysaccharides from Inonotus obliquus and its chromium (III) complex on advanced glycation end-products formation, α-amylase, α-glucosidase activity and H_2O_2-induced oxidative damage in hepatic L02 cells," *Food and Chemical Toxicology*, vol. 116, pp. 335–345, 2018.

[18] S. Raseetha, M. F. Zulkifli, M. Nurul-Nabilah, W. I. W. Ismail, and L. Jayasinghe, "Inhibition of lipid accumulation in 3T3-L1 adipocytes by chlorogenic acid derived from green coffee (Robusta sp.) beans and pulps," *Malaysian Applied Biology*, vol. 46, pp. 163–170, 2017.

[19] W. Chen, Y. Liu, G. Xue, L. Zhang, and S. Shao, "Diazoxide protects L6 skeletal myoblasts from H2O2-induced apoptosis via the phosphatidylinositol-3 kinase/Akt pathway," *Inflammation Research*, vol. 65, pp. 53–60, 2016.

[20] H. Lin, H. Zhu, J. Tan et al., "Comparative analysis of chemical constituents of *Moringa oleifera* leaves from China and India by ultra-performance liquid chromatography coupled with quadrupole-time-of-flight mass spectrometry," *Molecules*, vol. 24, no. 5, p. 942, 2019.

[21] M. Vijayarajan and R.-M. Pandian, "Cytotoxicity of methanol and acetone root bark extracts of *Moringa concanensis* against A549, hep-G2 and HT-29 cell lines," *J. Acad. ind. Res,* vol. 5, pp. 45–49, 2016.

[22] A. Gori, C. Brunetti, L. B. dos Santos Nascimento et al., "Photoprotective role of photosynthetic and non-photosynthetic pigments in *Phillyrea latifolia*: is their "Antioxidant" function prominent in leaves exposed to severe summer drought?" *International Journal of Molecular Sciences*, vol. 22, no. 15, p. 8303, 2021.

[23] K. Geoffrey, A. N. Mwangi, and S. M. Maru, "Sunscreen products: rationale for use, formulation development and regulatory considerations," *Saudi Pharmaceutical Journal*, vol. 27, no. 7, pp. 1009–1018, 2019.

[24] S. Kale, G. Gajbhiye, and N. Chaudhari, "Determination and comparison of in vitro SPF of topical formulation containing lutein ester from Formulation and in- vitro Evaluation of Moringa concanensis, Nimmo. Seed Oils Sunscreen Cream," *Int. J. Pharmtech Res,* vol. 2, pp. 2060–2062, 2010.

[25] A. R. Nunes, A. L. M. Rodrigues, D. B. de Queiróz et al., "Photoprotective potential of medicinal plants from Cerrado biome (Brazil) in relation to phenolic content and antioxidant activity," *Journal of Photochemistry and Photobiology B: Biology*, vol. 189, pp. 119–123, 2018.

[26] N. Lionetti and L. Rigano, "The new sunscreens among formulation strategy, stability issues, changing norms, safety and efficacy evaluations," *Cosmetics*, vol. 4, no. 2, p. 15, 2017.

[27] K. Maeda, "Analysis of ultraviolet radiation wavelengths causing hardening and reduced elasticity of collagen gels in vitro," *Cosmetics*, vol. 5, no. 1, p. 14, 2018.

[28] S. Iswarya, N. Radhakrishnan, V. Kavitha, A. B. Mandal, and A. Gnanamani, "Collagenase inhibition activity of Indian medicinal plants: an approach to moderate collagen turnover," *International Journal of Bioassays*, vol. 3, pp. 2075–2078, 2014.

[29] T. S. Thring, P. Hili, and D. P. Naughton, "Anti-collagenase, anti-elastase and anti-oxidant activities of extracts from 21 plants," *BMC Complementary and Alternative Medicine*, vol. 9, no. 1, p. 27, 2009.

[30] N. S. S. Ambarwati, B. Elya, Y. Desmiaty, and H. Omar, "Anti-elastase of leaves and stem bark extract of *Garcinia daedalanthera* Pierre," *International Journal of Pharma Sciences and Research*, vol. 12, pp. 592–596, 2020.

[31] V. Balamurugan, V. Balakrishnan, P. J. Robinson, and M. Ramakrishan, "Anti-cancer and apoptosis-inducing effects of *Moringa concanensis* using hepG2 cell lines," *Bangladesh Journal of Pharmacology*, vol. 9, pp. 604–609, 2014.

[32] D. Sivakumar, R. Manikandan, and P. Velu, "Antimicrobial activity of *Moringa concanensis* flower against human pathogens and its cytotoxic effects on HepG2 cell Line," *Research Journal of Microbiology*, vol. 15, pp. 51–60, 2020.

[33] B. Y. Sin and H. P. Kim, "Inhibition of collagenase by naturally-occurring flavonoids," *Archives of Pharmacal Research*, vol. 28, no. 10, pp. 1152–1155, 2005.

[34] N. Ł. Zofia, Z. D. Martyna, Z. Aleksandra, and B. Tomasz, "Comparison of the antiaging and protective properties of plants from the Apiaceae family," *Oxidative Medicine and Cellular Longevity*, vol. 2020, Article ID 5307614, 2020.

J. Indian bot. Soc. e-ISSN:2455-7218, ISSN:0019 - 4468 Vol. 101 (3) 2021: 214-223

INDIRECT ORGANOGENESIS AND REGENERATION OF *MACROTYLOMA UNIFLORUM* (LAM) VERDC

KARTHIKA PALANISAMY, VASANTH KRISHNAN AND DHANDAPANI GURUSAMY[1]

Molecular Biology Lab, Department of Botany, Bharathiar University, Coimbatore 641 046, Tamil Nadu, India. [1]Department of Botany, Kongunadu Arts and Science College (Autonomous), Bharathiar University, Coimbatore 641 029, Tamil Nadu, India.
E-mail: vasanthlabbu@gmail.com
Date of online publication: 30th September 2021
DOI: 10.5958/2455-7218.2021.00027.9

The present research was performed to develop an indirect organogenesis protocol in *Macrotyloma uniflorum* via callus by using cotyledon and epicotyledon explants. Cotyledon explants were produce the best result on MS medium supplemented with 3.0 mg/L BAP. The maximum percentage (97%) of regeneration was obtained with the combination of BAP+GA_3 (2.0+1.0 mg/L) from cotyledon explants. Well established root system was developed from regenerated shoot lets in the medium combination with BAP+NAA (1.0+1.0 mg/L). Cotyledon explants were showed more responsible than epicotyledon in terms of callus induction and plant regeneration. This *in vitro,* developed plant lets were successfully acclimatized to the pots and established in the green house. This standardized *in vitro* regeneration system will facilitate further to development of a reliable procedure to accomplish genetic manipulation in this genus.

Keywords: Cotyledon, Callus induction, Epicotyledon, Indirect organogenesis, Regeneration

Macrotyloma uniflorum (Lam.) Verdc. is a hardy pulse crop of the Fabaceae family cultivated mostly in the southern region especially Tamil Nadu, Andhra Pradesh, and Karnataka, and also in some parts of Maharashtra and Madhya Pradesh. It has been an important fodder crop since the beginning of agriculture in many parts of South Asia (Murphy and Fuller 2017). It is the most widely recovered pulse crop from the prehistoric or early historic sites in India and is also an underutilized and unexplored food legume (Reddy *et al*. 2008). Due to the many desirable characters such as tolerance to drought, salinity, and heavy metals, horse gram is considered as a potential crop for enhancing tolerance in cultivated crops (Reddy *et al*. 2008). Moreover, this species exhibits many medicinal properties such as antioxidant and antimicrobial activities and is also known to be effective in the dissolution and dislocation of kidney stones (Kawsar *et al*. 2008).

Macrotyloma uniflorum (Lam.) Verdc. have wide adaptability and thrives well under adverse climatic conditions and in poor soil (Bolbhat and Dhumal 2010). In the alarming environmental distress due to global warming and water scarcity, this crop can be considered as a future crop due to its high nutritional value and better adaptability to adverse environmental conditions. High-yielding and disease-resistant plant varieties can be developed through plant tissue culture (Kawsar *et al*. 2008). Hence this research is aimed to establish a suitable regeneration protocol and culture condition, which can be used in horse gram to make superior varieties adverse to the environmental conditions.

Tissue culture allows the production and propagation of genetically homogeneous, disease-free plant material (Chatenet *et al*. 2001). Plant tissue culture represents the most promising areas of application at present time and giving an outlook into the future. It is also essential to have sufficient mother culture and reduce the number of subcultures to avoid variation and plan the production of plants according to the demand. The *in vitro* culture has a unique has a role in sustainable and competitive agriculture and has been successfully applied in plant breeding for the rapid introduction of improved plants and it has become an integral part of plant breeding (Hussain *et al*. 2012).

In horse gram, shoot formation may occur as a result directly of explants without

Received on June 01, 2021 www.indianbotsoc.org Accepted on June 30, 2021

callus formation (Tejavathi and Nijalingappa, 1989) or from somatic embryos formed at the ends of leaf and immature cotyledon derived callus (Mohamed *et al*. 2004, 2005). In previous indirect organogenesis studies, multiple shoots regenerated from the callus which developed by shoot tip and cotyledonary node explants (Tejavathi *et al*. 2010). In this present study, plant regeneration was successfully established by indirect organogenesis with more number of shoots from callus which derived from cotyledon and epicotyledon explants.

MATERIALS AND METHODS

Surface Sterilization: Seeds (variety. Paiyur-2) were procured from Tamil Nadu Agriculture University (TNAU) regional research station, Dharmapuri, Tamil Nadu, India. The seeds were initially rinsed with running tap water for 3 min and rinsed with 3% sodium hypochlorite for 5 min. Later, the seeds were rinsed with distilled water thrice for 5 min, followed by rinsing with 70% ethanol for 2 min. The excess ethanol traces were removed by rinsing in distilled water thrice for 5 min. The seeds were then treated with 0.1% mercuric chloride (w/v) for 3 min and thoroughly washed the seeds three to five times with sterile double distilled water. The surface-sterilized seeds were inoculated in humidified tissue paper with sterilized petriplates and incubated at 16/8 hrs light condition for germination (25 ± 2°C with 50 μmol m−2 s−1).

Selection of explant and callus initiation: Cotyledon and epicotyls were separated from three days old germinated seedlings. The cotyledon explants (0.8 - 1.0 cm) were excised by removing the cotyledons. Epicotyls were cut into pieces of approximately 1cm. MS (Murashige and Skoog, 1962) basal medium was used for callus induction. The nutrient medium consists of inorganic nutrients, carbon sources, vitamins, iron, and amino acids essential for the development of callus.

The explants such as cotyledon and epicotyls were inoculated on MS medium containing different concentrations of plant growth regulators, such as 1.0-5.0 mg/L 6-Benzylaminopurine (BAP), 0.25-1.25mg/L Thidiazurone (TDZ), and the combination of 1.0-5.0 mg/L (BAP) and 0.5 mg/L TDZ for testing the best combination for callus induction. Thirty explants in triplicates were used in each experiment for callogenesis. The number of explants that formed callus and its response was recorded at regular intervals. Callus was sub-cultured regularly every 2 weeks.

Regeneration from callus: After 20 days, the embryonic callus was subcultured on shoot induction medium (SIM) in the culture tubes containing MS salts and vitamins, sucrose along with various concentrations of cytokinins such as (BAP) 0.5 – 4.0mg/L with 6-(γ, γ-Dimethylallylamino) purine (2iP) 0.25 - 3.3mg/L, (BAP), 0.5 - 4.0 mg/L with Picloram (PIC) 0.25 –3.0mg/L and (BAP) 0.5 – 4.0 with Gibberellic acid (GA_3) 2.5 – 3.0mg/L were used. Individual elongated shoots from cotyledonary and epicotyl explants were cultured a root induction medium comprising MS salts, vitamins, and sucrose along with various concentrations of Naphthalene acetic acid (NAA) 0.5-4.0mg/L, (BAP) 0.1 with (NAA) 0.5 – 2.5 mg/L and (BAP) 1.0 with Dichlorophenoxy acetic acid (2,4-D) 0.5 to 2.5 mg/L to optimize the ideal concentration for root induction.

In vitro grown healthy regenerated plants were washed thoroughly to remove adhered media and then transferred to small plastic cups containing a mixture of autoclaved sand, soil, and vermiculite (1:1:1). The potted plants were covered with transparent polythene bags with a minute puncture and were grown in a growth chamber at 25 ± 2ºC with 85% relative humidity for 2-3 weeks. The plants were irrigated once in 2 days. Upon new leaf growth, the plantlets were transferred to polythene bags and maintained in the greenhouse.

The analysis of variance (ANOVA) appropriate for the design was carried out to

detect the significance of differences among the treatment means. The data were statistically analyzed by the DMRT (Duncan's Multiple Range Test) (Harter, 1960) at $p<0.05$ significant level.

Histological studies: The callus was fixed in formalin, acetic acid and ethanol (FAA) in the ratio 1:1:9. After 24 hrs of fixing, the specimens were dehydrated in tertiary butyl alcohol as given by Sass, (1940). The paraffin-embedded specimens were sectioned with the help of the Rotary Microtome. The thickness of the sections was set to 10-12 µm. Dewaxing of the sections was carried out by customary procedure (Johnsen, 1940). The sections were stained with toluidine blue as per the method of O'Brien *et al*. (1964). For studying the stomatal morphology, venation pattern, and trichome distribution, parenchymal section (the section has taken parallel to the surface of the leaf) as well as clearing of the leaf with 5% sodium hydroxide or epidermal peeling by partial maceration employing Jeffrey's maceration fluid (Sass, 1940) were prepared. Glycerine mounted temporary preparations were made for macerated/cleared materials. Powdered materials of different parts were cleared with NaOH and mounted in a glycerine medium after staining, followed by different cell components were studied and measured.

RESULTS AND DISCUSSION

An efficient regeneration protocol of *M. uniflorum* has been successfully established using cotyledon and epicotyls explants. Based on Varisai Mohamed *et al*. (2005) report on cotyledon explants, the present study demonstrated and produced more shoots using cotyledon and epicotyls explants. Although, various sources of explants have been reported for regeneration, so far there is no report for regeneration from epicotyls explants. Cytokinins are necessary for plant cell division, induction of adventitious bud formation, and growth of lateral buds in the cell cycle control (Gatcia Arias *et al*. 2010). (BAP) is among the most widely used cytokinins for *in vitro* callus induction in a wide range of plant species. In the present study, successful induction of potentially organogenic callus from cotyledon and epicotyls was achieved using (BAP) 3.0 mg/L with 91% callus of 0.52 mg in weight from cotyledon explants (Fig 1) and 79.33% callus of 0.44 mg in weights from epicotyl explants (Fig 2).

The calluses are of varied morphologies, cotyledon-derived callus was compact and greenish-white whereas the epicotyl-derived callus is greenish-white with friable nature (Table 1). The fresh friable callus weighs 0.32 mg was observed in 0.12 µM (2,4-

Table1: Effect of Cytokinins on callus induction of cotyledon and epicotyledon explants of *M. uniflorum* paiyur-2 variety seeds

Explants		Cotyledon				Epicotyledon			
Plant Growth Regulators (mg/L)		Initiation of Callus (Days)	Percentage of Callus Response (%)	Callus Fresh Weight (mg)	Callus Type	Initiation of Callus (Days)	Percentage of Callus Response (%)	Callus Fresh Weight (mg)	Callus Type
BAP	1.0	14	64.4±1.29^{f}	70.00±3.05^{cd}	GW-C	15	62.3±1.85^{c}	58.3±1.45^{c}	W-F
	2.0	11	75.2±0.92^{e}	73.66±0.33^{b}	GW-C	15	73.67±2.02^{b}	67±1^{b}	GW-F
	3.0	**9**	**91.0 ±0.71^{a}**	**82.66±4.05^{a}**	**GW-C**	**11**	**79.33±1.76^{a}**	**74.67±1.45^{a}**	**GW-F**
	4.0	9	80.6±0.51^{b}	78.33±1.45^{b}	G-C	13	70.33±1.45^{b}	65.67±0.33^{a}	GW-F
	5.0	12	76±1.05^{c}	69.33±2.84^{cde}	G-C	16	63.67±0.67^{c}	61.34±0.89^{c}	GW-F
TDZ	0.25	14	72.6±1.44^{c}	61.33±0.88^{def}	YW-C	14	70±1.25^{b}	62±0.58^{b}	YW-F
	0.50	10	78.8±0.38^{b}	66.33±3.52^{bc}	YW-C	12	74.67±0.89^{a}	68.67±0.89^{bc}	YW-F
	0.75	13	68.2±1.02^{ef}	58.00±1.15^{def}	Y-F	15	65.35±1.45^{c}	57.67±2.60^{a}	YW-F
	1.0	13	65.8±0.73^{fg}	56.66±1.20^{efg}	Y-F	16	59.67±0.89^{d}	54.33±1.76^{ab}	W-F
	1.25	15	56.2±0.58^{h}	54.66±1.76^{fg}	Y-F	16	53.67±1.45^{e}	59.67±0.89^{c}	W-F
BAP + TDZ	1.0±0.5	12	46±0.71^{j}	47.33±1.45^{h}	YG-F	12	57.66±1.45^{d}	51.33±0.89^{c}	GW-F
	2.0±0.5	14	53.2±0.80^{i}	49.33±2.40^{gh}	G-F	12	62.67±1.20^{bc}	56.33±0.89^{bc}	GW-F
	3.0±0.5	10	72.8±0.86^{d}	63.33±0.88^{cde}	YG-F	10	68.67±0.89^{a}	60±1.00^{a}	GW-F
	4.0±0.5	13	69.6±0.51^{e}	60.00±0.57^{cdef}	G-F	14	65.33±0.67^{b}	57.33±1.45^{bc}	GW-F
	5.0±0.5	12	63.8±1.36^{g}	51.00±0.57^{gh}	G-F	15	61.33±.089^{c}	53.33±0.89^{a}	G-F

GW-C-Greenish white compact, **G-C-** Greenish compact, **YW-C-**Yellowish white compact, **Y-F-**Yellowish friable, **YG-**Yellowish green friable, **G-F-**Greenish friable, **WF**-Whitish friable, **GW-F**-Greenish white friable, **YW-F-**Yellowish white friable. For each treatment, 50 explants were used and repeated three times. Values represent the means ± standard error. Mean values followed by the same letters within a column are not significantly different according to Duncan's multiple range test at 5% level.

Table 2: Effect of different concentrations and combinations of BAP on shoot regeneration from cotyledon and epicotyls

Explants		Cotyledon				Epicotyledon			
Plant Growth Regulators (mg/L)		Initiation Days	Percentage of Responses (%)	Mean Number of Shoots	Shoot Length (cm)	Initiation Days	Percentage of Responses (%)	Mean Number of Shoots	Shoot Length (cm)
BAP+2iP	0.5 + 0.25	13	54.00±3.77^{efg}	7.66±0.33^{fgh}	2.07±0.22^{ef}	12	58.67±0.67^{c}	9.67±0.89^{bc}	1.27±0.15^{d}
	1.0 + 0.5	13	61.25±4.40^{cdef}	12.67±1.00^{ab}	2.93±0.52^{cde}	09	61±0.57^{b}	3.67±0.67^{b}	1.93±0.09^{c}
	2.0 + 1.0	13	67.50±3.65^{bc}	17.33±1.45^{efgh}	4.10±0.21^{b}	**07**	63.67±1.33^{a}	15.33±0.88^{a}	3.3±0.17^{a}
	3.0 + 2.0	17	55.00±4.22^{cdefg}	8.00±1.15^{b}	3.83±0.20^{bc}	11	57±1.15^{c}	10.67±0.89^{c}	2.63±0.13^{b}
	4.0 + 3.0	17	47.50±5.26^{fg}	2.66±0.33^{fgh}	3.20±0.31^{bcd}	11	54.67±0.88^{d}	7.33±0.89^{bc}	1.6±0.17^{cd}
BAP+ Picloram	0.5 + 0.25	11	66.75±4.97^{cdefg}	15.33±1.45^{efgh}	2.10±0.21^{ef}	16	63.33±0.89b	11±100^{b}	1.2±0.11^{c}
	1.0 + 0.5	9	72.50±5.59^{cde}	18.67±0.88^{cd}	2.77±0.26^{de}	12	68±0.57a	14.67±0.89^{a}	1.93±0.08^{b}
	2.0 + 1.0	12	61.25±3.98^{defg}	11.67±1.45^{c}	3.43±0.23^{bcd}	12	62.69±0.89c	10±1.00^{c}	2.8±0.15^{a}
	3.0 + 2.0	11	53.00±4.62^{efg}	4.00±1.00^{ab}	2.77±0.15^{de}	15	58.67±0.33bc	7.66±0.89^{bc}	1.07±0.07^{c}
	4.0 + 3.0	8	49.00±5.00^{g}	3.33±0.33^{hi}	1.83±0.18^{f}	17	55.33±0.89^{d}	5.67±0.89^{c}	1.86±0.08^{b}
BAP + GA_3	0.5 + 0.25	8	67.50±3.65^{bc}	17.00±1.15^{ab}	3.96±0.88^{b}	12	74.67±1.45^{c}	17±0.57^{b}	3.1±0.20^{b}
	1.0 + 0.5	8	**83.00±4.19^{a}**	**26.00±0.57^{a}**	**5.13±0.27^{a}**	14	**77±1.15^{a}**	**19.33±0.89^{a}**	**4.23±0.14^{a}**
	2.0 + 1.0	10	76.25±3.72^{ab}	21.33+1.20^{ab}	4.06±0.39^{b}	12	72.33±1.2^{b}	15.38±0.33^{b}	3.4±0.20^{b}
	3.0 + 2.0	7	65.00±4.22^{bcd}	16.33±1.45^{c}	3.26±0.39^{bcd}	12	61.33±0.66^{c}	9.33±0.89^{c}	2.5±0.23^{c}
	4.0 + 3.0	10	61.25±3.98^{cdef}	11.67±0.88^{cd}	2.8±0.23^{de}	11	58.33±0.89^{d}	5.67±0.89^{d}	1.87±0.08^{d}

For each treatment, 50 shoots initiated on callus were used and repeated three times. Values represent the means ± standard error. Mean values followed by the same letters with in a column are not significantly different according to Duncan's multiple range test at 5% level.

D) (Tejavathi *et al*. 2010) and nature is found to be closely linked to the obtained greenish-white friable calli of cotyledon explants (4.5 µM NAA and 10 µM Zeatin) in another study (Mohamed *et al*. 2004, Zambre *et al*. 1988).

There are no reports on efficient plant regeneration from epicotyls explants of *Macrotyloma uniflorum*. In *Arachis hypogea,* 90.4 % callus induction was observed with epicotyl-explants in the combination of 0.2 mg/L (NAA) with 0.5 mg/L Kinetin from (Venkatachalam *et al*. 1998).

Various horse gram explants that have been used to regenerate plants via organogenesis such as shoot tip (Tejavathi and Nijalingappa 1989), shoot apices and cotyledonary node (Tejavathi *et al*. 2009), cotyledon (Varisai Mohamed 2005), leaf (Mohamed *et al*. 2004) and seeds (Amal *et al*. 2020). But the present study showed a differential response from the explants tested from paiyur -2 variety of horse gram using cotyledon and epicotyl explants.

Recently, Verma *et al*. (2011) reported differential shoot development response based on the concentration of (TDZ) used in the culture medium. Thus, both (BAP) and (TDZ) are effective cytokinin for shoot organogenesis in horse gram. In the present study, BAP showed effective shoot responses with cotyledon and epicotyls explants was tested (Table 2).

In line with our results, similar results were obtained for best shoot regeneration from

Table 3: Effect of auxins on root induction with different growth regulators and concentration from elongated *in vitro* shoots on callus derived cotyledon and epicotyl explants

Explants		Cotyledon				Epicotyledon			
Plant Growth Regulators (mg/L)		Initiation Days	Percentage of Responses (%)	Mean Number of Roots	Root Length (cm)	Initiation Days	Percentage of Responses (%)	Mean Number of Roots	Root Length (cm)
NAA	0.5	15	59.00±5.77^{bcd}	4.20±1.00^{abcd}	4.56±0.42^{bcde}	24	59.83±1.01^{b}	2.33±0.33^{b}	3.07±0.18^{c}
	1.0	18	68.33±3.33^{ab}	5.66±0.57^{abc}	5.43±0.29^{b}	21	65±0.87^{a}	5.6±0.33^{a}	4.77±0.15^{a}
	2.0	18	65.00±0.00^{bcd}	4.33±1.20^{abcd}	4.63±0.29^{bcde}	21	63.33±0.89^{b}	4±0^{b}	3.73±0.20^{b}
	3.0	16	57.66±3.33^{cd}	3.00±1.52^{bcd}	3.76±0.31^{defg}	23	52±0.58^{c}	3.33±0.33^{b}	2.8±0.15^{a}
	4.0	15	52.00±5.77^{de}	2.43±0.33^{d}	2.96±0.14^{fg}	23	20.33±1.45^{d}	1±0^{c}	1.53±0.14^{d}
BAP+NAA	1.0+0.5	15	61.00±0.00^{bcd}	4.00±1.15^{abc}	4.10±0.66^{cdef}	21	66.67±0.88^{b}	4.67±0.89^{b}	2.9±0.15^{d}
	1.0+1.0	17	**73.33±3.33^{a}**	**7.00±1.00^{a}**	**7.40±0.32^{a}**	22	**69.67±0.88^{a}**	**5.67±0.33^{a}**	**6.33±0.08^{a}**
	1.0+1.5	16	68.33±3.33^{bcd}	6.0±0.88^{abcd}	5.03±0.18^{bcd}	21	57.83±0.60^{c}	3.67±0.33^{a}	5.43±0.17^{b}
	1.0+2.0	16	67.00±5.77^{bc}	5.66±0.57^{ab}	4.50±0.40^{bcde}	21	42.33±0.89^{d}	2.66±0.33^{b}	4.43±0.18^{c}
	1.0+2.5	13	57.66 ± 6.66^{cd}	3.00±1.73^{bcd}	3.56±0.38^{efg}	18	31.67±0.89^{e}	1.85±0.58^{c}	3.13±0.09^{d}
BAP + 2,4-D	1.0+0.5	22	52.00 ± 5.77^{f}	2.33±0.33^{cd}	2.60±0.30^{g}	19	52.5±0.76^{c}	1.33±0.33^{d}	1.67±0.19^{d}
	1.0+1.0	22	59.33 ± 5.77^{ef}	3.33±1.20^{abcd}	3.90±0.37^{cdef}	19	57±0.58^{d}	2±0.00^{c}	3.23±0.78^{c}
	1.0+1.5	24	71.00 ± 0.00^{bcd}	5.00±0.57^{abc}	4.13±0.63^{cdef}	22	68.83±0.44^{c}	4.53±0.33^{b}	3.9±00.06^{a}
	1.0+2.0	21	67.55±0.00^{bc}	4.66±0.88^{abcd}	5.13±0.35^{bc}	24	65.5±0.76^{a}	3±0.00^{a}	3.2±0.11^{b}
	1.0+2.5	21	64.66 ± 3.53^{cd}	3.66±0.66^{abcd}	3.40±0.30^{efg}	20	60.5±1.26^{b}	2.60±0.33^{b}	2.33±0.09^{c}

For each treatment, 50 elongated shoots were used and repeated three times. Values represent the means ± standard error. Mean values followed by the same letters within a column are not significantly different according to Duncan's multiple range test at 5% level.

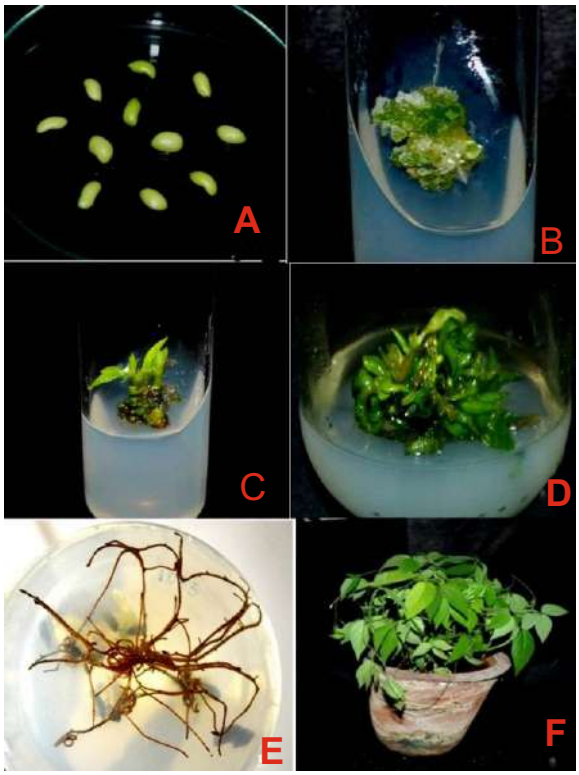

Figure 1 (A-F): - Indirect organogenesis of Horse gram, *Macrotyloma uniflorum* Var. Paiyur- B**.** using cotyledon explants **A.** Cotyledon explants prepared from *in vitro* raised seedlings 2) Nodular and green compact callus induction on MS medium BAP (3.0 mg/L) **C.** Adventitious shoot bud formation on organogenic callus **D.** Proliferation of multiple shoots in BAP+GA3 (1.0+0.5 mg/L) **E.** Regenerated shoots produce roots in BAP + NAA (0.2+1.0 mg/L) **F.** Hardened plants

the callus of *P. vulgaris* on medium supplemented with 5.0 mg/L of (BAP). Also, other reports affirm that (BAP) is effective for shoot induction in *P. vulgaris* (Arellano *et al*. 2009, Mukeshimana *et al*. 2013).

When 0.5 mg (TDZ) were used alone in the MS medium, 0.66 mg of callus fresh weight was observed within 10 days and when (TDZ) is used with a combination of (BAP), the shoot formation is observed from callus. Collado *et al*., 2013 report that the highest callus weight was observed within 21 days in the concentration of 0.04 mg/L (TDZ) with Gamborg B5 medium. But unfortunately, the callus was turned dark brown when the same concentration of hormone was used for shoots induction from callus.

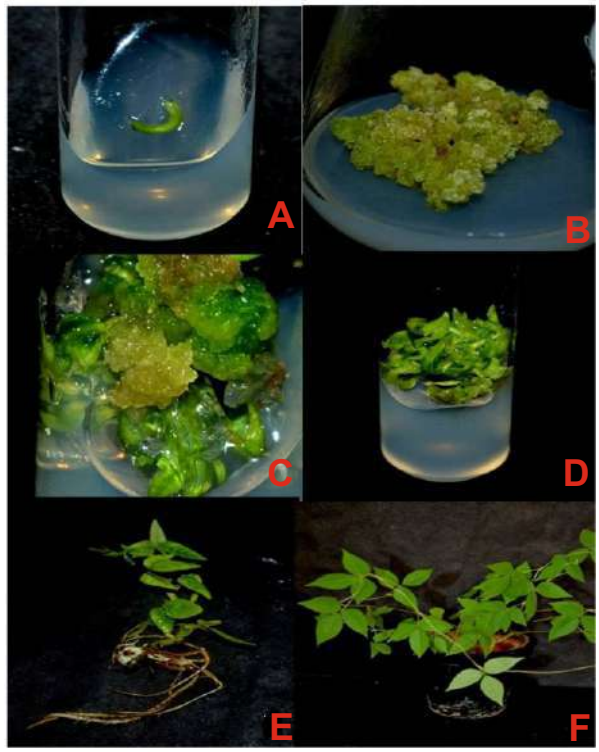

Figure 2 (A-F):- Indirect organogenesis of Horse gram, *Macrotyloma uniflorum* Var. Paiyur-2 using epicotyl explants **A.** Epicotyl explants from *in vitro* germinated seeds **B.** Callus production from Epicotyl explants **C.** Differentiation of induced callus tissue into multiple shoot buds **D.** Proliferation of multiple shoot buds **E.** Elongated shoot buds produced root system **F.** *In vitro* grown seedlings established in the pot

Shoot Regeneration and Elongation: Callus cultured on multiple shoots induction medium containing (BAP+GA_3) 1.0+0.5 mg/L) started to produce adventitious shoot bud formation along with small nodules on organogenic callus pieces of cotyledon explants within 28 days and epicotyledon explants within 31 days. The light green areas of the calli were most competent for adventitious shoot bud differentiation. A cluster of shoot primordia formed in the nodule area and leaf-like structures emerged from the shoot primordia. Maximum shoots of 26 with an average length of 5.13cm and regeneration response of 83% was observed from callus of cotyledon explants and 19 shoots with an average length of 4.23cm and regeneration response of 77% were observed with epicotyls explants supplemented with (BAP+GA_3)

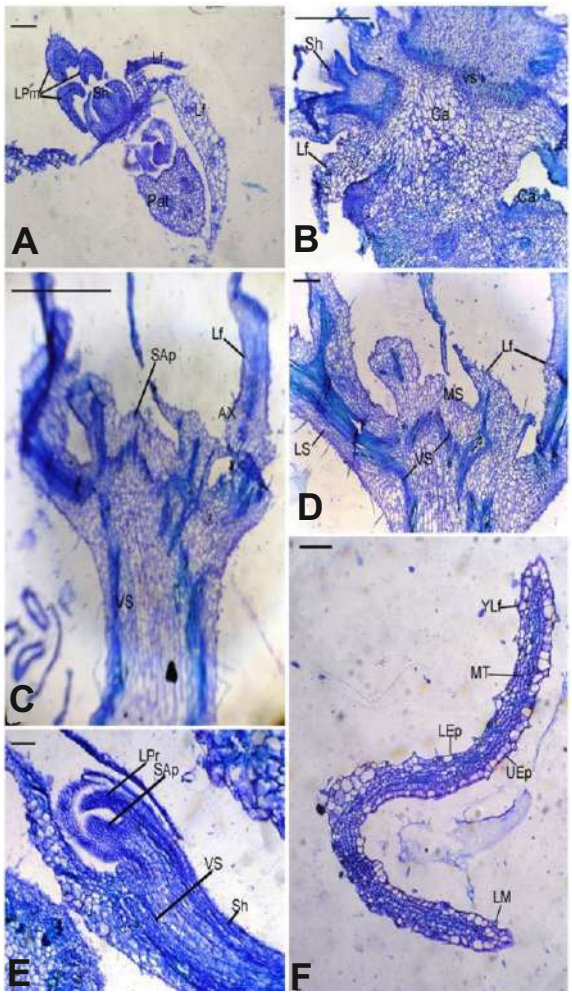

Figure 3(A-F):-- Histological section of Horse gram, *Macrotyloma uniflorum* Var. Paiyur-2 regenerating callus showing initial development of shoot buds **A.** T.S of shoot apex of young shoots developed by the callus. **B.** T.S of callus showing vascular cylinder and axillary formed in the axil of a leaf. **C.** Callus masses from which a shoot complex develops. **D.** L.S of shoot complex formed from the callus. **E.** L.S of young shoot, with shoot apex and leaf primordia. **F.** T.S of young leaves produced by the callus. Abbreviations: LPm-Leaf Primordia; Pet-Petiole; Sh-Shoot Primordia; VS-Vascular Strand; Ca-Callus; Lf-Leaf; Ax-Axis of the Shoot; MS-Main Shoot; SAp-Shoot Apex; MT-Mesophyll Tissue; UEp-Upper Epidermis; LEp-Lower Epidermis; LM-Leaf Margin; Ylf- Young Leaf

1.0+0.5 mg/L (Table 2). However, as the concentrations of both BAP and GA3 increased, the regeneration efficiency was decreased gradually. The present study reported more efficient and producible outcomes when compared to similar studies reported earlier (Tejavathi *et al*. 2010; Venkatachalam *et al*.1988).

It is suggested that (GA_3) along with the cytokinin stimulates the development of shoot primordial induced by (BAP) (Ghulam *et al*. 2017). Adding GA_3 to (BAP) containing media at any concentration has been reported to improve the frequency of somatic embryogenesis (Li *et al*. 2002). GA_3 stimulates the production of numerous enzymes, notably α-amylase, in germinating cereal grains. Besides, (GA_3) Gibberellic acids promote seed germination in some species that otherwise require cold stratification and/or light for inducing seed germination (Davies, 1995). Experimental results suggest that the *Gibberellin Responsive* gene (*HvGR*) (Localized to pockets of subepidermal cells from where shoot primordial originate) is responsible for (GA_3) induced shoot induction. (*HvGR)* shows a high level of expression in the regeneration stage of the initiated shoots where the signal was localized primarily in the developing shoot primordial (Seong *et al*. 2004).

Shoot regeneration was also induced from cotyledon and nodal explants for six cultivars from other regions of the world (Hamdy and Hattori, 2006a, b). The percentage of adventitious shoot development was varied from 0-55.1% depending on the cultivar, type and concentration of growth regulators (Hamdy and Hattori 2006a). Edyta *et al*. (2012) reported along with (NAA) and (BAP) supplementation of (GA_3) was increases the callus viability and shoot regeneration by independent of genotype and tannin content, in contrast to other reports (Hamdy and Hattori, 2006, Bahget *et al*. 2008).

Rooting and Acclimatization: The recalcitrant nature of legumes to rooting in culture conditions has limited the successful application of any biotechnological approaches for crop improvement. The auxins (2,4-D) and (NAA) at various concentrations are commonly used to induce rooting from the

explants in both *in vitro* and *in vivo* cultures. Rooting is much favored when auxins are used along with cytokinins whereas 73.33% (Table 3) root formation (7 roots of 7.40cm length) was observed in the callus derived from cotyledon explants and in the case of epicotyl derived callus, 69.67% root formation was observed with 5.67 roots of 6.33cm in length when treated with 1.0mg/L of (BAP) and 1.0mg/L (NAA) within 17 and 22 days after exposure to rooting medium, respectively.

Regeneration of shoots from both cotyledon and epicotyls was found to occur via the indirect organogenesis method. It is noteworthy that more shoots were differentiated on the cotyledon-derived callus compare to the epicotyl-derived callus. It indicates that lower cytokinin concentrations and a significantly higher amount of auxin ratio were suitable for root induction. The well-rooted plantlets were transferred to plastic cups containing sterile sand, soil, and vermiculite (1:1:1 v/v/v). 84% percent of the plantlets that survived during acclimatization and acclimatized plants (Fig 1&2(6) were transferred to the greenhouse. The regenerated plants did not show detectable variation in morphological or growth characteristics compared to the parent plant. Whereas reports show that about 60% of survival plants were achieved using soil:sand:manure (1:1:1) (Tejavathi *et al*. 2010) and about 55% of survival plants were achieved using Vermiculite: sand and red soil mixture (1:1:1) was tested (Mohamed *et al*. 2005).

In vitro induction of organogenesis depends on the endogenous concentration of plant growth regulators, their distribution in the cultured tissue, and interaction with an exogenously supplied growth regulator. Efficient (83%) shoot organogenesis was observed using (BAP) in combination with (GA_3) from cotyledon derived callus as the similar effect of this combination was noted previously (Ananthakrishnan *et al*. 2003).

To date, there are reports available on the culture of horse gram with various explants derived from the reliable protocol for mass multiplication of plantlets (Tejavathi *et al.*, 2010). It has been suggested that the tissue culture of legumes from cotyledon explants has been regarded as a good explants source. In this study, were successfully produced from the embryogenic callus of *M. uniflorum* from cotyledon and epicotyl explants in the indirect organogenesis method.

The explants (young petals and leaves) carrying different sets of epigenetic regulators will probably decide the regeneration conditions (for example, exogenous amino acids and plant growth regulators in media) and affect the regeneration outcomes (for example, cytosine methylation variation in regenerates) by mediating responses to external stimuli and initiating epigenetic alterations that influence adaptation to stresses (Miguel and Marum 2011).

With proper selection of explants and optimization of the culture medium and hormones, *in vitro* micropropagation of this plant can be carried out successfully. The media described in this paper for horse gram regeneration was independent of the genotype.

Histological studies: Histological observations revealed that the origin of shoot buds directly from the cultures of cotyledon and epicotyls raised on (MS+BAP) 3.0 µM. As the callus grows, it produces small shoots at several points of the callus. The shoot primordial has shoot apex with young leaf primordial. The leaf primordia are curved with shortleaf lamina. The mature leaf produced a well-developed lamina with homogenous mesophyll tissue and lateral veins. The callus has a well-differentiated vascular cylinder with xylem and phloem. When the shoot develops from the callus, the vascular traces originate from the main vascular cylinder of the callus and enter into the shoot axis. From the shoot axis, the vascular traces enter into the leaves to form the veins. The young leaves have a small collateral vascular bundle and wide

parenchymatous shows ground parenchyma cells. Small non-glandular trichomes are common in the outer (lower) surface of the lamina. The shoot apical meristem has cytoplasmic callus forming lateral initials of leaf primordial and it was grow into mature leaves which possess district midrib and lateral veins, young leaves are folded into V- or U-shaped outline (Fig 3).

CONCLUSION

This study developed an efficient and reproducible regeneration protocol via indirect organogenesis from the cotyledon and epicotyl explants of horse gram, var. paiyur-2. Freshly collected seeds are optimal for callus formation without affecting the regeneration capability of calli with anatomical proof. The formation of calli strongly determines the explant's type and seed age. The number of shoots per callus was dependent on both the concentration of (BAP) used during callus proliferation and the combination of (BAP) with (GA_3) concentration used for shoot formation and elongation. The regeneration frequency that we reported is high when compared with the results obtained in the previous studies. The present study concluded that established protocol applies to two different explants and may therefore be used to regenerate other genotypes. The results presented here are expected to be helpful for genetic transformation study to improve the traits of the cultivars.

REFERENCES

Amal TC, Karthika P, Dhandapani G, Selvakumar S and Vasanth K 2020 A simple and efficient Agrobacterium mediated in planta transformation protocol for horse gram (*Macrotyloma uniflorum* Lam. Verdc.). *J. Gen. Eng. Biotech.* **18** 1-9.

Ananthakrishnan, G.X, Xia C, Elman S, Singer HS. Paris A, Gal-On and Guba V 2003 Shoot production in Squash (*Cucurbita pepo*). by *in vitro* organogenesis. Pl. Cell Rep. **21** 739-746.

Bahget S, Shabban OA, EL-Shiny O, Lightfood DA and EL-Shemy HA 2008 Establishment of the regeneration system for *Vicia faba* L. *Curr. Issues Mol. Biol.* **11** 47-54.

Bolbhat SN and Dhumal KN 2010 Desirable mutants for pod and maturity characteristics in M_2 generation of horsegram [*Macrotyloma uniflorum* (Lam.) Verdc]. Research on Crops. **2** 437-440.

Chatenet M, Delage C, Ripolles M, Irey M, Lockhart BLE, Rott P 2001 Detection of sugarcane yellow leaf virus in quarantine and production of virus-free sugarcane by apical meristem culture. *Pl. Dis*. **85** 1177-1180.

Davies PJ 1995 *The plant hormones: their nature, occurrence, and functions. In: Plant hormones: physiology, biochemistry, and molecular biology.* Kluwer Academic Publishers, Boston, Pp 13-38.

Gatcia A, Munoz Valverde J, Ramírez Fonseca P and Valdez Melara M 2010 *In vitro* plant regeneration system for common bean (*Phaseolus vulgaris*): effect of N6-benzylaminopurine and adenine sulphate. *Electron. J. Biotech.* **13** 6–7.

Hamdy MA and Hattori K 2006a Regeneration of (*Vicia faba* L.) cultivars from mature seed cotyledons. *Asian J. Pl. Sci.* **5** 623-629.

Hamdy MA and Hattori K 2006ab *In vitro* micropropagation of (*Vicia faba* L). cultivars 'waza soramame' and 'Cairo 241' by nodal explants proliferation and somatic embryogenesis. *Biotech.* **5** 32-37.

Harter HL 1960 Critical values for Duncan's new multiple range test. *Biometrics*. 671-685.

Hussain A, Qarshi IA, Nazir H and Ullah I 2012 Plant tissue culture: current status and opportunities. *Rec. adv. in pl. in vitro cul*. 1-28.

Johansen DA 1940 *Plant Microtechnique*. Mc Graw Hill Book Co; New York

Kawsar SMA, Huq E and Nahar N 2008 Cytotoxicity assessment of the aerial parts of (*Macrotyloma uniflorum* (Lam.) Verdc). *Int. J. Pharmacol.* **4** 297-300.

Li X, Krasnyanski SF and Korban SS 2002 Somatic embryogenesis, secondary somatic embryogenesis, and shoot organogenesis in Rosa. *J. Pl. Physiol.* **159** 313-319.

Miguel C, Marum L 2011 An epigenetic view of plant cells cultured *in vitro*: somaclonal variation and beyond. *J. Exp. Bot.* **62** 3713–3725.

Mohamed SV, Wang CS, Thiruvengadam M and Jayabalan N 2004 *In vitro* plant regeneration via somatic embryogenesis through cell suspension cultures of horse gram *Macrotyloma uniflorum* (Lam.) Verdc. *In vitro cell Dev. Biol-Pl.* **40** 284-289.

Mohamed VS, Jih-Min S, Toong-Long J, Chang-Sheng W 2005 Optimization of Somatic embryogenesis in suspension cultures of horse gram (*Macrotyloma uniflorum* (Lam.) Verdc.]-A hardy grain legume. Sci. Horti. **106** 427-439.

Murashige T and Skoog F (1962) A Revised Medium for Rapid Growth and Bio Assays with Tobacco Tissue Cultures Physiol. Plant **15**.

Murphy C and Fuller DQ 2017 Seed coat thinning during horse gram (*Macrotyloma uniorum*) domestication documented through synchrotron tomography of archaeological seeds. *Sci. Rep*. **7** 1-9.

O'Brien TP, Feder N and Mc Cull ME 1964 Poychromatic Staining of Plant Cell walls by toluidine blue-O. *Protoplasma* **59** 364-373.

Raza G, Singh MB and Bhalla PL 2017 *In vitro* plant regeneration from commercial cultivars of soybean. *BioMed. Res. Int*.

Reddy P C O, Sairanganayakulu G, Thippeswamy M, Reddy PS, Reddy MK and Sudhakar C 2008 Identification of stress-induced genes from the drought tolerant semi-arid legume crop Horse gram (*Macrotyloma uniflorum* (Lam.) Verdc). through analysis of substracted expressed sequence tags. *Pl. sci.* **175** 372-384.

Rout GR, Mohapatra A and Jain SM 2006 Tissue culture of ornamental pot plant: A critical review on present scenario and future prospects. *Biotech. Advan.* **24** 531-560.

Sass JE 1940 *Elements of Botanical Microtechnique*. Mc Graw Hill Book Co; New York

Seong RC, Kim JY, Haam JW and Seo YW 2004 *Isolation and Characterization a Gibberellin Responsive Gene (HvGR) from initiated shoots from calli derived from mature embryo of barley. In: Proceedings of the 4th International Crop Science Congress, Brisbane, Australia. Published on website.* URL: www.cropscience.org.au/icsc2004.

Skrzypek E, Czyczylo-Mysza I and Marcinska I 2012 Indirect organogenesis of Faba bean (*Vicia faba* L. Minor). *Acta boil. Cracov. Bot.* **54** 102-108.

Tejavathi DH and Nijalingappa BHM 1989 Shoot tip culture in *Dolichos biflorus* L. *Reprinted from Curr. Sci.* **58** 1385-1388.

Tejavathi DH, Devaraj VR, Savitha M, Anitha P and Nijagunaiah R 2010 Regeneration of multiple shoots from the callus cultured of *Macrotyloma uniflorum* (Lam.) Verdc. *Indian J. Biotech.* **9** 101-105.

Venkatachalam P, Geetha N and Jayabalan N 1998 Influence of Growth Regulators on Plant Regeneration from Epicotyl and Hypocotyl

Cultures of Two Groundnut *(Arachis hypogea* L.) Cultivars. *J. Pl. Biol.* **41** 1-8.

Verma K, Rani A and Saini R 2011 An efficient plant regeneration system from half seed explants of soybean [*Glycine max* (L.) Merrill] using thidiazuron. *Soybean. Research*. **8** 12–23.

Zambre MA, De Clercq J, Vranová E, Van Montagu M, Angenon G and Dillen W 1998 Plant regeneration from embryo-derived callus in *Phaseolus vulgaris* L. (common bean) and *P. acutifolius* A. Gray (tepasry bean). *Pl. Cell Rep.* **17** 626-630.

Vegetos
https://doi.org/10.1007/s42535-021-00218-w

RESEARCH ARTICLES

Plant regeneration from direct organogenesis of *Pandanus canaranus* Warb, an endemic medicinal plant

Venkatachalam Balamurugan[1] · Palanisamy Karthika[1] · Gurusamy Dhandapani[2] · Kumarasamy Pradeepa Veerakumari[3] · Krishnan Vasanth[1]

Received: 12 June 2020 / Revised: 15 April 2021 / Accepted: 19 April 2021
© Society for Plant Research 2021

Abstract

Pandanus canaranus is an endemic medicinal plant that has been used for traditional medicines and many pharmaceutical applications. The current study is the first report for a development of efficient protocol for in vitro regeneration by direct or indirect organogenesis, which is necessary for the conservation of this important medicinal plant species. In the current study, we standardize the culture medium supplemented with different plant growth regulators (PGRs) of various concentrations using shoot tip, leaf, shoot and root meristematic explants. The shoot and root meristematic explants did not produce any callus whereas, leaf explants initiated callus combination with 1.5 mgl^{-1} of each 2ip + BAP PGRs. But, there was no further development and the callus was also browned in each and every subculture on same combination of the medium contains PGRs. After various PGRs and different concentration tested, cytokinin and auxins were influenced and showed multiple shoots formation from the shoot tip explants. The maximum number of multiple shoots and shoot length (elongation) were observed with 4 mgl^{-1} 2ip and 3 mgl^{-1} of each BAP + GA_3, respectively. Further, maximum number of root induction/development from elongated shoots were observed in the MS medium supplemented with 3 mgl^{-1} IBA. As per our knowledge and references, current study is the first report of successful development and establishment of in vitro regeneration in *P. canaranus*.

Keywords *Pandanus canaranus* · Endemic · Medicinal plant · Regeneration · Acclimatization

Abbreviations

PGRs	Plant growth regulators
MS	Murashige and Skoog
BAP	6-Benzylaminopurine
2ip	Isopentenyl adenine
GA_3	Gibberellic acid
IBA	Indole-3-butyric acid
NAA	Naphthalene acetic acid
Z	Zeatin
ANOVA	Analyze of variance

Introduction

Pandanus canaranus belongs to the family Pandanaceae. The plants primarily grow in Alappuzha, Pathanamthitta, Palakkad, Kannur, Kozhikkode, Wayanad districts in Kerala, India (Sasidharan 2004). More than seven hundred species of *Pandanus* genus were reported and distributed in subtropical and tropical regions; approximately 30–40 species are known to occur in India (Charterjee and Pakrashi 2001; Jose et al. 2016). This plant is also called as "pandan" and is native to Asia and tropical regions of Australia. The leaves are commonly used for Southeast Asian food preparation (Thomson et al. 2006). The five cultivated species, such as *P. tectorius*, *P. amaryllyfolius*, *P. utilis*, *P. boninesis* and *P. pygmaeus* are used for commercial purposes (Stone 1974). Though, a majority of species are spiny, some spineless garden varieties have been reported. Moreover, *P. leram* acts as barrier against encroachment of the sea and thus protects human settlements along the coast lines (Panda et al. 2000). Previous studies also discovered that coastal vegetations can play a considerable role in reducing the kinetic

✉ Krishnan Vasanth
vasanthlabbu@gmail.com

[1] Department of Botany, School of Life Sciences, Bharathiar University, Coimbatore, Tamil Nadu 641 046, India

[2] Department of Botany, Kongunadu Arts and Science College (Autonomous), Bharathiar University, Coimbatore, Tamil Nadu 641 029, India

[3] Department of Statistics, Bharathiar University, Coimbatore, Tamil Nadu 641 046, India

energy from a potential tsunami (Mascarenhas and Jayakumar 2008; Thuy et al. 2012). This species is widely planted in seashores for tsunami force mitigation (Paterson 2008). Anthropogenic destruction of *Pandanus* plants from its usual habitats along rivers, sea shores, and land water bodies and their substitution with concrete, stone or other structures is among the major reasons for slow decline of screw pines (Raina et al. 2004; Jose et al. 2016). It is important that we replenish these bio resources via technical intervention due to the challenges involved. Simultaneously, particular consideration has to be accorded to the very slow growing nature and to the actuality that there is shrinkage of suitable costal area with the specific microclimatic environment required for growth (Jose et al. 2016). The *Pandanus* genus has a lot of natural product which is used for a flavoring and food preparation (Son 2019). The leaves and fruits from this family are used to treat cold/flu, hepatitis, asthma, boils, and cancer, (Meilleur et al. 1997) and fruits are staple foods in Micronesia include the Marshall Islands, Federated States of Micronesia and Kiribati provide that up to 50% of energy intake, the main staple food in Nauru (Kayser 2002). Adults regularly consume 20–50 keys every day during the main fruiting seasons (Englberger 2003; Adkar and Bhaskar 2014). Especially, *P. tectorius* fruits have 60–70% of polyphenols were proved and valuable for human health (Wu et al. 2019).

This plant can be regenerated through growth and development of existing axillary and apical shoots or apical meristems or regeneration of adventitious shoots. The adventitious buds and shoots are formed de novo and meristem start from explants. Micropropagation has become a significant part of the possible propagation of several plants system (Razdan 2003; Iliev et al. 2010). The mass propagation of homogeneous, healthy plants through tissue culture is the only viable technique for production of huge numbers of cloned plants in a short time (Amoo et al. 2012). Conventional propagation is not always sufficient to produce large pool of plants to be used for germplasm conservation during reintroduction (Behera et al. 2018). However, so far only few studies are available on in vitro propagation in *Pandanus* species. Therefore, the present study is aimed to investigate the effects of various concentrations of plant growth regulators (PGRs), on in vitro organogenesis from various explants to establish a suitable and reproducible protocol for in vitro development of *P. canaranus*.

Materials and methods

Explant preparation and surface sterilization

The plants were initially collected from Nilgiri district, Gudalur village, Tamil Nadu and established in the green house, Department of Botany, Bharathiar University Coimbatore, Tamil Nadu, India. The plant specimen was referred and authenticated by Botanical Survey of India (Identification No: BSI/SRC/5/23/2016/Tech/1788), Southern region of Coimbatore. The leaf and shoot tip (Fig. 1) explants were used for surface sterilization by washing using running tap water for 20 min followed by 2% sodium hypochlorite for 5 min. Further, sterilized with 70% ethanol for 10 min and treated with 0.2% mercuric chloride ($HgCl_2$) for 10 min. Finally, the explants were washed 2 or 3 times in sterile double distilled water following which, the surface sterilized explants were inoculated to medium supplemented with various growth regulator combinations under aseptic conditions.

Media and culture condition

Murashige and Skoog (1962) medium was supplemented with 30 gl^{-1} sucrose and solidified with 0.8% agar. The pH of the medium was adjusted to 5.8 and then autoclaved at 121 °C for 15 min. Thermo-liable growth regulators were added to the post autoclaved media and distributed in to test tubes or tissue culture jars under aseptic conditions. The explants inoculated in culture tubes were incubated at 25 ± 2 °C under 16 h light and 8 h dark conditions; irradiance was provided by cool white fluorescence light (Philips, India).

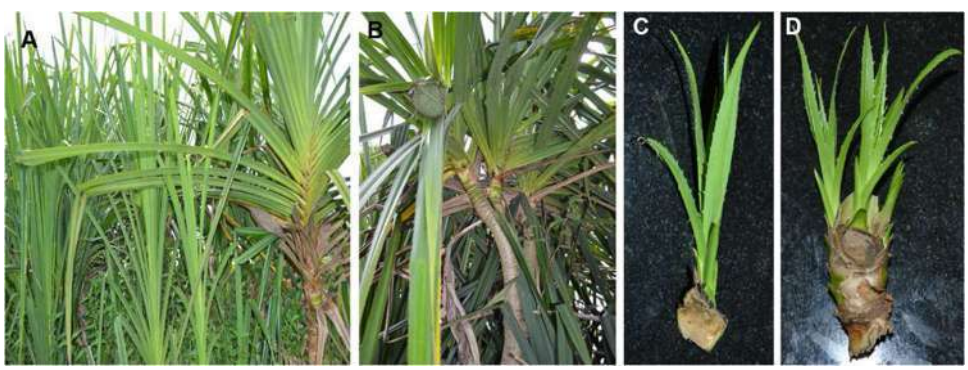

Fig. 1 *Pandanus canaranus* habitat and explants used for the in vitro culture. **a**, **b** Well established plants in the university campus, **c**, **d** shoot tip explants

Callus induction

The leaf segments, about 5–8 mm in length were excised to employ as explants for callus formation (Fig. 2). Various concentrations and combinations of cytokines and auxins were used such as, BAP (1.0–5.0 mgl^{-1}), BAP + 2ip, (0.5–2.5 mgl^{-1}), BAP + Z (1.0–5.0 mgl^{-1}) and BAP + Z + NAA (1.0–4.0 mgl^{-1}) were tested for the induction of different types of callus and the frequency (%) of callus induction was measured.

Shoot regeneration

Shoot tip explants (Fig. 3) were grown on MS medium supplemented with various growth regulators with different concentrations used for direct organogenesis such as, 2ip (1.0–7.0 mgl^{-1}) and 1–5 mgl^{-1} of each Z, BAP, BAP + NAA, BAP + Z, BAP + 2ip for shoot organogenesis. After 25 days post inoculation of the explants, shoot tips were subcultured in to fresh media, followed by two more rounds of subculture until a multiple healthy shoots were obtained. The percent of shoot organogenesis and average number of shoots per explant was recorded. The regenerated and multiplied shoots were transferred to shoot elongation medium containing 1.0–5.0 mgl^{-1} of each GA_3 alone and in combination with BAP.

Root formation

The elongated shoots (3–5 cm long) were subcultured in the medium supplemented with 1.0–5.0 mgl^{-1} of NAA and IBA for adventitious rooting development. The number and length of the roots was observed followed by calculation of percent root formation.

Acclimatization

The plantlets regenerated through direct organogenesis from shoot tip explants were gently washed with sterile distilled water to eliminate the adhering agar. Moreover, the plantlets were once again washed with half strength MS medium without any hormones and transferred to the plastic pots containing a soilrite for a week in the culture room for initial acclimatization. Thereafter, the acclimatized plants were transferred to plastic pots containing red soil: vermicompost: sandy soil (1:1:1 ratio) in the greenhouse to establish complete plants.

Statistical analysis

All the experiments were performed thrice with 10 replicates for each experiment and the results were analyzed by one-way ANOVA to calculate the significance of difference among the treatment means compared using Duncan's

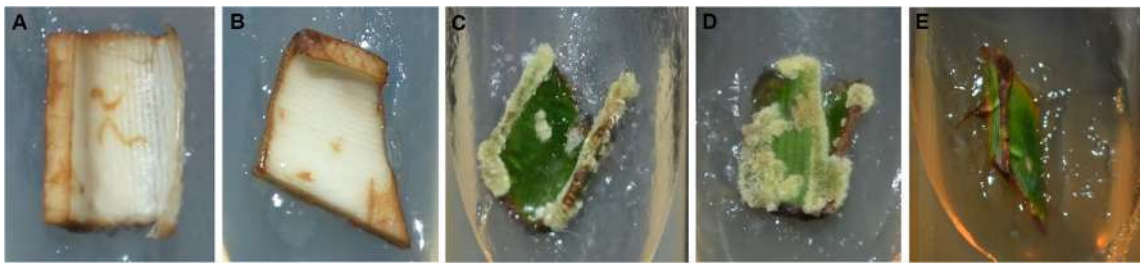

Fig. 2 In direct organogenesis of *P. canaranus* using leaf explants. **a**, **b** Leaf explants, **c**, **d** initiation of callus, **e** phenolic compounds segregation

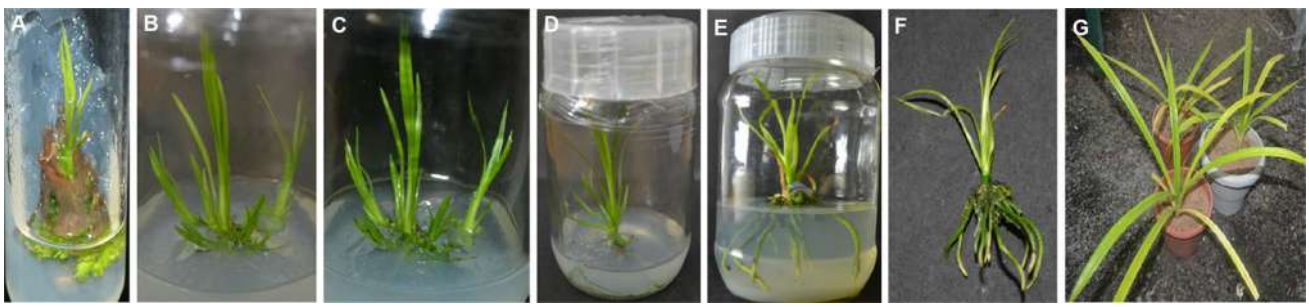

Fig. 3 Direct organogenesis of *P. canaranus* using shoot tip explants. **a** Shoot tip explants inoculated in the culture medium. **b, c** Multiplication, regeneration and elongation of shoots, **d**, **e** initiation and development of root system from elongated shoots, **f** well established plantlets, **g** plantlets transferred to pots for acclimatization

Multiple Range Test (DMRT) at $P < 0.05\%$ level using by IBM SPSS 20 software.

Result and discussion

Effect of plant growth regulators on callus induction

Of the *P. canaranus* leaf explants inoculated in MS-medium supplemented with different combination and concentration of plant growth regulators, callus induction was higher (57.33%) with a combination of 1.5 mgl^{-1} of each BAP and 2ip hormones. White friable callus was observed within 45 days after inoculation of leaf explant with the above hormonal combination (Table 1 and Fig. 2). While other combinations, such as BAP + Zeatin showed between 29.99 and 35% white friable callus inductions with 1–5 mgl^{-1} of each hormones were tested and also duration of the callus induction increased from 45 to 60 days. The 1.0–4.0 mgl^{-1} of BAP alone tested showed 26.00–32.75% white friable callus induction within 60 days. Further, BAP + NAA + Zeatin (each 1.0–4.0 mgl^{-1}) combination tested showed higher percent (37.25%) white friable callus induction with 4 mgl^{-1} of each hormone tested, while other concentrations reduced the callus induction from 37.25 to 21.70% at 50 days post inoculation of the explants. All three different hormone concentrations and combinations tested showed white friable callus whereas, the explants inoculated with kinetin alone did not respond to any callus induction even after 60 days of culture with 1.0–5.0 mgl^{-1} hormones tested (Table 1). However, the callus initiated from the leaf explants did not develop and produced mature calluses and organogenesis. Because, the leaf explants released phenolics that exudate to medium even with repeated subculture to fresh medium. In previous study reported that *P. canaranus* leaves were observed as rich of secondary metabolites such as flavonoids, phenols and tannin (Balamurugan et al. 2020). In addition to that, the shoot and root meristem (Table S1 & Fig. S1) were tested for culturing in the medium supplemented with 1.0–5.0 mgl^{-1} of each combination with BAP + Zeatin, BAP + 2ip, BAP + NAA + Zeatin and 0.5–2.5 mgl^{-1} of 2,4-D alone. With these hormonal combinations and concentrations tested by using shoot and root meristem, none of them induced or responded any callus even at 60 days post culture and consequently, the explants were secreted phenolics contents to the medium (Table S1 & Fig. S1).

Generally, auxins are necessary for callus induction and proliferation, while redifferentiation of callus and formation of organized structure is brought about with a combination of both cytokinins and auxins (Wang et al. 2008; Dhir et al. 2014). Several other studies have demonstrated

Table 1 Effect of different concentration of plant growth regulators on callus induction from leaf explants

PGRs (mgl^{-1})			Number of days	Callus induction (%)	Callus type and colour
Control			60	[a]	[a]
BAP	Z				
1	1		60	29.66 ± 1.04^{f}	WF
2	2			32.33 ± 0.76^{ef}	WF
3	3			35.00 ± 0.50^{de}	WF
4	4			40.00 ± 2.17^{cd}	WF
5	5			34.66 ± 0.28^{de}	WF
BAP	2ip				
0.5	0.5		45	35.00 ± 1.80^{de}	WF
1	1			43.33 ± 0.76^{cd}	WF
1.5	1.5			57.33 ± 0.57^{a}	WF
2	2			51.00 ± 2.02^{b}	WF
2.5	2.5			45.33 ± 1.52^{c}	WF
BAP					
1			60	26.00 ± 2.91^{fg}	WF
2				32.75 ± 2.28^{ef}	WF
3				30.25 ± 3.68^{efg}	WF
4				26.00 ± 2.04^{fg}	WF
BAP	Z	NAA			
1	1	1	50	21.50 ± 4.62^{g}	WF
2	2	2		33.50 ± 0.64^{e}	WF
3	3	3		36.50 ± 0.64^{d}	WF
4	4	4		37.25 ± 0.47^{d}	WF
Kinetin					
1			60	[a]	[a]
2				[a]	[a]
3				[a]	[a]
4				[a]	[a]
5				[a]	[a]

WF white friable callus

Values are represented as means ± standard error (SE) of triplicate determinations and experiments with 10 replicates

Means significantly different to DMRT at ($P \leq 0.05$)

[a]No respond

that the MS-medium is one of the best medium for callus initiation and plant regenerations (Chaudhury and Qu 2000; Jain et al. 2005; Zhang et al. 2007). PGRs play an important role in the induction and development of callus from explants. The 2,4-D was induced high level of callus initiation in some grass species (Li et al. 2006). Further, combination of BA with 2,4-D, NAA and IBA, were effectively induce the callus formation in *Gleditsia caspica* (Zarinjoei et al. 2014). A research study by Wakte et al (2009) observed and demonstrated that, 2,4-D induced fragile callus from lateral bud explant of *P. amaryllifolius*.

Effect of plant growth regulators on shoot induction and elongation

Direct organogenesis is regarded as one of the most reliable method for clonal propagation as it upholds genetic homogeny among progenies. Various concentrations of cytokinins and auxins were tested for shoot induction using shoot bud explants. Explants inoculated with 1.0–7.0 mgl^{-1} 2ip showed 3.75–12.25 shoots per explant. Further, maximum number of shoots per explant were observed using with 4 mgl^{-1} 2ip at 75 days post inoculation of the explants (Table 2 and Fig. 3). Followed by, explants inoculated with 1.0–5.0 mgl^{-1} of BAP showed 2.25–5.50 shoots per explant at 95 days post incubation and maximum number of shoots were observed with 4 mgl^{-1} BAP. In medium exposed with Zeatin showed 2.75–8.25 shoots per explant at 95 days post incubation and maximum number of shoots was observed with 4 mgl^{-1} Zeatin (Table 2). In addition to that, explants exposed to 1.0–5.0 mgl^{-1} of BAP + Zeatin medium showed 2.0–5.0 shoots per explant at 90 days post incubation and maximum number of shoots was observed with 2 mgl^{-1} of each BAP and Zeatin tested. Finally, the explants exposed with 1.0–5.0 mgl^{-1} of each BAP and 2ip combination showed 5.0–10.75 shoots per explant at 85 days post culture and maximum number of shoots were obtained with 3 mgl^{-1} of each BAP and 2ip used (Table 2). In conclusion, the present study showed variation in the response of explants with different growth regulators and results showed that 4 mgl^{-1} of 2ip alone tested induced and developed good multiple microshoots.

Table 2 Effect of different growth regulators on shoot induction from shoot tip explants

PGRs (mgl^{-1})		Number of days	Number of shoots
Control		95	00
2ip			
1		75	3.75 ± 0.25^{hi}
2			5.00 ± 0.40^{efg}
3			8.00 ± 0.40^{c}
4			12.25 ± 0.47^{a}
5			10.00 ± 0.40^{b}
6			7.25 ± 0.47^{cd}
7			4.00 ± 0.40^{gh}
BAP			
1		95	2.25 ± 0.25^{jk}
2			3.00 ± 0.40^{hij}
3			4.50 ± 0.28^{gh}
4			5.50 ± 0.28^{ef}
5			2.74 ± 0.25^{j}
Z			
1		95	2.75 ± 0.28^{j}
2			4.00 ± 0.40^{gh}
3			5.50 ± 0.28^{ef}
4			8.25 ± 0.47^{c}
5			7.00 ± 0.40^{d}
BAP	Z		
1	1	90	2.50 ± 0.28^{j}
2	2		5.00 ± 0.40^{efg}
3	3		3.50 ± 0.28^{hi}
4	4		2.50 ± 0.28^{j}
5	5		2.00 ± 0.40^{jk}
BAP	2ip		
1	1	85	5.25 ± 0.47^{ef}
2	2		8.00 ± 0.40^{c}
3	3		10.75 ± 0.47^{b}
4	4		6.25 ± 0.25^{de}
5	5		5.00 ± 0.40^{efg}

Values are represented as means ± standard error (SE) of triplicate determinations and experiments with 10 replicates. Means significantly different to DMRT at ($P \leq 0.05$)

For shoot elongation, regenerated shoots were subcultured into MS medium supplemented with 3 mgl^{-1} of BAP and GA_3 and a showed maximum shoot elongation (6.0 cm) at 40 days post culture (Table 3). Further, the length of the shoot elongation was reduced from 6.0 to 3.25 cm when the concentration of the both hormones were increased or decreased. While, GA_3 alone was tested, the maximum shoot elongation was observed at 3.75 cm 40 days post culture (Table 3). Cytokinins have a positive effect for axillary bud proliferation and coefficients of axillary shoots. Jana and Shekhawat (2011a, b) and Balamurugan et al. (2019) already reports the mass multiplication of *Gloriosa superba* using leave explants through in vitro culture technique. When increased, the concentration of cytokinins also increased

Table 3 Effect of shoot elongation with different growth regulators from in vitro generated shoots

PGRs (mgl^{-1})		Number of days	Shoots length (cm)
Control		40	00
GA_3			
1		40	2.00 ± 0.40^{e}
2			3.75 ± 0.47^{bc}
3			3.25 ± 0.25^{bcd}
4			2.50 ± 0.28^{cde}
5			2.25 ± 0.25^{de}
BAP	GA_3		
1	1	0	3.50 ± 0.28^{bc}
2	2		4.00 ± 0.40^{bc}
3	3		6.00 ± 0.70^{a}
4	4		4.25 ± 0.47^{b}
5	5		3.25 ± 0.75^{b}

Values are represented as means ± standard error (SE) of triplicate determinations and experiments with 10 replicates

Means significantly different to DMRT at ($P \leq 0.05$)

the number of shoots (Liang et al. 2020). The lower concentration of auxin and cytokinin promoted the morphogenic response exhibit a synergistic effect. Recently, in vitro regeneration by using shoot tip explants exposed to MS medium containing cytokinins (BA, mT, or Kn) and auxins (NAA, IAA) in different concentrations and combinations showed stimulatory effect on the regeneration in *Pterocarpus marsupium* (Ahmad et al. 2020). The tender leaf segments inoculated on MS media supplemented with different concentrations of 2,4-D exhibited differential responses in callus initiation in *Phoenix dactylifera* L. (Kurup et al. 2014). The multiple shoot bud proliferation was observed with 0.022 mM of BA tested with stepwise sub-culture of *P. amaryllifolius* (Gangopadhyay et al. 2004). The broad range of BAP and NAA are mainly suitable media composition for shoot growth and development was reported (Tripathi et al. 2018).

There are few reports on micropropagation of *Stevia* plantlets with different explants used for direct and indirect regenerations (Mathur et al. 2017). The number of shoots increased when increasing the BAP and constant level of Kinetin concentration, further there was insignificant changes of shoot proliferation with increased Kinetin level and study showed that differential responses with each cytokinine was tested in *P. amaryllifolius* (Thimmaraju et al. 2005). Organogenesis is a complex morphogenetic process that involves the formation of monopolar structures of certain appearance to shoots or roots. Sometimes, cytokinins combined with auxins induced the *in-vitro* shoot organogenesis (Saxena et al. 1992). The absence of any kind of growth regulator did not produce any shoot proliferation (Dhir and Shekhawat 2014a, b). In *Gloriosa superba,* desirable shoot regeneration was observed from corm buds calluses in half strength MS medium supplemented with minor concentration and combination of cytokinins. But shoot initiation was decreased, while concentration of cytokines was increased (Arumugam and Gopinath 2012). Indirect regeneration methods often lead to the somaclonal variation and direct regeneration is essential to obtain the true type of plants (Ahmad and Anis 2005). The shoot apex explant is an excellent choice for plant regeneration in monocots (Ceasar and Ignacimuthu 2010; Ramakrishnan et al. 2013) and induced multiple buds when culturing medium was supplemented with 2ip (Sharmin et al. 2013). While different explants were tested for shoot induction, highest shoots responses were observed with transverse thin cell layer segments then compared to shoot apical meristem and nodal explants supplemented with various BAP, NAA and kinetin concentrations in *Boerhaavia difusa* (Pandey et al. 2019).

Various concentrations and combinations of BA and Kin were tested (0.05–0.54 µM) for multiple shoots emergence using shoot tip explants in *Ceropegia bulbosa* (Dhir and Shekhawat 2014a, b). In the current study, similar results were observed with multiple shoots induction in the same medium supplemented with 2ip followed by shoot elongation after induction with 0.5–3.0 mgl^{-1} of GA_3 (Jose et al. 2016).

Effect of plant growth regulators on root induction

To induce roots from elongated shoots, 1.0–5.0 mgl^{-1} of NAA and IBA were tested individually and results showed maximum root formation (5.75 roots/shoot) with 3 mgl^{-1} NAA used at 35 days post culture, but, only 2.62 cm in length of roots was observed (Table 4 & Fig. 3f). When the concentration of the NAA was increased or decreased, the number and length of the roots formation was reduced. Maximum number of roots (3.25 roots/shoot) was showed with medium contains 3 mgl^{-1} of IBA and increased the length of roots with 4.75 cm at 35 days post culture. In our current study showed that, IBA induced less number of shoots (3.25) when compared to NAA (5.75). The length of roots (4.75 cm) was increased when culturing the explants on medium supplemented with IBA (Table 4). Generally, root formation and developments is very hard and difficult in these plants. The induction of healthy roots was observed when the shoots were inoculated in full strength medium with or without auxin supplements. Out of the two auxins used for root induction, IBA has induced healthier roots, increased in length and is most suitable for the species. The acclimatized plantlets have been successfully established in the green house or field condition and more than 85.3% of transformed plants survived (Table 5). All plants were healthy; grow vigorously and are morphologically similar to in vivo plants. Past studies have shown that,

Table 4 Effect of root induction with different growth regulators and concentration from elongated in vitro shoots

PGRs (mgl^{-1})	Number of days	Number of roots initiation	Roots length (cm)
Control	35	0.5 ± 0.28^{e}	0.87 ± 0.23^{e}
IBA			
1		2.25 ± 0.25^{cd}	3.25 ± 0.25^{bc}
2		3.00 ± 0.40^{bc}	4.00 ± 0.40^{ab}
3	35	3.25 ± 0.25^{bc}	4.75 ± 0.47^{a}
4		2.25 ± 0.28^{cd}	2.50 ± 0.28^{cd}
5		1.75 ± 0.25^{d}	2.50 ± 0.64^{cd}
NAA			
1		3.25 ± 0.25^{bc}	1.50 ± 0.28^{de}
2		4.00 ± 0.40^{b}	2.00 ± 0.40^{de}
3	35	5.75 ± 0.47^{a}	2.62 ± 0.37^{cd}
4		4.00 ± 0.40^{b}	2.50 ± 0.28^{cd}
5		2.50 ± 0.28^{cd}	2.25 ± 0.25^{cd}

Values are represented as means ± standard error (SE) of triplicate determinations and experiments with 10 replicates

Means significantly different to DMRT at ($P \leq 0.05$)

Table 5 Acclimatization of in vitro regenerated plants

No of plants acclimatization	No of plants survived	% of survived	Total % of plants survived
20	18	90	
15	12	80	85.3 ± 2.51
15	13	86	

Values are represented as means ± standard error (SE) of triplicate determinations

Means significantly different to DMRT at ($P \leq 0.05$)

using half strength medium with reduced sucrose level and higher percent agar in *P. amaryllifolius* resulted spontaneous development of root formation (Thimmaraju et al. 2005). Root induction was observed on half-strength MS-medium supplemented with 0.5 mgl^{-1} NAA in *Jatropha curcas* (Astha et al. 2006). The effective root formation was showed in *Catharanthus roseus* when the combination of IBA and BA were used (Junaid et al. 2007). In *Acorus calamus*, shoots induction was increased when the auxiliary bud explants were cultured in the medium contain Kinetin and also IBA induced and developed healthy roots (Sharma and Sharma 2017).

IBA was more effective for root induction than IAA (Jana and Shekhawat 2011a, b). Higher concentrations of NAA or IBA induced more number of roots in *Scaevola sericea* (Liang et al. 2020). *Salvadora persica* showed highest percentage of root induction in half strength MS-medium supplemented with 3.0 mgl^{-1} IBA (Mathur et al. 2002a, b). A single white stilt root was produced when shoots were cultured in the semi-solid charcoal medium supported with filter paper wraps; thick roots were also observed to develop when increasing the agar concentration. Screw pines were transferred to polybags containing sand soil and cow dung (2:1) kept in a shade house conditions for acclimatization with regular irrigations (Jose et al. 2016). In *Azadirachta indica*, 80–83.5% of plantlets survived and were transferred to the pots for hardening and final transfer to field conditions (Shekhawat et al. 2009). 60–70% of in vitro developed *Salvadora persica* plantlets were successfully transplanted to garden followed by establishment in natural conditions (Mathur et al. 2002a, b). Growing large number of *Pandanus* species in the coastal area should improve the coastal vegetation and reduced the tsunami energy and other natural calamities in the coastal zone (Tsuji et al. 1995; Lynett et al. 2003; Danielsen et al. 2005).

Conclusion

An efficient regeneration and reliable in vitro protocol for clonal propagation of shoot tip explants of *P. canaranus* was successfully developed. This is the first report of an in vitro regenerated protocol for this species. This reproducible protocol has been efficiently adopted for mass production of clonally uniform plantlets. Furthermore, development of complete plantlets by indirect organogenesis from leaf, shoot and root meristem needs to be studied by optimizing the culture medium, growth hormones and various other factors that will influence the efficient regeneration.

Supplementary Information The online version contains supplementary material available at https://doi.org/10.1007/s42535-021-00218-w.

Acknowledgements We thankfully acknowledge the Botanical Survey of India, Southern region of Coimbatore, Tamil Nadu, for identifying and authenticating the plant specimen. We thank Bharathiar University, Coimbatore, for the financial support and access the lab facility.

Declarations

Conflict of interest The authors declare no conflict of interest.

References

Adkar PP, Bhaskar VH (2014) *Pandanus odoratissimus* (Kewda): a review on ethnopharmacology, phytochemistry, and nutritional aspects. Adv Pharmacol Sci. https://doi.org/10.1155/2014/120895

Ahmad N, Anis M (2005) In vitro mass propagation of *Cucumis sativus* L. from nodal segments. Turk J Bot 29(3):237–240

Ahmad A, Anis M, Khanam MN, Alatar AA (2020) Direct shoot organogenesis from shoot tip explants of a highly medicinal valued tree *Pterocarpus marsupium* Roxb. Vitro Cell Dev Biol Plant 56(5):670–681. https://doi.org/10.1007/s11627-020-10115-7

Amoo SO, Aremu AO, Van Staden J (2012) *In vitro* plant regeneration, secondary metabolite production and antioxidant activity of micropropagated *Aloe arborescens* Mill. Plant Cell Tiss Organ Cult 111(3):345–358. https://doi.org/10.1007/s11240-012-0200-3

Arumugam A, Gopinath K (2012) *In vitro* micropropagation using corm bud explants: an endangered medicinal plant of *Gloriosa superba* L. Asian J Biotechnol 4(3):120–128. https://doi.org/10.3923/ajbkr.2012.120.128

Astha S, Nidhi K, Shekhawat GS (2006) *In vitro* culture and plant regeneration of economically potent plant species *Jatropha curcas*. Biochem Cell Arch 6(2):323–327

Balamurugan V, Amal TC, Karthika P, Selvakumar S, Vasanth K (2019) Somatic embryogenesis and plant regeneration in *Gloriosa superba* L.: an Endangered Medicinal Plant. In: i*n vitro* plant breeding towards novel agronomic traits. Springer Singapore, pp 27–42. https://doi.org/10.1007/978-981-32-9824-8_2

Balamurugan V, Raja K, Selvakumar S, Vasanth K (2020) Phytochemical screening, antioxidant, anti-diabetic and cytotoxic activity of leaves of *Pandanus canaranus* Warb. Mater Today Proc. https://doi.org/10.1016/j.matpr.2020.07.603

Behera S, Kamila PK, Rout KK, Barik DP, Panda PC, Naik SK (2018) An efficient plant regeneration protocol of an industrially important plant, *Hedychium coronarium* J. Koenig and establishment of genetic & biochemical fidelity of the regenerants. Ind Crops Prod 126:58–68. https://doi.org/10.1016/j.indcrop.2018.09.058

Ceasar SA, Ignacimuthu S (2010) Effects of cytokinins, carbohydrates and amino acids on induction and maturation of somatic embryos in kodo millet (*Paspalum scorbiculatum* Linn). Plant Cell Tiss Organ Cult 102(2):153–162. https://doi.org/10.1007/s11240-010-9716-6

Charterjee A, Pakrashi SC (2001) The Treatise of Indian Medicinal Plants, vol 6. National Institute of Science Communication, New Delhi (**2nd edition**)

Chaudhury A, Qu R (2000) Somatic embryogenesis and plant regeneration of turf type bermudagrass: effect of 6-benzyladenin in callus induction medium. Plant Cell Tiss Org Cult 60(2):113–120. https://doi.org/10.1023/A:1006456005961

Danielsen F, Sorensen MK, Olwig MF, Selvam V, Parish F, Burgess ND, Quarto A (2005) The Asian tsunami: a protective role for coastal vegetation. Science 310(5748):643–643. https://doi.org/10.1126/science.1118387

Dhir R, Shekhawat GS (2014a) Ecorehabilitation and biochemical studies of *Ceropegia bulbosa* Roxb.: a threatened medicinal succulent. Acta Physiol Plant 36(6):1335–1343. https://doi.org/10.1007/s11738-014-1512-1

Dhir R, Shekhawat GS (2014b) In vitro propagation using transverse thin cell layer culture and homogeneity assessment in *Ceropegia bulbosa* Roxb. J Plant Growth Regul 33(4):820–830. https://doi.org/10.1007/s00344-014-9432-2

Dhir R, Shekhawat GS, Alam A (2014) Improved protocol for somatic embryogenesis and calcium alginate encapsulation in *Anethum graveolens* L.: a medicinal herb. Appl Biochem Biotech 173(8):2267–2278. https://doi.org/10.1007/s12010-014-1032-x

Englberger L (2003) Are Pacific islanders still enjoying the taste of *Pandanus*? Pac Islands Nutri 58:10–11

Gangopadhyay G, Bandyopadhyay T, Modak BK, Wongpornchai S, Mukherjee KK (2004) Micropropagation of Indian pandan (*Pandanus amaryllifolius* Roxb.), a rich source of 2-acetyl-1-pyrroline. Curr Sci 87:11589–1592

Iliev I, Gajdosova A, Libiakova G, Jain SM (2010) Plant micropropagation. In: Plant cell culture: essential methods. John Wiley Sons, pp 1–23, https://doi.org/10.1002/9780470686522

Jain M, Chengalrayan K, Gallo-meagher M, Mislevy P (2005) Embryogenic callus induction and regeneration in a pentaploid hybrid bermudagrass CV. Tifton 85. Crop Sci 45(3):1069–1072. https://doi.org/10.2135/cropsci2004.0337

Jana S, Shekhawat GS (2011a) Plant growth regulators, adenine sulfate and carbohydrates regulate organogenesis and *in vitro* flowering of *Anethum graveolens*. Acta Physiol Plant 33(2):305–311. https://doi.org/10.1007/s11738-010-0548-0

Jana S, Shekhawat GS (2011b) Critical review on medicinally potent plant species: *Gloriosa superba*. Fitoterapia 82(3):293–301. https://doi.org/10.1016/j.fitote.2010.11.008

Jose B, Harikumar K, Krishnan PN, Satheeshkumar K (2016) In vitro mass multiplication of screw pines (*Pandanus* spp.)—an important costal bio-resource. J Coast Conserv 20(6):443–453. https://doi.org/10.1007/s11852-016-0458-4

Junaid A, Mujib A, Bhat MA, Sharma MP, Samaj J (2007) Somatic embryogenesis and plant regeneration in *Catharanthus roseus*. Biol Plant 51(4):641–646. https://doi.org/10.1007/s10535-007-0136-3

Kayser A (2002) Nauru One Hundred Years Ago, 1 Pandanus. Nauru: University of the South Pacific Centre; Suva: Institute of Pacific Studies, Universityof the South Pacific

Kurup SS, Aly MA, Lekshmi G, Tawfik NH (2014) Rapid *in vitro* regeneration of date palm (Phoenix dactylifera L.) cv. Kheneizi using tender leaf explant. Emir J Food Agric 25:539–544. https://doi.org/10.9755/ejfa.v26i6.18051

Li R, Bruneau AH, Qu R (2006) Improved plant regeneration and in vitro somatic embryogenesis of St Augustine grass *Stenotaphrum secundatum* (Walt.) Kuntze. Plant Breed 125(1):52–56. https://doi.org/10.1111/j.1439-0523.2006.01193.x

Liang H, Xiong Y, Guo B, Yan H, Jian S, Ren H, Zheng F (2020) Shoot organogenesis and somatic embryogenesis from leaf and root explants of *Scaevola sericea*. Sci Rep 10(1):1–11. https://doi.org/10.1038/s41598-020-68084-1

Lynett PJ, Borer J, Liu PLF, Synolasis CE (2003) Field survey and Numerical modeling of the 1998 Papua New Guinea tsunami. Pure Appl Geophys 160:2119–2146. https://doi.org/10.1007/978-3-0348-7995-8_16

Mascarenhas A, Jayakumar S (2008) An environmental perspective of the post-tsunami scenario along the coast of Tamil Nadu, India: role of sand dunes and forests. J Environ Manag 89(1):24–34. https://doi.org/10.1016/j.jenvman.2007.01.053

Mathur S, Shekhawat GS, Batra A (2002a) Micropropagation of *Salvadora persica* via cotyledonary nodes. J Biotechnol 1:197–200

Mathur S, Shekhawat GS, Batra A (2002b) An efficient in vitro method for mass propagation of *Salvadora persica* via apical meristem. J Plant Biochem Biot 11(2):125–127. https://doi.org/10.1007/BF03263149

Mathur S, Bulchandani N, Parihar S, Shekhawat GS (2017) Critical review on steviol glycosides: Pharmacological, toxicological and therapeutic aspects of high potency zero caloric sweetener. Int J Pharmacol 13(7):916–928. https://doi.org/10.3923/ijp.2017.916.928

Meilleur BA, Maigret MB, Manshardt R (1997) Hala and Wauke in Hawaii. Bishop Mus Bull Anthropol 7:1–55

Murashige T, Skoog F (1962) A revised medium for rapid growth and bio assays with tobacco tissue cultures. Physiol Plant 15(3):473–497. https://doi.org/10.1111/j.1399-3054.1962.tb08052.x

Panda KK, Mohapatra S, Das LN, Mishra MK, Panda BB (2000) Optimal utilization of kewda *Pandanus fascicularis* to ameliorate economy and ecology of coastal India. J Med Arom Plant Sci 22(4a):679–682

Pandey N, Tripathi D, Pandey-Rai SKRS (2019) Transverse thin cell layer culture for high frequency shoot germination in *Boerhaavia difusa* L., its conservation and assessment of genetic fidelity. Plant Arch 19(1):1093–1101

Paterson CN (2008) The ecological restoration of coastal terrestrial ecosystems in Southern Sri Lanka. In: Proceedings from International Conference on building education and research (BEAR), pp 1368–1383

Raina VK, Kumar A, Srivastava SK, Syamsundar KV, Kahol AP (2004) Essential oil composition of 'kewda'(*Pandanus odoratissimus*) from India. Flavour Frag J 19(5):434–436. https://doi.org/10.1002/ffj.1331

Ramakrishnan M, Ceasar SA, Duraipandiyan V, Daniel MA, Ignacimuthu S (2013) Efficacious somatic embryogenesis and fertile plant recovery from shoot apex explants of onion (*Allium cepa*. L.). Vitro Cell Dev Biol Plant 49(3):285–293. https://doi.org/10.1007/s11627-013-9510-3

Razdan MK (2003) Introduction to plant tissue culture. Science Publishers, Inc., Enfield, Plymouth

Sasidharan N (2004) Biodiversity documentation for Kerala: flowering plants. KFRI Handbook. Kerala Forest Research Institute, Peechi

Saxena PK, Malik KA, Gill R (1992) Induction by thidiazuron of somatic embryogenesis in intact seedlings of peanut. Planta 187(3):421–424. https://doi.org/10.1007/BF00195667

Sharma P, Sharma J (2017) Ethnobotany and *In vitro*regeneration of *Acorus calamus* L (Acoraceae): a high valued medicinal and economic plant. Ann Pl Sci 6:1568–1571. https://doi.org/10.21746/aps.2017.02.006

Sharmin SA, Alam MJ, Sheikh MMI, Zaman R, Khalekuzzaman M, Mondal SC, Alam I (2013) Micropropagation and antimicrobial activity of *Curcuma aromatica* Salisb. a threatened aromatic medicinal plant. Turk J Biol 37(6):698–708. https://doi.org/10.3906/biy-1212-11

Shekhawat GS, Mathur S, Batra A (2009) Role of phytohormones and nitrogen in somatic embryogenesis induction in cell culture derived from leaflets of *Azadirachta indica*. Biol Plant 53(4):707. https://doi.org/10.1007/s10535-009-0127-7

Son NT (2019) Secondary metabolites of genus *Pandanus*: an aspect of phytochemistry. Mini Rev Org Chem 16(7):689–710. https://doi.org/10.2174/1570193X16666181206102740

Stone BC (1974) Towards an improved infrageneric classification in *Pandanus* (Pandanaceae). Bot Jahrb Syst 94:459–540

Thimmaraju R, Bhagyalakshmi N, Narayan MS, Venkatachalam L, Ravishankar GA (2005) In vitro culture of Pandanus amaryllifolius and enhancement of 2-acetyl-1-pyrroline, the major flavouring compound of aromatic rice, by precursor feeding of L-proline. J Sci Food Agric 85(15):2527–2534. https://doi.org/10.1002/jsfa.2286

Thomson LA, Englberger L, Guarino L, Thaman RR, Elevitch CR (2006) *Pandanus tectorius* (pandanus). In: Elevitch CR (ed) Species profiles for pacific Island agroforestry. Permanent Agriculture Resources, Holualoa, Hawaii, USA

Thuy NB, Tanaka N, Tanimoto K (2012) Tsunami mitigation by coastal vegetation considering the effect of tree breaking. J Coast Conserv 16(1):111–121. https://doi.org/10.1007/s11852-011-0179-7

Tripathi D, Rai KK, Rai SK, Rai SP (2018) An improved thin cell layer culture system for efficient clonal propagation and *in vitro* withanolide production in a medicinal plant *Withania coagulans* Dunal. Ind Crop Prod 119:172–182. https://doi.org/10.1016/j.indcrop.2018.04.012

Tsuji Y, Imamura F, Matsutomi H, Synolakis CE, Nanang PT, Jumadi HS, Han SS, Arai K, Cook B (1995) Field survey of the east java earthquake and tsunami June 3, 1994. Pageoph 144:839–854. https://doi.org/10.1007/978-3-0348-7279-9_25

Wakte KV, Nadaf AB, Thengane RJ, Jawali N (2009) In vitro regenerating plantlets in *Pandanus amaryllifolius* Roxb. as a model system to study the development of lower epidermal papillae. Vitro Cell Dev Biol 45(6):701. https://doi.org/10.1007/s11627-009-9191-0

Wang W, Zhao X, Zhuang G, Wang S, Chen F (2008) Simple hormonal regulation of somatic embryogenesis and/or shoot organogenesis in caryopsis cultures of *Pogonatherum paniceum* (Poaceae). Plant Cell Tiss Organ Cult 95(1):57–67. https://doi.org/10.1007/s11240-008-9414-9

Wu C, Tian Y, Yu J, Zhang R, Zhang X, Guo P (2019) The *Pandanus tectorius* fruit extract (PTF) modulates the gut microbiota and exerts anti-hyperlipidaemic effects. Phytomedicine 58:152863. https://doi.org/10.1016/j.phymed.2019.152863

Zarinjoei F, Rahmani MS, Shabanian N (2014) In vitro plant regeneration from cotyledon-derived callus cultures of leguminous tree Gleditsia caspica Desf. New For 45(6):829–841. https://doi.org/10.1007/s11056-014-9440-x

Zhang S, Hanna W, Ozias-Akins P (2007) Comparison of callus induction and plant regeneration from different explants in triploid and tetraploid turf-type bermudagrasses. Plant Cell Tiss Org Cult 90(1):71–78. https://doi.org/10.1007/s11240-007-9255-y

Publisher's Note Springer Nature remains neutral with regard to jurisdictional claims in published maps and institutional affiliations.

भा.कृ.अनु.प.-केन्द्रीय कपास अनुसंधान संस्थान
(भारतीय कृषि अनुसंधान परिषद)
पोस्ट बैग नं.02, शंकर नगर, पो.ऑ., नागपुर-440010 (महाराष्ट्र), भारत

ICAR-CENTRAL INSTITUTE FOR COTTON RESEARCH
(Indian Council of Agricultural Research)
Post Bag No.2, Shankar Nagar, P.O., Nagpur-440010 (M.S.), India
Ph.(O) :07013-275536, Fax :07013–275529 EPBAX:07103-275637-39, 275549,275617
Email (O):director.cicr@icar.gov.in, cicrnagpur@gmail.com, Website:www.cicr.org.in

डॉ. वाय. जी. प्रसाद
निदेशक
Dr. Y. G. Prasad
Director

F. No.: T-I/4/2021 **By Email** Date: 15.11.2021

To,

Dr. G. Dhandapani,
Assistant Professor,
PG & Research Department of Botany,
Kongunadu Arts and Science College (Autonomous),
Affiliated to Bharathiar University,
Coimbatore- 641029

Subject: In-principle approval is given to Dr. M. Amutha to get associated in the collaborative research work -reg.

Sir,

With reference to your email dated September 19, 2021 regarding above cited subject, In-principle approval is given to Dr. M. Amutha to get associated in the collaborative research work on pest management aspect related to cotton. Further it is requested to prepare and submit a joint research proposal containing the detailed technical programme of both the institutes for consideration by the our Institute Research Council. Based on the merit of the proposal, cost and time involved, an MoU can be signed for the collaborative research work at a later stage.

Thanking you,

Yours faithfully

(Y.G. Prasad) 15.11.21
Director
ICAR-CICR, Nagpur

Copy to:
1. **Dr. A. H. Prakash**, PC & Head, ICAR-CICR, Regional Station, Coimbatore
2. **Dr. M. Amutha,** Senior Scientist, ICAR-CICR, Regional Station Coimbatore.
3. **Dr. G. Balasubramani,** I/c ITMU, ICAR-CICR, Nagpur

Marutham
Honey

25a, Indira nagarMtp Road, Kavundampalayam,Coimbatore - 641030. Mobile: +919442532228
www.maruthamhoney.com

Date: 16/10/2018

To Whom It May Concern

This is to certify that Dr S Rajeshkumar, Assistant Professor, Department of Zoology, Kongunadu Arts and Science College, Coimbatore since 2018 in association with Diploma in apiculture, Department of Zoology, Kongunadu Arts and Science College (Autonomous), Coimbatore-29 have organized many scientific Beekeeping training programmed to students, farmers and self-help group to promote the beekeeping for the betterment of Indian economy.

Thank you.

For MARUTHAM HONEY BEE FARM

Proprietor

Signature

பாரதியார் பல்கலைக்கழகம்
BHARATHIAR UNIVERSITY
COIMBATORE – 641 046, TAMILNADU, INDIA
State University | Re-Accredited with "A" Grade by NAAC | Ranked 14th among Indian Universities by MOE-NIRF

Dr. R.Kalai Selvan, Ph.D,
Assistant Professor

07.10.2022

Dear Dr. C. Shobana,

I am pleased to be working with your research team. Let me start by saying thank you for bringing prospective graduate students to my group. Despite the fact that our research on green synthesis, characterization, and application methods for nanotechnology has been published in SCI and SCIE publications, I am looking forward to our groups working together on long-term research projects. Your students might benefit from exposure to cutting-edge methods and relevant publications. Additionally, it might be helpful for our groups' joint research efforts.

Thanking you

Yours sincerely

(R.Kalai Selvan) 11/10/2022

To

Dr. C. Shobana
Assistant professor
Department of Zoology
Kongunadu Arts and Science College
Coimbatore - 641 029, Tamil Nadu, India

Division of Biotechnology
College of Environmental and Bioresource Sciences
CHONBUK NATIONAL UNIVERSITY

194-5 Ma-dong Iksan Jeollabuk-do 570-752, Korea
Phone +82-63-850-0835 / Fax +82-63-850-0834
http://www.chonbuk.ac.kr/biotech

Acceptance Letter for Research Collaboration

To

Dr. C. Shobana
Assistant Professor
Department of Zoology
Kongunadu Arts and Science College
Coimbatore-641 029
Tamil Nadu, India.

Dear Dr. Shobana,

Thank you for your request and interest regarding the research collaboration with my group. It is my pleasure to accept your invitation to have collaboration with you especially (i) Participation in seminars and academic meetings, (ii) Exchange of academic materials and other permissible information, (iii) Sharing of available instrumentation facilities and, (iv) Preparation of database by the outcome of scientific findings. I hope the research collaborations could be useful for your students to get exposure with advanced molecular techniques and publications in reputed high impact international journals.

Thanks

Dr. S. Kamala-Kannan
Professor
Division of Biotechnology
College of Environmental and Bioresource Sciences
Chonbuk National University
194-5 Madong, Iksan-City-54596
Jeonbuk, South Korea
Phone: 0082-63-850-0842
Fax: 0082-63-850-0834
Email: kannan@jbnu.ac.kr

Journal of Experimental Biology and Agricultural Sciences

http://www.jebas.org

ISSN No. 2320 – 8694

TOXICITY OF ZINC OXIDE NANOPARTICLES ON HUMAN SKIN DERMAL CELLS

Harshyini Maheswaran[1], Ling Shing Wong[2], Anto Cordelia Tanislaus Antony Dhanapal[3], Ramasamy Thangavelu Narendhirakannan[4], Ashok Kumar Janakiraman[5], Sinouvassane Djearamane[1*]

[1]Department of Biomedical Science, Faculty of Science, Universiti Tunku Abdul Rahman, Kampar, 31900 Malaysia
[2]Life Science Division, Faculty of Health and Life Sciences, INTI International University, Nilai, 71800 Malaysia
[3]Department of Chemical Science, Faculty of Science, Universiti Tunku Abdul Rahman, Kampar, 31900 Malaysia
[4]Department of Biochemistry, Kongunadu Arts and Science College, Affiliated to Bharathiar University, Coimbatore, Tamil Nadu, India
[5]Department of Pharmaceutical Technology, Faculty of Pharmaceutical Sciences, UCSI University, 56000 Cheras, Kuala Lumpur, Malaysia

Received – July 18, 2020; Revision – September 17, 2020; Accepted – January 03, 2021
Available Online – March 25, 2021

DOI: http://dx.doi.org/10.18006/2021.9(Spl-1-GCSGD_2020).S95.S100

Keywords

Zinc oxide nanoparticles

Zinc

Skin dermal cells

Toxicity

ABSTRACT

Zinc oxide (ZnO) has special physical and chemical characteristics which enable it to be utilized in numerous applications including electronics, sunscreens, pigments, and most notably in biomedical applications. Nanoemulsions containing zinc oxide nanoparticles (ZnO NPs) are progressively sought-after as an active component in cosmetic formulations and are used in sunscreens, moisturizers, and antiaging products. Zinc paste bandages including Unna boot consist of open wove cotton gauze treated with ZnO paste are now common medicaments for leg ulcers. The damaged and broken skins are vulnerable to ZnO NPs uptake. This being the case, ZnO NPs on the skin surface can affect the functions of surrounding cells in numerous ways by penetrating into the skin cells. This could exert toxicity effects on the skin cells over time depending on the concentration and site of ZnO NPs exposure. This review brings together some findings regarding the toxicity of ZnO NPs on human skin dermal cells and thus in turn enlightens the safer usage of ZnO NPs in skin care applications.

* Corresponding author

E-mail: sinouvassane@utar.edu.my; biochsinouvas07@gmail.com (Sinouvassane Djearamane)

Peer review under responsibility of Journal of Experimental Biology and Agricultural Sciences.

Production and Hosting by Horizon Publisher India [HPI] (http://www.horizonpublisherindia.in/).
All rights reserved.

All the articles published by Journal of Experimental Biology and Agricultural Sciencesare licensed under a Creative Commons Attribution-NonCommercial 4.0 International License Based on a work at www.jebas.org.

1 Introduction

Richard Feynman, the Nobel Prize winner in 1959, was the foremost to foresee the advent of modern technology that might work with materials on just a range of 1–100 nm. Nanotechnology's true promise lies in the potential for manipulating materials at the same unimaginably small scale (Tocco et al., 2012). The reverberations that nanotechnology has in our lives at this moment in time are mountainous. Current implementations contribute to the instigation of devices, systems, and structures that are capable of revolutionizing medical therapeutics and diagnostics which have yet to be seen (Rajeshkumar et al., 2019). According to a study from the Consumer Product Inventory of Nanotechnology, silver nanoparticles (Ag NPs) are the most commonly used nanomaterials as they are present in 435 (24%) consumer products on the market (Therapeutic Goods Administration, 2006; Vance et al., 2015; Zhang et al., 2016).

Most of the metal nanoparticles (MNPs) such as copper oxide, magnesium oxide, silver, and zinc oxide nanoparticles exhibit antimicrobial properties that have been imparted into the packaging to kill harmful microorganisms (Makhlouf &Tiginyanu, 2011). In this regard, antimicrobial MNPs have positive results in hindering food deterioration as well as prolonging food's shelf life because of the intrinsic physicochemical properties of inorganic MNPs which enable the unrestrained development of reactive oxygen species (ROS) that primes to oxidative stress and ensuing cell damage (Fu et al., 2014). Given their low toxicity, price, and ultraviolet barrier properties, zinc oxide nanoparticles (ZnO NPs) are favored over Ag NPs (Chaudhry et al., 2008; Llorens et al., 2012). Drug delivery has drawn awareness of researchers and pharmaceutical companies that nano-mediated systems could constitute an acceptable exchange therapy for conventional drugs since they can provide a more impactful drug build-up in the site of infection with reduced side effects (Grumezescu, 2016).

2 Zinc Oxide Nanoparticles

Since the early 1960s, ZnO has been synthesized in thin films to be used as catalysts, sensors, and transducers. Due to its distinctive and precise properties, ZnO has attracted attention for a broad array of applications like those of electrical conductors, optical (pigment applications), and thermal since it is stable at temperatures more than 1800°C (Moezzi et al., 2012). Zinc oxide nanoparticles (ZnO NPs) are also known as oxydatum, ketozinc, permanent white, zincioxicum, and oxozinc (AZoNano, 2013). ZnO NPs have inherent qualities determined primarily by size, crystallinity, composition, and morphology. Their characteristics, such as morphological, chemical, and mechanical features, alter concerning the nanometer level. In addition to the stated properties, ZnO NPs also have a high electrochemical coupling coefficient, high chemical stability, and high photostability (Kołodziejczak-Radzimska & Jesionowski, 2014). Not only ZnO NPs work as credible physical ultraviolet A (320-400 nm) as well as ultraviolet B (290-320 nm) filters (Nohynek et al., 2007; Zvyagin et al., 2008) that are present in sunscreens to shield users from the damaging outcomes of UV rays (Maverakis et al., 2010; Djearamane et al., 2019), it also reduces the reliance on systemically absorbable chemical sunscreen agents (Gonzalez et al., 2006). These formulations aimed to shield the skin from sun-induced erythema, decrease photoaging as well as possibly decrease the likelihood of skin cancer (Holmes et al., 2016) by lingering at or close by the surface of the skin because there is no reasoning for their entry into the skin (Gamer et al., 2006; Cross et al., 2007). However, contact with ZnO NPs through the usage of consumer products and also through occupational and environmental exposure might bring health hazards to humans.

3 Toxicity of ZnO NPs on Skin Cells

The skin as the body's key defence organ is well equipped to halt the penetration of materials through its surface (Lin et al., 2015). Mammalian skin is divided into many layers: stratum corneum (SC), epidermis, dermis, and subcutaneous layer. SC is the barricade that limits the penetration rate of many topically applied materials (Schaefer et al., 2003). Nanomaterials including nano-emulsions made up of oils, emulsifiers and aqueous vehicles are being processed to create a stable network of nano sized globules that are increasingly popular in cosmetics and medicine (Nohynek et al., 2007). For instance, the Nano Gel platform developed by Tri-K Industries presents a simplistic production process for refined nanoemulsion products that prevents transepidermal water loss (TEWL) and enables it suitable for many applications including anti-aging products, moisturizers, and sunscreens (Müller et al., 2002).

Zinc is an essential micronutrient for human health (Rostan et al., 2002). Zinc has a prominent part in influencing each stage of the wound alleviating phase; from membrane restoration, oxidative stress, coagulation, inflammation, and immune response, tissue re-epithelialization, angiogenesis, to scarring (Sekhon & Sen Gupta, 2017). Zinc is particularly essential to the skin (Rostan et al., 2002) because the skin contains high zinc in the epidermis (Gupta et al., 2014). Because of its multitude in the epidermis, a slight zinc inadequacy can lead to coarsened skin and hinder the curing of wounds (Lansdown et al., 2007). Unna boot bandages of zinc paste comprised of open wove cotton gauze infused with ZnO paste persist as the traditional procedure for leg ulcers (Williams, 1999).

Numerous factors possibly influence the absorption of ZnO NPs into the skin following its superficial application. Firstly, the surface area to volume ratio increases with smaller NP's that enhances the reactivity of NPs with penetration capacity into the

skin. The amount of cellular uptake of NPs increases with the decrease of size as the submicron ZnO or ZnO microparticles penetrate slower than ZnO NPs (He et al., 2010; Reed et al., 2012). Secondly, the type of zinc ion formed following ZnO dissolution and then readiness to penetrate into the skin cells is pH-dependent. The rate of dissolution of ZnO into Zn^{2+} is faster at lower pH (Han et al., 2010; Bian et al., 2011). Thirdly, high pH (>9) or low pH (<3) damages human skin integrity which brings the risk of NPs entry into the skin cells (Holmes et al., 2016). Fourthly, the capability of zinc ions and ZnO to traverse the SC is reliant on the essence of their engagement with the SC (Hostynek, 2003). The noticeably elevated uptake of Zn in human skin at lower pH occurred because human SC is semipermeable for cations as Zn is in the cationic form at lower pH (LareseFilon et al., 2011). Lastly, in the topical formulations, zinc absorption into the skin cells is determined by the concentration of zinc present in the topically applied substance (Zhong, 2004).

The controversy regarding the safety of ZnO to humans began in the late 1990s when ZnO had been utilized for obstructing UV radiation in sunscreens. Studies indicated that ZnO NPs cannot cross the skin barrier, so it stays on the skin's external layer and therefore does not cause toxicity (Klingshirn, 2007; Moezzi et al., 2012). Furthermore, ZnO NPs pooled on the exterior of skin and inside the skin furrows through the intact epidermis have not been reported to penetrate or cause cellular toxicity. Mohammed et al. (2019) also concluded the safe use of sunscreen products. However, the dermal absorption of ZnO has been documented with a ZnO cream (Triple Treatment, Smith & Nephew, Hull, UK) administered on the forearm for a duration of 3 hours (Gorodetsky et al., 1999). Another report showed low zinc ion uptake by skin in normozincemic humans through topical ZnO (Hostýnek et al., 1993). When the superficial keratinocytes are shed off naturally, the zinc ion in the epidermal keratin will be gone while a portion of zinc entering deeper skin layers will then be taken up into the circulatory system (Lansdown et al., 2007). Although topically spread ZnO does not enter the viable epidermis, ZnO hydrolyzes on the skin superficial, which raises the zinc ion concentration in SC and the epidermis, thus in the systemic circulation as well as in urine (Holmes et al., 2016). It has been mentioned that little quantities of zinc from ZnO do get absorbed through the human skin (Hayden et al., 1997). Zyyagin et al. (2008) demonstrated that the caprylic capric triglycerides formulation of ZnO NPs encouraged the passive diffusion of NPs through the lipophilic intercellular passage. This passage depicts the fundamental transdermal penetration pathway. ZnO NPs mineral constituents are found on the skin barrier as well as in the region of desquaming corne ocytes is shown by electron micrographs of human skin (Zvyagin et al., 2008; Espitia et al., 2012). At lower pH, more ZnO undergoes acid-catalyzed hydrolysis to liberate zinc ions. Zn^{2+}will be the main ion in the solution and that zinc ion penetrates the SC and thence into the viable epidermis (Bian et al., 2011). An insoluble precipitate forms at pH 9 as the zinc is in the $Zn(OH)_{2(s)}$ form because of the existence of a zero charge point at around pH 9.4. Hence, the amount of zinc ions accessible to pass through the skin is lesser at higher pH due to a decrease in $Zn(OH)^{+}$ ions dissolution (Holmes et al., 2016). The uncertainty now is if the rise in free zinc may affect the intracellular zinc homeostasis. Studies on the toxicity of skin cells by differing labile zinc concentrations are doubtful. It turned out to be that the viability of human skin fibroblasts with the company from oxidative stress from UVB as well as UVA radiation has been assisted with the rise in intracellular zinc (Richard et al., 1993).

The clinical relevance of the transdermal route in alleviating the symptoms of zinc deficiency is uncertain. After covering the extensive skin areas using topical ZnO in petrolatum, neither Morgan et al. (1980) nor Derry et al. (1983) managed to track an elevated serum zinc level. Systemic zinc uptake by topical zinc is significantly enhanced in the absence of a skin barrier. Following the usage of ZnO-medicated adhesive dressing, serum zinc concentration elevated was reported among the victims of substantial partial-thickness as well as a full-thickness burn injury. There were no substantial variations in serum zinc among ZnO-treated and control-treated patients with small wounds about $10cm^2$ (Lansdown et al., 2007). Skin diseases like psoriasis vulgaris produce hyperkeratosis that might end in reduced topically applied substance uptake (Korting et al., 1990). This is reasoned by the thickening of the epidermis as a result of inflamed skin which ultimately enhances the skin as a barricade (Walker et al., 2003). Other skin diseases such as eczema and podoconiosis (elephantiasis) with rupture in the SC permit the penetration of topically applied substances as the reduction in the barrier capacity of the skin (Korting et al., 1990). Hence, the studies have confirmed that the damaged skin is susceptible to ZnO uptake (Williams, 1999, Walker et al., 2003, Lansdown et al., 2007). Earlier studies reported that exogenous zinc ions are useful as they can avoid herpes infections (Read et al., 2019) and serve to shield the skin as an antioxidant (Prasad, 2014). Two modes of action involving zinc ions applied topically as an antioxidant was suggested. Firstly, Zn^{2+} substitutes Fe^{2+} and Cu^{2+} on cell membranes along with proteins. Secondly, Zn^{2+} might stimulate metallothione in forming a zinc-thiolate moiety that operates as a chelating agent for damaging free radicals (Rostan et al., 2002). In a hamster ear experiment, the topical formulation of zinc ions was proven to simulate metallothionein. The skin contains metallothionein, which will cling to additional labile zinc to ensure an ideal concentration of zinc ions. Small concentrations of free zinc originating from ZnO that enter intact skin may be advantageous to serve as an antioxidant (Morgan et al. 1993).

Besides, when ZnO NPs undergoes hydrolysis, it produces zinc ions and reactive oxygen species (ROS). This further activates different cytotoxic pathways such as intracellular calcium flux, plasma membrane leakage, and mitochondrial depolarization (George et al., 2009).

Conclusion and Recommendation for Future Research

From the earlier study findings, it is evident that ZnO NPs do not penetrate the intact healthy skin and therefore do not cause toxicity effect. On the other hand, some studies have reported the penetration of zinc ions through the stratum corneum of damaged and compromised skin. The information regarding the toxic effects of ZnO NPs in skin cells is scarce. Therefore, future research studies are needed in both *in vitro* and *in vivo* to address the dose and duration of exposure required causing the potential toxic effects of ZnO NPs upon entry into the skin cells.

References

AzoNano (2013) Zinc Oxide (ZnO) Nanoparticles – Properties & Applications. [Online] AZoNano.com. Available at https://www.azonano.com/article.aspx?ArticleID=3348 access on 29th April 2020.

Bian SW, Mudunkotuwa IA, Rupasinghe T, Grassian VH (2011) Aggregation and Dissolution of 4 nm ZnO Nanoparticles in Aqueous Environments: Influence of pH, Ionic Strength, Size, and Adsorption of Humic Acid. Langmuir 27(10): 6059-6068.

Chaudhry Q, Scotter M, Blackburn J, Ross B, Boxall A, Castle L, Aitken RJ, Watkins R (2008) Applications and implications of nanotechnologies for the food sector. Food Additives & Contaminants: Part A Chemistry, Analysis, Control, Exposure, and Risk Assessment 25(3): 241-258.

Cross SE, Innes B, Roberts MS, Tsuzuki T, Robertson TA, McCormick P (2007) Human Skin Penetration of Sunscreen Nanoparticles: In-vitro Assessment of a Novel Micronized Zinc Oxide Formulation. Skin Pharmacology and Physiology 20(3): 148-154.

Derry JE, McLean WM, Freeman JB (1983) A Study of the Percutaneous Absorption from Topically Applied Zinc Oxide Ointment. Journal of Parenteral and Enteral Nutrition 7(2): 31-135.

Djearamane S, Wong LS, Lim YM, Lee PF (2019) Cytotoxic Effects of Zinc Oxide Nanoparticles on *Chlorella vulgaris.* Pollution Research 38(2):479-484.

Espitia PJP, Soares DNFF, Coimbra JDSR, de Andrade NJ, Cruz RS, Medeiros EAA (2012) Zinc oxide nanoparticles: synthesis, antimicrobial activity, and food packaging applications. Food Bioprocess Technology 5: 1447-1464.

Fu P, Xia Q, Hwang H, Ray P, Yu H (2014) Mechanisms of Generation of reactive oxygen species. Journal of Food and Drug Analysis 22(1): 64-75.

Gamer AO, Leibold E, van Ravenzwaay B (2006) The in vitro absorption of microfine zinc oxide and titanium dioxide through porcine skin. Toxicology in Vitro 20(3): 301-307.

George S, Pokhrel S, Xia T, Gilbert B, Ji Z, Schowalter M, Rosenauer A, Damoiseaux R, Bradley KA, Mädler L Nel AE (2009) Use of a Rapid Cytotoxicity Screening Approach to Engineer a Safer Zinc Oxide Nanoparticle through Iron Doping. ACS Nano 4(1): 15-29.

Gonzalez H, Farbrot A, Larko O, Wennberg AM (2006) Percutaneous absorption of the sunscreen benzophenone-3 after repeated whole-body applications, with and without ultraviolet irradiation. British Journal of Dermatology 154(2): 337-340.

Gorodetsky R, Andriessen A, Poliansky I, Vexter A (1999) Measurement of breast skin viscoelasticity and a pilot study on the potential radioprotective effect of a zinc-based cream. Journal of Wound Care 8(10): 514-518.

Grumezescu A, (2016) Surface Chemistry of Nanobiomaterials. Elsevier Science, United States.

Gupta M, Mahajan VK, Mehta KS, Chauhan PS (2014) Zinc Therapy in Dermatology: A Review. Dermatology Research and Practice 2014: 1-11.

Han J, Qiu W, Gao W (2010) Potential dissolution and photo-dissolution of ZnO thin films. Journal of Hazardous Materials 178: 115-122.

Hayden C, Roberts M, Benson H (1997) Systemic absorption of sunscreen after topical application. The Lancet 350(9081): 863-864.

He C, Hu Y, Yin L, Tang C, Yin C (2010) Effects of particle size and surface charge on cellular uptake and biodistribution of polymeric nanoparticles. Biomaterials 31(13): 3657-3666.

Holmes AM, Song Z, Moghimi HR, Roberts MS (2016) Relative Penetration of Zinc Oxide and Zinc Ions into Human Skin after Application of Different Zinc Oxide Formulations. ACS Nano 10(2): 1810-1819.

Hostynek JJ (2003) Factors determining percutaneous metal absorption. Food and Chemical Toxicology 41(3): 327-345.

Hostýnek JJ, Hinz RS, Lorence CR, Price M, Guy RH (1993) Metals and the Skin. Critical Reviews in Toxicology 23(2):171-235.

Klingshirn C (2007) ZnO: from basics towards applications. Physics Status Solid B 244(9): 3027-3073.

Kołodziejczak-Radzimska A, Jesionowski T (2014) Zinc oxide - from synthesis to application: A review. Materials 7(4): 2833-2881.

Korting HC, Zienecke H, Schafer-Korting M, Braun-Falco O (1990) Liposome encapsulation improves efficacy of betamethasonedipropionate in atopic eczema but not in psoriasis vulgaris. European Journal of Clinical Pharmacology 39(4):349–351.

Lansdown ABG, Mirastschijski U, Stubbs N, Scanlon E, Ågren MS (2007) Zinc in wound healing: Theoretical, experimental, and clinical aspects. Wound Repair and Regeneration 15(1): 2-16.

LareseFilon F, Crosera M, Adami G, Bovenzi M, Rossi F, Maina G (2011) Human skin penetration of gold nanoparticles through intact and damaged skin. Nanotoxicology 5(4): 493-501.

Lin L, Nufer K, Tomihara S, Prow T (2015) Non-invasive nanoparticle imaging technologies for cosmetic and skincare products. Cosmetics 2:196-210.

Llorens A, Lloret E, Picouet PA, Trbojevich R, Fernandez A (2012) Metallic-based micro and nanocomposites in food contact materials and active food packaging. Trends in Food Science & Technology 24: 19-29.

Makhlouf ASH, Tiginyanu I (2011) Nanocoatingsand Ultra-Thin Films. Oxford: Woodhead Pub Ltd.

Maverakis E, Miyamura Y, Bowen MP, Correa G, Ono Y, Goodarzi H (2010) Light, including ultraviolet. Journal of Autoimmunity 34: 247-257.

Moezzi A, McDonagh AM, Cortie MB (2012) Zinc oxide particles: synthesis, properties, and applications. Chemical Engineering Journal 185186: 1-22.

Mohammed YH, Holmes A, Haridass IN, Sanchez WY, Studier H, Grice JE, Benson, HAE Roberts MS (2019) Support for the Safe Use of Zinc Oxide Nanoparticle Sunscreens: Lack of Skin Penetration or Cellular Toxicity after Repeated Application in Volunteers. Journal of Investigative Dermatology 139(2): 308-315.

Morgan AJ, Lewis G, Van den Hoven WE, Akkerboom PJ (1993) the effect of zinc in the form of erythromycin-zinc complex (Zineryt lotion) and zinc acetate on metallothionein expression and distribution in hamster skin. British Journal of Dermatology 129(5): 563-570.

Morgan ME, Hughes MA, Mcmillan EM, King I, Mackie RM (1980) Plasma zinc in psoriatic in-patients treated with local zinc applications. British Journal of Dermatology 102(5): 579-583.

Müller RH, Radtke M, Wissing SA (2002) Solid lipid nanoparticles (SLN) and nanostructured lipid carriers (NLC) in cosmetic and dermatological preparations. Advanced Drug Delivery Reviews 54: 131-155.

Nohynek GJ, Lademann J, Ribaud C, Roberts MS (2007) Grey Goo on the Skin? Nanotechnology, Cosmetic, and Sunscreen Safety. Critical Reviews in Toxicology 37(3): 251-277.

Prasad AS (2014) Zinc is an Antioxidant and Anti-Inflammatory Agent: Its Role in Human Health. Frontiers in Nutrition 1: 1-10.

Rajeshkumar S, Lakshmi T, Naik P (2019) Recent advances and biomedical applications of zinc oxide nanoparticles. Green Synthesis, Characterization, and Applications of Nanoparticles 445-457.

Read SA, Obeid S, Ahlenstiel C, Ahlenstiel G (2019) The Role of Zinc in Antiviral Immunity. Advances in Nutrition 10(4): 696-710.

Reed RB, Ladner DA, Higgins CP, Westerhoff P, Ranville JF (2012) Solubility of nano-zinc oxide in environmentally and biologically important matrices. Environmental Toxicology and Chemistry 31(1): 93-99.

Richard MJ, Guiraud P, Leccia MT, Beani JC, Favier A (1993) Effect of zinc supplementation on resistance of cultured human skin fibroblasts toward oxidant stress. Biological Trace Element Research 37(2-3): 187-199.

Rostan EF, DeBuys HV, Madey DL, Pinnell SR (2002) Evidence supporting zinc as an important antioxidant for skin. International Journal of Dermatology 41(9): 606-611.

Schaefer H, Redelmaier TE, Nohynek GJ, Lademann J (2003) Pharmacokinetics and topical application of drugs. Fitzpatrick's Dermatology in General Medicine 2313–2318.

Sekhon UDS, Sen Gupta A (2017) Platelets and Platelet-Inspired Biomaterials Technologies in Wound Healing Applications. ACS Biomaterials Science & Engineering 4(4): 1176-1192.

Therapeutic Goods Administration, Australia (2006) A Review of the Scientific Literature on the Safety of Nanoparticulate Titanium Dioxide or Zinc Oxide In Sunscreens. Australia: Australian Government, Department of Health and Ageing Therapeutic Goods Administration.

Tocco I, Zavan B, Bassetto F, Vindigni V (2012) Nanotechnology-Based Therapies for Skin Wound Regeneration. Journal of Nanomaterials 2012: 1-11.

Vance, M.E, Kuiken T, Vejerano EP, McGinnis SP, Hochella MF, Rejeski D, Hull MS (2015) Nanotechnology in the real world: Redeveloping the nanomaterial consumer products inventory. Beilstein Journal of Nanotechnology 6(1): 1769-1780.

Walker SL, Hawk JLM, Young AR (2003) Acute and chronic effects of ultraviolet radiation on the skin. Fitzpatrick's Dermatology in General Medicine 1275–1282.

Williams C (1999) Examining the range of medicated and paste-impregnated bandages. British Journal of Nursing 8(15):1019-1020.

Zhang H, Huang Q, Xu A, Wu L (2016) Spectroscopic probe to contribution of physicochemical transformations in the toxicity of aged ZnO NPs to Chlorella vulgaris: new insight into the variation of toxicity of ZnO NPs under aging process. Nanotoxicology 10(8): 1177–1187.

Zhong LW (2004) Zinc oxide nanostructures: growth, properties, and applications. Journal of Physics: Condensed Matter 16: 829-858.

Zvyagin AV, Zhao X, Gierden A, Sanchez W, Ross JA, Roberts MS (2008) Imaging of zinc oxide nanoparticle penetration in human skin in vitro and in vivo. Journal of Biomedical Optics 13(6): 064031.

Our ref: IPSR/RMC/UTARRF/2020-C2/S06
Date: 16 December 2020

Dr. Sinouvassane Djearamane
Faculty of Science
Universiti Tunku Abdul Rahman

Dear Dr. Sinouvassane Djearamane,

RE: UTAR RESEARCH FUND 2020 CYCLE 2

Thank you for your application for funding from the UTAR Research Fund (UTARRF). We are pleased to inform you that your application has been successful. The details of your approved research project are as follows:

Research Title	**:**	**Effects of Chemically and Biologically Synthesised Zinc Oxide Nanoparticles on Human Skin Dermal Cells and Cancer Cells**
Period of Research	**:**	**21 December 2020 - 20 December 2021**
Grant Approved	**:**	**RM32000.00**
Project Number	**:**	**IPSR/RMC/UTARRF/2020-C2/S06**
Vote Number	**:**	**6200/SB7**
Co-Researcher(s)	**:**	**1. Dr Lim Chan Kiang** **2. Dr Anto Cordelia Tanislaus Antony Dhanapal** **3. Prof. Dr Wong Ling Shing (INTI International University)** **4. Dr Narendhirakannan R. T. (Kongunadu Arts and Science College, India)**

You are required to fulfill the following conditions:

1. To send the grant offer acceptance reply slip to Institute of Postgraduate Studies and Research within one week from this offer letter date.
2. To sign one (1) copy of the UTAR Research Fund Agreement on the terms and conditions governing the research funding.
3. To submit application for external funding in UTAR within the project duration

The University wishes you all the best in your research.

Thank you.

Yours sincerely,

Prof Ts Dr Faidz bin Abd Rahman
Vice President (R&D and Commercialisation)

c.c.
President, Universiti Tunku Abdul Rahman
Director, Institute of Postgraduate Studies and Research

UTAR RESEARCH FUND 2020 CYCLE 2 REPLY SLIP

Name	**:**	**Dr. Sinouvassane Djearamane**
Research Title	**:**	**Effects of Chemically and Biologically Synthesised Zinc Oxide Nanoparticles on Human Skin Dermal Cells and Cancer Cells**
Period of Research	**:**	**21 December 2020 - 20 December 2021**
Grant Approved	**:**	**RM32000.00**
Project Number	**:**	**IPSR/RMC/UTARRF/2020-C2/S06**
Vote Number	**:**	**6200/SB7**
Co-Researcher(s)	**:**	**1. Dr Lim Chan Kiang** **2. Dr Anto Cordelia Tanislaus Antony Dhanapal** **3. Prof. Dr Wong Ling Shing (INTI International University)** **4. Dr Narendhirakannan R. T. (Kongunadu Arts and Science College, India)**

I accept / decline the offer of the above funding from the UTAR Research Fund and agree to abide by the terms and conditions stipulated by the University.*

Signature **:** 

Name **: Dr. Sinouvassane Djearamane**

I/C No. / Passport No. **: N8631226**

Date **:** 17/12/2020

Department of Applied Mathematics I
School of Building Engineering
University of Seville
Seville, Spain

Dr. N. Mohanaprija
Assistant Professor
Kongunadu Arts and Science College
Coimbatore – 641 029
Tamil Nadu, India

Seville, 9th October 2022

TO WHOM IT MAY CONCERN

This letter certifies that **Dr. N. Mohanapriya,** Assistant Professor of Mathematics in the Kongunadu Arts and Science College (Coimbatore,Tamil Nadu, India) has been working on joint research with the research group FQM-016 "Design, Codes and Cryptography" of the Universidad de Sevilla (Seville, Spain) since April 2021. So far, the list of joint works that have been developed with this collaboration is the following one:

Paper published:

R. M. Falcón, N. Mohanapriyah and V. Aparna, ***Optimal shadow allocations of secret sharing schemes arisen from the dynamic coloring of extended neighborhood coronas***. Mathematics 10:12 (2022), paper 2018. DOI: 10.3390/math10122018.

Paper submitted:

R. M. Falcón, V. Aparna, N. Mohanapriya, ***Dynamic coloring of degree splitting graphs.***

Contribution to Conference:

R. M. Falcón, N. Mohanapriya, V. Aparna. ***Minimizing the total number of shadows in secret sharing schemes based on extended neighborhood coronas***. XVII Reunión Española sobre Criptología y Seguridad de la Información RECSI 2022. (Santander, Spain, 19-21 October, 2022).

I remain at your disposal for any further information you may require at this respect. You may contact me at rafalgan@us.es.

DEPARTAMENTO DE MATEMÁTICA APLICADA I

Raúl Manuel Falcon Ganfornina
Deputy Director of Research
Department of Applied Mathematics I
School of Building Engineering
Universidad de Sevilla
41012 - Seville, Spain.

Palestine Journal of Mathematics

Vol. 10 (Special Issue II, 2021) , 169–177 © Palestine Polytechnic University-PPU 2021

On the Resolving Strong Domination Number of Corona and Cartesian Product of Graphs

Dafik*,1,2, I.H Agustin[1], A.C Prihandoko[1,3], E.Y Kurniawati[1], R Nisviasari[1], N. Mohanapriya[4]

∗Corresponding Author
Communicated by M. Venkatachalam

MSC 2010 Classifications: 05C12, 05C69.

Keywords and phrases: Resolving strong domination number, Corona product, Cartesian product.

Abstract. The two popular research of interests in graph theory are dominating set theory and metric dimension theory. The two no tions can clearly model the real life problems and give a breakthrough to analysing a graph representation in term of distance and domination. In this paper, we try to combine the two concepts, it rises a new notion, namely a resolving strong domination set. A set $R_D \subset V(H)$ is said to be a resolving strong domination of H if R_D satisfies two conditions, namely resolving set and strong dominating set in H. The minimum cardinality of R_D such that R_D satisfies resolving set and strong dominating set is called the resolving strong domination number of H, denoted by $\gamma_{rst}(H)$. In this paper, we have obtained the exact value of the resolving strong domination number of corona and cartesian product of graphs, i.e. the corona and cartesian product of path and cycles.

1 Introduction

A graph (also known as an undirected graph or a simple graph to distinguish it from a multi-graph) is a pair of $H = (V, E)$, where V is a set of vertices (singular: vertex) and E is a set of paired vertices with elements called edges (sometimes links or lines). In this study, we only use a finite, simple, un-directed and connected graph. In graph H, the vertex set V represents some elements, they could be computers, cities, bus, train, plane, etc and the edge set E represents some connection or relation between those elements. For detail definition of graph and its elements, it can be referred to Chartrand *et. al* [1].

The two popular research of interests in graph are dominating set theory and metric dimension theory. The two notions can clearly model the real life problems and give a breakthrough to analysing a graph representation in term of distance and domination. We refer to Slater [2] for the concept of resolving set of graph. Let H be a connected graph of order p and let $W = \{v_1, v_2, ..., v_k\}$ be an ordered set of vertices of G. For a vertex u of G, the k-vector $r(u|W) = (d(u, v_1), d(u, v_2), ..., d(u, v_k))$, where $d(u, v)$ represents the distance between the vertices u and v, is called the representation of vertices with respect to W. The set W is a resolving set for H if $r(u|W) = r(v|W)$ implies that $u = v$ for every pair u, v of vertices of H. A resolving set of minimum cardinality is called a minimum resolving set. The minimum cardinality of resolving set of H is its *dimension* of H, denoted by $dim(H)$. The concepts of resolving set and minimum resolving set have previously appeared in the literature [2, 3].

A subset D of the vertex set V of a graph H is said to be a dominating set of H if every vertex in $D - V$ is adjacent to a vertex in D . The minimum cardinality of a dominating set is called the domination number of H and is denoted by $\gamma(H)$[4]. In this paper we study a variant of this classical notion, namely the strong domination. A set $D \subseteq V$ is called a strong dominating set if for every vertex $v \in V - D$, there exists a vertex $u \in D$ such that $uv \in E(H)$ and $deg(u) \geq deg(v)$. The minimum cardinality of a strong dominating set is called the strong domination number of H and is denoted by $\gamma_{st}(H)$ [5, 6].

We initiate to study a new notion, namely the combination resolving set and strong dominating set. A set $R_D \subset V(H)$ is said to be a resolving strong domination of H if R_D satisfies two

conditions, namely resolving set and strong dominating set in H. The minimum cardinality of R_D such that R_D satisfies resolving set and strong dominating set is called the resolving strong domination number of H, denoted by $\gamma_{rst}(H)$. Dafik et al [10] have obtained the bound of the resolving strong domination number of any graph. Furthermore, Wardani *et al* [7, 8, 9] have determined some results on the domination number of some graphs, while Dafik *et al* have studied the resolving domination number of some graphs in [10, 11].

Lemma 1.1. *[10] The strong domination number of any graph H satistisfies*

$$max\{\gamma_{st}(H), dim(H)\} \leq \gamma_{rst}(H) \leq min\{\gamma_{st}(H) + dim(H), |V(H)| - 1\}.$$

Now, we recall the definition of corona and cartesian product of graphs. Let H_1 and H_2 be two graphs of order n and m, respectively. The corona product of graph H_1 and H_2, denoted by $H_1 \odot H_2$ is defined as the graph obtained from H_1 and H_2 by taking one copy of H_1 and n copies of H_2 and joining by an edge each vertex from the ith-copy of H_2 with the ith-vertex of H_1. While the cartesian product of H_1 and H_2 denoted by $H_1 \times H_2$ is the graph of order $n \times m$ with vertex set $V(H_1) \times V(H_2) = \{(x, y)|x \in V(H_1)\ and\ y \in V(H_2)\}$ such that two vertices $(x, y), (x', y')$ are adjacent if only if either $x = x'$ in H_1 and yy' in $E(H_2)$ or xx' in $E(H_1)$ and $y = y'$ in H_2. Iswadi e̊t. al stated the exact value of dimension number of corona product of any two graphs as follows.

Theorem 1.2. *[12] Let G, H be connected graph, with H with order of at least 2. The dimension number of $dim(G \odot H)$ is*

$$dim(G \odot H) = \begin{cases} |G|dim(H), & \text{if } H \text{ contains a dominant vertex;} \\ |G|dim(K_1 + H), & \text{otherwise} \end{cases}$$

From now on, we start to give our result on resolving strong domination number in the following sections.

2 The Resolving Strong Domination Number of Corona Product Graphs

We have obtained the resolving strong domination number of the corona product of graphs, i.e. path and cycle, denoted by $\gamma_{rst}(P_n \odot P_m)$.

Theorem 2.1. *For every positive integer $n, m \geq 3$,*

$$\gamma_{rst}(P_n \odot P_m) = n\left\lceil \frac{m}{2} \right\rceil.$$

Proof. Graph $P_n \odot P_m$ is a connected graph with vertex set $V(P_n \odot P_m) = \{x_i; 1 \leq i \leq n\} \cup \{y_j^i; 1 \leq j \leq m, 1 \leq i \leq n\}$ and edge set $E(P_n \odot P_m) = \{x_i x_{i+1}; 1 \leq i \leq n-1\} \cup \{y_j^i y_{j+1}^i; 1 \leq j \leq m-1, 1 \leq i \leq n\} \cup \{x_i y_j^i; 1 \leq j \leq m, 1 \leq i \leq n\}$. The cardinality of vertex set $V(P_n \odot P_m)$ is $n + m$ and the cardinality of edge set $E(P_n \odot P_m)$ is $2nm - 1$.

We divide two cases to show the proof. First, determining the lower bound and upper bound of $\gamma_{rst}(P_n \odot P_m)$. We use Lemma 1.1 to show the lower bound of $\gamma_{rst}(P_n \odot P_m)$, thus we have $\gamma_{rst}(P_n \odot P_m) \geq max\{\gamma_{st}(P_n \odot P_m), dim(P_n \odot P_m)\}$. Based on Theorem 1.2 we know that $dim(P_n \odot P_m) = n\ dim(K_1 + P_m) = n\lceil \frac{m}{2} \rceil$. It is easy to see that $\gamma_{st}(P_n \odot P_m) = n$. Hence, it implies

$$\begin{aligned} \gamma_{rst}(P_n \odot P_m) &\geq max\{\gamma_{st}(P_n \odot P_m), dim(P_n \odot P_m)\} \\ &= max\{n, n\lceil \tfrac{m}{2} \rceil\} = n\left\lceil \frac{m}{2} \right\rceil \end{aligned}$$

Furthermore, we determine the upper bound of $\gamma_{rst}(P_n \odot P_m)$ by defining the resolving strong dominating set $R_D(P_n \odot P_m)$. By considering the above vertex and edge sets, we define the following resolving strong dominating set $R_D = \{x_i, y_j^i; 1 \leq i \leq n, 2 \leq j \leq m-1\ and\ j \equiv 0(mod 2)\}$.

Secondly, we need to show the distinction of $r(u|R_D)$ showing the distance between the vertices $u \in V(P_n \odot P_m)$ and $v \in R_D$. They are all different and it can be shown in Table 1. It concludes the proof. □

Table 1. The distinction of $r(u|R_D)$ where $u \in V(P_n \odot P_m)$

	Resolving Strong Dominating Set (R_D)																				
$V(P_n \odot P_m)$	x_1	x_2	x_3	...	x_n	y_2^1	y_4^1	y_6^1	...	y_2^2	y_4^2	y_6^2	...	y_2^3	y_4^3	y_6^3	...	...	y_2^n	y_4^n	y_6^n	...
x_1	0	1	2	...	n-1	1	1	1	...	2	2	2	...	3	3	3	...	...	n	n	n	...
x_2	1	0	1	...	n-2	2	2	2	...	1	1	1	...	2	2	2	...	...	n-1	n-1	n-1	...
x_3	2	1	0	...	n-3	3	3	3	...	2	2	2	...	1	1	1	...	...	n-2	n-2	n-2	...
⋮	⋮	⋮	⋮	⋮	⋮	⋮	⋮	⋮	⋮	⋮	⋮	⋮	⋮	⋮	⋮	⋮	⋮	⋮	⋮	⋮	⋮	⋮
x_n	n-1	n-2	n-3	...	0	n	n	n	...	n-1	n-1	n-1	...	n-2	n-2	n-2	...	...	1	1	1	...
y_1^1	1	2	3	...	n	1	2	2	...	3	3	3	...	4	4	4	...	...	n+1	n+1	n+1	...
y_2^1	1	2	3	...	n	0	2	2	...	3	3	3	...	4	4	4	...	...	n+1	n+1	n+1	...
y_3^1	1	2	3	...	n	1	1	2	...	3	3	3	...	4	4	4	...	...	n+1	n+1	n+1	...
⋮	⋮	⋮	⋮	⋮	⋮	⋮	⋮	⋮	⋮	⋮	⋮	⋮	⋮	⋮	⋮	⋮	⋮	⋮	⋮	⋮	⋮	⋮
y_m^1	1	2	3	...	n	2	2	2	...	3	3	3	...	4	4	4	...	...	n+1	n+1	n+1	...
y_1^2	2	1	2	...	n-1	n-2	3	3	...	1	2	2	...	3	3	3	...	...	n	n	n	...
y_2^2	2	1	2	...	n-1	n-2	3	3	...	0	2	2	...	3	3	3	...	...	n	n	n	...
y_3^2	2	1	2	...	n-1	n-2	3	3	...	1	1	2	...	3	3	3	...	...	n	n	n	...
⋮	⋮	⋮	⋮	⋮	⋮	⋮	⋮	⋮	⋮	⋮	⋮	⋮	⋮	⋮	⋮	⋮	⋮	⋮	⋮	⋮	⋮	⋮
y_m^2	2	1	2	...	n-1	n-2	3	3	...	2	2	2	...	3	3	3	...	...	n	n	n	...
y_1^3	3	2	1	...	n-2	n-2	4	4	...	3	3	3	...	1	2	2	...	...	n-1	n-1	n-1	...
y_2^3	3	2	1	...	n-2	4	4	4	...	3	3	3	...	0	2	2	...	...	n-1	n-1	n-1	...
y_3^3	3	2	1	...	n-2	4	4	4	...	3	3	3	...	1	1	2	...	...	n-1	n-1	n-1	...
⋮	⋮	⋮	⋮	⋮	⋮	⋮	⋮	⋮	⋮	⋮	⋮	⋮	⋮	⋮	⋮	⋮	⋮	⋮	⋮	⋮	⋮	⋮
y_m^3	3	2	1	...	n-2	4	4	4	...	3	3	3	...	2	2	2	...	...	n-1	n-1	n-1	...
⋮	⋮	⋮	⋮	⋮	⋮	⋮	⋮	⋮	⋮	⋮	⋮	⋮	⋮	⋮	⋮	⋮	⋮	⋮	⋮	⋮	⋮	⋮
y_1^n	n	n-1	n-2	...	1	n+1	n+1	n+1	...	n	n	n	...	n-1	n-1	n-1	...	...	1	2	2	...
y_2^n	n	n-1	n-2	...	1	n+1	n+1	n+1	...	n	n	n	...	n-1	n-1	n-1	...	...	0	2	2	...
y_3^n	n	n-1	n-2	...	1	n+1	n+1	n+1	...	n	n	n	...	n-1	n-1	n-1	...	...	1	1	2	...
⋮	⋮	⋮	⋮	⋮	⋮	⋮	⋮	⋮	⋮	⋮	⋮	⋮	⋮	⋮	⋮	⋮	⋮	⋮	⋮	⋮	⋮	⋮
y_m^n	n	n-1	n-2	...	1	n+1	n+1	n+1	...	n	n	n	...	n-1	n-1	n-1	...	...	2	2	2	...

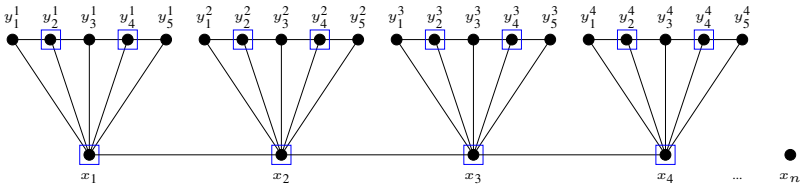

Figure 1. The illustration of the resolving strong dominating set of $P_4 \odot P_5$

For more detail explanation, we give an illustration of the resolving strong domination of $P_4 \odot P_5$ in Figure 1. Based on the Figure 1, the resolving strong dominating set $R_D(P_4 \odot P_5) = \{x_1, x_2, x_3, x_4, y_2^1, y_4^1, y_2^2, y_4^2, y_2^3, y_4^3, y_2^4, y_4^4\}$. Thus $\gamma_{rst}(P_4 \odot C_5) = 4\left\lceil \frac{5}{2} \right\rceil = 12$. We present the $r(u|R_D)$ showing the distance between the vertices $u \in V(P_4 \odot P_5)$ and $v \in R_D$ in the following.

$$x_1 = (0,1,2,3,1,1,2,2,3,3,4,4),\ x_2 = (1,0,1,2,2,2,1,1,2,2,3,3),$$
$$x_3 = (2,1,0,1,3,3,2,2,1,1,2,2),\ x_4 = (2,1,0,1,3,3,2,2,1,1,2,2),$$
$$y_1^1 = (1,2,3,4,1,2,3,3,4,4,5,5),\ y_2^1 = (1,2,3,4,0,2,3,3,4,4,5,5),$$
$$y_3^1 = (1,2,3,4,1,1,3,3,4,4,5,5),\ y_4^1 = (1,2,3,4,2,0,3,3,4,4,5,5),$$
$$y_5^1 = (1,2,3,4,2,1,3,3,4,4,5,5),\ y_1^2 = (2,1,2,3,3,3,1,2,3,3,4,4),$$
$$y_2^2 = (2,1,2,3,3,3,0,2,3,3,4,4),\ y_3^2 = (2,1,2,3,3,3,1,1,3,3,4,4),$$
$$y_4^2 = (2,1,2,3,3,3,2,0,3,3,4,4),\ y_5^2 = (2,1,2,3,3,3,2,1,3,3,4,4),$$
$$y_1^3 = (3,2,1,2,4,4,3,3,1,2,3,3),\ y_2^3 = (3,2,1,2,4,4,3,3,0,2,3,3),$$
$$y_3^3 = (3,2,1,2,4,4,3,3,1,1,3,3),\ y_4^3 = (3,2,1,2,4,4,3,3,2,0,3,3),$$
$$y_5^3 = (3,2,1,2,4,4,3,3,2,1,3,3),\ y_1^4 = (4,3,2,1,5,5,4,4,3,3,1,2),$$
$$y_2^4 = (4,3,2,1,5,5,4,4,3,3,0,2),\ y_3^4 = (4,3,2,1,5,5,4,4,3,3,1,1),$$
$$y_4^4 = (4,3,2,1,5,5,4,4,3,3,2,0),\ y_5^4 = (4,3,2,1,5,5,4,4,3,3,2,1).$$

Theorem 2.2. *For every positive integer* $n, m \geq 3$,

$$\gamma_{rst}(P_n \odot C_m) = n\left\lceil \frac{m}{2} \right\rceil.$$

Proof. Graph $P_n \odot C_m$ is a connected graph with vertex set $V(P_n \odot C_m) = \{x_i; 1 \leq i \leq n\} \cup \{y_j^i; 1 \leq j \leq m, 1 \leq i \leq n\}$ and edge set $E(P_n \odot C_m) = \{x_i x_{i+1}; 1 \leq i \leq n-1\} \cup \{y_j^i y_{j+1}^i; 1 \leq$

$j \leq m-1, 1 \leq i \leq n\} \cup \{y_i^i y_m^i; 1 \leq i \leq n\} \cup \{x_i y_j^i; 1 \leq j \leq m, 1 \leq i \leq n\}$. The cardinality of vertex set $V(P_n \odot C_m)$ is $n+m$ and the cardinality of edge set $E(P_n \odot C_m)$ is $2nm+n-1$.

To prove this theorem, We divide two cases, namely determining the lower bound and upper bound of $\gamma_{rst}(P_n \odot C_m)$. We use Lemma 1.1 to show the lower bound of $\gamma_{rst}(P_n \odot C_m)$, thus we have $\gamma_{rst}(P_n \odot C_m) \geq max\{\gamma_{st}(P_n \odot C_m), dim(P_n \odot C_m)\}$. Based on Theorem 1.2 we know that $dim(P_n \odot C_m) = n\, dim(K_1 + C_m) = n\lceil \frac{m}{2} \rceil$. It is easy to see that $\gamma_{st}(P_n \odot C_m) = n$. Hence, it implies

$$\begin{aligned}\gamma_{rst}(P_n \odot C_m) &\geq max\{\gamma_{st}(P_n \odot C_m), dim(P_n \odot C_m)\} \\ &= max\{n, n\lceil \tfrac{m}{2} \rceil\} = n\left\lceil \tfrac{m}{2} \right\rceil\end{aligned}$$

Furthermore, we determine the upper bound of $\gamma_{rst}(P_n \odot C_m)$ by defining the resolving strong dominating set $R_D(P_n \odot C_m)$. By considering the above vertex and edge sets, we define the following resolving strong dominating set $R_D = \{x_i, y_j^i; 1 \leq i \leq n, 2 \leq j \leq m-1 \text{ and } j \equiv 0(mod 2)\}$.

Secondly, we need to show the distinction of $r(u|R_D)$ showing the distance between the vertices $u \in V(P_n \odot C_m)$ and $v \in R_D$. They are all different and it can be shown in Table 1. It completes the proof. □

3 The Resolving Strong Domination Number of Cartesian Product Graphs

In this section, We show two theorems on the resolving strong domination of the cartesian product of graphs, namely path and cycle. The definition of this graph are shown in the introduction.

Theorem 3.1. *For every positive integer $n, m \geq 3$ and $m \geq n$,*

$$\gamma_{rst}(P_n \times P_m) = \begin{cases} n+1, & \text{if } m = 3 \\ \lceil \frac{m}{3} \rceil n, & \text{otherwise} \end{cases}$$

Proof. Path graph, namely P_n and P_m have vertex set $V(P_n) = \{u_1, u_2, u_3, \ldots, u_n$ and $V(P_m) = \{v_1, v_2, v_3, \ldots, v_m\}$, respectively. Graph $P_n \times P_m$ is a connected graph with vertex set $\{(u,v)|u \in V(P_n)$ and $v \in V(P_m)$, such that two vertices $(u_1, v_1), (u_2, v_2)$ are adjacent if only if either $u_1 = u_2$ in P_n and $v_1 v_2$ in $E(P_m)$ or $u_1 u_2$ in $E(P_n)$ and $v_1 = v_2$ in P_m. We divide two cases to show the proof.

Case 1. For $m = 3$.

First, determining the lower bound and upper bound of $\gamma_{rst}(P_n \times P_3)$. We use Lemma 1.1 to show the lower bound of $\gamma_{rst}(P_n \times P_3)$, thus we have $\gamma_{rst}(P_n \times P_3) \geq max\{\gamma_{st}(P_n \times P_3), dim(P_n \times P_3)\}$. We know that $\gamma_{st}(P_n \times P_3) = n$ and $dim(P_n \times P_3) = 2$. Hence, it implies

$$\begin{aligned}\gamma_{rst}(P_n \times P_3) &\geq max\{\gamma_{st}(P_n \times P_3), dim(P_n \times P_3)\} \\ &= max\{n, 2\} = n\end{aligned}$$

Furthermore, we determine the upper bound of $\gamma_{rst}(P_n \times P_3)$ by defining the resolving strong dominating set $R_D(P_n \times P_3)$. Suppose $R_D(P_n \times P_3) = \{(u_i, v_2) : 1 \leq i \leq n\}$ and we illustrate this resolving strong dominating set in Figure 2. Based on the illustration in Figure 2, the vertices (u_i, v_1) and (u_i, v_3) will receive the same representation for $1 \leq i \leq n$. Hence, we add 1 vertex to the resolving strong dominating set $R_D(P_n \times P_3)$, such that the representations of vertices in $V(P_n \times P_3)$ are all distinct. The resolving strong dominating set of $(P_n \times P_3)$ is $R_D(P_n \times P_3) = \{(u_2, v_1), (u_i, v_2) : 1 \leq i \leq n\}$, see Figure 3 to this illustration. Based on the Figure 3, we give the all representation of each vertex in $V(P_n \times P_3)$ in the following.

$$\begin{aligned}(u_1, v_1) &= (1, 1, 2, 3, ..., n-2, n-1, n) \\ (u_2, v_1) &= (0, 2, 1, 2, ..., n-3, n-2, n-1) \\ (u_3, v_1) &= (1, 3, 2, 1, ..., n-4, n-3, n-2) \\ &\vdots\end{aligned}$$

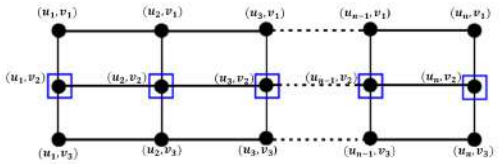

Figure 2. The illustration of the resolving strong dominating set of $P_n \odot P_3$.

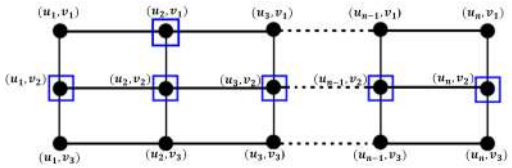

Figure 3. The illustration of the resolving strong dominating set of $P_n \odot P_3$.

$$
\begin{gathered}
(u_{n-1}, v_1) = (n-3, n-1, n-2, n-3, ..., 2, 1, 2) \\
(u_n, v_1) = (n-2, n, n-1, n-2, ..., 3, 2, 1) \\
(u_1, v_2) = (2, 0, 1, 2, ..., n-3, n-2, n-1) \\
(u_2, v_2) = (1, 1, 0, 1, ..., n-4, n-3, n-2) \\
(u_3, v_2) = (2, 2, 1, 0, ..., n-5, n-4, n-3) \\
\vdots \\
(u_{n-1}, v_2) = (n-2, n-2, n-3, n-4, ..., 3, 2, 1) \\
(u_n, v_2) = (n-1, n-1, n-2, n-3, ..., 2, 1, 0)
\end{gathered}
$$

$$
\begin{gathered}
(u_1, v_3) = (3, 1, 2, 3, ..., n-2, n-1, n) \\
(u_2, v_3) = (2, 2, 1, 2, ..., n-3, n-2, n-1) \\
(u_3, v_3) = (3, 3, 2, 1, ..., n-4, n-3, n-2) \\
\vdots \\
(u_{n-1}, v_3) = (n-1, n-1, n-2, n-3, ..., 2, 1, 2) \\
(u_n, v_3) = (n, n, n-1, n-2, ..., 3, 2, 1)
\end{gathered}
$$

It It completes the proof that $\gamma_{rst}(P_n \times P_3) = n + 1$ for $m = 3$. □

Case 2. For m otherwise.
First, determining the lower bound and upper bound of $\gamma_{rst}(P_n \times P_m)$. We use Lemma 1.1 to show the lower bound of $\gamma_{rst}(P_n \times P_m)$, thus we have $\gamma_{rst}(P_n \times P_m) \geq max\{\gamma_{st}(P_n \times P_m), dim(P_n \times P_m)\}$. We know that $\gamma_{st}(P_n \times P_m) = \left\lceil \frac{m}{3} \right\rceil n$ and $dim(P_n \times P_m) = 2$. Hence, it implies

$$
\begin{aligned}
\gamma_{rst}(P_n \times P_m) &\geq max\{\gamma_{st}(P_n \times P_m), dim(P_n \times P_m)\} \\
&= max\{\left\lceil \tfrac{m}{3} \right\rceil n, 2\} = \left\lceil \tfrac{m}{3} \right\rceil n
\end{aligned}
$$

Furthermore, we determine the upper bound of $\gamma_{rst}(P_n \times P_m)$ by defining the resolving strong dominating set $R_D(P_n \times P_m)$. We divide three cases for defining the resolving strong dominating set of $(P_n \times P_m)$, namely

(i) For $m \equiv 0(mod)$, $R_D(P_n \times P_m) = \{(u_l, v_k) : 1 \leq l \leq n, 1 \leq k \leq m \; and \; k \equiv 2(mod\ 3)\}$

(ii) For $m \equiv 2(mod)$, $R_D(P_n \times P_m) = \{(u_l, v_{m-1}), (u_l, v_k) : 1 \leq l \leq n, 1 \leq k < m \; and \; k \equiv 2(mod\ 3)\}$

(iii) For $m \equiv 1(mod)$, $R_D(P_n \times P_m) = \{(u_l, v_{m-1}), (u_l, v_k) : 1 \leq l \leq n, 1 \leq k < m - 1 \; and \; k \equiv 2(mod\ 3)\}$

Let the representations of each vertex in $V(P_n \times P_m)$ to R_D is $r[(u_i, v_j)|R_D] = (\alpha_l^k : 1 \leq l \leq n, 1 \leq k \leq m \; and \; k \equiv 2(mod\ 3))$. α_l^k is a distance of a vertex $(u_i, v_j) \in V(P_n \times P_m)$ to every vertices in $R_D(P_n \times P_m)$ by the function $f : d[(u_i, v_j), R_D(P_n \times P_m)] \longrightarrow \alpha_l^k$, where

$$\alpha_l^k = \begin{cases} l - i + |j - k|, & \text{if } i \leq l \\ i - l + |j - k|, & \text{if } i > l \end{cases}$$

It easy to see that the representations of vertices in $V(P_n \times P_3)$ are all distinct. It It completes the proof that $\gamma_{rst}(P_n \times P_3) = \left\lceil \frac{m}{3} \right\rceil n$ for m otherwise. □

Theorem 3.2. *For every positive integer $n, m \geq 3$ and $m \geq n$,*

$$\gamma_{rst}(P_n \times C_m) = \begin{cases} n + 1, & \textit{if } m = 3 \\ \lceil \frac{m}{3} \rceil n, & \textit{otherwise} \end{cases}$$

Let P_n and C_m are path and cycle graph, respectively. The vertex set of path is $V(P_n) = \{u_1, u_2, u_3, \ldots, u_n$ and vertex set of cycle is $V(C_m) = \{v_1, v_2, v_3, \ldots, v_m\}$. Graph $P_n \times C_m$ is a connected graph with vertex set $\{(u, v)|u \in V(P_n)$ and $v \in V(C_m)$, such that two vertices $(u_1, v_1), (u_2, v_2)$ are adjacent if only if either $u_1 = u_2$ in P_n and v_1v_2 in $E(C_m)$ or u_1u_2 in $E(P_n)$ and $v_1 = v_2$ in C_m. We divide into two cases to prove the resolving strong domination number of $P_n \times C_m$.

Case 1. For $m = 3$.

First, determining the lowerbound and upperbound of $\gamma_{rst}(P_n \times C_3)$. We use Lemma 1.1 to show the lowerbound of $\gamma_{rst}(P_n \times C_3)$, thus we have $\gamma_{rst}(P_n \times C_3) \geq max\{\gamma_{st}(P_n \times C_3), dim(P_n \times C_3)\}$. We know that $\gamma_{st}(P_n \times C_3) = n$ and $dim(P_n \times C_3) = 2$. Hence, it implies

$$\begin{aligned} \gamma_{rst}(P_n \times C_3) &\geq max\{\gamma_{st}(P_n \times C_3), dim(P_n \times C_3)\} \\ &= max\{n, 2\} = n \end{aligned}$$

Furthermore, we determine the upperbound of $\gamma_{rst}(P_n \times C_3)$ by defining the resolving strong dominating set $R_D(P_n \times C_3)$. By considering the above vertex and edge sets, we define resolving strong dominating set $R_D(P_n \times C_3) = \{(u_i, v_2) : 1 \leq i \leq n\}$ and we illustrate this resolving strong dominating set in Figure 4. Based on the illustration in Figure 4, the vertices (u_i, v_1) and (u_i, v_3) will receive the same representation for $1 \leq i \leq n$. Hence, we add 1 vertex to the resolving strong dominating set $R_D(P_n \times C_3)$, such that the representations of vertices in $V(P_n \times C_3)$ are all distinct. The resolving strong dominating set of $(P_n \times C_3)$ is $R_D(P_n \times C_3) = \{(u_2, v_1), (u_i, v_2) : 1 \leq i \leq n\}$, see Figure 5 to this illustration. Based on the Figure 5, we give the all representation of each vertex in $V(P_n \times C_3)$ in the following.

$$\begin{gathered} (u_1, v_1) = (1, 1, 2, 3, ..., n-2, n-1, n) \\ (u_2, v_1) = (0, 2, 1, 2, ..., n-3, n-2, n-1) \\ (u_3, v_1) = (1, 3, 2, 1, ..., n-4, n-3, n-2) \\ \vdots \\ (u_{n-1}, v_1) = (n-3, n-1, n-2, n-3, ..., 2, 1, 2) \\ (u_n, v_1) = (n-2, n, n-1, n-2, ..., 3, 2, 1) \\ (u_1, v_2) = (2, 0, 1, 2, ..., n-3, n-2, n-1) \\ (u_2, v_2) = (1, 1, 0, 1, ..., n-4, n-3, n-2) \\ (u_3, v_2) = (2, 2, 1, 0, ..., n-5, n-4, n-3) \\ \vdots \\ (u_{n-1}, v_2) = (n-2, n-2, n-3, n-4, ..., 3, 2, 1) \\ (u_n, v_2) = (n-1, n-1, n-2, n-3, ..., 2, 1, 0) \end{gathered}$$

$$\begin{gathered} (u_1, v_3) = (2, 1, 2, 3, ..., n-2, n-1, n) \\ (u_2, v_3) = (1, 2, 1, 2, ..., n-3, n-2, n-1) \\ (u_3, v_3) = (2, 3, 2, 1, ..., n-4, n-3, n-2) \end{gathered}$$

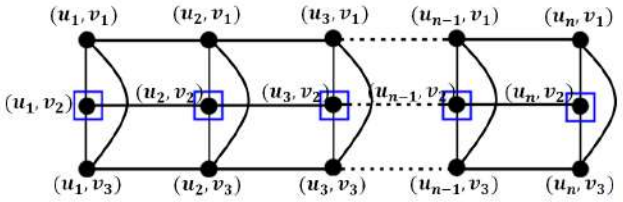

Figure 4. The illustration of the resolving strong dominating set of $P_n \odot C_3$.

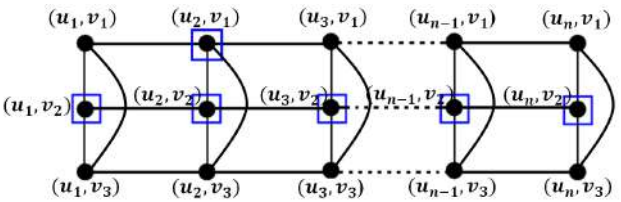

Figure 5. The illustration of the resolving strong dominating set on $P_n \odot C_3$.

$$\vdots$$
$$(u_{n-1}, v_3) = (n-2, n-1, n-2, n-3, ..., 2, 1, 2)$$
$$(u_n, v_3) = (n-1, n, n-1, n-2, ..., 3, 2, 1)$$

It completes the proof that $\gamma_{rst}(P_n \times P_3) = n + 1$ for $m = 3$.□
Case 2. For m otherwise.
First, determining the lowerbound and upperbound of $\gamma_{rst}(P_n \times C_m)$. We use Lemma 1.1 to show the lowerbound of $\gamma_{rst}(P_n \times C_m)$, thus we have $\gamma_{rst}(P_n \times C_m) \geq max\{\gamma_{st}(P_n \times C_m), dim(P_n \times C_m)\}$. We know that $\gamma_{st}(P_n \times C_m) = \left\lceil \frac{m}{3} \right\rceil n$ and $dim(P_n \times C_m) = 2$. Hence, it implies

$$\gamma_{rst}(P_n \times C_m) \geq max\{\gamma_{st}(P_n \times C_m), dim(P_n \times C_m)\}$$
$$= max\{\left\lceil \frac{m}{3} \right\rceil n, 2\} = \left\lceil \frac{m}{3} \right\rceil n$$

Furthermore, we determine the upper bound of $\gamma_{rst}(P_n \times C_m)$ by defining the resolving strong dominating set $R_D(P_n \times C_m)$. We divide three cases for defining the resolving strong dominating set of $(P_n \times C_m)$, namely

(i) For $m \equiv 0(mod)$, $R_D(P_n \times C_m) = \{(u_l, v_k) : 1 \leq l \leq n, 1 \leq k \leq m \text{ and } k \equiv 2(mod\ 3)\}$

(ii) For $m \equiv 2(mod)$, $R_D(P_n \times C_m) = \{(u_l, v_{m-1}), (u_l, v_k) : 1 \leq l \leq n, 1 \leq k < m \text{ and } k \equiv 2(mod\ 3)\}$

(iii) For $m \equiv 1(mod)$, $R_D(P_n \times C_m) = \{(u_l, v_{m-1}), (u_l, v_k) : 1 \leq l \leq n, 1 \leq k < m - 1 \text{ and } k \equiv 2(mod\ 3)\}$

Let the representations of each vertex in $V(P_n \times C_m)$ to R_D is $r[(u_i, v_j)|R_D] = (\alpha_l^k : 1 \leq l \leq n, 1 \leq k \leq m \text{ and } k \equiv 2(mod\ 3))$. α_l^k is a distance of a vertex $(u_i, v_j) \in V(P_n \times C_m)$ to every vertices in $R_D(P_n \times C_m)$ by the function $f : d[(u_i, v_j), R_D(P_n \times C_m)] \longrightarrow \alpha_l^k$, where

$$\alpha_l^k = \begin{cases} l-i+|j-k|, & \text{if } i \le l, k < n \text{ and } j < (k+n) \text{ or} \\ & k > n \text{ and } j > (k+n) \text{mod } m \\ i-l+|j-k|, & \text{if } i > l, k < n \text{ and } j < (k+n) \text{ or} \\ & k > n \text{ and } j > (k+n) \text{mod } m \\ l-i+2n-|j-k|-1, & \text{if } i \le l, k < n \text{ and } j \ge (k+n) \text{ or} \\ & k > n \text{ and } j \le (k+n) \text{mod } m \\ i-l+2n-|j-k|-1, & \text{if } i > l, k < n \text{ and } j \ge (k+n) \text{ or} \\ & k > n \text{ and } j \le (k+n) \text{mod } m \end{cases}$$

It easy to see that the representations of vertices in $V(P_n \times C_m)$ are all distinct. It completes the proof that $\gamma_{rst}(P_n \times C_3) = \left\lceil \frac{m}{3} \right\rceil n$ for m otherwise. □

4 Concluding Remark

The results in this paper are finding the exact values of $\gamma_{rst}(H)$, where H are $P_n \odot P_m$, $P_n \odot C_m$, $P_n \times P_m$ and $P_n \times C_m$. However, to determine γ_{rst} of any graph H is considered to be an NP-problem. Therefore we propose the following open problems.

(i) Determine γ_{rst} of any graph H apart from above investigated graphs.

(ii) Determine the sharpest lower and upper bound of γ_{rst} for any coronation and cartesian product of graphs.

Acknowledgments

We gratefully an acknowledge the support from Combinatorics, Graph Theory, and Network Topology (CGANT) Research Group University of Jember and Department of Mathematics, Kongunadu Arts and Science College of year 2021.

References

[1] G. Chartrand, L. Lesniak, P. Zhang, Graphs and Digraphs, sixth ed., Taylor and Francis Group, Boca Raton, New York

[2] P.J. Slater, Leaves of trees, Congr. Numer. 14 (1975) 549âĂŞ559.

[3] P.J. Slater, Dominating and reference sets in a graph, J. Math. Phys. Sci. 22 (1988) 445âĂŞ455.

[4] T.W. Haynes, S.T. Hedetniemi, P.J. Slater, Fundamentals of domination in graphs, Marcel Dekker, New York, 1998.

[5] Dieter Rautenbach, Bounds on the strong domination number, Discrete Mathematics 215 (2000) 201-212.

[6] S. K. Vaidya, S. H. Karkar, On Strong Domination Number of Graphs, *Applications and Applied Mathematics*: An International Journal (AAM) **12** pp. 604-612

[7] Wardani, D.A.R., Dafik, Agustin, I.H., The locating dominating set (LDS) of generalized of corona product of path graph and any graphs, 2020, Journal of Physics: Conference Series **1465**(1).

[8] Dafik, Agustin, I.H., Wardani, D.A.R., The number of locating independent dominating set on generalized corona product graphs, 2020, Advances in Mathematics: Scientific Journal 9(7), pp. 4873-4891.

[9] Yuliana, I., Dafik, Agustin, I.H., Wardani, D.A.R. On the power domination number of corona product and join graphs, 2019, Journal of Physics: Conference Series **1211**(1).

[10] Dafik, Agustin, I.H., Retno Wardani, D.A., Kurniawati, E.Y., A study of local domination number of S n âŁţ H graph, 2018, Journal of Physics: Conference Series **943**(1).

[11] R Alfarisi, Dafik and AI Kristiana, Resolving domination number of graphs, Discrete Mathematics *Algorithms and Applications* **11** No. 06

[12] Iswadi H, Baskoro E.T, Simanjuntak R, On the Metric Dimension of Corona Product of Graphs, Far East Journal of Mathematical Sciences 2(2) 2011.

Author information

Dafik[*,1,2], I.H Agustin[1], A.C Prihandoko[1,3], E.Y Kurniawati[1],
R Nisviasari[1], N. Mohanapriya[4], [1]CGANT-University of Jember Indonesia, [2]Department of Mathematics Education University of Jember Indonesia, [3]Information Technology Department University of Jember Indonesia, [4]Department of Mathematics, Kongunadu Arts and Science College, India.
E-mail: d.dafik@unej.ac.id

Received : January 5, 2021
Accepted : April 15, 2021

More on Single Valued Neutrosophic R-dynamic Vertex Coloring and R-dynamic Edge Coloring of graphs

[1]Aparna V, [2]Mohanapriya N and [3]Broumi Said
[1,2]PG and Research Department of Mathematics, Kongunadu Arts and Science College,
Coimbatore-641 029, Tamil Nadu, India.
[3]Laboratory of Information Processing, Faculty of Science Ben M'Sik,
University Hassan II, Casablanca, Morocco.
aparnav18794@gmail.com[1], phdmohana@gmail.com[2], broumisaid78@gmail.com[3]

Abstract

The notion of neutrosophic sets facilitates the analysis of values that are unclear or indeterminate. In this paper, we discuss the single valued neutrosophic R-dynamic vertex coloring of Cartesian product of SVNG's and join of SVNG's. Further we have described the concept of single valued neutrosophic R-dynamic edge coloring and provided some examples and theorems.
Keywords: Single Valued Neutrosophic Graph; Single Valued Neutrosophic Vertex Coloring; Single Valued Neutrosophic R-dynamic Vertex Coloring; Single Valued Neutrosophic Edge Coloring; Single Valued Neutrosophic R-dynamic Edge Coloring.

1 Introduction

Rosenfeld [20], 10 years after Zadeh's seminal study in fuzzy sets [23], was the first to develop fuzzy graphs. Fuzzy graph theory is presently being used in a variety of domains in modern science and technology, including information theory, neural networks, expert systems, cluster analysis, medical diagnostics, control theory, and many others. In 2004, Munoz et al. [15] presented the fuzzy chromatic number, which was further developed in 2006 by C. Eslahchi and B. N. Onagh [11]. In 2009, S. Lavanya and R. Sattanathan [13] proposed the idea of fuzzy total coloring for the first time. Arindam Dey and Anita Pal discussed fuzzy vertex coloring with fuzzy graphs using the α-cut in the paper [7] in 2012. Anjaly Kishore, M.S.Sunitha, published a research paper [4] in 2014 on strong chromatic number of fuzzy graphs.
To deal with data on membership and non-membership values, intuitionistic fuzzy sets are utilised. Kassimir T. Atanassov [6] developed the concepts of intuitionistic fuzzy sets and intuitionistic fuzzy graphs in 1986 and 1999, respectively. Ismail and Rifayathali [12] addressed intuitionistic fuzzy graph coloring with (α, β) cuts in 2015, while Rifayathali et al. [16] published studies on intuitionistic fuzzy coloring and strong intuitionistic fuzzy coloring in 2017 and 2018.
The principles of membership and non-membership are insufficient to predict the result of all real-time circumstances. In situations when the vagueness or indeterminacy of a decision must be considered, intuitionistic fuzzy logic is unsuitable to provide a solution. F. Smarandache discovered a solution as a result of this condition: "Neutrosophic logic". Smarandache [21] developed the concept of Neutrosophic Sets in 1998, which is a generalised form of intuitionistic fuzzy sets that incorporates three categories of values: truth, indeterminacy, and falsity membership values. Single-valued neutrosophic sets were studied by Wang et al. [22] in 2010. In 2015, Dhavaseelan et al. [10] introduced and discussed Strong Neutrosophic graphs, and in 2016, Akram and Shahzadi [1-3] introduced and discussed Single Valued Neutrosophic graph definitions and operations of neutrosophic graphs. Broumi et al. [8, 9] expanded on their prior work with single-valued neutrosophic graphs. Rohini et al. established the concept of single valued neutrosophic vertex coloring, single valued neutrosophic edge coloring, and single valued neutrosophic total coloring of single valued neutrosophic graph with examples in the research publications [17, 18] published in 2019. In addition, Rohini et al. have expanded on their work on single valued neutrosophic vertex coloring and developed the concept of single valued neutrosophic irregular vertex coloring in [19].

DOI:https://doi.org/10.54216/IJNS.160102

Received: June 07, 2021 Accepted: October 19, 2021

Bruce Montgomery proposed the concept of r-dynamic coloring in [14]. The r-dynamic coloring of a graph is an appropriate coloring of the graph in which each vertex u receives $min\{r, d(u)\}$ different colors from its neighbours. In [5] we have introduced the concept of single valued neutrosophic R-dynamic vertex coloring and furthermore in this paper, we discuss the single valued neutrosophic R-dynamic vertex coloring of Cartesian product of SVNG's and join of SVNG's. Also we have introduce the concept of single valued neutrosophic R-dynamic edge coloring and provided some examples and theorems.

2 Preliminaries

Definition 2.1. [21] Consider S as a collection of objects(points). Then the **neutrosophic set** P in S is described by truth membership function $t_P(s)$, an indeterminacy function $i_P(s)$ and a falsity membership (non-membership) function $f_P(s)$. The mappings $t_P(s)$, $i_P(s)$ and $f_P(s)$ are real standard or non-standard subsets of $]0^-, 1^+[$ which means $t_P(s) : S \to]0^-, 1^+[$, $i_P(s) : S \to]0^-, 1^+[$ and $f_P(s) : S \to]0^-, 1^+[$. Also $0^- \leq t_P(s) + i_P(s) + f_P(s) \leq 3^+$.

Definition 2.2. [2] A **Single Valued Neutrosophic Graph (SNVG)** $G = (C, D)$ is a pair consisting of $C : N \to [0, 1]$ which is a single valued neutrosophic set on N and $D : N \times N \to [0, 1]$, a single valued neutrosophic relation on N with the following characteristics:
$t_D(uv) \leq min\{t_C(u), t_C(v)\}$
$i_D(uv) \leq min\{i_C(u), i_C(v)\}$
$f_D(uv) \leq max\{f_C(u), f_C(v)\}$
for all $u, v \in N$. The sets C and D are said to be single valued neutrosophic vertex set and edge set of G respectively. The single valued neutrosophic relation D is symmetric if it satisfies $t_D(uv) = t_D(vu)$, $i_D(uv) = i_D(vu)$ and $f_D(uv) = f_D(vu)$ for all $u, v \in N$.

Definition 2.3. [3] A **complete neutrosophic graph (CSVNG)** is an SVNG $G = (C, D)$ which complies criteria below:
$t_D(uv) = min\{t_C(u), t_C(v)\}$
$i_D(uv) = min\{i_C(u), i_C(v)\}$
$f_D(uv) = max\{f_C(u), f_C(v)\}$
for all $u, v \in C$.

Definition 2.4. [17] The collection $\Gamma = \{\gamma_1, \gamma_2, \cdots, \gamma_p\}$ of SVN fuzzy sets is termed as **p-Single Valued Neutrosophic Vertex Coloring(SVNVC)** of SVNG $G = (C, D)$ if the following criteria hold:
1. $\vee\gamma_s(u) = C, \forall u \in C$
2. $\gamma_s \wedge \gamma_t = 0$
3. For each incident vertices of the edge uv of G, $min\{\gamma_s(t_C(u)), \gamma_s(t_C(v))\} = 0$, $min\{\gamma_s(i_C(u)), \gamma_s(i_C(v))\} = 0$ and $max\{\gamma_s(f_C(u)), \gamma_s(f_C(v))\} = 1, (1 \leq s \leq p)$.
This is indicated as $\chi^v(G)$ and is termed as the SVN chromatic number of the SVNG G.

Definition 2.5. [5] A family $\Gamma = \{\gamma_1, \gamma_2, \cdots, \gamma_p\}$ of SVN fuzzy sets is termed as **p-Single Valued Neutrosophic R-dynamic Vertex Coloring (SVNRVC)** of a SVNG $G = (C, D)$ if the following criteria hold:
1. $\vee\gamma_s(u) = C, \forall u \in C$
2. $\gamma_s \wedge \gamma_t = 0$
3. For each incident vertices of the edge uv of G, $min\{\gamma_s(t_C(u)), \gamma_s(t_C(v))\} = 0$, $min\{\gamma_s(i_C(u)), \gamma_s(i_C(v))\} = 0$ and $max\{\gamma_s(f_C(u)), \gamma_s(f_C(v))\} = 1, (1 \leq s \leq p)$.
4. Every vertex u with m number of incident edges, the corresponding incident vertices of the vertex u receives atleast $min\{R, m\}$ different members(colors) from the set Γ.
Here, $1 \leq R \leq M$ where M represents the maximum number of incident edges of the vertices of SVNG G.
The least value of p is the SVNRVC of SVNG G which is denoted as $\chi^v_R(G)$, is called the Single Valued Neutrosophic R-dynamic chromatic number of the SVNG G.
Further we define Single Valued Neutrosophic dynamic chromatic number of the SVNG G, $\chi^v_2(G)$ by replacing $R = 2$ in criterion 4 i.e., (4) becomes every vertex u with m number of incident edges, the corresponding incident vertices of the vertex u receives atleast $min\{2, m\}$ different members(colors) from the set Γ.

Definition 2.6. [8] **Path** P_m in a single valued neutrosophic graph $G = (C, D)$ is an arrangement of distinct vertices $v_1, v_2, \cdots, v_m$ which complies the criteria $t_D(v_{k-1}, v_k) > 0$, $i_D(v_{k-1}, v_k) > 0$ and $f_D(v_{k-1}, v_k) > 0$ for $2 \leq k \leq m$.

DOI:https://doi.org/10.54216/IJNS.160102
Received: June 07, 2021 Accepted: October 19, 2021

Definition 2.7. [8] A **cycle** C_m in a single valued neutrosophic graph $G = (C, D)$ is a sequence of distinct vertices $v_1, v_2, \cdots, v_m, v_1$ which satisfies the condition $t_D(v_{k-1}, v_k) > 0$, $i_D(v_{k-1}, v_k) > 0$ and $f_D(v_{k-1}, v_k) > 0$ for $2 \leq k \leq$, together with $t_D(v_1, v_m) > 0$, $i_D(v_1, v_m) > 0$ and $f_D(v_1, v_m) > 0$.

Definition 2.8. [3] Consider $G_1 = (C_1, D_1)$ and $G_2 = (C_2, D_2)$ be two single valued neutrosophic graphs of $G_1^* = (V_1, E_1)$ and $G_2^* = (V_2, E_2)$ respectively. Then the cartesian product $G_1 \times G_2$ is defined to be the pair (C, D) such that
1. $t_C(u_1, u_2) = min\{t_{C_1}(u_1), t_{C_2}(u_2)\}$
$i_C(u_1, u_2) = min\{i_{C_1}(u_1), i_{C_2}(u_2)\}$
$f_C(u_1, u_2) = max\{f_{C_1}(u_1), f_{C_2}(u_2)\}$
2. $t_D((u, u_2)(u, v_2)) = min\{t_{C_1}(u), t_{D_2}(u_2v_2)\}$
$i_D((u, u_2)(u, v_2)) = min\{i_{C_1}(u), i_{D_2}(u_2v_2)\}$
$f_D((u, u_2)(u, v_2)) = max\{f_{C_1}(u), f_{D_2}(u_2v_2)\}$ for all $u \in V_1$ and for all $u_2v_2 \in E_2$.
3. $t_D((u_1, v), (v_1, v)) = min\{t_{D_1}(u_1v_1), t_{C_2}(v)\}$
$i_D((u_1, v), (v_1, v)) = min\{i_{D_1}(u_1v_1), i_{C_2}(v)\}$
$f_D((u_1, v), (v_1, v)) = max\{f_{D_1}(u_1v_1), f_{C_2}(v)\}$ for all $v \in V_2$ and for all $u_1v_1 \in E_1$.

Definition 2.9. [3] Consider $G_1 = (C_1, D_1)$ and $G_2 = (C_2, D_2)$ be two single valued neutrosophic graphs of $G_1^* = (V_1, E_1)$ and $G_2^* = (V_2, E_2)$ respectively. Then the join $G_1 + G_2$ is defined to be the pair (C, D) such that

$$1.t_C(u) = \begin{cases} t_{C_1}(u) & if \quad u \in V_1 \; and \; u \notin V_2 \\ t_{C_2}(u) & if \quad u \in V_2 \; and \; u \notin V_1 \\ max\{t_{C_1}(u), t_{C_2}(u)\} & if \quad u \in V_1 \cap V_2 \end{cases}$$

$$2.\ i_C(u) = \begin{cases} i_{C_1}(u) & if \quad u \in V_1 \; and \; u \notin V_2 \\ i_{C_2}(u) & if \quad u \in V_2 \; and \; u \notin V_1 \\ max\{i_{C_1}(u), i_{C_2}(u)\} & if \quad u \in V_1 \cap V_2 \end{cases}$$

$$3.\ f_C(u) = \begin{cases} f_{C_1}(u) & if \quad u \in V_1 \; and \; u \notin V_2 \\ f_{C_2}(u) & if \quad u \in V_2 \; and \; u \notin V_1 \\ min\{f_{C_1}(u), f_{C_2}(u)\} & if \quad u \in V_1 \cap V_2 \end{cases}$$

$$4.\ t_D(uv) = \begin{cases} t_{D_1}(uv) & if \quad uv \in E_1 \; and \; uv \notin E_2 \\ t_{D_2}(uv) & if \quad uv \in E_2 \; and \; uv \notin E_1 \\ max\{t_{D_1}(uv), t_{D_2}(uv)\} & if \quad uv \in E_1 \cap E_2 \\ min\{t_{C_1}(u), t_{C_2}(v)\} & if \quad uv \in E' \end{cases}$$

$$5.\ i_D(uv) = \begin{cases} i_{D_1}(uv) & if \quad uv \in E_1 \; and \; uv \notin E_2 \\ i_{D_2}(uv) & if \quad uv \in E_2 \; and \; uv \notin E_1 \\ max\{i_{D_1}(uv), i_{D_2}(uv)\} & if \quad uv \in E_1 \cap E_2 \\ min\{i_{C_1}(u), i_{C_2}(v)\} & if \quad uv \in E' \end{cases}$$

$$6.\ f_D(uv) = \begin{cases} f_{D_1}(uv) & if \quad uv \in E_1 \; and \; uv \notin E_2 \\ f_{D_2}(uv) & if \quad uv \in E_2 \; and \; uv \notin E_1 \\ min\{f_{D_1}(uv), f_{D_2}(uv)\} & if \quad uv \in E_1 \cap E_2 \\ max\{f_{C_1}(u), f_{C_2}(v)\} & if \quad uv \in E' \end{cases}$$

3 Single Valued Neutrosophic Dynamic Coloring of Graphs

In this section we have determined the Single Valued Neutrosophic Dynamic Chromatic Number of some graphs like Cartesian product of path with path, path with complete graph; join of path and path, path with cycle and path with complete SVNG.

Theorem 3.1. *Let $l \geq 2, m \geq 2$, then the single valued neutrosophic dynamic chromatic number of the cartesian product of path P_l with path P_m is $\chi_2^v(P_l \times P_m) = 4$.*

Proof. Consider path $P_l = (C_1, D_1)$ with SVN vertex set $C_1 = \{v_1, v_2, \cdots, v_l\}$ and path $P_m = (C_2, D_2)$ with SVN vertex set $C_2 = \{u_1, u_2, \cdots, u_m\}$. Then the cartesian product of path P_l with path P_m is SVNG $P_l \times P_m = (C, D)$ with SVN vertex set $C = \{(v_j, u_k) : 1 \leq j \leq l, 1 \leq k \leq m\}$ and edge set defined as in the definition 2.8.
Let $\Gamma = \{\gamma_1, \gamma_2, \gamma_3, \gamma_4\}$ be the collection of fuzzy sets determined on vertices of $P_l \times P_m$ for $R = 2$ as follows:

DOI:https://doi.org/10.54216/IJNS.160102
Received: June 07, 2021 Accepted: October 19, 2021

Case 1: When $m \equiv 0(mod\ 4)$ and $m \equiv 2(mod\ 4)$.

$$\gamma_1((v_j,u_k)) = \begin{cases} (t_C((v_j,u_k)), i_C((v_j,u_k)), f_C((v_j,u_k)) & for \quad j \equiv 1(mod\ 4)\ and\ k \equiv 1(mod\ 4), \\ & \quad j \equiv 2(mod\ 4)\ and\ k \equiv 3(mod\ 4), \\ & \quad j \equiv 3(mod\ 4)\ and\ k \equiv 2(mod\ 4,) \\ & \quad j \equiv 0(mod\ 4)\ and\ k \equiv 0(mod\ 4) \\ (0,0,1) & for \quad otherwise \end{cases}$$

$$\gamma_2((v_j,u_k)) = \begin{cases} (t_C((v_j,u_k)), i_C((v_j,u_k)), f_C((v_j,u_k)) & for \quad j \equiv 1(mod\ 4)\ and\ k \equiv 2(mod\ 4), \\ & \quad j \equiv 2(mod\ 4)\ and\ k \equiv 0(mod\ 4), \\ & \quad j \equiv 3(mod\ 4)\ and\ k \equiv 1(mod\ 4), \\ & \quad j \equiv 0(mod\ 4)\ and\ k \equiv 3(mod\ 4) \\ (0,0,1) & for \quad otherwise \end{cases}$$

$$\gamma_3((v_j,u_k)) = \begin{cases} (t_C((v_j,u_k)), i_C((v_j,u_k)), f_C((v_j,u_k)) & for \quad j \equiv 1(mod\ 4)\ and\ k \equiv 3(mod\ 4), \\ & \quad j \equiv 2(mod\ 4)\ and\ k \equiv 1(mod\ 4), \\ & \quad j \equiv 3(mod\ 4)\ and\ k \equiv 0(mod\ 4), \\ & \quad j \equiv 0(mod\ 4)\ and\ k \equiv 2(mod\ 4) \\ (0,0,1) & for \quad otherwise \end{cases}$$

$$\gamma_4((v_j,u_k)) = \begin{cases} (t_C((v_j,u_k)), i_C((v_j,u_k)), f_C((v_j,u_k)) & for \quad j \equiv 1(mod\ 4)\ and\ k \equiv 0(mod\ 4), \\ & \quad j \equiv 2(mod\ 4)\ and\ k \equiv 2(mod\ 4), \\ & \quad j \equiv 3(mod\ 4)\ and\ k \equiv 3(mod\ 4), \\ & \quad j \equiv 0(mod\ 4)\ and\ k \equiv 1(mod\ 4) \\ (0,0,1) & for \quad otherwise \end{cases}$$

Case 2 : When $m \equiv 1(mod\ 4)$.

$$\gamma_1((v_j,u_k)) = \begin{cases} (t_C((v_j,u_k)), i_C((v_j,u_k)), f_C((v_j,u_k)) & for \quad j \equiv 1(mod\ 4)\ and\ k \equiv 1(mod\ 4), \\ & \quad j \equiv 2(mod\ 4)\ and\ k \equiv 3(mod\ 4), \\ & \quad j \equiv 3(mod\ 4)\ and\ k \equiv 2(mod\ 4), \\ & \quad j \equiv 0(mod\ 4)\ and\ k \equiv 0(mod\ 4), \\ & \quad j \equiv 2(mod\ 4)\ and\ k = m \\ (0,0,1) & for \quad otherwise \end{cases}$$

$$\gamma_2((v_j,u_k)) = \begin{cases} (t_C((v_j,u_k)), i_C((v_j,u_k)), f_C((v_j,u_k)) & for \quad j \equiv 1(mod\ 4)\ and\ k \equiv 2(mod\ 4), \\ & \quad j \equiv 2(mod\ 4)\ and\ k \equiv 0(mod\ 4), \\ & \quad j \equiv 3(mod\ 4)\ and\ k \equiv 1(mod\ 4), \\ & \quad j \equiv 0(mod\ 4)\ and\ k \equiv 3(mod\ 4), \\ & \quad j \equiv 0(mod\ 4)\ and\ k = m \\ (0,0,1) & for \quad otherwise \end{cases}$$

$$\gamma_3((v_j,u_k)) = \begin{cases} (t_C((v_j,u_k)), i_C((v_j,u_k)), f_C((v_j,u_k)) & for \quad j \equiv 1(mod\ 4)\ and\ k \equiv 3(mod\ 4), \\ & \quad j \equiv 2(mod\ 4)\ and\ k \equiv 1(mod\ 4), \\ & \quad j \equiv 3(mod\ 4)\ and\ k \equiv 0(mod\ 4), \\ & \quad j \equiv 0(mod\ 4)\ and\ k \equiv 2(mod\ 4), \\ & \quad j \equiv 1(mod\ 4)\ and\ k = m \\ (0,0,1) & for \quad otherwise \end{cases}$$

$$\gamma_4((v_j,u_k)) = \begin{cases} (t_C((v_j,u_k)), i_C((v_j,u_k)), f_C((v_j,u_k)) & for \quad j \equiv 1(mod\ 4)\ and\ k \equiv 0(mod\ 4), \\ & \quad j \equiv 2(mod\ 4)\ and\ k \equiv 2(mod\ 4), \\ & \quad j \equiv 3(mod\ 4)\ and\ k \equiv 3(mod\ 4), \\ & \quad j \equiv 0(mod\ 4)\ and\ k \equiv 1(mod\ 4), \\ & \quad j \equiv 3(mod\ 4)\ and\ k = m \\ (0,0,1) & for \quad otherwise \end{cases}$$

Case 3 : When $m \equiv 3(mod\ 4)$.

$$\gamma_1((v_j,u_k)) = \begin{cases} (t_C((v_j,u_k)), i_C((v_j,u_k)), f_C((v_j,u_k)) & for \quad j \equiv 1(mod\ 4)\ and\ k \equiv 1(mod\ 4), \\ & \quad j \equiv 2(mod\ 4)\ and\ k \equiv 3(mod\ 4), \\ & \quad j \equiv 3(mod\ 4)\ and\ k \equiv 2(mod\ 4), \\ & \quad j \equiv 0(mod\ 4)\ and\ k \equiv 0(mod\ 4), \\ & \quad j \equiv 2(mod\ 4)\ and\ k = m-1, \\ & \quad j \equiv 0(mod\ 4)\ and\ k = m \\ (0,0,1) & for \quad otherwise \end{cases}$$

DOI:https://doi.org/10.54216/IJNS.160102
Received: June 07, 2021 Accepted: October 19, 2021

$$\gamma_2((v_j,u_k)) = \begin{cases} (t_C((v_j,u_k)), i_C((v_j,u_k)), f_C((v_j,u_k)) & for \quad j \equiv 1(mod\ 4)\ and\ k \equiv 2(mod\ 4), \\ & \quad j \equiv 2(mod\ 4)\ and\ k \equiv 0(mod\ 4), \\ & \quad j \equiv 3(mod\ 4)\ and\ k \equiv 1(mod\ 4), \\ & \quad j \equiv 0(mod\ 4)\ and\ k \equiv 3(mod\ 4), \\ & \quad j \equiv 0(mod\ 4)\ and\ k = m-1, \\ & \quad j \equiv 2(mod\ 4)\ and\ k = m \\ (0,0,1) & for \quad otherwise \end{cases}$$

$$\gamma_3((v_j,u_k)) = \begin{cases} (t_C((v_j,u_k)), i_C((v_j,u_k)), f_C((v_j,u_k)) & for \quad j \equiv 1(mod\ 4)\ and\ k \equiv 3(mod\ 4), \\ & \quad j \equiv 2(mod\ 4)\ and\ k \equiv 1(mod\ 4), \\ & \quad j \equiv 3(mod\ 4)\ and\ k \equiv 0(mod\ 4), \\ & \quad j \equiv 0(mod\ 4)\ and\ k \equiv 2(mod\ 4), \\ & \quad j \equiv 1(mod\ 4)\ and\ k = m-1, \\ & \quad j \equiv 3(mod\ 4)\ and\ k = m \\ (0,0,1) & for \quad otherwise \end{cases}$$

$$\gamma_4((v_j,u_k)) = \begin{cases} (t_C((v_j,u_k)), i_C((v_j,u_k)), f_C((v_j,u_k)) & for \quad j \equiv 1(mod\ 4)\ and\ k \equiv 0(mod\ 4), \\ & \quad j \equiv 2(mod\ 4)\ and\ k \equiv 2(mod\ 4), \\ & \quad j \equiv 3(mod\ 4)\ and\ k \equiv 3(mod\ 4), \\ & \quad j \equiv 0(mod\ 4)\ and\ k \equiv 1(mod\ 4), \\ & \quad j \equiv 3(mod\ 4)\ and\ k = m-1, \\ & \quad j \equiv 1(mod\ 4)\ and\ k = m \\ (0,0,1) & for \quad otherwise \end{cases}$$

Case 4 : For $P_3 \times P_3$.

$$\gamma_1((v_j,u_k)) = \begin{cases} (t_C((v_j,u_k)), i_C((v_j,u_k)), f_C((v_j,u_k)) & for \quad jk = 11, 13, 32 \\ (0,0,1) & for \quad otherwise \end{cases}$$

$$\gamma_2((v_j,u_k)) = \begin{cases} (t_C((v_j,u_k)), i_C((v_j,u_k)), f_C((v_j,u_k)) & for \quad jk = 12, 31, 33 \\ (0,0,1) & for \quad otherwise \end{cases}$$

$$\gamma_3((v_j,u_k)) = \begin{cases} (t_C((v_j,u_k)), i_C((v_j,u_k)), f_C((v_j,u_k)) & for \quad jk = 21, 23 \\ (0,0,1) & for \quad otherwise \end{cases}$$

$$\gamma_4((v_j,u_k)) = \begin{cases} (t_C((v_j,u_k)), i_C((v_j,u_k)), f_C((v_j,u_k)) & for \quad jk = 22 \\ (0,0,1) & for \quad otherwise \end{cases}$$

As a result, the family $\Gamma = \{\gamma_1, \gamma_2, \gamma_3, \gamma_4\}$ ensures that SVNRVC requirements are met. Families with fewer than four points did not match our defining criteria. Hence $\chi_2^v(P_l \times P_m) = 4$. □

Theorem 3.2. *Let $l \geq 2, m \geq 2$, then the single valued neutrosophic dynamic chromatic number of the cartesian product of path P_l with CSVNG K_m is $\chi_2^v(P_l \times K_m) = m$.*

Proof. Consider path $P_l = (C_1, D_1)$ with SVN vertex set $C_1 = \{v_1, v_2, \cdots, v_l\}$ and CSVNG $K_m = (C_2, D_2)$ with SVN vertex set $C_2 = \{u_1, u_2, \cdots, u_m\}$. Then the cartesian product of path P_l with CSVNG K_m is SVNG $P_l \times K_m = (C, D)$ with SVN vertex set $C = \{(v_j, u_k) : 1 \leq j \leq l, 1 \leq k \leq m\}$ and edge set defined as in the definition 2.8.

Let $\Gamma = \{\gamma_1, \gamma_2, \cdots, \gamma_m\}$ be the collection of fuzzy sets determined on vertices of $P_l \times K_m$ for $R = 2$ as follows:

$$\gamma_1((v_j,u_k)) = \begin{cases} (t_C((v_j,u_k)), i_C((v_j,u_k)), f_C((v_j,u_k)) & for \quad j \equiv 1(mod\ 2)\ and\ k = 1, \\ & \quad j \equiv 0(mod\ 2)\ and\ k = m \\ (0,0,1) & for \quad otherwise \end{cases}$$

For $2 \leq i \leq m$,

$$\gamma_i((v_j,u_k)) = \begin{cases} (t_C((v_j,u_k)), i_C((v_j,u_k)), f_C((v_j,u_k)) & for \quad j \equiv 1(mod\ 2)\ and\ k = i, \\ (t_C((v_j,u_k)), i_C((v_j,u_k)), f_C((v_j,u_k)) & \quad j \equiv 0(mod\ 2)\ and\ k = i-1 \\ (0,0,1) & for \quad otherwise \end{cases}$$

As a result, the family $\Gamma = \{\gamma_1, \gamma_2, \cdots, \gamma_m\}$ ensures that SVNRVC requirements are met. Families with fewer than m points did not match our defining criteria. Hence $\chi_2^v(P_l \times K_m) = m$. □

Theorem 3.3. *Let $l \geq 2, m \geq 2$, then the single valued neutrosophic dynamic chromatic number of the join of path P_l with path P_m is $\chi_2^v(P_l + P_m) = 4$.*

Proof. Consider path $P_l = (C_1, D_1)$ with SVN vertex set $C_1 = \{v_1, v_2, \cdots, v_l\}$ and path $P_m = (C_2, D_2)$ with SVN vertex set $C_2 = \{u_1, u_2, \cdots, u_m\}$. Also the vertex set of these SVNG's are disjoint. Then the join of path P_l with path P_m is SVNG $P_l + P_m = (C, D)$ with SVN vertex set $C = \{v_1, v_2, \cdots, v_l, u_1, u_2, \cdots, u_m\}$. Also the membership, indeterminacy and falsity functions of the vertices of $P_l + P_m$ is determined using the definition in 2.9 and edge set is also determined in the same way.

DOI:https://doi.org/10.54216/IJNS.160102
Received: June 07, 2021 Accepted: October 19, 2021

Let $\Gamma = \{\gamma_1, \gamma_2, \gamma_3, \gamma_4\}$ be the collection of fuzzy sets determined on vertices of $P_l + P_m$ for $R = 2$ as follows:

$$\gamma_1(v_j) = \begin{cases} (t_C(v_j), i_C(v_j), f_C(v_j)) & for \quad j \equiv 1(mod\ 2) \\ (0,0,1) & for \quad otherwise \end{cases}$$

$$\gamma_2(v_j) = \begin{cases} (t_C(v_j), i_C(v_j), f_C(v_j)) & for \quad j \equiv 0(mod\ 2) \\ (0,0,1) & for \quad otherwise \end{cases}$$

$$\gamma_3(u_k) = \begin{cases} (t_C(u_k), i_C(u_k), f_C(u_k)) & for \quad k \equiv 1(mod\ 2) \\ (0,0,1) & for \quad otherwise \end{cases}$$

$$\gamma_4(u_k) = \begin{cases} (t_C(u_k), i_C(u_k), f_C(u_k)) & for \quad k \equiv 0(mod\ 2) \\ (0,0,1) & for \quad otherwise \end{cases}$$

As a result, the family $\Gamma = \{\gamma_1, \gamma_2, \cdots, \gamma_4\}$ ensures that SVNRVC requirements are met. Families with fewer than four points did not match our defining criteria. Hence $\chi_2^v(P_l + P_m) = 4$. □

Theorem 3.4. *Let $l \geq 2, m \geq 3$, then the single valued neutrosophic dynamic chromatic number of the join of path P_l with cycle C_m is* $\chi_2^v(P_l + C_m) = \begin{cases} 4 & when \quad m\ is\ even \\ 5 & when \quad m\ is\ odd \end{cases}$.

Proof. Consider path $P_l = (C_1, D_1)$ with SVN vertex set $C_1 = \{v_1, v_2, \cdots, v_l\}$ and cycle $C_m = (C_2, D_2)$ with SVN vertex set $C_2 = \{u_1, u_2, \cdots, u_m\}$. Also the vertex set of these SVNG's are disjoint. Then the join of path P_l with cycle C_m is SVNG $P_l + C_m = (C, D)$ with SVN vertex set $C = \{v_1, v_2, \cdots, v_l, u_1, u_2, \cdots, u_m\}$. Also the membership, indeterminacy and falsity functions of the vertices of $P_l + C_m$ is determined using the definition in 2.9 and edge set is also determined in the same way.

Case 1 : When m is even.

Let $\Gamma = \{\gamma_1, \gamma_2, \gamma_3, \gamma_4\}$ be the collection of fuzzy sets determined on vertices of $P_l + C_m$ for $R = 2$ as follows:

$$\gamma_1(v_j) = \begin{cases} (t_C(v_j), i_C(v_j), f_C(v_j)) & for \quad j \equiv 1(mod\ 2) \\ (0,0,1) & for \quad otherwise \end{cases}$$

$$\gamma_2(v_j) = \begin{cases} (t_C(v_j), i_C(v_j), f_C(v_j)) & for \quad j \equiv 0(mod\ 2) \\ (0,0,1) & for \quad otherwise \end{cases}$$

$$\gamma_3(u_k) = \begin{cases} (t_C(u_k), i_C(u_k), f_C(u_k)) & for \quad k \equiv 1(mod\ 2) \\ (0,0,1) & for \quad otherwise \end{cases}$$

$$\gamma_4(u_k) = \begin{cases} (t_C(u_k), i_C(u_k), f_C(u_k)) & for \quad j \equiv 0(mod\ 2) \\ (0,0,1) & for \quad otherwise \end{cases}$$

As a result, the family $\Gamma = \{\gamma_1, \gamma_2, \cdots, \gamma_4\}$ ensures that SVNRVC requirements are met. Families with fewer than four points did not match our defining criteria.

Case 2 : When m is odd.

Let $\Gamma = \{\gamma_1, \gamma_2, \gamma_3, \gamma_4, \gamma_5\}$ be the collection of fuzzy sets determined on vertices of $P_l + C_m$ for $R = 2$ as follows:

$$\gamma_1(v_j) = \begin{cases} (t_C(v_j), i_C(v_j), f_C(v_j)) & for \quad j \equiv 1(mod\ 2) \\ (0,0,1) & for \quad otherwise \end{cases}$$

$$\gamma_2(v_j) = \begin{cases} (t_C(v_j), i_C(v_j), f_C(v_j)) & for \quad j \equiv 0(mod\ 2) \\ (0,0,1) & for \quad otherwise \end{cases}$$

$$\gamma_3(u_k) = \begin{cases} (t_C(u_k), i_C(u_k), f_C(u_k)) & for \quad k \equiv 1(mod\ 2)\ and\ k \neq m \\ (0,0,1) & for \quad otherwise \end{cases}$$

$$\gamma_4(u_k) = \begin{cases} (t_C(u_k), i_C(u_k), f_C(u_k)) & for \quad k \equiv 0(mod\ 2) \\ (0,0,1) & for \quad otherwise \end{cases}$$

$$\gamma_5(u_k) = \begin{cases} (t_C(u_k), i_C(u_k), f_C(u_k)) & for \quad k = m \\ (0,0,1) & for \quad otherwise \end{cases}$$

As a result, the family $\Gamma = \{\gamma_1, \gamma_2, \cdots, \gamma_5\}$ ensures that SVNRVC requirements are met. Families with fewer than five points did not match our defining criteria.

Hence $\chi_2^v(P_l + C_m) = \begin{cases} 4 & when \quad m\ is\ even \\ 5 & when \quad m\ is\ odd \end{cases}$. □

Theorem 3.5. *Let $l \geq 2, m \geq 2$, then the single valued neutrosophic dynamic chromatic number of the join of path P_l with CSVNG K_m is $\chi_2^v(P_l + K_m) = m + 2$.*

Proof. Consider path $P_l = (C_1, D_1)$ with SVN vertex set $C_1 = \{v_1, v_2, \cdots, v_l\}$ and CSVNG $K_m = (C_2, D_2)$ with SVN vertex set $C_2 = \{u_1, u_2, \cdots, u_m\}$. Also the vertex set of these SVNG's are disjoint. Then the join of path P_l with CSVNG K_m is SVNG $P_l + K_m = (C, D)$ with SVN vertex set

DOI:https://doi.org/10.54216/IJNS.160102
Received: June 07, 2021 Accepted: October 19, 2021

$C = \{v_1, v_2, \cdots, v_l, u_1, u_2, \cdots, u_m\}$. Also the membership, indeterminacy and falsity functions of the vertices of $P_l + K_m$ is determined using the definition in 2.9 and edge set is also determined in the same way.
Let $\Gamma = \{\gamma_1, \gamma_2, \cdots, \gamma_{m+2}\}$ be the collection of fuzzy sets determined on vertices of $P_l + K_m$ for $R = 2$ as follows:

$$\gamma_1(v_j) = \begin{cases} (t_C(v_j), i_C(v_j), f_C(v_j)) & for \quad j \equiv 1(mod\ 2) \\ (0,0,1) & for \quad otherwise \end{cases}$$

$$\gamma_2(v_j) = \begin{cases} (t_C(v_j), i_C(v_j), f_C(v_j)) & for \quad j \equiv 0(mod\ 2) \\ (0,0,1) & for \quad otherwise \end{cases}$$

For $3 \leq k \leq m+2$,

$$\gamma_k(u_i) = \begin{cases} (t_C(u_i), i_C(u_i), f_C(u_i)) & for \quad i = k-2 \\ (0,0,1) & for \quad otherwise \end{cases}$$

As a result, the family $\Gamma = \{\gamma_1, \gamma_2, \cdots, \gamma_{m+2}\}$ ensures that SVNRVC requirements are met. Families with fewer than $m+2$ points did not match our defining criteria. Hence $\chi_2^v(P_l + K_m) = m+2$. □

4 Single-Valued Neutrosophic Edge Coloring

Definition 4.1. [17] The collection $\Gamma = \{\gamma_1, \gamma_2, \cdots, \gamma_p\}$ of SVN fuzzy sets is termed as **p-Single Valued Neutrosophic Edge Coloring(SVNEC)** of SVNG $G = (C, D)$ if the following criteria hold:
1. $\vee\gamma_s(uv) = D, \forall uv \in D$
2. $\gamma_s \wedge \gamma_t = 0$
3. For each strong edge uv of G, $min\{\gamma_s(t_D(uv))\} = 0$, $min\{\gamma_s(i_D(uv))\} = 0$ and $max\{\gamma_s(f_D(uv))\} = 1$, $(1 \leq s \leq p)$.
This is indicated as $\chi^e(G)$ and is termed as the SVN edge chromatic number of the SVNG G.

Example 4.2. Consider the following SVNG $G_1 = (C, D)$ with SVN vertex set $C = \{v_1, v_2, v_3, v_4, v_5\}$ and SVN edge $D = \{v_j v_k | jk = 12, 23, 34, 45, 15\}$ with

$$(t_C(v_j), i_C(v_j), f_C(v_j)) = \begin{cases} (0.4, 0.2, 0.5) & j = 1 \\ (0.3, 0.4, 0.6) & j = 2, 4 \\ (0.4, 0.4, 0.7) & j = 3 \\ (0.2, 0.3, 0.8) & j = 5 \end{cases}$$

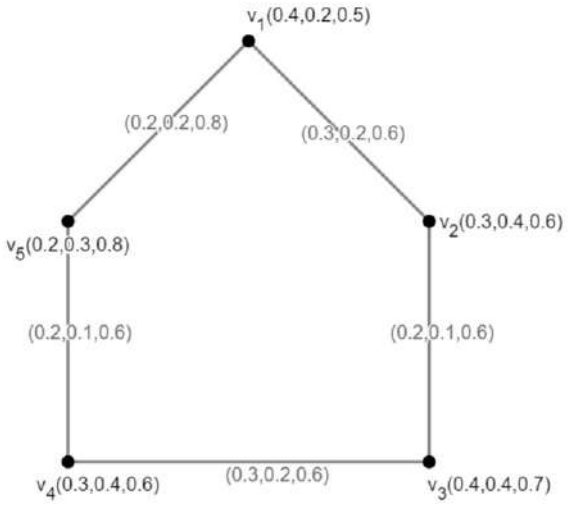

Figure 1: G_1

$$(t_D(v_j v_k), i_D(v_j v_k), f_D(v_j v_k)) = \begin{cases} (0.3, 0.2, 0.6) & jk = 12, 34 \\ (0.2, 0.1, 0.6) & jk = 23, 45 \\ (0.2, 0.2, 0.8) & jk = 15 \end{cases}$$

Figure 1 depicts the SVNG G_1.
Let $\Gamma = \{\gamma_1, \gamma_2, \gamma_3\}$ be collection of SVN fuzzy sets determined on D as below:

$$\gamma_1(v_j v_k) = \begin{cases} (0.3, 0.2, 0.6) & for \quad jk = 12, 34 \\ (0,0,1) & for \quad otherwise \end{cases}$$

DOI:https://doi.org/10.54216/IJNS.160102
Received: June 07, 2021 Accepted: October 19, 2021

$$\gamma_2(v_jv_k) = \begin{cases} (0.2, 0.1, 0.6) & for \quad jk = 23, 45 \\ (0, 0, 1) & for \quad otherwise \end{cases}$$
$$\gamma_3(v_jv_k) = \begin{cases} (0.2, 0.2, 0.8) & for \quad j = 15 \\ (0, 0, 1) & for \quad otherwise \end{cases}$$

Hence the family $\Gamma = \{\gamma_1, \gamma_2, \gamma_3\}$ ensures that SVNEC requirements are met. Families with fewer than 3 points did not match our defining criteria. Hence $\chi^e G_1 = 3$.

Definition 4.3. The collection $\Gamma = \{\gamma_1, \gamma_2, \cdots, \gamma_p\}$ of SVN fuzzy sets is termed as **p-Single Valued Neutrosophic R-dynamic Edge Coloring(SVNREC)** of SVNG $G = (C, D)$ if the following criteria hold:
1. $\vee\gamma_s(uv) = D, \forall uv \in D$
2. $\gamma_s \wedge \gamma_t = 0$
3. For each strong edge uv of G, $min\{\gamma_s(t_D(uv))\} = 0$, $min\{\gamma_s(i_D(uv))\} = 0$ and $max\{\gamma_s(f_D(uv))\} = 1$, $(1 \leq s \leq p)$.
4. For each edge uv with at least m number of incident edges, the corresponding edges receives at least $min\{R, m\}$ different members(colors) from the set Γ.
Here, $1 \leq R \leq M$ where M represents the maximum number of incident edges at the edges of SVNG G.
The least value of p is the SVNREC of SVNG G is denoted as $\chi^e_R(G)$, is called the Single Valued Neutrosophic R-dynamic edge chromatic number of the SVNG G.

Example 4.4. Consider the following SVNG $G_2 = (C, D)$ with SVN vertex set $C = \{v_1, v_2, v_3, v_4, v_5, v_6\}$ and SVN edge $D = \{v_jv_k | jk = 12, 23, 24, 34, 45, 56, 15, 16\}$ with

$$(t_C(v_j), i_C(v_j), f_C(v_j)) = \begin{cases} (0.5, 0.3, 0.4) & j = 1, 4 \\ (0.7, 0.6, 0.8) & j = 2 \\ (0.8, 0.4, 0.6) & j = 3, 6 \\ (0.6, 0.5, 0.7) & j = 5 \end{cases}$$

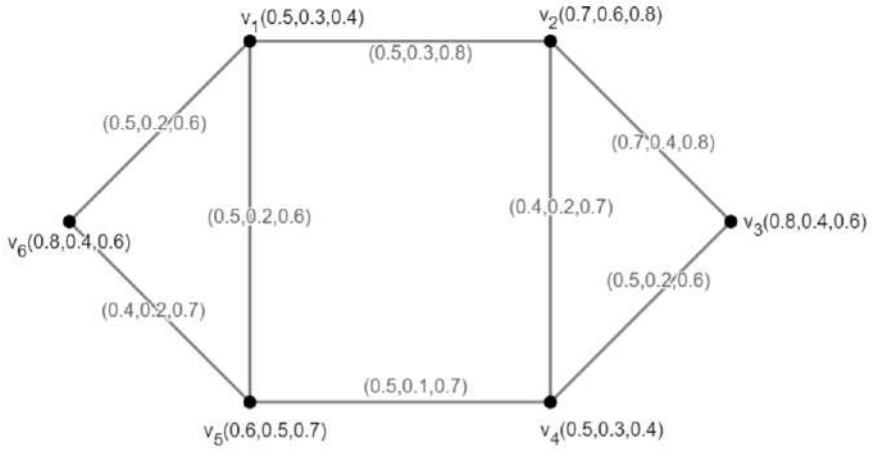

Figure 2: G_2

$$(t_D(v_jv_k), i_D(v_jv_k), f_D(v_jv_k)) = \begin{cases} (0.5, 0.3, 0.8) & jk = 12 \\ (0.4, 0.2, 0.7) & jk = 24, 56 \\ (0.5, 0.2, 0.6) & jk = 34, 15, 16 \\ (0.7, 0.4, 0.8) & jk = 23 \\ (0.5, 0.1, 0.7) & jk = 45 \end{cases}$$

Figure 2 depicts the SVNG G_2.
Here $M = 4$ so $1 \leq R \leq 4$.
For $1 \leq R \leq 2$ let $\Gamma = \{\gamma_1, \gamma_2, \gamma_3\}$ be collection of SVN fuzzy sets determined on D as below:

$$\gamma_1(v_jv_k) = \begin{cases} (0.5, 0.3, 0.8) & for \quad jk = 12 \\ (0.4, 0.2, 0.7) & for \quad jk = 56 \\ (0.5, 0.2, 0.6) & for \quad jk = 34 \\ (0, 0, 1) & for \quad otherwise \end{cases}$$
$$\gamma_2(v_jv_k) = \begin{cases} (0.5, 0.2, 0.6) & for \quad jk = 16 \\ (0.7, 0.4, 0.8) & for \quad jk = 23 \\ (0.5, 0.1, 0.7) & for \quad jk = 45 \\ (0, 0, 1) & for \quad otherwise \end{cases}$$

DOI:https://doi.org/10.54216/IJNS.160102
Received: June 07, 2021 Accepted: October 19, 2021

$$\gamma_3(v_jv_k) = \begin{cases} (0.4, 0.2, 0.7) & for \quad jk = 24 \\ (0.5, 0.2, 0.6) & for \quad jk = 15 \\ (0, 0, 1) & for \quad otherwise \end{cases}$$

Hence the family $\Gamma = \{\gamma_1, \gamma_2, \gamma_3\}$ ensures that SVNREC requirements are met. Families with fewer than 3 points did not match our defining criteria. Hence $\chi_R^e G_2 = 3$.

For $R = 3$ let $\Gamma = \{\gamma_1, \gamma_2, \gamma_3, \gamma_4\}$ be collection of SVN fuzzy sets determined on D as below:

$$\gamma_1(v_jv_k) = \begin{cases} (0.5, 0.2, 0.6) & for \quad jk = 34, 16 \\ (0, 0, 1) & for \quad otherwise \end{cases}$$

$$\gamma_2(v_jv_k) = \begin{cases} (0.4, 0.2, 0.7) & for \quad jk = 24, 56 \\ (0, 0, 1) & for \quad otherwise \end{cases}$$

$$\gamma_3(v_jv_k) = \begin{cases} (0.7, 0.4, 0.8) & for \quad jk = 23 \\ (0.5, 0.2, 0.6) & for \quad jk = 15 \\ (0, 0, 1) & for \quad otherwise \end{cases}$$

$$\gamma_4(v_jv_k) = \begin{cases} (0.5, 0.3, 0.8) & for \quad jk = 12 \\ (0.5, 0.1, 0.7) & for \quad jk = 45 \\ (0, 0, 1) & for \quad otherwise \end{cases}$$

Hence the family $\Gamma = \{\gamma_1, \gamma_2, \gamma_3, \gamma_4\}$ ensures that SVNREC requirements are met. Families with fewer than 4 points did not match our defining criteria. Hence $\chi_3^e G_2 = 4$.

For $R = 4$ let $\Gamma = \{\gamma_1, \gamma_2, \cdots, \gamma_6\}$ be collection of SVN fuzzy sets determined on D as below:

$$\gamma_1(v_jv_k) = \begin{cases} (0.5, 0.3, 0.8) & for \quad jk = 12 \\ (0, 0, 1) & for \quad otherwise \end{cases}$$

$$\gamma_2(v_jv_k) = \begin{cases} (0.5, 0.2, 0.6) & for \quad jk = 34, 16 \\ (0, 0, 1) & for \quad otherwise \end{cases}$$

$$\gamma_3(v_jv_k) = \begin{cases} (0.4, 0.2, 0.7) & for \quad jk = 24 \\ (0, 0, 1) & for \quad otherwise \end{cases}$$

$$\gamma_4(v_jv_k) = \begin{cases} (0.5, 0.2, 0.6) & for \quad jk = 15 \\ (0, 0, 1) & for \quad otherwise \end{cases}$$

$$\gamma_5(v_jv_k) = \begin{cases} (0.7, 0.4, 0.8) & for \quad jk = 23 \\ (0.4, 0.2, 0.7) & for \quad jk = 56 \\ (0, 0, 1) & for \quad otherwise \end{cases}$$

$$\gamma_6(v_jv_k) = \begin{cases} (0.5, 0.1, 0.7) & for \quad jk = 45 \\ (0, 0, 1) & for \quad otherwise \end{cases}$$

Hence the family $\Gamma = \{\gamma_1, \gamma_2, \gamma_3, \cdots, \gamma_6\}$ ensures that SVNREC requirements are met. Families with fewer than 6 points did not match our defining criteria. Hence $\chi_4^e G_2 = 6$.

Thus $\chi_R^e(G_2) = \begin{cases} 3 & for \quad 1 \leq R \leq 2 \\ 4 & for \quad R = 3 \\ 6 & for \quad R = 4 \end{cases}$

Theorem 4.5. *Let $n \geq 3$, P_l be a path graph then* $\chi_R^e(P_l) = \begin{cases} 2 & for \quad R = 1 \\ 3 & for \quad R = 2 \end{cases}$

Proof. Let the SVN vertex set of P_l be $C = \{u_1, u_2, \cdots, u_l\}$ and SVN edge set be $D = \{u_{j-1}u_j : 2 \leq j \leq l\}$. For the path graph P_l, $1 \leq R \leq 2$.

Let $\Gamma = \{\gamma_1, \gamma_2\}$ be collection of fuzzy sets determined on edges for $R = 1$ as follows:

$$\gamma_1(u_{j-1}u_j) = \begin{cases} (t_D(u_{j-1}u_j), i_D(u_{j-1}u_j), f_D(u_{j-1}u_j)) & for \quad j\ is\ even \\ (0, 0, 1) & for \quad otherwise \end{cases}$$

$$\gamma_2(u_{j-1}u_j) = \begin{cases} (t_D(u_{j-1}u_j), i_D(u_{j-1}u_j), f_D(u_{j-1}u_j)) & for \quad j\ is\ odd \\ (0, 0, 1) & for \quad otherwise \end{cases}$$

Thus the family $\Gamma = \{\gamma_1, \gamma_2\}$ ensures that SVNREC requirements are met. Families with fewer than 2 points did not match our defining criteria. Hence $\chi_R^e(P_l) = 2$.

When $R = 2$, let $\Gamma = \{\gamma_1, \gamma_2, \gamma_3\}$ be collection of fuzzy sets determined on edges as follows:

$$\gamma_1(u_{j-1}u_j) = \begin{cases} (t_D(u_{j-1}u_j), i_D(u_{j-1}u_j), f_D(u_{j-1}u_j)) & for \quad j \equiv 2(mod\ 3) \\ (0, 0, 1) & for \quad otherwise \end{cases}$$

$$\gamma_2(u_{j-1}u_j) = \begin{cases} (t_D(u_{j-1}u_j), i_D(u_{j-1}u_j), f_D(u_{j-1}u_j)) & for \quad j \equiv 0(mod\ 3) \\ (0, 0, 1) & for \quad otherwise \end{cases}$$

$$\gamma_3(u_{j-1}u_j) = \begin{cases} (t_D(u_{j-1}u_j), i_D(u_{j-1}u_j), f_D(u_{j-1}u_j)) & for \quad j \equiv 1(mod\ 3) \\ (0, 0, 1) & for \quad otherwise \end{cases}$$

Thus the family $\Gamma = \{\gamma_1, \gamma_2, \gamma_3\}$ ensures that SVNREC requirements are met. Families with fewer than 3

DOI:https://doi.org/10.54216/IJNS.160102
Received: June 07, 2021 Accepted: October 19, 2021

points did not match our defining criteria. Thus $\chi_2^e(P_l) = 3$.

Hence $\chi_R^e(P_l) = \begin{cases} 2 & for \quad R = 1 \\ 3 & for \quad R = 2 \end{cases}$ □

Theorem 4.6. *Let $l \geq 3$, C_l be a cycle then* $\chi_R^e(C_l) = \begin{cases} 2 & for \quad R = 1 \quad and\, l\, is\, even \\ 3 & for \quad R = 1 \quad and\, l\, is\, odd \\ 5 & for \quad R = 2 \quad and\, l = 5 \\ 3 & for \quad R = 2 \quad and\, l = 3n \\ 4 & for \quad R = 2 \quad and\, otherwise \end{cases}$

Proof. Let the SVN vertex set of C_l be $C = \{u_1, u_2, \cdots, u_l\}$ and SVN edge set be $D = \{u_{j-1}u_j, u_{1l} : 2 \leq j \leq l\}$. For the path graph C_l, $1 \leq R \leq 2$.

Case 1 : When $R = 1$ *and* l *is even.*

Let $\Gamma = \{\gamma_1, \gamma_2\}$ be collection of fuzzy sets determined on edges for $R = 1$ as follows:

$\gamma_1(u_ku_h) = \begin{cases} (t_D(u_{j-1}u_j), i_D(u_{j-1}u_j), f_D(u_{j-1}u_j)) & for \quad j\, is\, even \\ (0,0,1) & for \quad otherwise \end{cases}$

$\gamma_2(u_ku_h) = \begin{cases} (t_D(u_{j-1}u_j), i_D(u_{j-1}u_j), f_D(u_{j-1}u_j)) & for \quad j\, is\, odd \\ (t_D(u_ku_h), i_D(u_ku_h), f_D(u_ku_h)) & for \quad kh = 1l \\ (0,0,1) & for \quad otherwise \end{cases}$

Thus the family $\Gamma = \{\gamma_1, \gamma_2\}$ ensures that SVNREC requirements are met. Families with fewer than 2 points did not match our defining criteria. Hence $\chi_1^e(C_l) = 2$.

Case 2 : When $R = 1$ *and* l *is odd.*

Let $\Gamma = \{\gamma_1, \gamma_2\}$ be collection of fuzzy sets determined on edges for $R = 1$ as follows:

$\gamma_1(u_ku_h) = \begin{cases} (t_D(u_{j-1}u_j), i_D(u_{j-1}u_j), f_D(u_{j-1}u_j)) & for \quad j\, is\, even \\ (0,0,1) & for \quad otherwise \end{cases}$

$\gamma_2(u_ku_h) = \begin{cases} (t_D(u_{j-1}u_j), i_D(u_{j-1}u_j), f_D(u_{j-1}u_j)) & for \quad j\, is\, odd \\ (0,0,1) & for \quad otherwise \end{cases}$

$\gamma_3(u_ku_h) = \begin{cases} (t_D(u_ku_h), i_D(u_ku_h), f_D(u_ku_h)) & for \quad kh = 1l \\ (0,0,1) & for \quad otherwise \end{cases}$

Thus the family $\Gamma = \{\gamma_1, \gamma_2, \gamma_3\}$ ensures that SVNREC requirements are met. Families with fewer than 3 points did not match our defining criteria. Hence $\chi_1^e(C_l) = 3$.

Case 3 : When $R = 2$ *and* $l = 5$.

Let $\Gamma = \{\gamma_1, \gamma_2, \gamma_3, \gamma_4, \gamma_5\}$ be a family of fuzzy sets determined on edges for $R = 2$ as follows:

$\gamma_1(u_ku_h) = \begin{cases} (t_D(u_ku_h), i_D(u_ku_h), f_D(u_ku_h)) & for \quad kh = 12 \\ (0,0,1) & for \quad otherwise \end{cases}$

$\gamma_2(u_ku_h) = \begin{cases} (t_D(u_ku_h), i_D(u_ku_h), f_D(u_ku_h)) & for \quad kh = 23 \\ (0,0,1) & for \quad otherwise \end{cases}$

$\gamma_3(u_ku_h) = \begin{cases} (t_D(u_ku_h), i_D(u_ku_h), f_D(u_ku_h)) & for \quad kh = 34 \\ (0,0,1) & for \quad otherwise \end{cases}$

$\gamma_4(u_ku_h) = \begin{cases} (t_D(u_ku_h), i_D(u_ku_h), f_D(u_ku_h)) & for \quad kh = 45 \\ (0,0,1) & for \quad otherwise \end{cases}$

$\gamma_5(u_ku_h) = \begin{cases} (t_D(u_ku_h), i_D(u_ku_h), f_D(u_ku_h)) & for \quad kh = 15 \\ (0,0,1) & for \quad otherwise \end{cases}$

Thus the family $\Gamma = \{\gamma_1, \gamma_2, \gamma_3, \gamma_4, \gamma_5\}$ ensures that SVNREC requirements are met. Families with fewer than 5 points did not match our defining criteria. Hence $\chi_2^e(C_l) = 5$.

Case 4 : When $R = 2$ and $l = 3n, n = 1, 2, \cdots$.

Let $\Gamma = \{\gamma_1, \gamma_2, \gamma_3\}$ be a family of fuzzy sets determined on edges as follows:

$\gamma_1(u_ku_h) = \begin{cases} (t_D(u_{j-1}u_j), i_D(u_{j-1}u_j), f_D(u_{j-1}u_j)) & for \quad j \equiv 2(mod\, 3) \\ (0,0,1) & for \quad otherwise \end{cases}$

$\gamma_2(u_ku_h) = \begin{cases} (t_D(u_{j-1}u_j), i_D(u_{j-1}u_j), f_D(u_{j-1}u_j)) & for \quad j \equiv 0(mod\, 3) \\ (0,0,1) & for \quad otherwise \end{cases}$

$\gamma_3(u_ku_h) = \begin{cases} (t_D(u_{j-1}u_j), i_D(u_{j-1}u_j), f_D(u_{j-1}u_j)) & for \quad j \equiv 1(mod\, 3) \\ (t_D(u_ku_h), i_D(u_ku_h), f_D(u_ku_h)) & for \quad kh = 1l \\ (0,0,1) & for \quad otherwise \end{cases}$

Thus the family $\Gamma = \{\gamma_1, \gamma_2, \gamma_3\}$ ensures that SVNREC requirements are met. Families with fewer than 3 points did not match our defining criteria. Hence $\chi_2^e(C_l) = 3$ for $l = 3n$.

Case 5 : When $R = 2$ and otherwise.

Let $\Gamma = \{\gamma_1, \gamma_2, \gamma_3, \gamma_4\}$ be a family of fuzzy sets determined on edges as follows:

DOI:https://doi.org/10.54216/IJNS.160102
Received: June 07, 2021 Accepted: October 19, 2021

When $l = 3n+1, n = 1, 2, \cdots$.

$$\gamma_1(u_k u_h) = \begin{cases} (t_D(u_{j-1}u_j), i_D(u_{j-1}u_j), f_D(u_{j-1}u_j)) & for \quad j \equiv 2(mod\,3) \\ (0,0,1) & for \quad otherwise \end{cases}$$

$$\gamma_2(u_k u_h) = \begin{cases} (t_D(u_{j-1}u_j), i_D(u_{j-1}u_j), f_D(u_{j-1}u_j)) & for \quad j \equiv 0(mod\,3) \\ (0,0,1) & for \quad otherwise \end{cases}$$

$$\gamma_3(u_k u_h) = \begin{cases} (t_D(u_{j-1}u_j), i_D(u_{j-1}u_j), f_D(u_{j-1}u_j)) & for \quad j \equiv 1(mod\,3) \\ (0,0,1) & for \quad otherwise \end{cases}$$

$$\gamma_4(u_k u_h) = \begin{cases} (t_D(u_k u_h), i_D(u_k u_h), f_D(u_k u_h)) & for \quad kh = 1l \\ (0,0,1) & for \quad otherwise \end{cases}$$

When $l = 3n+2, n = 1, 2, \cdots$

$$\gamma_1(u_k u_h) = \begin{cases} (t_D(u_{j-1}u_j), i_D(u_{j-1}u_j), f_D(u_{j-1}u_j)) & for \quad j \equiv 2(mod\,3) \\ (t_D(u_k u_h), i_D(u_k u_h), f_D(u_k u_h)) & for \quad kh = (l-2)(l-1) \\ (0,0,1) & for \quad otherwise \end{cases}$$

$$\gamma_2(u_k u_h) = \begin{cases} (t_D(u_{j-1}u_j), i_D(u_{j-1}u_j), f_D(u_{j-1}u_j)) & for \quad j \equiv 0(mod\,3) \\ (t_D(u_k u_h), i_D(u_k u_h), f_D(u_k u_h)) & for \quad kh = (l-3)(l-2) \\ (0,0,1) & for \quad otherwise \end{cases}$$

$$\gamma_3(u_k u_h) = \begin{cases} (t_D(u_{j-1}u_j), i_D(u_{j-1}u_j), f_D(u_{j-1}u_j)) & for \quad j \equiv 1(mod\,3) \\ (t_D(u_k u_h), i_D(u_k u_h), f_D(u_k u_h)) & for \quad kh = 1l \\ (0,0,1) & for \quad otherwise \end{cases}$$

$$\gamma_4(u_k u_h) = \begin{cases} (t_D(u_k u_h), i_D(u_k u_h), f_D(u_k u_h)) & for \quad kh = (l-4)(l-3), (l-1)l \\ (0,0,1) & for \quad otherwise \end{cases}$$

Thus the family $\Gamma = \{\gamma_1, \gamma_2, \gamma_3, \gamma_4\}$ ensures that SVNREC requirements are met. Families with fewer than 4 points did not match our defining criteria. Thus $\chi_2^v(C_l) = 4$ when otherwise.

□

5 Conclusions

In this paper we have analysed about the single valued neutrosophic R-dynamic vertex coloring of Cartesian product of SVNG's and join of SVNG's. Also we have amalgamated the idea of Single Valued Neutrosophic edge Coloring and r-dynamic coloring to introduce a new concept Single Valued Neutrosophic R-dynamic Edge Coloring (SVNREC). We have defined the new coloring and provided some examples.

Funding: This research received no external funding.

Acknowledgments: The authors gratefully acknowledge the referees for their thorough reading, insightful remarks and helpful suggestions that have enhanced the quality of this manuscript.

Conflicts of Interest: The authors declare no conflict of interest.

References

[1] M. Akram, S. Siddique and B. Davvaz, "New concepts in neutrosophic graphs with application", Journal of Applied Mathematics and Computing, 57, pp.279-302, 2018.

[2] M. Akram and S. Shahzadi, "Neutrosophic soft graphs with application", Journal of Intelligent and Fuzzy Systems, 32(1), pp.841-858, 2017.

[3] M. Akram and S. Shahzadi, "Operations on single-valued neutrosophic graphs", Journal of Uncertain Systems, 11, pp.1-26, 2016.

[4] Anjaly Kishore and M. S. Sunitha, "Strong chromatic number of fuzzy graphs, Annals of Pure and Applied Mathematics, 7(2), pp.52-60, 2014.

[5] V. Aparna, N. Mohanapriya and Said Broumi, "Single Valued Neutrosophic R-dynamic Vertex Coloring of graphs"(Accepted).

[6] Arindam Dey and Anita Pal, "Vertex Coloring of a Fuzzy Graph using Alpa Cut", International Journal of Management, IT and Engineering, 2(8), pp.340-352, 2012.

[7] K. T. Atanassov, "Intuitionistic fuzzy sets", Fuzzy sets and systems, 20, pp.87-96, 1986.

DOI:https://doi.org/10.54216/IJNS.160102
Received: June 07, 2021 Accepted: October 19, 2021

[8] S. Broumi, M. Talea, M. Bakali and F. Smarandache, "Single-valued neutrosophic graphs", Journal of New Theory, 10, pp.86-101, 2016.

[9] S. Broumi, M. Talea, F. Smarandache and M. Bakali, "Single valued neutrosophic graphs: Degree, Order and Size", IEEE International Conference on Fuzzy Systems (FUZZ), pp.2444-2451, 2016.

[10] Changiz Eslahchi and B. N. Onagh, "Vertex strength of fuzzy graphs", International Journal of Mathematics and Mathematical Sciences, pp.1-9, 2005.

[11] R. Dhavaseelan, R. Vikramaprasad and V. Krishnaraj, "Certain types of neutrosophic graphs", International Journal of Mathematical Sciences and Applications, 5(2), pp.333-339, 2015.

[12] S. Ismail Mohideen and M. A. Rifayathali, "Coloring of Intuitionistic fuzzy graph using (α, β)-cuts", International Research Journal of Mathematical Engineering and IT, 2, pp.14-26, 2015.

[13] S. Lavanya and R. Sattanathan, "Fuzzy total coloring of fuzzy graph", International Journal of Information Technology and Knowledge Management, 2, pp.37-39, 2009.

[14] B. Montgomery, "Dynamic coloring of graphs", ProQuest LLC, Ann Arbor, MI, Ph.D Thesis, West Virginia University, 2001.

[15] M. A. Rifayathali, A. Prasanna and S. Ismail Mohideen, "Strong intuitionistic fuzzy graph coloring", International Journal of Latest Engineering Research and Applications, 2, pp.163-169, 2017.

[16] A. Rohini, M. Venkatachalam, S. Broumi and F. Smarandache, "Single Valued Neutrosophic Coloring", Neutrosophic Sets and Systems, 28, pp.13-22, 2019.

[17] A. Rohini, M. Venkatachalam, Dafik, S. Broumi and F. Smarandache, "Operations of Single Valued Neutrosophic Coloring", Neutrosophic Sets and Systems, 31, pp.172-178, 2020.

[18] A. Rohini, M. Venkatachalam, Dafik, S. Broumi and F. Smarandache, "Single Valued Neutrosophic Irregular Vertex Coloring", Acta Electrotechnica, 61, pp.56-60, 2020.

[19] A. Rosenfeld, "Fuzzy graphs", Fuzzy sets and their applications, Academic Press, New York, 1975.

[20] F. Smarandache, "Neutrosophy: Neutrosophic Probability, Set and logic", Ann Arbor, Michigan, USA, 105, 2002.

[21] Susana Munoz, M. Teresa Ortuno, Javier Ramirez and Javier Yanez, "Coloring fuzzy graphs", Omega, 33(3), pp.211-221, 2005.

[22] H. Wang, F. Smarandache, Y. Zhang and R. Sunderraman, "Single-valued neutrosophic sets", Multisspace Multiscriot, 4, pp.410-413, 2010.

[23] L. A. Zadeh, "Fuzzy sets", Information Control, 8, pp.338-353, 1965.

DOI:https://doi.org/10.54216/IJNS.160102
Received: June 07, 2021 Accepted: October 19, 2021

Notes on Number Theory and Discrete Mathematics
Print ISSN 1310–5132, Online ISSN 2367–8275
Vol. 27, 2021, No. 2, 191–200
DOI: 10.7546/nntdm.2021.27.2.191-200

On r-dynamic coloring of comb graphs

K. Kalaiselvi[1], N. Mohanapriya[2] and J. Vernold Vivin[3]

[1] Department of Mathematics, Dr. Mahalingam College of Engineering and Technology
Pollachi-642 003, Tamil Nadu, India
e-mail: kalaiselvi18577@gmail.com

[2] PG and Department of Mathematics, Kongunadu Arts and Science College
Coimbatore-641 029, Tamil Nadu, India
e-mail: n.mohanamaths@gmail.com

[3] Department of Mathematics, University College of Engineering Nagercoil
(A Constituent College of Anna University, Chennai)
Konam, Nagercoil-629 004, Tamil Nadu, India
e-mail: vernoldvivin@yahoo.in

Received: 4 May 2020 **Revised:** 25 February 2021 **Accepted:** 5 April 2021

Abstract: An r-dynamic coloring of a graph G is a proper coloring of G such that every vertex in $V(G)$ has neighbors in at least $\min\{d(v), r\}$ different color classes. The r-dynamic chromatic number of graph G denoted as $\chi_r(G)$, is the least k such that G has a coloring. In this paper we obtain the r-dynamic chromatic number of the central graph, middle graph, total graph, line graph, para-line graph and sub-division graph of the comb graph $P_n \odot K_1$ denoted by $C(P_n \odot K_1)$, $M(P_n \odot K_1)$, $T(P_n \odot K_1)$, $L(P_n \odot K_1)$, $P(P_n \odot K_1)$ and $S(P_n \odot K_1)$ respectively by finding the upper bound and lower bound for the r-dynamic chromatic number of the Comb graph.
Keywords: r-dynamic coloring, Comb graph, Central graph, Middle graph, Total graph, Line graph, Sub-division graph, Para-line graph.
2020 Mathematics Subject Classification: 05C15, 05C75.

1 Introduction

In this paper, all graphs are simple and finite. For a graph G, let $\delta(G)$ and $\Delta(G)$ denote the minimum and maximum degree of G. The r-dynamic coloring was first introduced by Montgomery [10]. An r-dynamic coloring of a graph is a map c from $V(G)$ to the set of colors such that:

(i) if $uv \in E(G)$, then $c(u) \neq c(v)$, and

(ii) for each vertex $v \in V(G)$, $|c(N(v))| \geq \min\{d(v), r\}$,

where $N(v)$ denotes the set of all vertices adjacent to v and $d(v)$ its degree and r is a positive integer. The first condition characterizes proper coloring and it is called the adjacency condition and second condition is the r-adjacency condition. The r-dynamic chromatic number of a graph G is denoted by $\chi_r(G)$, is the minimum k such that G admits such a proper k-coloring. The 1-dynamic chromatic number of a graph G is equal to its chromatic number. The 2-dynamic chromatic number of a graph G is studied by the name dynamic chromatic number in [1–4, 7].

There are many upper bounds and lower bounds for $\chi_d(G)$ in terms of graph parameters. For a graph G with $\Delta(G) \geq 3$, Lai et al. [7] proved that $\chi_d(G) \leq \Delta(G) + 1$, except for a cycle graph C_5. An upper bound for the dynamic chromatic number of a regular graph G and the independence number of the graph G, $\alpha(G)$, was introduced in [5]. In fact, it was proved that $\chi_2(G) \leq \chi(G) + 2\log_2 \alpha(G) + \mathcal{O}(1)$. Taherkhani gave [11] an upper bound for $\chi_2(G)$ in terms of the chromatic number, the maximum degree Δ and the minimum degree δ that is $\chi_2(G) - \chi(G) \leq [\Delta e/\delta \log(2e(\Delta^2 + 1))]$, where G is again a d-regular graph. Li et al. proved in [8] that in determining the value of $\chi_r(G)$ for planar bipartite graphs with maximum degree at most 3 and arbitrary high girth is an NP-hard problem. Furthermore, Li and Zhou [8] showed that to determine whether there exist a 3-dynamic coloring or not, for a claw free graph with the maximum degree 3 is an NP-complete problem.

2 Preliminaries

Let G be a simple and finite graph with vertex $V(G)$ and edge set $E(G)$. The middle graph [9] of G denoted by $M(G)$, is defined as follows, the vertex set of $M(G)$ is $V(G) \cup E(G)$. Two vertices x, y of $M(G)$ are adjacent in $M(G)$ in case one of the following holds: (i) x, y are in $E(G)$ and x, y are adjacent in G. (ii) x is in $V(G)$, y is in $E(G)$, and x, y are incident in G.

Let G be a graph with vertex set $V(G)$ and edge set $E(G)$. The total graph [9] of G, denoted by $T(G)$, is defined in the following way. The vertex set of $T(G)$ is $V(G) \cup E(G)$. Two vertices x, y of $T(G)$ are adjacent in $T(G)$ in case one of the following holds: (i) x, y are in $V(G)$ and x is adjacent to y in G. (ii) x, y are in $E(G)$ and x, y are adjacent in G. (iii) x is in $V(G)$, y is in $E(G)$, and x, y are incident in G.

The central graph [12] $C(G)$ of a graph G is obtained from G by adding an extra vertex on each edge of G, and then joining each pair of vertices of the original graph which were previously non-adjacent.

The line graph [6] of G, denoted by $L(G)$, is the graph whose vertex set is the edge set of G. Two vertices of $L(G)$ are adjacent whenever the corresponding edges of G are adjacent.

The sub-division graph $S(G)$ is obtained simply by inserting a new vertex for each edge of G.

The line graph of a sub-division graph is the para-line graph $P(G)$.

Let P_n be a path graph with n vertices and K_1 be a complete graph with one vertex. The comb graph $P_n \odot K_1$ is defined as the corona product of path graph P_n with the complete graph K_1 by taking one copy of P_n and $|V(P_n)|$ copies of K_1 and making the i^{th} vertex of P_n adjacent to the i^{th} copy of K_1 where $1 \leq i \leq n$. Comb graph has $2n$ vertices and $2n - 1$ edges.

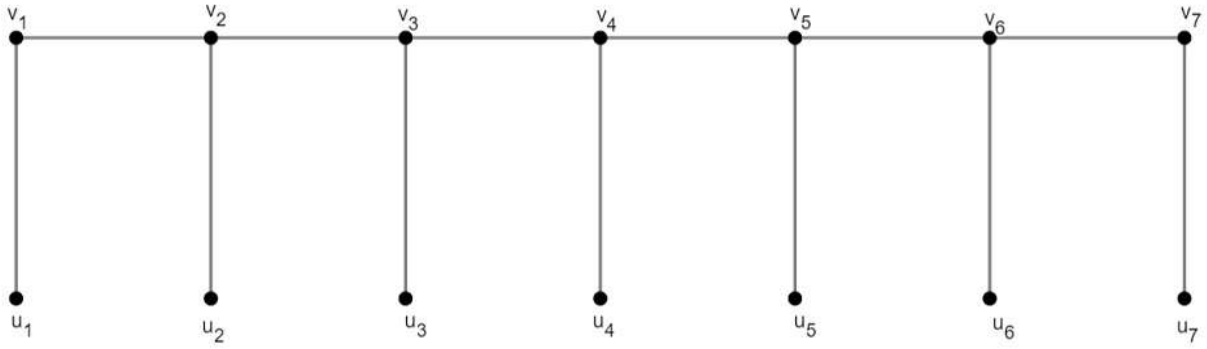

Figure 1. Comb graph $P_7 \odot K_1$

In the following section we obtain the r-dynamic chromatic number of the central graph, middle graph, total graph, line graph, para-line graph and sub-division graph of the comb graph $P_n \odot K_1$ denoted by $C(P_n \odot K_1)$, $M(P_n \odot K_1)$, $T(P_n \odot K_1)$, $L(P_n \odot K_1)$, $P(P_n \odot K_1)$ and $S(P_n \odot K_1)$, respectively.

3 Main results

Lemma 3.1. $\chi_r(G) \geq \min\{r, \Delta(G)\} + 1$.

Theorem 3.2. *Let $n \geq 3$, $C(P_n \odot K_1)$ be the central graph of comb graph then*

$$\chi_r(C(P_n \odot K_1)) = \begin{cases} n, & \text{for } r = 1 \\ 2n, & \text{for } 2 \leq r \leq \Delta - 1 \\ 2n+3, & \text{for } r = \Delta \end{cases}$$

Proof. Let

$$V(C(P_n \odot K_1)) = \{v_i : 1 \leq i \leq n\} \cup \{v_i' : 1 \leq i \leq n-1\} \cup \{u_i : 1 \leq i \leq n\} \cup \{u_i' : 1 \leq i \leq n\}$$

where v_i' and u_i' are the vertices corresponding to the edge $v_i v_{i+1}$ and $v_i u_i$ of $(P_n \odot K_1)$, $1 \leq i \leq n$. The maximum and minimum degrees of $C(P_n \odot K_1)$ are $\Delta(C(P_n \odot K_1)) = 2n-1$ and $\delta(C(P_n \odot K_1)) = 2$. Define the mapping $c : V \to Z^+$.

Case 1: When $r = 1$, the r-dynamic coloring is n are as follows:

- $c(v_i) = i, 1 \leq i \leq n$
- $c(u_i) = i, 1 \leq i \leq n$
- $c(v_i') = \begin{cases} 4, & \text{for } i \neq 3, 4,\ 1 \leq i \leq n-1 \\ 2, & \text{for } i = 3, 4,\ 1 \leq i \leq n-1 \end{cases}$
- $c(u_i') = \begin{cases} 3, & \text{for } i \neq 3,\ 1 \leq i \leq n \\ 4, & \text{for } i = 3,\ 1 \leq i \leq n \end{cases}$

Hence the r-adjacency condition is fulfilled, therefore $\chi_r(C(P_n \odot K_1)) = n$ for $r = 1$.

If $\chi_r(C(P_n \odot K_1)) < n$, then the r-adjacency condition will not be fulfilled.

Case 2: When $2 \leq r \leq \Delta - 1$, the r-dynamic coloring is $2n$ are as follows:

- $c(v_i) = i, 1 \leq i \leq n$
- $c(u_i) = i + n, 1 \leq i \leq n$
- $c(v_i^{'}) = i + n, 1 \leq i \leq n$
- $c(u_i^{'}) = \begin{cases} n, & \text{for } i = 1,\ 1 \leq i \leq n-1 \\ i-1, & \text{for } 2 \leq i \leq n-1 \end{cases}$

Hence the r-adjacency condition is fulfilled, therefore $\chi_r(C(P_n \odot K_1)) = 2n$ for $2 \leq r \leq \Delta - 1$. If $\chi_r(C(P_n \odot K_1)) < 2n$, then the r-adjacency condition will not be fulfilled.

Case: 3 When $r = \Delta$, the r-dynamic coloring is $2n + 3$ are as follows:

- $c(v_i) = i, 1 \leq i \leq n$
- $c(u_i) = i + n, 1 \leq i \leq n$
- $c(u_i^{'}) = 2n + 1, 1 \leq i \leq n$
- $c(v_i^{'}) = \begin{cases} 2n+2, & \text{for } i \text{ odd} \\ 2n+3, & \text{for } i \text{ even} \end{cases}$

Hence the r-adjacency condition is fulfilled, therefore $\chi_r(C(P_n \odot K_1)) = 2n+3$ for $r = \Delta$. If $\chi_r(C(P_n \odot K_1)) < 2n + 3$, then the r-adjacency condition will not be fulfilled. □

Lemma 3.3. *Let $n \geq 4$, $M(P_n \odot K_1)$ be the middle graph of comb graph then*

$$\chi_r(M(P_n \odot K_1)) \geq \begin{cases} 4, & \textit{for } 1 \leq r \leq 3 \\ r+1, & \textit{for } 4 \leq r \leq \Delta \end{cases}$$

Proof. Let

$$V(M(P_n \odot K_1)) = \{v_i : 1 \leq i \leq n\} \cup \{v_i^{'} : 1 \leq i \leq n-1\} \cup \{u_i : 1 \leq i \leq n\} \cup \{u_i^{'} : 1 \leq i \leq n\}$$

where $v_i^{'}$ and $u_i^{'}$ are the vertices corresponding to the edge $v_i v_{i+1}$ and $v_i u_i$ of $(P_n \odot K_1)$, $1 \leq i \leq n$. By the definition of middle graph the vertices $\{v_i^{'}, v_{i+1}^{'}, u_{i+1}^{'}, v_{i+1}\}$ induces a clique of order 4, hence $\chi_r(M(P_n \odot K_1)) \geq 4$. For $4 \leq r \leq \Delta$ by Lemma 3.1 $\chi_r(G) \geq \min\{r, \Delta(G)\} + 1$. This concludes the proof. □

Theorem 3.4. *Let $n \geq 4$, $M(P_n \odot K_1)$, then the r-dynamic chromatic number of the middle graph of a comb graph is*

$$\chi_r[M(P_n \odot K_1)] = \begin{cases} 4, & \textit{for } 1 \leq r \leq 3 \\ r+1, & \textit{for } 4 \leq r \leq \Delta \end{cases}.$$

Proof. The maximum and minimum degrees of $M(P_n \odot K_1)$ are $\Delta(M((P_n \odot K_1))) = 6$ and $\delta(M(P_n \odot K_1)) = 2$. Define the mapping $c : V \to Z^+$. We divide the proof into two cases.

Case 1: When $1 \leq r \leq 3$, by Lemma 3.3 the lower bound is $\chi_r(M((P_n \odot K_1))) \geq 4$. To show the upper bound, we use the following colorings:

- $c(v_1, v_2, \ldots, v_n) = \{3, 4, 3, 4, \ldots\}$
- $c(u_1^{'}, u_2^{'}, \ldots, u_n^{'}) = \{4, 3, 4, 3, \ldots\}$
- $c(u_1, u_2, \ldots, u_n) = 1$
- $c(v_1^{'}, v_2^{'}, \ldots, v_n^{'}) = \{2, 1, 2, 1, \ldots\}$

Thus we require 4 colors, that is $\chi_r(M(P_n \odot K_1)) \geq 4$. Hence $\chi_r(M(P_n \odot K_1)) = 4$.

Case 2: When $4 \leq r \leq \Delta$, by Lemma 3.3 the lower bound is $\chi_r(M((P_n \odot K_1))) \geq 4$. To show the upper bound, we use the following colorings.

Subcase (i): when $r = 4$, consider the coloring:

- $c(v_1, v_2, \ldots, v_n) = \{1, 2, 3, 1, 2, 3, \ldots\}$
- $c(v_1^{'}, v_2^{'}, \ldots, v_n^{'}) = \{3, 1, 2, 3, 1, 2, \ldots\}$
- $c(u_1^{'}, u_2^{'}, \ldots, u_n^{'}) = \{r, r+1, r, r+1, \ldots\}$
- $c(u_1, u_2, \ldots, u_n) = \{r+1, r, r+1, r, \ldots\}$

Thus we require $r + 1$ colors when $r = 4$.

Subcase (ii): When $r = 5$, consider the coloring:

- $c(v_1, v_2, \ldots, v_n) = \{2, 3, 2, 3, \ldots\}$
- $c(v_1^{'}, v_2^{'}, \ldots, v_n^{'}) = \{1, 4, 1, 4, \ldots\}$
- $c(u_1^{'}, u_2^{'}, \ldots, u_n^{'}) = \{r, r+1, r, r+1, \ldots\}$
- $c(u_1, u_2, \ldots, u_n) = \{r+1, r, r+1, r, \ldots\}$

Thus we require $r + 1$ colors when $r = 5$.

Subcase (iii): When $r = 6$, consider the coloring:

- $c(v_1, v_2, \ldots, v_n) = \{4, 1, 5, 2, 3, 4, 1, 5, 2, 3, \ldots\}$
- $c(v_1^{'}, v_2^{'}, \ldots, v_n^{'}) = \{2, 3, 4, 1, 5, 2, 3, 4, 1, 5, \ldots\}$
- $c(u_1^{'}, u_2^{'}, \ldots, u_n^{'}) = \{r, r+1, r, r+1, \ldots\}$
- $c(u_1, u_2, \ldots, u_n) = \{r+1, r, r+1, r, \ldots\}$

Thus we require $r + 1$ colors when $r = 6$.

Now from the subcases (i), (ii) and (iii) the r-adjacency condition is fulfilled. Therefore, $\chi_r(M(P_n \odot K_1)) \leq r + 1$. Hence $\chi_r(M(P_n \odot K_1)) = r + 1$. □

Lemma 3.5. *Let $n \geq 3$, $T(P_n \odot K_1)$ be the total graph of comb graph, then*

$$\chi_r(T(P_n \odot K_1)) \geq \begin{cases} 4, & \text{for } 1 \leq r \leq 3 \\ r+1, & \text{for } 4 \leq r \leq \Delta \end{cases}.$$

Proof. Let

$V(T(P_n \odot K_1)) = \{v_i : 1 \leq i \leq n\} \cup \{v_i^{'} : 1 \leq i \leq n-1\} \cup \{u_i : 1 \leq i \leq n\} \cup \{u_i^{'} : 1 \leq i \leq n\}$, where $v_i^{'}$ and $u_i^{'}$ are the vertices corresponding to the edge $v_i v_{i+1}$ and $v_i u_i$ of $(P_n \odot K_1)$, $1 \leq i \leq n$.

By the definition of total graph the vertices $\{v_i^{'}, v_{i+1}^{'}, u_{i+1}^{'}, v_{i+1}\}$ induce a clique of order 4, hence $\chi_r(T(P_n \odot K_1)) \geq 4$. For $4 \leq r \leq \Delta$ by Lemma 3.1 $\chi_r(G) \geq \min\{r, \Delta(G)\} + 1$. This concludes the proof. □

Theorem 3.6. *Let $n \geq 3$, $T(P_n \odot K_1)$ the r-dynamic chromatic number of the total graph of comb graph is*

$$\chi_r(T(P_n \odot K_1)) = \begin{cases} 4, & \text{for } 1 \leq r \leq 3 \\ r+1, & \text{for } 4 \leq r \leq \Delta \end{cases}$$

Proof. The maximum and minimum degrees of $T(P_n \odot K_1)$ are $\Delta(T(P_n \odot K_1)) = 6$ and $\delta(T(P_n \odot K_1)) = 2$. We divide the proof into two cases. Define the mapping $c : V \to Z^+$.

Case 1: When $1 \leq r \leq 3$, by Lemma 3.5 the lower bound is $\chi_r(T(P_n \odot K_1)) \geq 4$. To show the upper bound, we use the following colorings:

- $c(v_1, v_2, \ldots, v_n) = \{2, 3, 2, 3, \ldots\}$
- $c(u_1', u_2', \ldots, u_n') = \{3, 2, 3, \ldots\}$
- $c(u_1, u_2, \ldots, u_n) = \{1, 4, 1, 4, \ldots\}$
- $c(v_1', v_2', \ldots, v_n') = \{4, 1, 4, 1, \ldots\}$

Thus we require 4 colors that is $\chi_r(T(P_n \odot K_1)) \leq 4$. Hence $\chi_r(T(P_n \odot K_1)) = 4$.

Case 2: When $4 \leq r \leq \Delta$, by Lemma 3.5 the lower bound is $\chi_r(T(P_n \odot K_1)) \geq 4$. To show the upper bound, we use the following colorings:

Subcase (i): When $r = 4$, consider the coloring:

- $c(v_1, v_2, \ldots, v_n) = \{1, 2, 3, 1, 2, 3, \ldots\}$
- $c(v_1', v_2', \ldots, v_n') = \{3, 1, 2, 3, 1, 2, \ldots\}$
- $c(u_1', u_2', \ldots, u_n') = \{r, r+1, r, r+1, \ldots\}$
- $c(u_1, u_2, \ldots, u_n) = \{r+1, r, r+1, r, \ldots\}$

Thus we require $r + 1$ colors when $r = 4$.

Subcase (ii): When $r = 5$, consider the coloring:

- $c(v_1, v_2, \ldots, v_n) = \{2, 3, 2, 3, \ldots\}$
- $c(v_1', v_2', \ldots, v_n') = \{1, 4, 1, 4, \ldots\}$
- $c(u_1', u_2', \ldots, u_n') = \{r, r+1, r, r+1, \ldots\}$
- $c(u_1, u_2, \ldots, u_n) = \{r+1, r, r+1, r, \ldots\}$

Thus we require $r + 1$ colors when $r = 5$.

Subcase (iii): When $r = 6$, consider the coloring:

- $c(v_1, v_2, \ldots, v_n) = \{4, 1, 5, 2, 3, 4, 1, 5, 2, 3, \ldots\}$
- $c(v_1', v_2', \ldots, v_n') = \{2, 3, 4, 1, 5, 2, 3, 4, 1, 5, \ldots\}$
- $c(u_1', u_2', \ldots, u_n') = \{r, r+1, r, r+1, \ldots\}$
- $c(u_1, u_2, \ldots, u_n) = \{r+1, r, r+1, r, \ldots\}$

Thus we require $r + 1$ colors when $r = 6$.

Now from the subcases (i), (ii) and (iii) the r-adjacency condition fulfilled. Therefore, $\chi_r(T(P_n \odot K_1)) \leq r + 1$. Hence $\chi_r(T(P_n \odot K_1)) = r + 1$. □

Lemma 3.7. *Let $n \geq 4$, $L(P_n \odot K_1)$ be the line graph of comb graph, then*

$$\chi_r(L(P_n \odot K_1)) \geq \begin{cases} 3, & \text{for } 1 \leq r \leq 2 \\ 4, & \text{for } r = 3 \\ 5, & \text{for } r = 4 \end{cases}.$$

Proof. Let $V(L(P_n \odot K_1)) = e_1, e_2, e_3, \ldots, e_n, e_1^{'}, e_2^{'}, e_3^{'}, \ldots, e_{n-1}^{'}$. The maximum and minimum degrees of $L(P_n \odot K_1)$ are $\Delta(L(P_n \odot K_1)) = 4$ and $\delta(L(P_n \odot K_1)) = 1$. For $1 \leq r \leq 2$ by the definition of line graph the vertices $e_i, e_i^{'}, e_{i+1}^{'}$ induces a clique of order 3. Hence $\chi_r(L(P_n \odot K_1)) \geq 3$.

For $r = 3$ by Lemma 3.1

$$\chi_r(L(P_n \odot K_1)) \geq \min\{r, \Delta(L(P_n \odot K_1)\} \geq \min\{3, \Delta(L(P_n \odot K_1))\} + 1 = 3 + 1 = 4.$$

For $r = 4$ by Lemma 3.1

$$\chi_r(L(P_n \odot K_1)) \geq \min\{r, \Delta(L(P_n \odot K_1))\} \geq \min\{4, \Delta(L(P_n \odot K_1))\} + 1 = 4 + 1 = 5.$$

This concludes the proof. □

Theorem 3.8. *Let $n \geq 4$, $L(P_n \odot K_1)$ the r-dynamic chromatic number of a line graph of comb graph is*

$$\chi_r(L(P_n \odot K_1)) = \begin{cases} 3, & \text{for } 1 \leq r \leq 2 \\ 4, & \text{for } r = 3 \\ 5, & \text{for } r = 4 \end{cases}.$$

Proof. Define the mapping $c : V \to Z^+$. We divide the proof into three cases.

Case 1: For $1 \leq r \leq 2$. By the Lemma 3.7 the lower bound is $\chi_r(L(P_n \odot K_1)) \geq 3$. To show the upper bound, we use the following colorings:

- $c(e_1, e_2, \ldots, e_n) = 1$
- $c(e_1^{'}, e_2^{'}, \ldots, e_n^{'}) = \{2, 3, 2, 3, \ldots\}$

Thus we require 3 colors, that is $\chi_r(L(P_n \odot K_1)) \leq 3$. Hence $\chi_r(L(P_n \odot K_1)) = 3$ when $1 \leq r \leq 2$.

Case 2: For $r = 3$. By the Lemma 3.7 the lower bound is $\chi_r(L(P_n \odot K_1)) \geq 4$. The r-dynamic coloring are as follows:

- $c(e_1, e_2, \ldots, e_n) = \{1, 3, 1, 3, \ldots\}$
- $c(e_1^{'}, e_2^{'}, \ldots, e_n^{'}) = \{2, 4, 2, 4, \ldots\}$

Thus we require 4 colors, that is $\chi_r(L(P_n \odot K_1)) \leq 4$. Hence $\chi_r(L(P_n \odot K_1)) = 4$ when $r = 3$.

Case 3: For $r = 4$. By the Lemma 3.7 the lower bound is $\chi_r(L(P_n \odot K_1)) \geq 5$. The r-dynamic coloring are as follows:

- $c(e_1, e_2, \ldots, e_n) = \{1, 3, 1, 3, \ldots\}$
- $c(e_1^{'}, e_2^{'}, \ldots, e_n^{'}) = \{2, 4, 5, 2, 4, 5, \ldots\}$

Thus we require 5 colors, that is $\chi_r(L(P_n \odot K_1)) \leq 5$. Hence $\chi_r(L(P_n \odot K_1)) = 5$ when $r = 4$. □

Lemma 3.9. *Let $n \geq 3$, $P(P_n \odot K_1)$ be the para-line graph of comb graph then*

$$\chi_r(P(P_n \odot K_1)) \geq \begin{cases} 3, & \text{for } 1 \leq r \leq 2 \\ 4, & \text{for } r = \Delta \end{cases}.$$

Proof. Let $V(P(P_n \odot K_1)) = \{e_i; 1 \leq i \leq 2n\} \cup \{e_i^{'}; 1 \leq i \leq 2n-2\}$, where e_i is the vertex corresponding to the edge v_iv_{i+1} and $e_i^{'}$ is the vertex corresponding to the edge v_iu_i of $(P_n \odot k_1)$, $1 \leq i \leq n$. For $1 \leq r \leq 2$, by the definition of para-line graph the vertices $e_{2i+2}, e_{i+1}^{'}, e_{i+2}^{'}$ induces a clique of order 3. Hence $\chi_r(P(P_n \odot K_1)) \geq 3$.

For $r = \Delta$ by Lemma 3.1 $\chi_r(L(P_n \odot K_1)) \geq \min\{r, \Delta(P(P_n \odot K_1))\} + 1 = 3 + 1 = 4$. Therefore $\chi_r(L(P_n \odot K_1)) \geq 4$. This concludes the proof. □

Theorem 3.10. *Let $n \geq 3$, $P(P_n \odot K_1)$ the r-dynamic chromatic number of para-line graph of a comb graph is*

$$\chi_r(P(P_n \odot K_1)) = \begin{cases} 3, & \text{for } 1 \leq r \leq 2 \\ 4, & \text{for } r = \Delta \end{cases}.$$

Proof. The maximum and minimum degrees of $L(P_n \odot K_1)$ are $\Delta(L(P_n \odot K_1)) = 3$ and $\delta(L(P_n \odot K_1)) = 1$. Define the mapping $c : V \to Z^+$.

Case 1: For $1 \leq r \leq 2$. By the Lemma 3.9 the lower bound is $\chi_r(L(P_n \odot K_1)) \geq 3$. To show the upper bound, we assign colors as follows:

- $c(e_1, e_2, \ldots, e_n) = \{1, 2, 1, 2, \ldots\}$
- $c(e_1^{'}, e_2^{'}, \ldots, e_n^{'}) = \{1, 3, 1, 3, \ldots\}$

Thus we require 3 colors, that is $\chi_r(P(P_n \odot K_1)) \leq 3$. Hence $\chi_r(P(P_n \odot K_1)) = 3$ when $1 \leq r \leq 2$.

Case 2: For $r = 3$. By the Lemma 3.9 the lower bound is $\chi_r(P(P_n \odot K_1)) \geq 4$. To show the upper bound, we assign colors as follows:

- $c(e_1, e_2, \ldots, e_{2n-1}) = \{3, 1, 3, 1, \ldots\}$ and $c(e_{2n}) = 4$
- $c(e_1^{'}, e_2^{'}, \ldots, e_n^{'}) = \{1, 2, 1, 2, \ldots\}$

Thus we require 4 colors, that is $\chi_r(P(P_n \odot K_1)) \leq 4$. Hence $\chi_r(P(P_n \odot K_1)) = 4$ when $r = 3$. □

Theorem 3.11. *Let $n \geq 3$, and $S(P_n \odot K_1)$ be the sub-division graph of $(P_n \odot K_1)$, then*

$$\chi_r(S(P_n \odot K_1)) = r + 1, 1 \leq r \leq 3$$

Proof. Let $V(S(P_n \odot K_1)) = \{v_i : 1 \leq i \leq n\} \cup \{v_i^{'} : 1 \leq i \leq n-1\} \cup \{u_i : 1 \leq i \leq n\} \cup \{u_i^{'} : 1 \leq i \leq n\}$ where $v_i^{'}$ and $u_i^{'}$ are the vertex corresponding to the edge v_iv_{i+1} and v_iu_i of $(P_n \odot K_1)$, $1 \leq i \leq n$. The maximum and minimum degrees of $S(P_n \odot K_1)$ are $\Delta(S(P_n \odot K_1)) = 3$ and $\delta(S(P_n \odot K_1)) = 1$. By Lemma 3.1 $\chi_r(S(P_n \odot K_1)) \geq \min\{r, \Delta(S(P_n \odot K_1))\} + 1 = r + 1$, for $1 \leq r \leq 3$. To show the upper bound, we assign colors as follows:

Case 1: When $r = 1$,

- $c(v_1, v_2, \ldots, v_n) = 1$
- $c(v_1^{'}, v_2^{'}, \ldots, v_n^{'}) = 2$
- $c(u_1^{'}, u_2^{'}, \ldots, u_n^{'}) = 2$
- $c(u_1, u_2, \ldots, u_n) = 1$

Thus we require 2 colors, that is $\chi_r(S(P_n \odot K_1)) \leq 2$. Hence $\chi_r(S(P_n \odot K_1)) = 2$ when $r = 1$.

Case 2: When $r = 2$,

- $c(v_1, v_2, \ldots, v_n) = \{1, 2, 1, 2, \ldots\}$
- $c(v_1^{'}, v_2^{'}, \ldots, v_n^{'}) = 3$
- $c(u_1^{'}, u_2^{'}, \ldots, u_n^{'}) = \{2, 1, 2, 1, \ldots\}$
- $c(u_1, u_2, \ldots, u_n) = 3$

Thus we require 3 colors, that is $\chi_r(S(P_n \odot K_1)) \leq 3$. Hence $\chi_r(S(P_n \odot K_1)) = 3$ when $r = 2$.

Case 3: When $r = 3$,

- $c(v_1, v_2, \ldots, v_n) = \{1, 2, 1, 2, \ldots\}$
- $c(v_1^{'}, v_2^{'}, \ldots, v_n^{'}) = \{3, 4, 3, 4, \ldots\}$
- $c(u_1^{'}, u_2^{'}, \ldots, u_n^{'}) = \{2, 1, 2, 1, \ldots\}$
- $c(u_1, u_2, \ldots, u_n) = 4$

Thus we require 4 colors, that is $\chi_r(S(P_n \odot K_1)) \leq 4$. Hence $\chi_r(S(P_n \odot K_1)) = 4$ when $r = 3$. Therefore $\chi_r(S(P_n \odot K_1)) \leq r + 1, 1 \leq r \leq 3$. Hence $\chi_r(S(P_n \odot K_1)) = r + 1$, $1 \leq r \leq 3$. □

4 Conclusion

In this paper we have investigated the r-dynamic chromatic number of some operations such as central graph, middle graph, total graph, line graph, para-line graph, and subdivision graph of the comb graph $P_n \odot K_1$. We have used the upper bound and lower bound method to obtain the r-dynamic chromatic number. Let G be any connected graph, till now there is no sharp lower bound for the r-dynamic chromatic number, so it is left as an open problem.

Acknowledgements

The authors express their gratitude to the anonymous reviewers for their thorough reading, insightful remarks, and helpful suggestions that improved the content of this manuscript.

References

[1] Ahadi, A., Akbari, S., Dehghan, A., & Ghanbari, M. (2012). On the difference between chromatic number and dynamic chromatic number of graphs. *Discrete Mathematics*, 312, 2579–2583.

[2] Akbari, S., Ghanbari, M., & Jahanbekam, S. (2009). On the list dynamic coloring of graphs. *Discrete Applied Mathematics*, 157, 3005–3007.

[3] Akbari, S., Ghanbari, M., & Jahanbekam, S. (2010). On the dynamic chromatic number of graphs. *AMS Contemporary Mathematics*, 531, 11–18.

[4] Alishahi, M. (2012). Dynamic chromatic number of regular graphs. *Discrete Applied Mathematics*, 160, 2098–2103.

[5] Dehghan, A., & Ahadi, A. (2012). Upper bounds for the 2-hued chromatic number of graphs in terms of the independence number. *Discrete Applied Mathematics*, 160(15), 2142–2146.

[6] Harary, F. (1969). *Graph Theory*, Narosa Publishing home, New Delhi.

[7] Lai, H. J., Montgomery, B., & Poon, H. (2003). Upper bounds of dynamic chromatic number. *Ars Combinatorica*, 68, 193–201.

[8] Li, X., & Zhou, W. (2008). The 2nd-order conditional 3-coloring of claw-free graphs. *Theoretical Computer Science*, 396, 151–157.

[9] Michalak, D. (1983). On middle and total graphs with coarseness number equal 1. *Lecture Notes in Mathematics*, 1018, Springer Verlag Graph Theory, Lagow proceedings, Berlin Heidelberg, New York, Tokyo, 139–150.

[10] Montgomery, B. (2001). *Dynamic Coloring of Graphs*, ProQuest LLC, Ann Arbor, MI, Ph.D. Thesis, West Virginia University.

[11] Taherkhani, A. (2016). r-Dynamic chromatic number of graphs. *Discrete Applied Mathematics*, 201, 222–227.

[12] Vernold Vivin, J. (2007). *Harmonious Coloring of Total Graphs, n-leaf, Central Graphs and Circumdetic Graphs*, Ph.D. Thesis, Bharathiar University, Coimbatore, India.

VIT

Vellore Institute of Technology
(Deemed to be University under section 3 of UGC Act, 1956)

TO WHOM IT MAY CONCERN

This letter to certify that **Dr. C. Ravichandran,** Assistant Professor, Post Graduate and Research Department of Mathematics, Kongunadu Arts and Science College (Autonomous), Coimbatore, Tamil Nadu, India has been working on joint research works in the area of **"Fractional differential equations"** since 2013, the following joint papers are developed with his collaboration during June 2021 to August 2022:

1) Kamalendra Kumar, Rohit Patel, Velusamy Vijayakumar, Anurag Shukla, Chokkalingam Ravichandran, A discussion on boundary controllability of nonlocal impulsive neutral integro-differential evolution equations, Mathematical Methods in the Applied Sciences, 45(13), (2022), 8193-8215.

Futher any questions or clarification, you may contact me at **vijayakumarv@vit.ac.in** or mobile phone +91 9865406722

Sincerely yours,

10/11/22

Dr. V. VIJAYAKUMAR, M.Sc., M.Phil., Ph.D.,
Assistant Professor,
Department of Mathematics,
School of Advanced Science,
Vellore Institute of Technology (VIT),
Vellore - 632 014. Tamil Nadu.

Phone: +91 - 44 - 25613881
+91 - 44 - 25613888
e-mail : sk.kaliraj@gmail.com

RAMANUJAN INSTITUTE FOR ADVANCED STUDY IN MATHEMATICS

UNIVERSITY OF MADRAS

(Established under the Act of Incorporation
XXVII of 1857 Madras University Act 1923)
(State University)

Dr. K. Kaliraj
Assistant Professor

CHEPAUK
TRIPLICANE P.O.
CHENNAI - 600 005
INDIA

Date : 03/11/2022

TO WHOM IT MAY CONCERN

This letter to certify that **Dr. C. Ravichandran,** Assistant Professor, Post Graduate and Research Department of Mathematics, Kongunadu Arts and Science College (Autonomous), Coimbatore, Tamil Nadu, India has been working on joint research works in the area of **"Fractional differential equations"** since 2018, the following joint papers are developed with his collaboration during June 2021 to August 2022:

1) Kalimuthu Kaliraj, Mohan Manjula, Chokkalingam Ravichandran, Kottakkaran Sooppy Nisar, Results on neutral differential equation of sobolev type with nonlocal conditions, Chaos, Solitons & Fractals, Volume 158, May 2022, 112060

2) K.Kaliraj, M.Manjula, C. Ravichandran, New existence results on nonlocal neutral fractional differential equation in concepts of Caputo derivative with impulsive conditions, Chaos, Solitons & Fractals, Volume 161, August 2022, 112284

3) K. Kaliraj, K. S. Viswanath, K. Logeswari & C. Ravichandran, Analysis of Fractional Integro–Differential Equation with Robin Boundary Conditions Using Topological Degree Method, International Journal of Applied and Computational Mathematics, 8, 176 (2022). https://doi.org/10.1007/s40819-022-01379-1.

Further any questions or clarification, you may contact me at **kaliraj@unom.ac.in** or mobile phone +91 9940998443

Sincerely yours, 3/11/22

Dr. K. KALIRAJ, M.Sc.,M.Phil.,Ph.D.,
Assistant Professor
Ramanujan Institute for
Advanced Study in Mathematics
University of Madras
Chepauk, Chennai-600 005.

Journal of Industrial and Engineering Chemistry xxx (xxxx) xxx

Contents lists available at ScienceDirect

Journal of Industrial and Engineering Chemistry

journal homepage: www.elsevier.com/locate/jiec

Facile green synthesis of nano-sized ZnO using leaf extract of *Morinda tinctoria*: MCF-7 cell cycle arrest, antiproliferation, and apoptosis studies

Jaganathan Anitha[a,*], Rajendran Selvakumar[b], Senthilnayagam Hema[c], Kadarkarai Murugan[d], Thathan Premkumar[e,*]

[a] Department of Biochemistry, Kongunadu Arts and Science College (Autonomous), Coimbatore, Tamil Nadu 641029, India
[b] Department of Science and Humanities, Sri Krishna Polytechnic College, Coimbatore, Tamil Nadu 641042, India
[c] Department of Chemistry, Government College of Technology, Coimbatore, Tamil Nadu 641013, India
[d] Department of Zoology, Bharathiar University, School of Life Science, Coimbatore, Tamil Nadu 641046, India
[e] The University College, Department of Chemistry, Sungkyunkwan University, Suwon, Gyeonggi 16419, Republic of Korea

ARTICLE INFO

Article history:
Received 16 July 2021
Revised 21 September 2021
Accepted 5 October 2021
Available online xxxx

Keywords:
Breast cancer
Green synthesis
Morinda tinctoria
Nuna
Zinc oxide nanoparticles

ABSTRACT

Zinc oxide nanoparticles (ZnO NPs) were prepared by a facile, one-pot, greener approach using aqueous leaf extract of the medicinal plant Nuna (*Morinda tinctoria*) and were analyzed by ultraviolet–visible (UV–Vis) and Fourier-transform infrared (FT-IR) spectroscopy, powder X-ray diffraction (PXRD), field emission scanning electron microscopy (FESEM), and transmission electron microscopy (TEM) techniques. The TEM images confirmed that the as-prepared greener Nuna (Nu)-mediated ZnO NPs (Nu-ZnO NPs) were spherical in shape, with an average diameter of 8–10 nm. Further, the single phase and crystallinity of the Nu-ZnO NPs were observed by PXRD pattern. In addition, the biogenic Nu-ZnO NPs showed high cytotoxicity in human breast adenocarcinoma (MCF-7) cells *in vitro*. These tiny spherical bodies produced profound toxicity according to the MTT assay, with IC_{50} of 46 μg/mL. Apoptosis and morphological changes were studied using acridine orange/ethidium bromide and 4′,6-diamidino-2-phenylindole fluorescence staining and MTT assays. Finally, the anticancer efficacy of biosynthesized Nu-ZnO NPs was imparted by dysregulation of cell division through arrest of growth-promoting and inhibiting signals in the S phase, with further reduction in the G2/M phase of the cell cycle. In conclusion, Nu-ZnO NPs conferred MCF-7 cell toxicity by modulating proliferation and inducing apoptosis.

© 2021 The Korean Society of Industrial and Engineering Chemistry. Published by Elsevier B.V. All rights reserved.

Introduction

Breast cancer is a commonly known cancer among women and a foremost cause of death. It is a heterogeneous group of diseases with differences in gene expression, genomic instability, and cell signaling [1]. The symptoms of breast cancer comprise swelling of the breast or skin, dimpling, irritation, redness, scaliness, breast pain, and thickening of the nipple or breast skin. While widespread mammography and poly-chemotherapy with adjuvant tamoxifen treatment have reduced the mortality of early diagnosed breast cancer [2,3], it remains the most dangerous disease due to recurrence and metastasis. Despite developments in diagnosis and treatment of breast cancer over the past 10 years, morbidity and mortality in young (<45 years old) patients have increased considerably. Many of these parameters are affected by the tumor microenvironment, significantly impacting tumor progression and therapeutic response [4]. Nevertheless, traditional chemotherapeutic agents produce high toxicity to normal cells and create several severe side effects. Various platforms have been established to overcome such drawbacks.

The concurrence between nanotechnology and nanomedicine has produced new opportunities in the therapeutic and pharmaceutical fields [5]. Current nanotechnology has a wide range of applications in diagnosis, food industry, drug delivery, environmental cleanup, paints, electrical systems and electronics, sunscreens, cosmetics, sports, and other biomedical fields [6]. ZnO NPs are semiconducting metal oxide NPs that are utilized extensively in biomedicine as an anti-cancer drug and a tool for imaging biological systems; cosmetic applications of ZnO NPs also are well established. Interactions between NPs and biological systems have some unpredictable outcomes. Hence, understanding NP toxicity is necessary to preventing dangerous effects on the human body [7].

* Corresponding authors.
E-mail addresses: janibiochem@gmail.com (J. Anitha), thathanpremkumar@gmail.com (T. Premkumar).

https://doi.org/10.1016/j.jiec.2021.10.009

University of Madras
Department of Inorganic Chemistry
Guindy Campus, Chennai-600 025
Email: jeevapandian@yahoo.co.uk

Dr.K.PANDIAN, M.Sc.; Ph.D
Professor

21st July 2021

It is with great enthusiasm and interest that I support and collaborate with Dr. K. Kalpanadevi, Associate Professor and Head, PG and Research Department of Chemistry, Kongunadu Arts and Science College, Coimbatore. I had a long-time association with that august institution as Board of Studies in Chemistry, resource person in various seminars and workshops, Doctoral committee member and Ph.D. viva examiner. Therefore, I would like to extend my research collaboration in the area of nanomaterials with the Department of Chemistry in both student exchange programme and joint publications. As our research interests are alike, I believe that the proposed collaboration will have the potential to contribute a significantly production of novel materials in recent applications. I look forward to collaborating with you on all phases of research.

(K.PANDIAN)

Dr. P. SHANMUGA VELAN M.Sc., M.Phil., Ph.D.
Assistant Professor
Department of Chemistry
School of Science
Tamil Nadu Open University
Saidapet, Chennai - 600 015
Tamil Nadu, India.

17.03.2021

To

Dr. A. Amuthavalli
Assistant Professor
Department of Chemistry (PG & Research)
Kongunadu Arts and Science College
Coimbatore - 641 029.

Dear madam,

Greetings.

This letter is to confirm our interest in collaboration with you on the research work in the field of "Synthesis and Applications of Novel Organic Compounds".

As you know well, my research team has strong interest in synthesising novel organic compounds and studying their applications. With similar researches, I am pleased to give all support in the areas which are deemed appropriate for us for achieving the research goal.

We are looking forward to an active role in this collaboration.

17/3/2021

Yours Sincerely,

Dr. P. SHANMUGA VELAN, M.Sc.,M.Phil.,Ph.D.
Assistant Professor of Chemistry
School of Sciences
Tamil Nadu Open University
Saidapet, Chennai-600 015.
Tamil Nadu, INDIA

Hello: +91 89404 09751 (mobile); 044-24306641 (phone)
E.mail: shanchemmku@gmail.com (personal); shanmugavelan@tnou.ac.in (official)
URL: www.tnou.ac.in

Biocatalysis and Agricultural Biotechnology 45 (2022) 102483

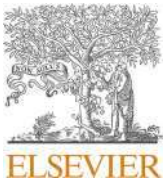

Contents lists available at ScienceDirect

Biocatalysis and Agricultural Biotechnology

journal homepage: www.elsevier.com/locate/bab

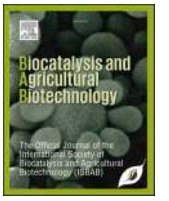

Study on spray-drying of *Bacillus velezensis* NKMV-3 strain, its formulation and bio efficacy against early blight of tomato

Murthy Vignesh [a,*], ShankarRamakrishanan Madhan Shankar [b,**], Nagaraj Subramani [c], Bodethala Narayanan VedhaHari [d], Durai Ramyadevi [d]

[a] Centre for Research & Evaluation, Bharathiar University, Coimbatore, 641 046, Tamil Nadu, India
[b] PG Department of Biotechnology, Kongunadu Arts and Science College (Autonomous), Coimbatore, 641 029, India
[c] Centre for Advanced Studies in Botany, University of Madras, Chennai, 600025, Tamil Nadu, India
[d] School of Chemical and Biotechnology, SASTRA Deemed University, Thanjavur, 613401, Tamil Nadu, India

ARTICLE INFO

Keywords:
Bacillus velezensis
Spray-drying
Tablet
Microbial bio control agent
Alternaria solani
Early blight
Tomato

ABSTRACT

Early blight caused by *Alternaria solani* (*A.solani*) is a serious disease affecting the tomato crop. Due to resistance built up in pathogens to fungicides, alternate methods of disease control have been explored. This research article details on the efficacy of whole cells of *Bacillus velezensis* (*B. velezensis*) NKMV-3 strain and its lipopeptide extract (LPE) against *A.solani*. *B.velezensis* NKMV-3 strain and its LPE was spray-dried using laboratory spray dryer. The highest powder recovery (55%) and viability (81.5%) was achieved when spray dried with 10%$MgSO_4$ + 10% Whey protein +0.1% SiO_2. The stability of the spray dried whole cell tablets was observed for 180 days (at 4 °C and 37 °C) with a maximum cfu.g^{-1} of 2.3 × 10^8 at 4 °C. The spray-dried tablets of LPE of *B.velezensis* NKMV-3 was stable for 2 years as per CIPAC guidelines with a very low degradation of lipopeptides namely iturin, surfactin and fengycin. Greenhouse studies also revealed that *B. velezensis* NKMV-3 tablets along with its LPE tablets showed inhibitory effects against *A.solani*. Hence, *B.velezensis* NKMV-3 was found to be a suitable candidate to be pursued for the development of a bio control agent against early blight of tomato.

1. Introduction

Early blight disease in tomatoes caused by *A.solani* is one of the most disastrous diseases of tomatoes leading to heavy economic losses of 70–80% in yield (Adhikari et al., 2017). The disease is considered to be the most devastating one, because of its significant cause of losses in both quantity and quality of fruit harvest. Favorable conditions for the onset of disease include warm and consistent moist environment which may be due to frequent rain showers or any overhead irrigation systems (Sahu et al., 2014). Major control measures for early blight of tomato involves the usage of synthetic fungicides. But continuous usage of fungicides may lead to resistance among plant pathogens (Todorova and Kozhuharova, 2010). Hence, in order to overcome this, safe and sustainable control measures such as use of microbial bio control agents are required.

Bacillus spp. has been verified as a plant growth promoter and systemic resistance inducer, in addition to the production of a broad range of antimicrobial compounds and as competitors for growth factors with other pathogenic microbes. Rhizospheric dwelling bacteria play an vital role in antagonistic activity against the plant pathogens, particularly through the induction of systemic induced

* Corresponding author.
** Corresponding author.
E-mail addresses: nanovignesh@gmail.com (M. Vignesh), srmadhanshankar@gmail.com (S.M. Shankar).

https://doi.org/10.1016/j.bcab.2022.102483
Received 3 August 2022; Received in revised form 22 August 2022; Accepted 3 September 2022
Available online 9 September 2022
1878-8181/© 2022 Elsevier Ltd. All rights reserved.

resistance in the host (Bhattacharyya and Jha, 2012). Hence, bacterial bio control agents targeting species of *Bacillus* genus are potential candidates for development of bio control agents against various plant pathogens(Andrić et al., 2020; Shafi et al., 2017). Also, *Bacillus* based bio control agents occupy a major part in the field of commercialized biopesticides (Fravel, 2005). In our previous results, we have shown an antagonistic species of *Bacillus* namely *B.velezensis* NKMV-3 capable of controlling the early blight pathogen (*A.solani*) in tomato(Vignesh et al., 2022).

Many reports have been published for the development of formulations using microbial bio control agents. The most common type of formulations using *Bacillus* spp. is either a liquid or a wettable powder formulation. Though there was bio control activity using these formulations, they lacked shelf-life and viability over a period of time. Further, it was also difficult for production and transportation of these formulations (Lee et al., 2006). Hence, the requirement for an alternate and more efficient type of formulation was the need of the hour. In order to overcome these drawbacks, scientists resorted to drying processes such as freeze drying and spray drying of bacteria. Since freeze drying was a more expensive technique due to its energy requirements, spray drying was an ideal choice (Peighambardoust et al., 2011).

Though, there were initial reports of reduction in cell viability and bio efficacy due to spray drying of bacteria (Abadias et al., 2005), further studied provided successful methodologies using spray drying for the development of bacterial formulations which were shelf-stable, viable and efficacious (Prabakaran and Hoti, 2008; Yánez-Mendizábal et al., 2012).

Previous results have suggested that *B.velezensis* strain was able to control early blight of potato (Gorai et al., 2021). Further, scientists were able to elucidate the inhibitory effects of volatiles produced by *B. velezensis* strain ZSY-1 against early blight in tomato. Ready to use tables from autoclaved cell free extract of *B.subtilis* CMs026 strain and its bio efficacy against early blight of Chinese Kale were also studied (Weerapol et al., 2019).

In the current study, an antagonistic bacteria *B.velezensis* NKMV-3 strain and its LPE were spray-dried. The spray dried powder was tableted. The tablets were examined for various physio-chemical properties. The stability of the tables were also examined in this study followed by a preliminary greenhouse study to understand the bio efficacy of whole cell tablets and its LPE tablets against *A.solani* in tomato.

2. Materials and methods

2.1. Microorganism and growth conditions for endospore production and viability

Bacillus velezensis NKMV-3 previously isolated from the rhizospheric soil of tomato plants from a tomato growing region of Tamil Nadu state, India was used in this study (Vignesh et al., 2022). Endospore production test was done as per Yánez-Mendizábal et al. (2012). Briefly, a loop full culture from an actively growing nutrient agar slant was taken and inoculated into nutrient broth amended with 2% Glucose. The bacteria were incubated for 48 h at 37 °C in a rotatory shaker with constant shaking of 130 rotations min^{-1}. Samples were drawn at 24h and 48h and subjected to heating at 80 °C for 12 min to kill vegetative cells and generate endospores. This was followed by serial dilution in water and plating on nutrient agar media from corresponding dilutions. The plates were incubated at 30 °C for 48h and observed for bacterial growth. A similar set of experiment was carried out without heat treating the bacterial culture at 80 °C. The $cfu.ml^{-1}$ was compared between heat treated and untreated cultures at 24h and 48h. The study was conducted in triplicates.

2.2. Spray-drying of bacteria

Spray-drying of *B.velezensis* NKMV-3 was conducted using a laboratory spray dryer (Spray Mate, Jay Instruments & Systems Pvt. Ltd). *B.velezensis* NKMV-3 grown in 100 ml Nutrient Broth amended with 2% Glucose for 48h at 130 rotations min^{-1} was used for Spray-drying. Based on literature survey, carrier materials such as maltodextrin (10% w/v), Skimmed milk powder (10% w/v) and whey protein (10% w/v) were used (Abadias et al., 2005; Bhagwat et al., 2020; Costa et al., 2002; Palazzini et al., 2020). 10% (w/v) $MgSO_4$was used as a cell protectant and 0.1% (w/v) SiO_2 was used as anticaking agent in each combination during the process of spray-drying. The spray-drying parameters were as follows: inlet and outlet temperatures were 140 °C and 65 °C respectively. The flow rate of the suspension was maintained as 300 ml/h and the atomization pressure was 1.30 kg/cm^2. The spray dried powder from each combination was collected into sterile borosilicate bottles and placed at room temperature until further use.

The total dry matter in the initial 48h old bacterial suspension and the final spray dried powder was calculated by placing 5 ml/0.5g of the suspension/powder respectively at 105 °C for 24 h in a hot air oven. The difference between the final weight of the spray dried powder and the suspended solids in the initial suspension was used to calculate the percentage of powder recovery. The experiment was repeated thrice.

To determine the viability of the spray dried bacterial combinations using different carriers, the $cfu.ml^{-1}$ of the initial suspension and final spray-dried powder was calculated. 1 ml of the initial bacterial suspension was serially diluted and plated on nutrient agar medium. In case of spray dried powder, 0.1 g of the sample was rehydrated in water for 10 min and serially diluted and plated on nutrient agar media. The percentage of viability was calculated as below:

$$\% \text{ Viability} = (cfu.g^{-1} \text{ of final spray dried powder}/cfu.ml^{-1} \text{ of initial NKMV-3 Suspension}) \times 100$$

The experiment was repeated thrice.

2.3. Preparation of lipopeptide extract spray dried powder

B.velezensis NKMV-3 was grown in nutrient broth amended with 2% glucose for 30 h at 37 °C in a rotatory shaker with constant

shaking of 130 rotations min^{-1}. The cells were harvested by centrifugation at 6000×*g* for 15 min followed by the reduction of pH of the cell free extract to 2.0 by the addition of 3N HCl and left for overnight precipitation at 4 °C. The precipitated lipopeptides was separated by centrifugation at 8000×*g* for 30 min at 4 °C. The pellet was dissolved in methanol and extracted thrice and evaporated under vacuum using a rotatory evaporator at 50 °C and 65 rpm (Lin et al., 2020; Zouari et al., 2016). The resulting viscous liquid was left for drying at 50 °C for 48h in a hot air oven. The dried lipopeptide extract was scrapped and stored until further use.

Spray dried powder of lipopeptide extract was prepared using a laboratory spray dryer (Spray Mate, Jay Instruments & Systems Pvt. Ltd). The spray dried powder was prepared as follows: 5% (w/v) of NKMV-3 lipopeptide extract was dissolved in 20% (w/v) of methanol. This was followed by addition of 20% (w/v) of whey protein and 0.1% (w/v) SiO_2. The remaining portion was made up with cell free extract of NKMV-3. The Spray-drying parameters were as follows: inlet and outlet temperatures were 140 °C and 65 °C respectively. The flow rate of the suspension was maintained as 300 ml/h and the atomization pressure was 1.30 kg/cm^2. The spray dried powder was recovered and stored in borosilicate bottles at room temperature until further use.

2.4. Preparation of tablets

The spray dried powder of microbial sample and their derived lipopeptide extract were designed as tablets with 200 mg dose/tablet by direct compression and wet granulation process, respectively using an optimized formula (Table 1). The active ingredient and the individual excipients like sodium starch glycolate for disintegrating agent along with microcrystalline cellulose and lactose for diluents were passed through sieve no. 60 and triturated in a mortar. For direct compression of *B.velezensis* NKMV-3, 7.5% of dry corn starch as binder was preferred, due to hygroscopic nature of the spray dried powder and also to maintain the viability and stability of the bacterium. For the formulation of secondary metabolites as tablets, required amount of polyvinyl pyrrolidone dissolved in isopropyl alcohol was used as binder for granulation. The granules were passed through sieve no. 32 and then dried in hot air oven at 40 °C for 5 min. The granules and the direct compression mixture were individually lubricated with talc and magnesium stearate (2% each) and then compressed as tablets using semi-automatic single punch compression machine (Khera Instruments, Mumbai) with 8 mm diameter concave punches and dyes. The tablets were subjected to quality control standard testing and stored in desiccator for further evaluation (Coelho et al., 2018; Yánez-Mendizábal et al., 2012).

2.5. Pre-compression parameters for tableting

The wet granules and the direct compression mixture were evaluated for pre-compression parameters such as flow property, density, compressibility index and Hausner ratio before the pill compression process to ensure the suitability for the material for punching as solid unique tablets without any issues like weight variation, capping, breaking, etc (Weerapol et al., 2019). Angle of repose was measured to check the flow behavior of the samples using funnel method. Each sample was allowed to freely fall through a funnel fixed at height of 20 cm from base, to form a symmetrical cone on a paper. The height and base (diameter) of the cone was measured (n = 3 trials) and the angle of repose was calculated by the formula,

$$Tan\ \theta = \frac{Height\ of\ cone}{Radius\ of\ cone}$$

The bulk volume of samples was noted in a measuring cylinder and the tapped volume was confirmed by placing the known quantity of the granules in the Tapped Density Apparatus (Lab India), which runs up and down continuously for about 500 tapping at the height of 3–5 inches. The bulk and tapped density of the granules was assessed from bulk and tapped volume, correlated to the total weight of the granules using the formulae,

$$Bulk\ density\ (V0) = \frac{Bulk\ Volume\ of\ granules}{Weight\ of\ the\ sample\ taken}$$

$$Tapped\ density\ (Vt) = \frac{Tapped\ Volume\ of\ granules}{Weight\ of\ the\ sample\ taken}$$

These values were used to determine the compressibility nature of the materials through the compressibility index and Hausner

Table 1
Formulation of Tablets for of *B.velezensis* NKMV-3 and its LPE.

S. No.	Name of the ingredient	Quantity/Tablet (mg)	
		NKMV-3whole cells	NKMV-3 Lipopeptide extract
1	Active ingredient	200	200
2	Micro crystalline cellulose	42.5	42.5
3	Lactose	17	17
4	Starch	22.5	–
5	Poly vinyl pyrrolidone	–	22.5
6	Isopropyl alcohol	–	Quantity sufficient
6	Sodium starch glycolate	6	6
7	Talc	6	6
8	Magnesium stearate	6	6
	Total weight of a tablet	300	300

ratio calculation.

$$\%\ Compressibility\ Index = 100x\frac{V0 - Vt}{V0}$$

$$Hausner\ Ratio = \frac{V0}{Vt}$$

2.6. Evaluation of tablets

The formulated tablets were evaluated for standard quality parameters such as uniformity in dimensions and weight, hardness, disintegration time and friability (Ch et al., 2012). All the tablets were evaluated for diameter and thickness using a Vernier Caliper scale. The individual weight of tablets and their average weight deviation was calculated as the monograph standards. The hardness of the tablets was checked with Monsanto hardness tester. The time taken for the disintegration of the tablets was estimated in disintegration testing apparatus (Lab India) as per the specifications, using distilled water as media. The tablets were placed in vessels without disc (n = 6) and immersed and raised in the media until the tablets fragmented into pieces that passes through the mesh at the bottom of the vessel. Friability of the 10 tablets was evaluated using Tablet Friability Tester (Lab India), wherein the tablets were subjected to rolling and falling process at the optimum height of 6 cm for 100 revolutions in 4 min (25 rpm/minute). The initial and final weight of the tablets were considered to calculate the % friability using the formula,

$$\%\ Friability = \frac{Initial\ weight - Final\ weight}{Initial\ weight}x100$$

2.7. Shelf-life study of tablets

The prepared bacterial tablets were subjected to real time shelf-life studies at two pre-set temperatures namely 4 °C and 37 °C. The tablets were stored in airtight borosilicate screw cap containers and placed inside stability chambers (Remi, India) maintained at 4 °C and 37 °C with 50% RH. Triplicate samples were maintained (Meng et al., 2015). Tablets equivalent to 1g dry weight was taken at intervals of 30, 60, 90, 120 and 180 days from whole cell tablet formulation and serially diluted in sterile distilled water and plated on nutrient agar medium. The plates were incubated at 30 °C for 48h and observed for bacterial growth (Jayaraj et al., 2005).The number of bacterial colonies were counted and expressed as CFU g^{-1}.

The tablets of NKMV-3 lipopeptide extracts were subjected to accelerated shelf life studies in accordance with Collaborative International Pesticides Analytical Council limited., 2000; (Yánez-Mendizábal et al., 2011). Briefly tablets were stored in airtight borosilicate screw cap containers and placed inside stability chambers (Remi, India) maintained at 54°Cand50% RH for 14 days. Samples were quantified through liquid chromatography as adapted from (Dhanarajan et al., 2016) for lipopeptides namely iturin, surfactin and fengycin. Triplicate samples were maintained for the experiment.

2.8. Water solubility of tablets

The dissolution capacity of both bacterial tablet and that of the lipopeptide extract of NKMV-3 was determined as follows; 250 mg of each tablet were suspended in 50 ml of water and stirred using a magnetic stirrer at 829 rpm. The time for complete solubility was calculated in seconds and expressed as dissolution time/tablet (Fritzen-Freire et al., 2012). The experiment was repeated thrice.

2.9. Inhibitory effects of NKMV-3 lipopeptide extract tablets against A.solani

The effect of lipopeptide extract tablets of *B.velezensis* NKMV-3 was evaluated for any inhibitory effect on the mycelial growth of *A. solani*. 1%, 2.5% and 5% concentrations of the lipopeptide extract tablets were added to 100 ml of Potato dextrose broth. Each flask was inoculated with a 5 mm disc of *A.solani* from an actively growing plate. The flasks were incubated at 28 °C in a rotatory shaker with constant shaking of 130 rotations min^{-1} for 5 days. A control flask was maintained with only a 5 mm A.*solani* disc and without the

Table 2
Treatment details for greenhouse studies.

Treatment No.	Treatment details	Dosage (g/l)
T1	Un treated control	–
T2	NKMV-3T	1
T3	NKMV-3T	2
T4	NKMV-3T	3
T5	NKMV-3 LPET	1
T6	NKMV-3 LPET	2.5
T7	NKMV-3 LPET	5
T8	NKMV-3T + LPET	1g each
T9	NKMV-3T + LPET	2g + 2.5g
T10	NKMV-3T + LPET	3g+5g
T11	NKMV-3T + LPET	5g+5g
T12	Mancozeb	2g

NKMV-3T – B.velezensis tablet
LPET – Lipopeptide extract tablet of NKMV-3

addition of NKMV-3 lipopeptide extract tablet. Samples were drawn from each flask after 5 days of incubation and observed under a light microscope (Olympus CX 31) for any abnormalities in the hyphal structures and photographed.

2.10. Greenhouse studies of bacterial and lipopeptide extract tablets against A.solani in tomato

A completely randomized block designed greenhouse study was conducted to evaluate the effect of NKMV-3 and its lipopeptide extract tablets on tomato for the control of early blight of tomato. Twelve treatments as provided in Table 2 were evaluated. PKM-1 variety tomato seedlings were used for the study. Thirty days old seedlings were transplanted into 5 Kg pots and used for the trial. The potting mixture consisted of red soil, farmyard manure and river sand in the ratio 1:2:1.

The plants were grown for another 45 days until it reached 10–15 leaf stage. A spore suspension with min 3×10^5 conidia/ml was prepared from a 10 day old *A.solani* plate using 0.1% Tween-80 (Awan and Shoaib, 2019). In order to provide the bacterial cells time to establish on the leaf surface, treatments T2 to T4 were sprayed two days prior to the application of the conidial suspension. While all other treatments were sprayed two days after inoculation of conidial suspension. An untreated control was maintained with no application of conidial suspension. Plants were enclosed inside plastic covers for 48h after conidial application with a relative humidity of 60% to improve conditions for onset of disease. Each treatment was replicated thrice. The percentage of early blight disease severity was evaluated 20 days after inoculation based on the visual score of the symptoms on leaves as follows in Table 3 (Vakalounakis, 1983):

The percentage of early blight disease index was calculated using the above scoring of visual symptoms using the below formula (Pandey et al., 2003; Ravikumar et al., 2016):

Percentage disease index = Sum of all ratings x 100 /

No. of sampled leaves x maximum score in rating.

2.11. Statistical analysis

All data was analyzed statistically using WASP - Web Agri Stat Package 2.0 and Microsoft excel (2016), to assess statistically significant differences among the various treatments.

3. Results

3.1. Endospore production and viability of NKMV-3

Bacillus velezensis NKMV-3 was found to produce endospores when subjected to heat treatment. The CFU ml^{-1} including vegetative and endospore cells was 6.3×10^8 and 2.7×10^9 respectively before heat treatment at 24h and 48h after inoculation. The CFUml^{-1}gradually reduced to 2.3×10^6 and 3.3×10^8 respectively after heat treatment at 24h and 48h after inoculation respectively. The reduction in CFU ml^{-1} was lesser in 48h old culture in comparison to 24h culture. The highest viability of cells (88.9%) was observed when 48h old culture was subjected to endospore formation (Table 4).

3.2. Moisture content, percentage recovery percent, viability and survival of spray dried powder of B.velezensis NKMV-3 and its LPE

Spray-drying of *B.velezensis* NKMV-3 yielded a dull white powder which was hygroscopic when exposed to air due to the presence of maltodextrin, skim milk or whey protein based on the composition. There was a significant influence on the usage of different carrier materials in the preparation of spray-dried powder of *Bacillus velezensis* NKMV-3. On an average, the percentage powdery recovery was ranging between 27 and 55%. Similarly, the moisture percentage of the spray dried powder was significantly varying between 5 and 11% when using different carrier materials (Table 5). The maximum powder recovery was observed while using whey protein as carrier while the least percentage of moisture was observed when skim milk was used as the carrier.

In order to scale up the production of *B. velezensis* NKMV-3, 10% $MgSO_4$, 10% whey protein and 0.1% SiO_2 was shortlisted as it produced the maximum powdery recovery with moderate moisture percentage (Table 5).The viability of the cells ranged from 70 to 82% based on the carrier material. Whey protein carrier combination with 10% $MgSO_4$ was found to have the maximum percent viability of 81.5, while skim milk combination with 10% $MgSO_4$ showed the least percent viability of 70.4% (Fig. 1). 48h culture of *B. velezensis* NKMV-3 had a cfu.ml^{-1} of 1.3×10^9. The survival of *B.velezensis* NKMV-3 was greatly influenced by various carrier materials. The average cfu.g^{-1} when maltodextrin was used as a carrier was 1.4×10^7.Whey protein as carrier produced a slightly better cell survivability of 4.9×10^8 cells g^{-1}. Skim milk as carrier produced a viability of 2×10^7 cfu g^{-1}. Whey protein which was found to have the maximum powder recovery and viability was used for the spray-drying of the LPE of NKMV-3. The powder recovery of LPE of

Table 3
Scoring chart for *A.solani* lesions.

Score	Details
0	No visible lesions on the leaf
1	Up to 10% of the leaf affected
2	11–25% of the leaf affected
3	26–50% of the leaf is affected
4	51–75% of the leaf is affected
5	>75% of the leaf is affected or leaf abscised

Table 4
Viability of *B.velezensis* NKMV-3 after heat treatment for endospore formation.

S.No	Time point	$CFUml^{-1}$ Before heat Treatment	$CFUml^{-1}$ After heat Treatment	% Viability
1	24h	$6.3 \times 10^{8}(\pm 3.1)$	$2.3 \times 10^{6}(\pm 1.5)$	75.0
2	48h	$2.7 \times 10^{9}(\pm 1.5)$	$3.3 \times 10^{8}(\pm 2.5)$	88.9

Table 5
Percentage powdery recovery and moisture with inlet and outlet temperatures during spray drying using different carrier materials Each value is a mean of three replications. Different letters indicate significant differences between different treatments ($P < 0.05$) using WASP.

S. No	Treatment details	Inlet Temperature (°C)	Outlet Temperature (°C)	Powder Recovery (%)	Moisture (%)
1	NKMV-3 + 10%$MgSO_4$ + 10% Maltodextrin +0.1% SiO_2	140	65	27.32^{c}	11.70^{a}
2	NKMV-3 + 10%$MgSO_4$ + 10% Skim Milk + 0.1% SiO_2	140	65	49.50^{b}	3.70^{b}
3	NKMV-3 + 10%$MgSO_4$ + 10% Whey protein +0.1% SiO_2	140	65	55.33^{a}	5.00^{b}
4	NKMV-3 LPE +10% Whey protein +0.1% SiO_2	140	65	44.05 ± 1.63^{d}	6.80 ± 0.38^{c}

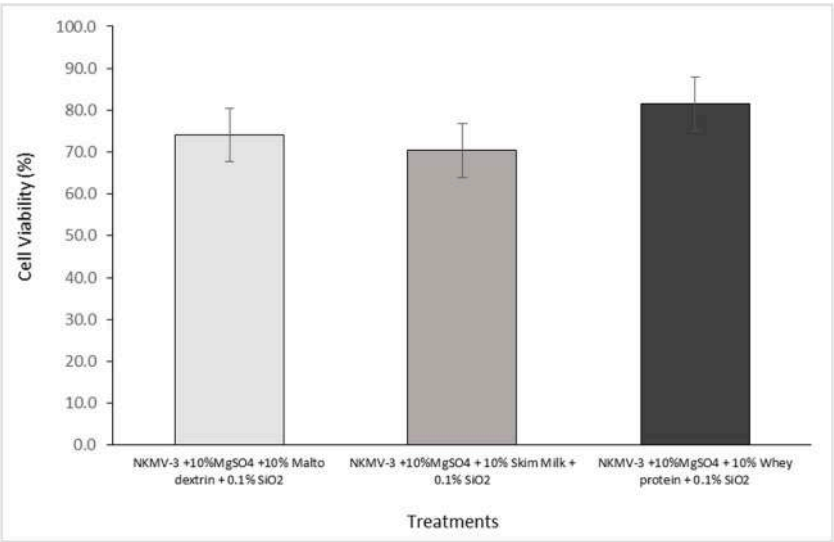

Fig. 1. Cell viability of *B.velezensis* NKMV-3 using different carrier materials while spray-drying at 140 °C inlet temperature and 65 °C as outlet temperature. Each value is a mean of three replications. Significant difference between treatments ($P < 0.05$) using WASP.

NKMV-3 was 44.05% with moisture of 6.80%.

3.3. Preparation of bacterial and NKMV-3 LPE tablets

The spray dried samples of *B.velezensis* and their derived metabolites both exhibited hygroscopic nature when exposed to air. The secondary metabolites sample was wet granulated with PVP binder, which resulted in free-flowing granules with required flow behavior as confirmed by the angle of repose value 39°. In case of the spray dried microbes, the direct compression mixture exhibited poor flow property due to cohesive nature of the raw materials(Al-Zoubi et al., 2021). However, addition of the lubricants improved the flow nature of the sample, which was manually compressed into tablets (Ch et al., 2012). The bulk and tapped density measurement of both the samples confirmed their optimum compressibility index and Hausner ratio that was suitable for compression of the materials into solid unit tablets. The results obtained are provided in Table 6 & Fig. 2.

Table 6
Pre-compression parameters of the granules.

S. No.	Parameters	NKMV-3 whole cells	NKMV-3 Lipopeptide extract
1	Angle of repose (θ°)	15.983 ± 1.086	39.028 ± 1.714
2	Bulk density (g/mL)	0.298 ± 0.006	0.321 ± 0.001
3	Tapped density (g/mL)	0.411 ± 0.010	0.403 ± 0.004
4	Compressibility Index (%)	27.376 ± 0.892	25.474 ± 0.904
5	Hausner Ratio	1.377 ± 0.017	1.254 ± 0.009

3.4. Evaluation of tablets

The dimensions of both formulated tablets were 8.1 mm diameter and 5.1 mm thickness without any variation. The average weight of the tablets was about 285 mg and 297 mg for the direct compressed microbes and wet granulated metabolites, respectively. Both tablets were found to be within the standard narrow limits of 5% deviation of the average weight, which ensured uniform distribution of the active ingredients at required dose in all the tablets. The hardness of tablets containing the microbes and metabolites was found to be 3.5 and 4 kg/cm^{2}respectively. This provided the optimum compression force and strength of the tablets. The disintegration time of 10 and 14 min for the former and later, respectively, is considered suitable due to addition of sodium starch glycolate. The friability of less than 0.1% in both batches of tablets signified the negligible weight loss due to crack or damage of edges (Weerapol et al., 2019). Further, the time to dissolve for microbial tablets was slightly less (613s) in comparison to LPE tablets (854s). The result of the study is shared in Table 7.

3.5. Stability study of B. velezensis NKMV-3 and its lipopeptide extract tablets

B. velezensis tablets prepared as described were stored at 4 °C and 37 °C. The real time stability (cfu.g^{-1}) data for the bacterial pellets was observed for 180 days on a monthly basis. Table 8 provide details of the stability at the two storage temperatures. At both storage temperatures, a cfu.g^{-1} of x10^8 was achieved. Though statistically not significant, the cfu.g^{-1} of the bacterial pellets was slightly better at 4 °C in comparison to stability at 37 °C.

Previous studies have reported that *B. velezensis* NKMV-3 can produce iturin, surfactin and fengycin (Vignesh et al., 2022). LPE tablets of NKMV-3 was prepared as described earlier and subjected to accelerated stability study. After 14 days at 54 °C, iturin degraded by 3.98%, fengycin by 2.43% and surfactin by 3.87% (Table 9). This clearly proved that the LPE tablets were stable for 2 years as per CIPAC guidelines.

3.6. Inhibitory effect of NKMV-3 lipopeptide extracts tablets on A.solani

B.velezensis NKMV-3 LPE tablets were inoculated into PDB at various concentrations along with mycelial plugs of *A.solani*. NKMV-3 LPE tablets were found to be effective in at all tested dosages against *A.solani* producing swelling in the mycelium, leading to deformation of the hyphae. There was a gradual increase in the deformed hyphae as the concentration of the tablets increased from 1 to 5%. The malformations in the hyphae are shown in Fig. 3.

3.7. Greenhouse studies of bacterial and lipopeptide extract tablets against A.solani in tomato

A greenhouse study was performed to evaluate the efficacy of the tablets of the bacteria and its LPE's against *A.solani* in tomato. The percentage disease index was calculated after 20 days inoculation of the conidial suspension on the tomato plants. The results revealed that, the combination of LPE tablets and the bacterial tablets when used together as tank mix provided a better control of the disease in comparison to the stand-alone usage of either the LPE tablets or the bacterial tablets. The least PDI was obtained in the chemical treatment (Mancozeb) followed by combination of LPE tablets and bacterial tablets used at a dosage of 5 g/l each. The least control of the disease was found when the bacterial tablets were used alone at a dosage of 1 g/l. The results of the greenhouse study are presented in Fig. 4.

4. Discussion

In the present study, experiments were performed to evaluate the ability of the formation of endospores by *B.velezensis* NKMV-3, spray-drying of whole cells and its lipopeptide extracts, tableting of whole cells and its lipopeptide extract and inhibitory effect of both the tablets against *A.solani* under greenhouse conditions in tomato plants.

Due to various reasons such as resistance to fungicides, evolution of pathogens, change in climatic conditions, a shift from chemical pesticides to microbial bio-fungicides has begun. *Bacillus* spp. are an important candidate among other genera of bacteria because they produce a wide array of secondary metabolites finding applications in agriculture and healthcare (Zhao et al., 2017). Ongena and Jacques. (2008) have reviewed the mechanisms of plant disease control by various lipopeptides produced by *Bacillus* spp.

This study as described above, involves the spray-drying of antagonistic bacteria. The main criteria for a bacterium to be able to be spray dried are its ability to tolerate high temperatures for a certain duration of time (Golowczyc et al., 2010). Thermo tolerance for

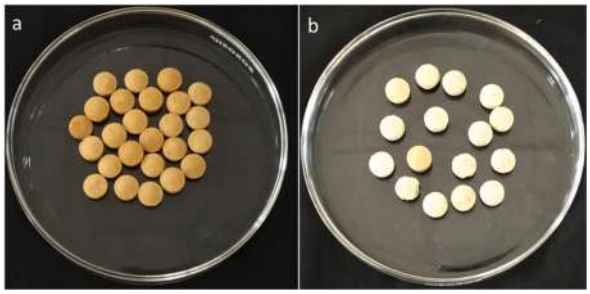

Fig. 2. a. Compressed tablets of *B. velezensis* NKMV-3 whole cells, b. Compressed tablets of LPE of *B. velezensis* NKMV-3.

Table 7
Evaluation of the Tablets of *B.velezensis* NKMV-3 Whole cells and its Lipopeptide extract.

S. No.	Parameters	NKMV-3 Whole cells	Lipopeptide extract
1	Average weight (mg)	285.2 ± 2.15	297.2 ± 3.12
2	Diameter (mm)	8.1 ± 0.002	8.1 ± 0.002
3	Thickness (mm)	5.1 ± 0.003	5.1 ± 0.003
4	Hardness (Kg/cm^2)	3.5 ± 0.1	4.33 ± 0.28
5	Disintegration Time (min)	10 ± 1.0	14.33 ± 0.57
6	Friability (%)	0.05 ± 0.002	0.04 ± 0.002
7	Dissolution time (s)	613.67 ± 6.03	854.33 ± 13.58

Table 8
Real time shelf-life study of compressed tablets of *B. velezensis* spray dried powder. The values are averages of three replicates.

Storage time (Days)	Mean $cfu.g^{-1}(x\ 10^8)$	
	4 °C	37 °C
0	5.3 ± 0.58	5.3 ± 0.58
30	4.7 ± 1.15	4.3 ± 1.53
60	3.7 ± 0.58	3.7 ± 2.08
90	3.3 ± 0.58	2.3 ± 0.58
120	3.0 ± 1.00	2.0 ± 1.00
150	2.7 ± 0.58	1.7 ± 1.15
180	2.3 ± 1.53	1.3 ± 0.58

Table 9
Accelerated stability study of compressed tablets of *B. velezensis* LPE spray dried powder. The values are averages of three replicates.

S.No	Analysis parameter	% Degradation of lipopeptides after 14 days of Accelerated stability study
1	Iturin	3.98 ± 0.100
2	Fengycin	2.43 ± 0.005
3	Surfactin	3.87 ± 0.004

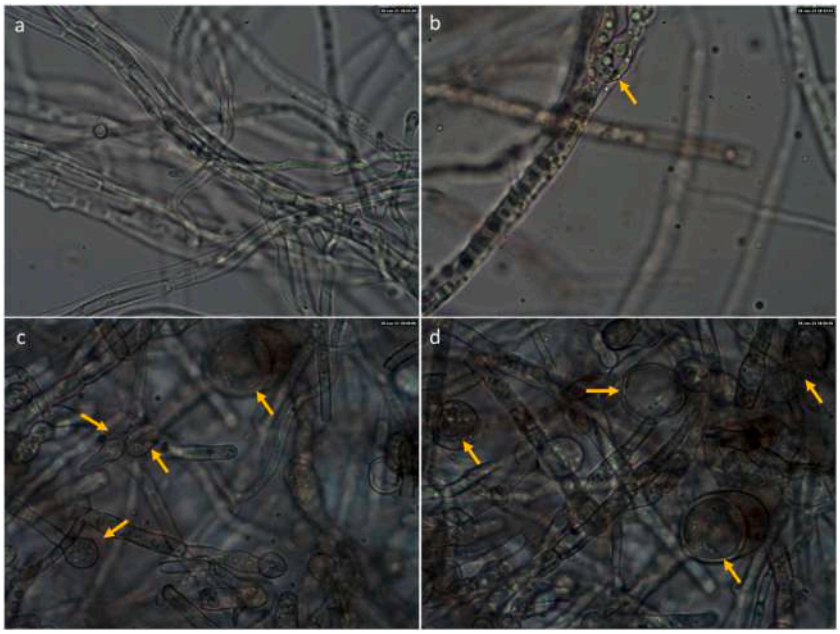

Fig. 3. Effect of NKMV-3 LPE tablets against *A.solani* under *in vitro* conditions. a. Control without LPE tablets, b. LPE compressed tablets at 1% concentration against *A. solani*, c. LPE compressed tablets at 2.5% concentration against *A.solani*, d. LPE compressed tablets at 5% concentration against *A.solani*. Arrows indicate deformations in the mycelial structures upon exposure to NKMV-3 LPE tablets.

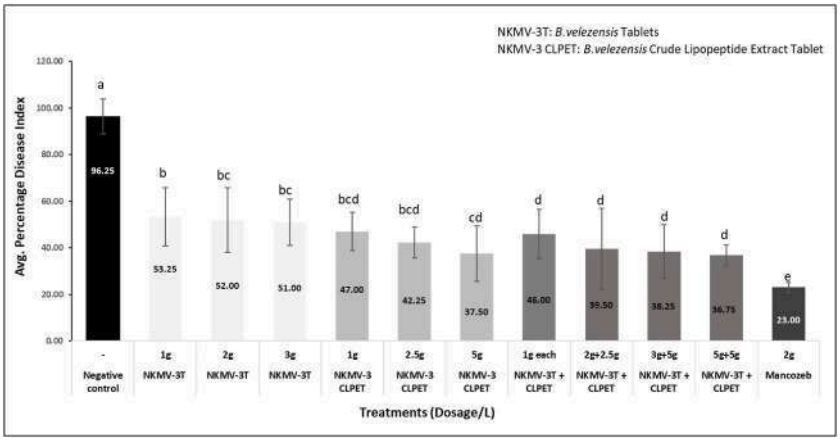

Fig. 4. Bio efficacy results of various treatments of *B.velezensis* NKMV-3 strain and its LPE tablets against *A.solani* under greenhouse conditions. Each bar represents average of three replicates. Different letters indicate significant differences in between treatments. ($P < 0.05$) according to WASP.

bacteria especially *Bacillus* spp. is achieved through the formation of specialized heat resistant vegetative structures called endospores. Endospores help in tiding over unfavorable conditions and may survive even over millions of years (Nicholson et al., 2000). Errington (2003) determined that when *Bacillus* spp. was exposed to 80–85 °C, they were able to form endospores. Our results also suggest that *B. velezensis* NKMV-3 is able to form endospores when exposed to 80 °C. This will enhance the viability of spores during the spray-drying process.

Spray-drying of bacterial formulations was considered to be a non-viable option for producing bio control agents mainly due to the reduction in cell viability and lower bio efficacy among other reasons (Abadias et al., 2005). On further research and development in this area, success was achieved by several scientists to produce a stable and efficacious spray dried product. Prabakaran and Hoti. (2008) and Yánez-Mendizabal et al. (2012), were able to produce spray dried *B.subtilis* and *B. thuringiensis* var. *Israelensis* that was stable and also effective in controlling brown rot caused by *Monilinia* spp. in nectarines & peaches and third instars of *Ades aegypti* mosquito larvae respectively. Further, spray-drying of bacterial cells is determined by several parameters such as inlet temperature, outlet temperature, atomization pressure, cells protectants, carriers and others. A detailed reading of these parameters affecting the spray-drying process is provided by Huang et al. (2017). Of all the parameters, outlet temperature is very critical for the survival of spray dried cells. Zhou et al. (2008) suggested an optimal outlet temperature of not more than 65 °C for the spray-drying of *B.thuringiensis*. Though Palazzini et al. (2020) used a slightly lower outlet temperature of 55 °C for the spray-drying of *B.velezensis* for the control of *Fusarium* head blight in wheat, we have optimized 65 °C as outlet temperature for the spray-drying of *B.velezensis* NKMV-3 strain which is concurrence with Zhou et al. (2008).

Another factor critical to the success of spray-drying is the growth phase of the bacteria used for spray-drying. We have used a 48h old culture which is in the log phase for spray drying. This maximizes the chances of survival of cells after spray drying. Similar results were obtained by Yánez-Mendizábal et al. (2012) when they compared the survival percentage of 24h and 72 h *B.subtilis* culture after spray-drying.

The current studies were conducted using a lab scale spray-dryer, hence the losses were more. A maximum powdery recovery of 55% was achieved in this study. This in accordance with the results obtained by Costa et al. (2002). In general, there is always a reduction in the number of cells before and after spray drying (Palazzini et al., 2020; Yánez-Mendizábal et al., 2012). Our results also concurred with a reduction in cfu.g^{-1} by 10^1–10^2 folds after spray drying depending on the carrier used.

Tablet formulations of both *B.velezensis* NKMV-3 and its LPE were prepared from their respective spray-dried powders. All tablets so prepared were found acceptable to normal tableting standards. This can be used while scaling up the process for preparing commercial quantities of the formulation. As described by Weerapol et al. (2019) the addition of 6% Sodium starch glycolate provided the necessary hardness to the tablets which increased the disintegration time. The friability of less than 0.1% in both batches of tablets signified the negligible weight loss due to crack or damage. Since Silicon dioxide (anti caking agent) was added during the preparation of spray drying, it resulted in a free flowing powder (Pingali et al., 2011).

B.velezensis has known to exhibit antagonistic activity against early blight pathogen in Potato (Gorai et al., 2021). Gao et al. (2017) had demonstrated that volatile compounds produced by *B.velezensis* strain ZSY-1 were able to control the growth of *A.solani* in tomato. Cao et al. (2018) demonstrated that lipopeptides produced by *B.velezensis* isolates consisting of iturin, surfactin and fengycin played important role in controlling plant pathogens namely *Ralstonia solanacearum* and *Fusarium oxysporum*. On similar lines, *B.velezensis* NKMV-3 strain and its lipopeptide extract (containing iturin, surfactin and fengycin) was already shown to exhibit inhibitory effect against *A.solani* in tomato (Vignesh et al., 2022). The stability of the whole cell tablets was studied at two storage temperatures (4 °C and 37 °C).Our results indicated that there was only a slight reduction of viable cells at 37 °C in comparison to 4 °C. These results are in concurrence with results obtained by Palazzini et al. (2020). Weerapol et al. (2019) studied the degradation of surfactin over a period of three months in tablets derived from *B.subtilis* strain CMs026 and reported no degradation in surfactin content when stored at 4 °C. In order to confirm the stability of LPE tablets, iturin, surfactin and fengycin were quantified through liquid chromatography after 14

days at accelerated conditions in accordance with CIPAC guidelines. Our results showed less than 5% degradation in all three lipopeptides analyzed, suggesting the stability of the LPE tablets. The reason for this could be that these lipopeptides are stable and not degraded even when autoclaved (Weerapol et al., 2019).Tablets derived from *B.subtilis* strains were previously used effectively for the control of *A.solani*, *A. brassicicola* in Chinese kale under pot conditions and for the control of damping off in tomato under greenhouse and field conditions. Similar experiments were conducted under greenhouse conditions to evaluate the efficacy of *B.velezensis* strain NKMV-3 against *A.solani* in tomato. Spray dried tablets of whole cells and LPE of *B.velezensis* strain NKMV-3 was effective in controlling *A.solani* in tomato.

In conclusion, in this study, spray drying of whole cells and LPE of *B.velezensis* strain NKMV-3 was standardized. Addition of silicon dioxide to the spray dried powder provided free flow properties to it. Tablets of each, whole cells of B.velezensis NKMV 3 strain and its LPE were prepared using sodium starch glycolate to provide hardness. Further, tablets of whole cells of NKMV-3 were stable up to 180 days at both 4 °C and 37 °C storage temperatures. Similarly, LPE tablets exhibited a 2-year shelf life under accelerated stability testing conditions. Both the tablets were found to be effective in controlling *A.solani* under greenhouse conditions. Hence, all the results indicate that *B.velezensis* strain NKMV-3 can be an effective bio control agent for the control of early blight in tomato. Future experiments should focus on the scale up of fermentation of *B.velezensis* strain NKMV-3 and its downstream processing for obtaining commercial quantities of LPE. Field trials should also be conducted to ascertain the extent of control of *A.solani* under field conditions.

Authors contributions

VM: data acquisition, manuscript writing; BNV and RD: data analysis; NS: proofreading; characterization and SRM: project guidance and correspondence.

Declaration of competing interest

The authors declare that they have no known competing financial interests or personal relationships that could have appeared to influence the work reported in this paper.

Data availability

The data that has been used is confidential.

References

Abadias, M., Teixidó, N., Usall, J., Solsona, C., Viñas, I., 2005. Survival of the postharvest biocontrol yeast *Candida sake* CPA-1 after dehydration by spray-drying. Biocontrol Sci. Technol. 15, 835–846. https://doi.org/10.1080/09583150500187041.

Adhikari, P., Oh, Y., Panthee, D., 2017. Current status of early blight resistance in tomato: an update. Int. J. Mol. Sci. 18, 2019. https://doi.org/10.3390/ijms18102019.

Al-Zoubi, N., Gharaibeh, S., Aljaberi, A., Nikolakakis, I., 2021. Spray drying for direct compression of pharmaceuticals. Processes 9, 267. https://doi.org/10.3390/pr9020267.

Andrić, S., Meyer, T., Ongena, M., 2020. Bacillus responses to plant-associated fungal and bacterial communities. Front. Microbiol. 11, 1350. https://doi.org/10.3389/fmicb.2020.01350.

Awan, Z.A., Shoaib, A., 2019. Combating early blight infection by employing Bacillus subtilis in combination with plant fertilizers. Curr. Plant Biol. 20, 100125 https://doi.org/10.1016/j.cpb.2019.100125.

Bhagwat, A., Bhushette, P., Annapure, U.S., 2020. Spray drying studies of probiotic Enterococcus strains encapsulated with whey protein and maltodextrin. Beni-Suef Univ. J. Basic Appl. Sci. 9, 33. https://doi.org/10.1186/s43088-020-00061-z.

Bhattacharyya, P.N., Jha, D.K., 2012. Plant growth-promoting rhizobacteria (PGPR): emergence in agriculture. World J. Microbiol. Biotechnol. 28, 1327–1350. https://doi.org/10.1007/s11274-011-0979-9.

Cao, Y., Pi, H., Chandrangsu, P., Li, Y., Wang, Y., Zhou, H., Xiong, H., Helmann, J.D., Cai, Y., 2018. Antagonism of two plant-growth promoting Bacillus velezensis isolates against Ralstonia solanacearum and Fusarium oxysporum. Sci. Rep. 8, 4360. https://doi.org/10.1038/s41598-018-22782-z.

Ch, S., Debnath, S., R, S.K., S, R.S., B, M., 2012. Formulation & evaluation of lactic acid Bacillus & zinc sulphate fast dispersible tablets. J. Drug Deliv. Therapeut. 2 https://doi.org/10.22270/jddt.v2i1.62.

Coelho, A.G., Lima Neto, J. de S., Moura, A.K.S., Morais, I.C.P. da S., Cunha, F.V.M., Melo-Neto, B., Medeiros, M. das G.F. de, Vasconcelos, E.A.F., Arcanjo, D.D.R., Nunes, L.C.C., Citó, A.M. das G.L., 2018. Pharmaceutical development of tablets containing a spray-dried optimized extract from Lippia origanoides H. B. K.: influence of excipients and toxicological assessment. Braz. J. Pharm. Sci. 54 https://doi.org/10.1590/s2175-97902018000217226.

Costa, E., Teixidó, N., Usall, J., Fons, E., Gimeno, V., Delgado, J., Viñas, I., 2002. Survival of pantoea agglomerans strain CPA-2 in a spray-drying process. J. Food Protect. 65, 185–191. https://doi.org/10.4315/0362-028X-65.1.185.

Dhanarajan, G., Rangarajan, V., Sridhar, P.R., Sen, R., 2016. Development and scale-up of an efficient and green process for HPLC purification of antimicrobial homologues of commercially important microbial lipopeptides. ACS Sustainable Chem. Eng. 4, 6638–6646. https://doi.org/10.1021/acssuschemeng.6b01498.

Errington, J., 2003. Regulation of endospore formation in Bacillus subtilis. Nat. Rev. Microbiol. 1, 117–126. https://doi.org/10.1038/nrmicro750.

Fravel, D.R., 2005. Commercialization and implementation of biocontrol. Annu. Rev. Phytopathol. 43, 337–359. https://doi.org/10.1146/annurev.phyto.43.032904.092924.

Fritzen-Freire, C.B., Prudêncio, E.S., Amboni, R.D.M.C., Pinto, S.S., Negrão-Murakami, A.N., Murakami, F.S., 2012. Microencapsulation of bifidobacteria by spray drying in the presence of prebiotics. Food Res. Int. 45, 306–312. https://doi.org/10.1016/j.foodres.2011.09.020.

Gao, Z., Zhang, B., Liu, H., Han, J., Zhang, Y., 2017. Identification of endophytic Bacillus velezensis ZSY-1 strain and antifungal activity of its volatile compounds against Alternaria solani and Botrytis cinerea. Biol. Control 105, 27–39. https://doi.org/10.1016/j.biocontrol.2016.11.007.

Golowczyc, M.A., Silva, J., Abraham, A.G., De Antoni, G.L., Teixeira, P., 2010. Preservation of probiotic strains isolated from kefir by spray drying: preservation of probiotic strains. Lett. Appl. Microbiol. 50, 7–12. https://doi.org/10.1111/j.1472-765X.2009.02759.x.

Gorai, P.S., Ghosh, R., Konra, S., Mandal, N.C., 2021. Biological control of early blight disease of potato caused by Alternaria alternata EBP3 by an endophytic bacterial strain Bacillus velezensis SEB1. Biol. Control 156, 104551. https://doi.org/10.1016/j.biocontrol.2021.104551.

Huang, S., Vignolles, M.L., Chen, X.D., Le Loir, Y., Jan, G., Schuck, P., Jeantet, R., 2017. Spray drying of probiotics and other food-grade bacteria: A review. Trends Food Sci. Technol. 63, 1–17. https://doi.org/10.1016/j.tifs.2017.02.007.

Jayaraj, J., Radhakrishnan, N.V., Kannan, R., Sakthivel, K., Suganya, D., Venkatesan, S., Velazhahan, R., 2005. Development of new formulations of *Bacillus subtilis* for management of tomato damping-off caused by *Pythium aphanidermatum*. Biocontrol Sci. Technol. 15, 55–65. https://doi.org/10.1080/09583150400015920.

Lee, J.P., Lee, S.-W., Kim, C.S., Son, J.H., Song, J.H., Lee, K.Y., Kim, H.J., Jung, S.J., Moon, B.J., 2006. Evaluation of formulations of Bacillus licheniformis for the biological control of tomato gray mold caused by Botrytis cinerea. Biol. Control 37, 329–337. https://doi.org/10.1016/j.biocontrol.2006.01.001.

Lin, L.-Z., Zheng, Q.-W., Wei, T., Zhang, Z.-Q., Zhao, C.-F., Zhong, H., Xu, Q.-Y., Lin, J.-F., Guo, L.-Q., 2020. Isolation and characterization of fengycins produced by Bacillus amyloliquefaciens JFL21 and its broad-spectrum antimicrobial potential against multidrug-resistant foodborne pathogens. Front. Microbiol. 11, 579621 https://doi.org/10.3389/fmicb.2020.579621.

Meng, X., Yu, J., Yu, M., Yin, X., Liu, Y., 2015. Dry flowable formulations of antagonistic Bacillus subtilis strain T429 by spray drying to control rice blast disease. Biol. Control 85, 46–51. https://doi.org/10.1016/j.biocontrol.2015.03.004.

Nicholson, W.L., Munakata, N., Horneck, G., Melosh, H.J., Setlow, P., 2000. Resistance of *Bacillus* endospores to extreme terrestrial and extraterrestrial environments. Microbiol. Mol. Biol. Rev. 64, 548–572. https://doi.org/10.1128/MMBR.64.3.548-572.2000.

Ongena, M., Jacques, P., 2008. Bacillus lipopeptides: versatile weapons for plant disease biocontrol. Trends Microbiol. 16, 115–125. https://doi.org/10.1016/j.tim.2007.12.009.

Palazzini, J.M., Llabot, J.M., Cantoro, R., Chiotta, M.L., Allemandi, D.A., Torres, A.M., Chulze, S.N., 2020. Spray-drying process as a suitable tool for the formulation of *Bacillus velezensis* RC218, a proved biocontrol agent to reduce Fusarium Head Blight and deoxynivalenol accumulation in wheat. Biocontrol Sci. Technol. 30, 329–338. https://doi.org/10.1080/09583157.2019.1709621.

Pandey, K.K., Pandey, P.K., Kalloo, G., Banerjee, M.K., 2003. Resistance to early blight of tomato with respect to various parameters of disease epidemics. J. Gen. Plant Pathol. 69, 364–371. https://doi.org/10.1007/s10327-003-0074-7.

Peighambardoust, S.H., Golshan Tafti, A., Hesari, J., 2011. Application of spray drying for preservation of lactic acid starter cultures: a review. Trends Food Sci. Technol. 22, 215–224. https://doi.org/10.1016/j.tifs.2011.01.009.

Pingali, K., Mendez, R., Lewis, D., Michniak-Kohn, B., Cuitino, A., Muzzio, F., 2011. Mixing order of glidant and lubricant – influence on powder and tablet properties. Int. J. Pharm. 409, 269–277. https://doi.org/10.1016/j.ijpharm.2011.02.032.

Prabakaran, G., Hoti, S.L., 2008. Optimization of spray-drying conditions for the large-scale preparation ofBacillus thuringiensis var.israelensis after downstream processing. Biotechnol. Bioeng. 100, 103–107. https://doi.org/10.1002/bit.21722.

Ravikumar, M.C., Singh, H., Garampalli, R.H., 2016. Comparative evaluation of long-term storage techniques on viability and virulence of *Alternaria solani*. J. Taibah Univ. Sci. 10, 607–613. https://doi.org/10.1016/j.jtusci.2015.12.008.

Sahu, D., Khare, C., Patel, R., 2014. Eco friendly management of early blight of tomato using botanical plant extracts. J. Ind. Pollut. Control 30 (2), 215–218.

Shafi, J., Tian, H., Ji, M., 2017. *Bacillus* species as versatile weapons for plant pathogens: a review. Biotechnol. Biotechnol. Equip. 31, 446–459. https://doi.org/10.1080/13102818.2017.1286950.

Todorova, S., Kozhuharova, L., 2010. Characteristics and antimicrobial activity of Bacillus subtilis strains isolated from soil. World J. Microbiol. Biotechnol. 26, 1207–1216. https://doi.org/10.1007/s11274-009-0290-1.

Vakalounakis, D., 1983. Evaluation of tomato cultivars for resistance to Alternaria blight. Ann. Appl. Biol. 102, 138–139.

Vignesh, M., Shankar, S.R.M., MubarakAli, D., Hari, B.N.V., 2022. A novel rhizospheric bacterium: Bacillus velezensis NKMV-3 as a biocontrol agent against Alternaria leaf blight in tomato. Appl. Biochem. Biotechnol. 194, 1–17. https://doi.org/10.1007/s12010-021-03684-9.

Weerapol, Y., Nimraksa, H., Paradornuwat, A., Sriamornsak, P., 2019. Development of ready-to-use products derived from Bacillus subtilis strain CMs026 for plant disease control. BioControl 64, 173–183. https://doi.org/10.1007/s10526-019-09929-1.

Yánez-Mendizábal, V., Usall, J., Viñas, I., Casals, C., Marín, S., Solsona, C., Teixidó, N., 2011. Potential of a new strain of *Bacillus subtilis* CPA-8 to control the major postharvest diseases of fruit. Biocontrol Sci. Technol. 21, 409–426. https://doi.org/10.1080/09583157.2010.541554.

Yánez-Mendizabal, V., Viñas, I., Usall, J., Cañamás, T., Teixidó, N., 2012. Endospore production allows using spray-drying as a possible formulation system of the biocontrol agent Bacillus subtilis CPA-8. Biotechnol. Lett. 34, 729–735. https://doi.org/10.1007/s10529-011-0834-y.

Yánez-Mendizábal, V., Viñas, I., Usall, J., Torres, R., Solsona, C., Abadias, M., Teixidó, N., 2012. Formulation development of the biocontrol agent Bacillus subtilis strain CPA-8 by spray-drying: Bacillus subtilis CPA-8 spray-drying formulation. J. Appl. Microbiol. 112, 954–965. https://doi.org/10.1111/j.1365-2672.2012.05258.x.

Zhao, H., Shao, D., Jiang, C., Shi, J., Li, Q., Huang, Q., Rajoka, M.S.R., Yang, H., Jin, M., 2017. Biological activity of lipopeptides from Bacillus. Appl. Microbiol. Biotechnol. 101, 5951–5960. https://doi.org/10.1007/s00253-017-8396-0.

Zhou, X., Dong, J., Gao, J., Yu, Z., 2008. Activity-loss characteristics of spores of Bacillus thuringiensis during spray drying. Food Bioprod. Process. 86, 37–42. https://doi.org/10.1016/j.fbp.2007.10.017.

Zouari, I., Jlaiel, L., Tounsi, S., Trigui, M., 2016. Biocontrol activity of the endophytic Bacillus amyloliquefaciens strain CEIZ-11 against Pythium aphanidermatum and purification of its bioactive compounds. Biol. Control 100, 54–62. https://doi.org/10.1016/j.biocontrol.2016.05.012.